


2011

In Situ Biofiltration of Dissolved Organic Carbon in Reverse Osmosis Membrane Filtration

Russell Rosario Ferlita

University of South Florida, rferlita@mail.usf.edu

Follow this and additional works at: <http://scholarcommons.usf.edu/etd>

 Part of the [American Studies Commons](#), and the [Environmental Engineering Commons](#)

Scholar Commons Citation

Ferlita, Russell Rosario, "In Situ Biofiltration of Dissolved Organic Carbon in Reverse Osmosis Membrane Filtration" (2011).
Graduate Theses and Dissertations.
<http://scholarcommons.usf.edu/etd/3101>

This Dissertation is brought to you for free and open access by the Graduate School at Scholar Commons. It has been accepted for inclusion in Graduate Theses and Dissertations by an authorized administrator of Scholar Commons. For more information, please contact scholarcommons@usf.edu.

In Situ Biofiltration of Dissolved Organic Carbon in
Reverse Osmosis Membrane Filtration

by

Russell Rosario Ferlita

A dissertation submitted in partial fulfillment
of the requirements for the degree of
Doctor of Philosophy
Department of Civil and Environmental Engineering
College of Engineering
University of South Florida

Major Professor: Dr. Daniel H. Yeh, Ph.D.
Jeffrey Cunningham, Ph.D.
Sarina Ergas, Ph.D.
Valerie Harwood, Ph.D.
John Wolan, Ph.D.

Date of Approval:
February 28, 2011

Keywords: Autopsy, Biofouling, Biofilm, Characterization, Fouling

Copyright © 2011, Russell Rosario Ferlita

Dedication

I dedicate this dissertation to my loving wife, Lisa for her emotional support and financial assistance. She has always been there to provide an extra boost of encouragement and reassurance when it was most needed. Without her, this process would have been much more difficult. I would also like to include my son Vincent, whose timing has provided a little extra push. I would like to thank my parents, for always believing in me and providing the much needed ego boost from time to time.

I would also like to thank my friends for their guidance and support. Especially Kenneth Nilsson, who went through this process just prior to myself and was able to lend support, insight, and the much needed down time to help blow off steam. Additionally, I would like to thank my friends for their encouragement, not the least among them being Samuel DuPont, Rafael Urena, Jamie Fargen, Tov Vestgaarden, Brain Piech, and Bob Wenslow.

Acknowledgements

I would like to thank my advisor, Dr. Daniel Yeh, and the members of my committee, Dr. Jeffrey Cunningham, Dr. Sarina Ergas, Dr. Valerie Harwood, and Dr. John Wolan for their insight and encouragement throughout the process of my matriculation. I would also like to thank the scientists at Orange County Water District in Orange County California, especially Don Phipps, Ken Ishida, Jana Safarik, and Menu Leddy for lending their scientific expertise throughout my studies. I would also like to thank Jay Bieber and the rest of the staff at the Nanotechnology Education Research Center (NREC) at USF for sharing their microscopy expertise with me. Additionally, I would like to thank Leigh West and FCoE-BITT for sharing his microbiological expertise with me.

Additionally, I would like to thank the City of Dunedin for sharing their facility with me and allowing me to work on my project using their site as well as lending their financial support. I would especially like to thank Robert Kyle for helping me build my pilot system, Fred Hemerich for his support in siring, sensors, and data acquisition technology for my pilot, Irvin Ketty, Paul Stanek, and John Van Amburg for their insight and expertise with the plant, and all the Dunedin operators and staff for their help and support. I also would like to thank the National Science Foundation (NSF) Students Teachers And Resources in the Sciences (STARS) program for their financial support for my last year of study.

Last but not least, I would like to thank Joshua Goldman, Michael Keen, George Sunderland, Lauren Valdez, Ryan Eck, Michael Gerdjikian, and Sandy Pettit for their contributions to this project and my research in particular. They were all extraordinarily helpful and I enjoyed working with each of them. I would also like to thank my lab mates, Anh Do, Ana Prieto, and Ana Garcia. We had a great lab group that was always willing to help each other with advice or insight.

Table of Contents

List of Tables	v
List of Figures	x
Abstract	xvii
Chapter 1 Introduction	1
1.1 Membrane Background.....	1
1.2 Components in Water.....	6
1.2.1 Organic Carbon	7
1.2.1.1 Organic Carbon Analysis	7
1.3 Membrane Fouling.....	9
1.3.1 Scaling.....	9
1.3.2 Colloidal Fouling	10
1.3.3 Biofouling	11
1.4 Fouling Diagnosis	12
1.5 Pretreatment Methods	13
1.5.1 Conventional Pretreatment.....	13
1.5.2 Membrane Pretreatment.....	14
1.6 Biofiltration.....	15
1.6.1 Biofilters for Membrane Pretreatment	19
1.7 Research Objectives.....	23
1.7.1 Experimental Phases	23
1.7.1.1 Phase I: Literature Investigation and Equipment Setup	24
1.7.1.2 Phase II: Membrane Autopsies at Three Points of Skid	24
1.7.1.3 Phase III: Plant Analysis of Carbon Mass Balance	24
1.7.1.4 Phase IV: Flat Sheet Module Pilot Testing with Fouled Membrane Element.....	25
Chapter 2 Background.....	26
2.1 Dunedin Reverse Osmosis Water Treatment Plant.....	26
2.1.1 Dunedin Pretreatment Process	26
2.1.2 Dunedin Reverse Osmosis Process	29
Chapter 3 Materials and Methods	31
3.1 Experimental Objectives.....	31

3.2	Design of Experiments.....	31
3.3	Experimental Protocols and Analytical Methods.....	32
3.3.1	Carbohydrate Assay	32
3.3.2	Total Direct Count	35
3.3.3	Fourier-Transform Infrared Spectroscopy (FTIR)	37
3.3.4	Heterotrophic Plate Count.....	37
3.3.5	Protein Assay	40
3.3.6	Total Dry Mass.....	43
3.3.7	Total Organic Carbon/Total Nitrogen Analysis.....	43
3.3.8	UV ₂₅₄ Absorption.....	44
3.3.9	Specific UV Absorbance (SUVA)	44
3.3.10	Microscopic Evaluation.....	44
Chapter 4 Cryo-Snap: A Simple Modified Freeze-Fracture Method for SEM		
	Imaging of Membrane Cross-Sections.....	46
4.1	Introduction.....	46
4.2	Experimental	49
4.2.1	Materials and Sample Preparation	49
4.2.1.1	Razor Sectioning	49
4.2.1.2	Direct Freeze Fracture	50
4.2.1.3	Cryo-Snap.....	50
4.2.1.4	SEM Analysis.....	51
4.3	Results and Discussion.....	51
4.3.1	Ultrafiltration Membrane	51
4.3.2	Reverse Osmosis Membrane.....	53
4.3.3	Hollow Fiber Membrane.....	54
4.4	Conclusions.....	57
Chapter 5 Characterization of Membrane Fouling by Autopsies: A Plant Scale		
	Evaluation	59
5.1	Introduction.....	59
5.2	Autopsy Procedure.....	60
5.3	Autopsy Results From Orange County	60
5.3.1	External Evaluation.....	61
5.3.2	Protein and Carbohydrate Analysis.....	62
5.3.3	Total Direct Count and Heterotrophic Plate Count.....	65
5.3.4	ATR-FTIR.....	67
5.3.5	Microbial Community Profile.....	71
5.3.6	SEM/EDS.....	75
5.3.7	AFM.....	76
5.4	Plant-Wide Autopsies	77
5.4.1	External Evaluation.....	78
5.4.2	Dry Mass Analysis	79
5.4.3	Protein and Carbohydrate Analysis.....	81
5.4.4	Total Direct Count and Heterotrophic Plate Count.....	84
5.4.5	ATR-FTIR.....	86

5.4.6	SEM/EDS.....	89
5.4.7	AFM.....	94
5.5	Conclusions.....	96
5.5.1	Orange County Autopsy.....	96
5.5.2	Plant-Wide Autopsies.....	96
5.5.3	Overall Autopsy Conclusions.....	97
Chapter 6	Mass Balance Analysis of Dissolved Organic Carbon in a Reverse Osmosis Membrane Water Treatment Plant: Implications for Biofouling Control.....	99
6.1	Introduction.....	99
6.2	Sample Collection.....	101
6.3	Mass Balance Calculation.....	103
6.4	Results and Discussion.....	104
6.5	Conclusions.....	113
Chapter 7	Pilot System Analysis of Biofilm Effect on Downstream Membrane Material.....	115
7.1	Introduction.....	115
7.2	Pilot Design and Testing.....	115
7.2.1	Membrane Sampling.....	120
7.2.2	Zero External Carbon Loading.....	121
7.2.3	Carbon Loading.....	121
7.3	Results.....	123
7.3.1	Surface Fouling Characterization.....	123
7.3.1.1	Zero External Carbon Loading.....	123
7.3.1.1.1	Protein and Carbohydrate Data.....	124
7.3.1.1.2	Microbiological Data.....	129
7.3.1.1.3	ATR-FTIR.....	133
7.3.1.1.4	SEM-EDS.....	135
7.3.1.1.5	AFM.....	137
7.3.1.2	Carbon Loading.....	140
7.3.1.2.1	Protein and Carbohydrate Data.....	141
7.3.1.2.2	Microbiological Data.....	150
7.3.1.2.3	ATR-FTIR.....	155
7.3.1.2.4	SEM-EDS.....	157
7.3.1.2.5	AFM.....	158
7.3.1.3	Overall Foulant Trends.....	160
7.3.2	Flat Sheet Module Performance Characterization.....	163
7.3.2.1	Flux Characterization.....	163
7.3.2.2	Transmembrane Pressure Characterization.....	168
7.3.3	Flow Rate.....	169
7.3.4	Carbon and Nitrogen Mass Balance.....	170
7.4	Discussion.....	171
7.5	Conclusions.....	173
Chapter 8	Conclusions.....	175

8.1	Summary of Work.....	175
8.2	Impacts of Proposed Activities	177
8.3	Recommendations for Future Work.....	178
References		181
Appendices		192
	Appendix A Plant Diagram	193
	Appendix B Analytical Methods SOPs	194
	Appendix C Pilot System Operation	204
	Appendix D Additional Carbon Balance Information.....	212
	Appendix E Additional Pilot Study Information	228

List of Tables

Table 3-1 Typical dilution series for carbohydrate calibration curve	34
Table 3-2 Typical dilution series for protein calibration curve.....	42
Table 5-1 Concentrations with standard deviations of protein and carbohydrate and the ratio of carbohydrate to protein for indicated sample area	63
Table 5-2 Number of total bacteria ($\# \times 10^6/\text{cm}^2$) and heterotrophic bacteria ($\# \times$ $10^4/\text{cm}^2$) on indicated sample area.....	65
Table 5-3 Roughness data for indicated membrane samples	77
Table 5-4 The dry mass concentrations on the surface of the membranes	80
Table 5-5 The protein and carbohydrate concentrations on the surface of the membranes and the carbohydrate/protein ratio.....	82
Table 5-6 Number of culturable microorganisms for each section of each autopsied membrane	85
Table 5-7 AFM Roughness data for front middle and end sections of all three autopsied membrane elements.....	94
Table 7-1 The protein and carbohydrate concentrations of the pilot feed and concentrate swatches for the zero external carbon loading portion of the study.....	125
Table 7-2 The carbohydrate/protein for the feed and concentrate swatches and the feed/concentrate ratio data for protein and carbohydrate concentrations.....	127
Table 7-3 Total direct count for feed and concentrate swatches and feed/concentrate ratio	130
Table 7-4 HPC data for the feed and concentrate swatches as well as feed/concentrate ratio data for these counts.....	131

Table 7-5	The AFM roughness data for the feed and concentrate membrane swatches as a function of sampling date.....	139
Table 7-6	Protein and carbohydrate concentration on pilot membrane swatches from the 0.1 g/m ² day portion of study.....	141
Table 7-7	The carbohydrate/protein ratio data for the feed and concentrate swatches and feed/concentrate ratio data for protein and carbohydrates from the 0.1 g/m ² day portion of study	142
Table 7-8	Protein and carbohydrate concentrations on pilot membrane swatches from the 0.5 g/m ² day portion of study.....	143
Table 7-9	The carbohydrate/protein ratio data for the feed and concentrate swatches and feed/concentrate ratio data for protein and carbohydrates from the 0.5 g/m ² day portion of study	144
Table 7-10	Protein and carbohydrate concentration on pilot membrane swatches from the 2.0 g/m ² day portion of study.....	145
Table 7-11	The carbohydrate/protein ratio data for the feed and concentrate swatches and feed/concentrate ratio data for protein and carbohydrates from the 2.0 g/m ² day portion of study	146
Table 7-12	Total culturable microorganisms on the feed and concentrate membrane swatches from the 0.1 g C/m ² day portion of the study and the feed/concentrate ratio.....	152
Table 7-13	Total culturable microorganisms on the feed and concentrate membrane swatches from the 0.5 g C/m ² day portion of the study and the feed/concentrate ratio.....	152
Table 7-14	Total culturable microorganisms on the feed and concentrate membrane swatches from the 2.0 g C/m ² day portion of the study and the feed/concentrate ratio.....	153
Table 7-15	Ratio of initial flux decline for feed to concentrate with their standard deviations at each carbon loading condition as well as the number of samples used and the t-value for the difference from M=1	166
Table 7-16	Two-tailed t-test results between each carbon loading condition showing degrees of freedom (df), t-value, and indication of significance at 0.05	168
Table 7-17	Feed/concentrate ratio of foulants for each carbon loading level at 50GPM	170

Table 7-18 Feed/concentrate ratio of foulants for each carbon loading level at 25GPM	170
Table 7-19 The percent removal of carbon and nitrogen and percent increase in SUVA along with statistical results for the pilot system.....	171
Table B-1 Dilution series for carbohydrate calibration.....	196
Table B-2 Dilution series for protein calibration	203
Table D-1 Influent carbon into membrane treatment train and % removal to 04/07/09	216
Table D-2 Influent carbon into membrane treatment train and % removal from 04/14/09	217
Table D-3 Carbon removal on skid and individual stage levels to 04/07/09	218
Table D-4 Carbon removal on skid and individual stage levels from 04/14/09	219
Table D-5 Feed and concentrate SUVA and % change on plant level to 04/07/09	221
Table D-6 Feed and concentrate SUVA and % change on plant level from 04/14/09	222
Table D-7 SUVA data for the skid and stage levels with % removal to 04/07/09.....	223
Table D-8 SUVA data for the skid and stage levels with % removal from 04/14/09	224
Table D-9 Influent nitrogen with removal on plant, skid and stage levels and C:N ratio	226
Table E-1 The total number of microorganisms on the feed and concentrate pilot membrane swatches and the respective feed/concentrate ratio for the carbon loading portion of the study	229
Table E-2 RMS and Ra roughness data and feed/concentrate ratio data	231
Table E-3 Overall feed/concentrate ratio data for protein, carbohydrate, and HPC at each carbon loading condition	233
Table E-4 Feed/concentrate ratio for initial flux decline for the zero external carbon loading portion of the study	240

Table E-5	Feed/concentrate ratio for initial flux decline for the 0.1 g C/m ² day portion of the study.....	241
Table E-6	Feed/concentrate ratio for initial flux decline for the 0.5 g C/m ² day portion of the study.....	241
Table E-7	Feed/concentrate ratio for initial flux decline for the 2.0 g C/m ² day portion of the study.....	241
Table E-8	The t-test results from feed/concentrate ratio of protein concentration on pilot membrane samples	242
Table E-9	The t-test results from feed/concentrate ratio of carbohydrate concentration on pilot membrane samples	242
Table E-10	The t-test results from feed/concentrate ratio of total direct count numbers on pilot membrane samples	243
Table E-11	The t-test results from feed/concentrate ratio of HPC concentration on pilot membrane samples	243
Table E-12	The t-test results from feed/concentrate ratio of root mean squared (RMS) roughness values for pilot membrane samples.....	243
Table E-13	The t-test results from feed/concentrate ratio of average roughness (Ra) values for pilot membrane samples	243
Table E-14	Two-tailed t-test results between each carbon loading condition for protein concentration showing degrees of freedom (df), t-value, and indication of significance at 0.05.....	244
Table E-15	Two-tailed t-test results between each carbon loading condition for carbohydrate concentration showing degrees of freedom (df), t-value, and indication of significance at 0.05.....	245
Table E-16	Two-tailed t-test results between each carbon loading condition for feed carbohydrate/protein ratio showing degrees of freedom (df), t-value, and indication of significance at 0.05	245
Table E-17	Two-tailed t-test results between each carbon loading condition for concentrate carbohydrate/protein ratio showing degrees of freedom (df), t-value, and indication of significance at 0.05.....	246
Table E-18	Two-tailed t-test results between each carbon loading condition for total direct count showing degrees of freedom (df), t-value, and indication of significance at 0.05.....	246

Table E-19	Two-tailed t-test results between each carbon loading condition for HPC concentration showing degrees of freedom (df), t-value, and indication of significance at 0.05.....	247
Table E-20	Two-tailed t-test results between each carbon loading condition for RMS roughness showing degrees of freedom (df), t-value, and indication of significance at 0.05.....	247
Table E-21	Two-tailed t-test results between each carbon loading condition for average roughness (Ra) showing degrees of freedom (df), t-value, and indication of significance at 0.05.....	248
Table E-22	Two-tailed t-test results for the foulant analyses for 0.1 g C/m ² day showing degrees of freedom (df), t-value, and indication of significance at 0.05	248
Table E-23	Two-tailed t-test results for the foulant analyses for 0.5 g C/m ² day showing degrees of freedom (df), t-value, and indication of significance at 0.05	249
Table E-24	Two-tailed t-test results for the foulant analyses for 2.0 g C/m ² day showing degrees of freedom (df), t-value, and indication of significance at 0.05	249

List of Figures

Figure 1-1 Membrane Filtration Spectrum, adapted from Ultrapure Industries [6].....	3
Figure 1-2 Spiral Wound Reverse Osmosis Element.....	5
Figure 1-3 Concentrate Staging Membrane Treatment Design	6
Figure 1-4 Schematic of carbon fractions	8
Figure 1-5 Salt concentration gradient at an RO membrane boundary layer, i.e. concentration polarization	10
Figure 1-6 Typical Conventional Pretreatment Scheme	14
Figure 1-7 Typical Membrane Pretreatment Scheme	15
Figure 1-8 Diagram showing biofilm growth on fixed media in a biofilter.....	17
Figure 1-9 Diagram showing biofilm growth on membrane filter surface	22
Figure 2-1 Cross section of a horizontal green sand filter unit: A) 21.5” concrete base, B) 20” support gravel, C) 6” silica gravel, D) 15” manganese green sand, E) 30” Anthracite, F) 16” underdrain header, G) air scour header, and H) 16” inlet.....	28
Figure 2-2 Product side of skid detailing the numbering convention for pressure vessels.....	30
Figure 3-1 Dilution series from calibration curve from most concentrated to least concentrated, left to right.....	34
Figure 3-2 Microscope setup in FCoE-BITT used for total direct count	36
Figure 3-3 Russell Ferlita loading sample in FTIR (left) and sample in ATR- FTIR (right)	37
Figure 3-4 R2A agar plate with countable microbial colonies	40

Figure 3-5 Dilution series from a protein calibration curve from most concentrated to least concentrated, left to right	42
Figure 4-1 Cross-sectional SEM image of uncoated PVDF ultra-filtration membrane prepared using a) razor sectioning, b) freeze fracture, and c) Cryo-snap method.	52
Figure 4-2 Cross-sectional SEM image of Koch polyamide reverse osmosis membrane prepared using a) razor sectioning, b) freeze fracture, c) Cryo-snap method, and d) the EDS spectrum of a portion of the foulant layer from c (indicated by circle)	54
Figure 4-3 Cross-sectional SEM image of virgin polypropylene hollow fiber MF membrane material prepared via a) razor sectioning, b) freeze fracture, c) Cryo-snap method without membrane pore hydration, and d) Cryo-snap method with membrane pore hydration.....	57
Figure 5-1 Membrane element autopsied in Orange County showing the feed channel with debris deposited.....	61
Figure 5-2 Membrane leaf surface indicating flow direction (top) and areas of the membrane sampled, front (bottom left), middle (bottom center), and end (bottom right)(scale in cm)	62
Figure 5-3 Concentration of protein per unit area as a function of membrane section sampled (error bars indicate standard deviation)	64
Figure 5-4 Carbohydrate concentration per unit area for each section of membrane sampled (error bars indicate standard deviation).....	64
Figure 5-5 The carbohydrate/protein ratio for each section of the membrane sampled (error bars indicate standard deviation).....	65
Figure 5-6 The number of total microorganisms and heterotrophic microorganisms on the indicated sections of membrane surface (error bars indicate standard deviation)	67
Figure 5-7 ATR-FTIR spectra for A) front, B) middle, and C) end sections; D) difference spectra for each section with the reference spectrum	69
Figure 5-8 Difference spectra for each membrane section and reference spectrum	70
Figure 5-9 Capillary electrophoresis results of base pair lengths 34 through 215 (shaded regions indicate presence of fragment of specified length in sample indicated).....	73

Figure 5-10 Capillary electrophoresis results of base pair lengths 216 through 270 (shaded regions indicate presence of a fragment of specified length in sample indicated).....	74
Figure 5-11 Cryosnap images of front (top left), middle (top right), and end (bottom left) sections; and EDS spectrum for foulant on front section (bottom right).....	75
Figure 5-12 AFM top view images for autopsied membrane front (top left), middle (top right), and end (bottom left) sections as well as virgin membrane material (bottom right).....	76
Figure 5-13 Feed channel for membrane 1 (left), membrane 2 (middle), and membrane 3 (right).....	79
Figure 5-14 The concentration of dry mass measured for each section of membrane area autopsied (error bars indicate standard deviation)	81
Figure 5-15 The protein concentration measured for each section of membrane area autopsied (error bars indicate standard deviation)	83
Figure 5-16 The carbohydrate concentration measured for each section of membrane area autopsied (error bars indicate standard deviation)	84
Figure 5-17 Number of culturable microorganisms per unit area on each section of each autopsied membrane element (error bars indicate standard deviation).....	86
Figure 5-18 FTIR spectra for the front, middle, and end sections of the autopsied membranes for membrane 1 (top left), membrane 2 (top right), and membrane 3 (bottom left); and difference spectra for a representative spectrum from each autopsied membrane (bottom right).....	88
Figure 5-19 ATR-FTIR spectra from a representative sample from each autopsied membrane and virgin membrane material displayed from 2000-600 cm ⁻¹	89
Figure 5-20 Debris particle deposited on feed channel of membrane 1	90
Figure 5-21 EDS spectrum of a particle lodged in feed channel of membrane 1	91

Figure 5-22 SEM images of the surface for membrane 1 front (Top left), membrane 1 middle (top center), membrane 1 end (top right), membrane 2 front (middle left), membrane 2 middle (middle center), membrane 2 end (middle right), membrane 3 front (bottom left), membrane 3 middle (bottom center), and membrane 3 end (bottom right)	92
Figure 5-23 EDS spectrum from the end section of membrane 3.....	93
Figure 5-24 AFM images of the membrane sections from membrane 1 front (top left), membrane 1 middle (top center), membrane 1 end (top right), membrane 2 front (middle left), membrane 2 middle (middle center), membrane 2 end (middle right), membrane 3 front (bottom left), membrane 3 middle (bottom center), and membrane 3 end (bottom right)	95
Figure 6-1 Representation of plant sampling points: A) plant feed, B) plant permeate, and C) plant concentrate	102
Figure 6-2 Temporal profile of the concentration of DOC and TN in the plant feed-water	105
Figure 6-3 Temporal profile of calculated SUVA of the plant feed-water	106
Figure 6-4 Temporal profiles of the concentration of DOC in the plant feed-water and monthly precipitation.....	106
Figure 6-5 SUVA of the plant feed-water plotted as a function of plant feed-water DOC.....	107
Figure 6-6 Temporal profiles of percent removal of DOC and TN from RO treatment train.....	108
Figure 6-7 Removal of DOC within the RO treatment train plotted against the unit DOC loading based on the total membrane area in operation at the time of sampling top) percent removal of DOC and bottom) unit removal of DOC	110
Figure 6-8 Temporal profile of the percent change in SUVA from feed-water to concentrate.....	111
Figure 7-1 Schematic of pilot system	118
Figure 7-2 Sterlitech Flat Sheet Module	119
Figure 7-3 FSM portion of pilot system.....	120

Figure 7-4	Time function of protein concentration on pilot feed and concentrate swatches.....	126
Figure 7-5	Carbohydrate concentration on pilot feed and concentrate swatches as a function of sampling date	126
Figure 7-6	The feed/concentrate ratio for protein and carbohydrate concentrations plotted as a function of date sampled	128
Figure 7-7	The carbohydrate/protein ratio for the feed an concentrate swatches of the pilot system.....	129
Figure 7-8	The number of culturable bacteria per unit area on the feed and concentrate pilot swatches	132
Figure 7-9	The feed/concentrate ratio of the number of culturable bacteria on the membrane surface.....	133
Figure 7-10	ATR-FTIR spectra for virgin membrane material and pilot feed and concentrate membrane swatches from the zero external carbon loading portion of the study.....	134
Figure 7-11	Difference spectra for pilot feed and concentrate	135
Figure 7-12	SEM images of feed (top left) and concentrate (top right) and EDS images of feed (bottom left) and concentrate (bottom right).....	136
Figure 7-13	AFM images of the pilot membrane surface swatches: top view for feed (top left), top view for concentrate (top right), surface view for feed (bottom left), and surface view for concentrate (bottom right)	138
Figure 7-14	Protein concentration on the feed and concentrate pilot swatches for the carbon loading portion of the study	147
Figure 7-15	Carbohydrate concentration on the feed and concentrate swatches from the pilot system during the carbon loading portion of the study.....	148
Figure 7-16	The feed/concentrate ratio for protein and carbohydrate concentrations on the pilot membrane surfaces.....	149
Figure 7-17	The carbohydrate/protein ratio for the pilot feed and concentrate membrane surfaces during the carbon loading portion of the study.....	149
Figure 7-18	The total number of culturable microorganisms as a function of sampling date for the carbon loading portion of the study	154

Figure 7-19	The feed/concentrate ratio of culturable microorganisms as a function of sampling date for the carbon loading portion of the study	154
Figure 7-20	FTIR spectra of feed and concentrate membrane swatches from the carbon loading portion of the study along with virgin membrane material	155
Figure 7-21	FTIR difference spectra for feed and concentrate membrane swatches.....	156
Figure 7-22	SEM images of pilot membrane swatch surface for feed (top left) and concentrate (top right) and EDS spectra for feed (bottom left) and concentrate (bottom right)	158
Figure 7-23	AFM images of the pilot membrane swatch surfaces: top view for feed (top left), top view for concentrate (top right), surface view for feed (bottom left), and surface view for concentrate (bottom right)	159
Figure 7-24	The feed/concentrate ratio of protein concentration, carbohydrate concentration, HPC (error bars indicate standard deviation).....	161
Figure 7-25	Carbohydrate/protein ratio for the pilot feed and concentrate membrane swatches plotted against carbon loading rate (error bars indicate standard deviation).....	162
Figure 7-26	Initial flux decline data for FSM#4 during the 2 g C/m ² day portion of the study.....	165
Figure 7-27	Relationship of fouling rate ratio, M, to carbon loading rate (error bars indicate standard deviation)	167
Figure 7-28	The pressure for FSM#1 feed and concentrate membrane swatches and their differential pressure	169
Figure A-1	Plant Diagram.....	193
Figure C-1	Schematic of pilot system, not including flat sheet module portion.....	208
Figure C-2	Pump interface for pilot system.....	209
Figure C-3	Schematic of flat sheet module portion of pilot system	210
Figure D-1	Sampling scheme for individual skid and stage level	213
Figure D-2	Temporal profile of individual skid and stage level carbon removal	220

Figure D-3	Temporal profile of change in SUVA on individual skid and stage level	225
Figure D-4	Temporal profile of nitrogen removal on an individual skid and stage level	227
Figure E-1	RMS roughness for feed and concentrate and feed/concentrate ration throughout pilot study.....	232
Figure E-2	Average roughness for feed and concentrate and feed/concentrate ration throughout pilot study	232
Figure E-3	The feed/concentrate ratio for the protein, carbohydrate and HPC concentrations plotted against carbon loading rate for the 50 GPM flow rate.....	234
Figure E-4	The feed/concentrate ratio for the protein, carbohydrate and HPC concentrations plotted against carbon loading rate for the 25 GPM flow rate.....	234
Figure E-5	Initial rate of fouling, m, for the no carbon loading portion of the study for all four FSMs.....	236
Figure E-6	Initial rate of fouling, m, for the 0.1 g C/m ² day portion of the study for all four FSMs	237
Figure E-7	Initial rate of fouling, m, for the 0.5 g C/m ² day portion of the study for all four FSMs	238
Figure E-8	Initial rate of fouling, m, for the 2.0 g C/m ² day portion of the study for all four FSMs	239

Abstract

Biofouling, or the formation of biofilm on membrane surfaces, can decrease the performance (decreased flux and/or increased operating pressure) of a reverse osmosis (RO) membrane system in a water treatment plant. However, biofilms have been used in water treatment systems to remove organic carbon from water via biofilters and successfully reduce biofilm growth downstream. This research investigates the possibility that the heterotrophic biofilm present on membrane surfaces removes nutrients from the treatment water, thereby making it nutrient deprived as it travels along the treatment train. This may potentially be exploited as an *in situ* biofilter to actively remove dissolved organic carbon (DOC) from the treatment water, thereby protecting downstream membrane surfaces from biofouling. Analysis of fouled membranes from the Dunedin water treatment plant in Dunedin, FL indicates the presence of biofilm on membrane surfaces in a gradient pattern with a higher level of fouling at the front of the element. Additionally, the community structure of the biofilm at the front of the element is unique with respect to the feed-water and downstream membrane material. Additionally, a carbon (and nitrogen) mass balance study was performed at the water treatment plant in Dunedin, FL through extensive sampling of DOC at multiple locations of the RO membrane system over a 20 month period. Plant-level mass balance results indicate a significant pool of DOC was consistently unaccounted for, and presumably assimilated or otherwise removed within the membrane system. Sampling also indicated

a removal of total nitrogen. Additionally, the specific UV absorbance (SUVA) of the DOC in concentrate was consistently greater than that of the feed water, suggesting the removal of labile aliphatic carbon as the feed water travels through the feed channel of the membrane system.

A pilot system was designed and built to operate under plant conditions (flow rate and pressure) to test if the biofilm on the surface of the membrane can have a protective effect for downstream membrane material. A fouled membrane element was pulled from the plant at the same time and general location as an autopsied element (to determine composition on the surface) and used in the pilot system. Feed and concentrate water from the pilot was directed to flat sheet modules for performance testing and surface characterization. This allowed for characterization of the two sections without disturbing the membrane element. Differences in performance and foulant deposition were characterized for the two sections as a function of carbon addition and flow rate. The results from this testing suggest the membrane element, or the biofilm on its surface, has both a performance and a foulant deposition benefit for downstream membranes as compared to feed membrane material. This benefit also displayed an increasing trend as the concentration of organic carbon fed into the system increases.

Chapter 1 Introduction

1.1 Membrane Background

Water is a precious resource and is vital to life and the proper function of bodily systems. Due to the increasing scarcity of clean water sources, nontraditional water sources with relatively high levels of contaminants are increasingly being used [1-4]. In order to remove these contaminants and to meet increasingly stringent water quality regulations, there have been technological advances in processes and materials to make clean drinking water from these relatively contaminated sources. One such field of study is membrane technology, in which thin films are used to separate and purify gases and/or liquids. The use of membranes to purify water has great promise for increasing the world's water supply, thereby reducing the strain on current water resources.

There are various types of membrane filters, each having characteristic size cut-offs they are capable of filtering. These membrane filters make use of two distinct filtration mechanisms. First, size-exclusion filtration, or the pore flow model, refers to membranes with pores of a specific size or range of sizes. These pores act as a physical barrier, allowing particles and/or molecules that are smaller than the pore to pass through while blocking all particles and/or molecules that are larger [5]. The second mechanism is solution diffusion. Solution diffusion is different from size exclusion filtration in that there are no distinct pores in the membrane surface. Instead, this type of filtration relies

on physical interactions of the membrane material and the materials that compose the solution based on their chemical and physical properties. The material being filtered can be said to dissolve in the membrane material and is transmitted through in voids by diffusion down a concentration gradient [5]. In order to make use of this mechanism for water filtration, the osmotic pressure of the filter water must be overcome to obtain water from a diluted phase to a more concentrated phase (i.e. concentrating the water on the permeate side and the solutes in the effluent).

Microfiltration, ultrafiltration, and particle filtration are all examples of membranes that function by the pore flow model [5]. All these filters are capable of reducing turbidity in water by removing suspended particles, bacteria, and viruses. Reverse osmosis (RO) membranes function on the solution diffusion model and are capable of filtering charged particles and materials that are at the smallest portion of the membrane filtration spectrum, such as monovalent and multivalent ions as small as 1 nanometer and organic compounds (although small organics tend to be permeable due to their small size and neutral charge) [5]. Nanofiltration membranes are in the grey area between pore flow and solution diffusion. These membranes are capable of removing multivalent ions with varying efficiencies and organic compounds, although they suffer from the same shortfalls with small, neutral organic compounds as RO membranes, Figure 1-1 [5].

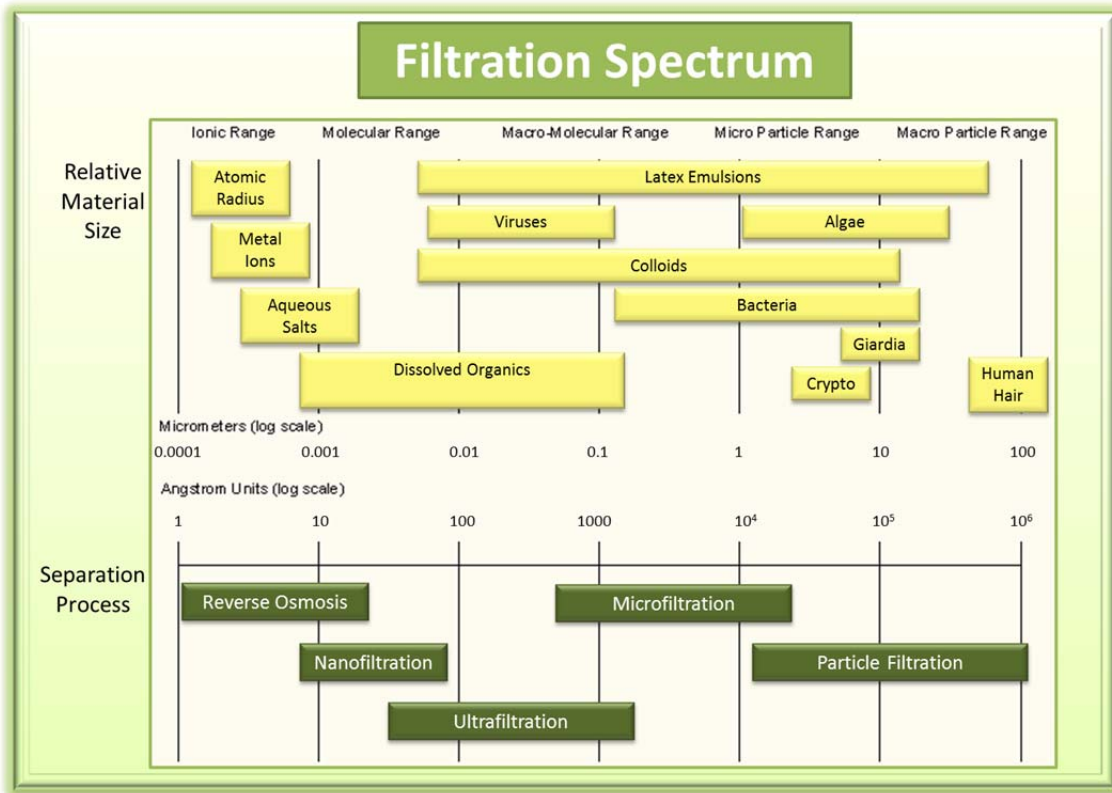


Figure 1-1 Membrane Filtration Spectrum, adapted from Ultrapure Industries [6]

Asymmetric RO membranes were introduced over forty years ago, originating from the Loeb Sourirajan process for the production of anisotropic cellulose acetate membrane materials [7-9]. These membranes were a tremendous advance due to their ability to desalinate water without the use of heated distillation and greatly reduced the amount of energy required for pressurized reverse osmosis processes. This is due to the very thin, dense cellulose acetate separation layer of these membranes formed during the phase inversion process. Advantages of these membranes include their resistance to chlorine and their smooth surface morphology, which makes them more resistant to foulant adhesion [10]. Additionally, their surface is uncharged, leading to more stable performance. However, the cellulose acetate is susceptible to biological degradation.

Cellulose acetate membranes also have a narrow pH range of operation, are sensitive to high temperatures, and have limited rejection of salts and low molecular weight compounds, so more advanced materials were studied, leading to advances in material science and engineering. Thin film composite (TFC) membranes with a dense aromatic polyamide separation layer on a porous support are the recent and popular evolution of this research [11]. These membranes have a very thin (0.01-0.1 μm) charged surface giving them higher rejection capabilities of salts and small molecules and the material has a wide tolerance to pH. Their thin separation layer lends them higher flux than cellulose acetate membranes, and they are resistant to biological degradation. However, TFC membranes are sensitive to chemical oxidants such as chlorine. Due to the advantages of TFC membranes over cellulose acetate membranes, they have become the most commonly used material for large scale purification processes [12-14]. RO membranes have received a lot of attention for a variety of applications, including drinking water, municipal wastewater, and industrial wastewater [3, 4, 15-18]. However, their most common application is for drinking water via desalination and/or softening of seawater and brackish groundwater sources [19].

The typical configuration for RO membranes is the spiral wound configuration, Figure 1-2. This configuration is a collection of flat-sheet membrane material that is rolled into a cylindrical housing. The individual membrane leafs are separated by feed and permeate spacers and glue lines to prevent cross-contamination of the feed, permeate, and concentrate streams. This configuration allows for a large surface area of membrane

material, typically 400 ft² (37.2 m²) for the standard 8" x 40" membrane element, to be housed in a small volume that is easily handled and occupies a small footprint.

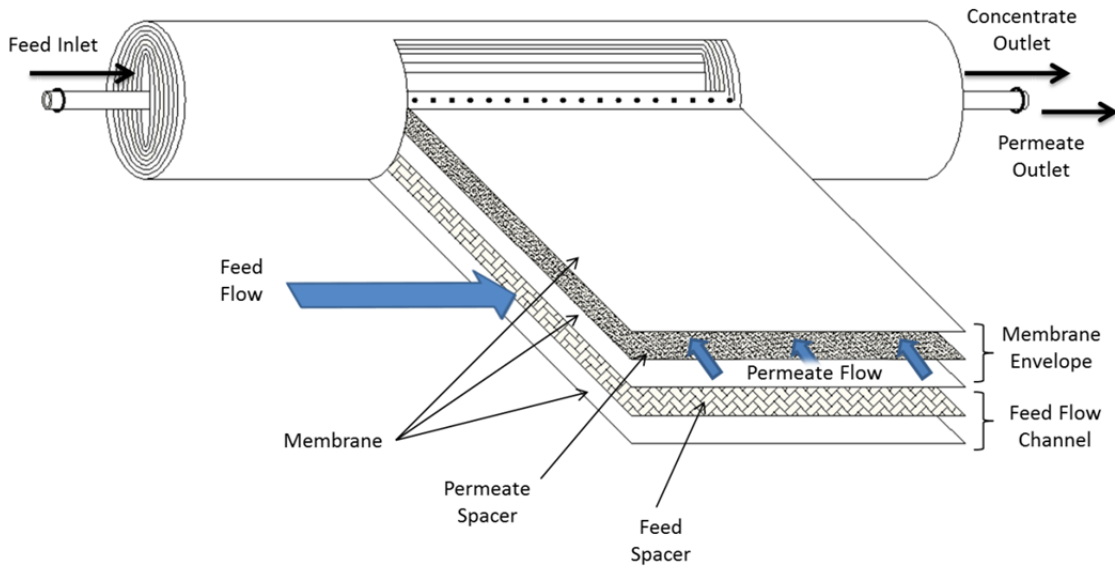


Figure 1-2 Spiral Wound Reverse Osmosis Element

The majority of RO systems in use today are spiral-wound, plug-flow configurations. In order to increase the water yield, multiple stages may be used where the concentrate from one stage becomes the feed for the next stage. This process is known as concentrate staging, Figure 1-3. This configuration (also known as the Christmas-tree array) squeezes out as much pure water as is economically feasible from the treatment water and minimizes concentrate disposal. These arrays may be two or three stages, although two stage arrays with first stage: second stage pressure vessel ratios of 2:1 and 3:2 being most common in drinking water applications [20]. As the membranes separate pure water from the solutes and contaminants, the feed-water becomes progressively concentrated along the flow axis. This increase in concentration of solutes and contaminants can lead

a loss in rejection performance as well as the deposition and/or adhesion of solutes on the membrane surface, resulting in fouling.

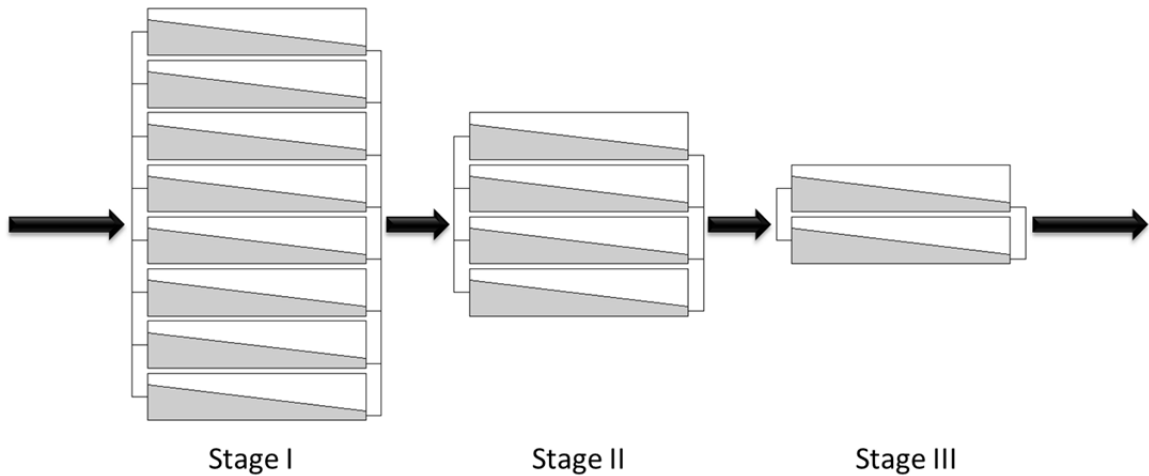


Figure 1-3 Concentrate Staging Membrane Treatment Design

1.2 Components in Water

Water can contain a variety of components, each presenting unique challenges for their removal in water treatment. Among these components are salts, ionic species, organic and inorganic materials, and metals. The primary focus of the research presented here is carbon, which can exist in an inorganic form (carbonate salts, carbon dioxide) or in an organic form. The removal of inorganic carbon is well studied and not a focus of this research. Organic carbon has implications in the formation of disinfection byproducts, membrane fouling, and growth of microorganisms in treatment and distribution systems [21-24].

1.2.1 Organic Carbon

Most of the organic carbon found in natural water resources is natural organic matter (NOM) and comes from the decomposition of plants and animals [25]. The presence of NOM in solution can lead to high levels of disinfection byproducts, colloidal fouling, and biofouling [26-28]. NOM can be divided into two categories, dissolved organic carbon (DOC) and particulate organic carbon (POC). POC can be removed through filtration and/or coagulation/sedimentation [29, 30]. DOC is of particular interest in its potential fouling effect for membrane filtration. DOC can be further divided into a biodegradable organic matter (BOM) and a refractory fraction, Figure 1-4 [31]. The refractory portion is not easily biodegradable and does not significantly contribute to microbial growth, although refractory organic carbon can be converted to BOM through oxidation (i.e. chlorine disinfection) [32].

1.2.1.1 Organic Carbon Analysis

Due to the issues listed above, the amount and type of organic carbon present in treatment waters is of interest. A common method for determining the amount of organic carbon present is through the use of a total organic carbon (TOC) analyzer. This method is capable of determining both the amount of carbon present (total carbon) and/or the TOC content. Although this is an effective method for determining the amount of organic carbon present, the downfall of this measurement is the lack of information on the type of organic carbon in solution. In order to further characterize the organic carbon measured with a TOC analyzer, the specific UV absorbance (SUVA) can be determined by normalizing the TOC to the UV absorbance at 254nm. The value of SUVA for a

treatment water has been strongly correlated to its aromatic character, and thus gives insight to the amount that is biodegradable [21].

The biodegradable fraction of organic carbon is typically characterized using biodegradable dissolved organic carbon (BDOC) and/or assimilable organic carbon (AOC) assays [31]. These measurements are powerful in that they give a direct measurement to the amount of organic carbon that is readily degradable by microorganisms. However, BDOC measurements have limitations at low levels (0.1-0.2 mg/L) and AOC detection is time consuming and requires a high level of expertise [31]. Additionally, AOC results are typically lower than BDOC results [33].

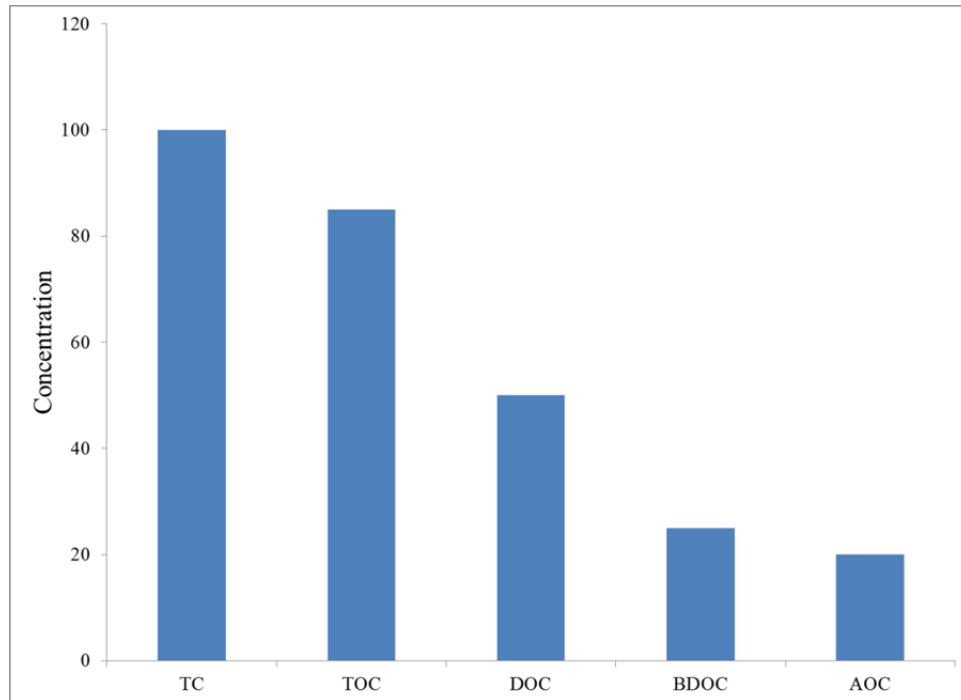


Figure 1-4 Schematic of carbon fractions

1.3 Membrane Fouling

Membrane fouling is defined as the gradual accumulation of contaminants on a membrane surface or within a porous membrane structure that inhibits the passage of water, thus decreasing productivity [20]. It remains the most pressing issue for RO system operation and leads to higher energy use, greater cleaning frequency and a reduction in the lifetime of the membrane. Cleaning fouled membranes begets considerable costs in terms of down time, personnel hours, and chemical costs and disposal. Further, excessive cleaning can damage membranes and decrease their lifespan. The contaminants that lead to membrane fouling include precipitated salts (scaling), the deposition of colloidal organic materials, and bacterial colonization (biofilms) [20].

1.3.1 Scaling

Scaling is the precipitation and/or accumulation of salts that have exceeded their solubility limit in solution and typically occurs with sparingly soluble salts [20, 34, 35]. There are two mechanisms that contribute to the concentration of these solutes exceeding their solubility limit. First, the concentration of solutes increases as the treatment water progresses through the treatment train. Second, the concentration of the salts at the surface of the membrane is higher than in the bulk solution due to a phenomenon known as concentration polarization, Figure 1-5 [5]. This phenomenon occurs when pure water is passed through the membrane and the treatment water immediately on the treatment side of the membrane is inadequately mixed creating a laminar boundary layer. To combat this, modifications in the feed spacer can be made to increase turbulence at the boundary layer. Common materials forming scales include calcium carbonate, calcium

sulfate, and barium sulfate, as well as many more [36-39]. The precipitation of these materials on the membrane surface and within the pores leads to flux decline as well as increase in operational costs [39].

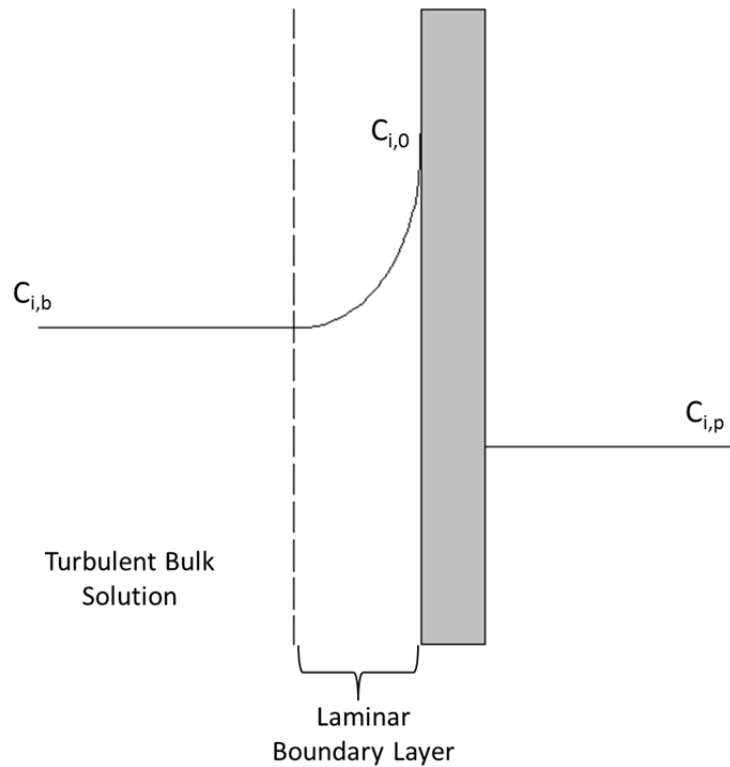


Figure 1-5 Salt concentration gradient at an RO membrane boundary layer, i.e. concentration polarization

1.3.2 Colloidal Fouling

Colloidal Fouling is caused by the deposition of organic materials, namely humic substances, polysaccharides, and proteins on the membrane surface. It can be an important contributing factor to flux decline, especially when treating waters that have high levels of NOM [26, 40, 41].

1.3.3 Biofouling

Organic, colloidal, and to some extent, inorganic fouling can be controlled by limiting their concentrations in solution [42]. However, biofouling is difficult to control due to the ability of microorganisms to survive and multiply on a limited amount of nutrients, including dead bacteria [43]. As bacteria colonize surfaces, they excrete extracellular polymeric substances (EPS) which are composed of polysaccharides, proteins, nucleic acids, and other polymeric materials. This mixture of bacteria and the EPS they secrete is known as biofilms [44, 45]. EPS enhances the structural integrity of biofilms by providing electrostatic interactions, hydrogen bonds, and nonpolar interactions within the matrix. Biofilms act as an ecological habitat for bacteria, condition the membrane surfaces to aid colonization, help shield bacteria from biocides and oxidizing agents, retain water for the bacteria, and are resistant to shear forces [43, 44, 46]. Due to the ability of bacteria to grow and reproduce, biofilms can accumulate rapidly and seemingly suddenly while other types of fouling are typically more gradual [47]. Once attached to a surface, the multiplication of bacteria is a function of the concentration of biodegradable material in the feed-water [47].

Like other types of fouling, biofouling can lead to serious issues, such as loss of permeate flux, increase in pressure and operational costs, and in some instances, biological degradation of the membrane material. The loss of permeate flux attributed to biofouling can be caused by the physical clogging of pores by particulates, allowing less water to pass through; and/or the formation of a layer of EPS causing significant resistance [47]. The resistance increases proportionally to the thickness of the foulant layer, which

increases pumping costs and decreases salt rejection due to concentration polarization [47]. Studies have shown that some membrane surfaces, such as cellulose acetate, are damaged by biofouling [48]. Although no studies have indicated biological degradation of TFC membranes, they contain carbon and nitrogen, so the potential does exist [47].

There are several factors that contribute to membrane fouling, mostly related to the solution chemistry, hydrophobicity of the surfaces, and/or the presence of microorganisms in the treatment water. Studies have shown that the morphology of the membrane surface also contributes to their fouling potential. Namely, the degree of fouling is directly proportional to the degree of roughness of a membrane surface [10]. Membrane surfaces with a higher degree of roughness will have an increased surface area of the membrane, which enables more bacteria to attach. Rough surfaces also immobilize colloids and/or particles, attracting them to the membrane surface. Studies have shown that polyamide membranes generally have a higher degree of roughness than cellulose acetate membranes [10].

1.4 Fouling Diagnosis

If a plant is experiencing problems with membrane performance and fouling, it is advisable to observe the membrane surface to determine the source of the performance issue, thereby enabling better pretreatment design to reduce or eliminate the problem. In order to observe the membrane surface in a spiral wound membrane element, the fiberglass shell must be cut open to reveal the membrane surfaces in a process called a membrane autopsy. During an autopsy, tests are performed on the membrane surface and

on the material deposited on it to ascertain its chemical and/or biological composition. In a survey of 150 membrane autopsies, biofouling was the most frequently observed problem, occurring in approximately 83% of the reverse osmosis plants surveyed [23, 47, 49].

1.5 Pretreatment Methods

To date, much of the research effort has focused on operational fouling mitigation strategies and system design improvements. To this end, efforts have focused on two fronts: improved pretreatment of feed water to minimize fouling propensity, and membrane material and surface modification to combat fouling [50-53]. Common pretreatment methods for RO systems include conventional pretreatment, membrane filtration with microfiltration or ultrafiltration, and biofiltration.

1.5.1 Conventional Pretreatment

Conventional pretreatment for RO systems typically includes an intake, screens for coarse filtration, chemical addition paired with coagulation/flocculation, single or double stage multimedia filtration, and cartridge filtration, Figure 1-6. This type of pretreatment is capable of delivering high quality feed water for RO systems. However, fluctuations in the raw water quality can be detrimental to the system and can lead to increased turbidity, decreased removal efficiency, filter breakthrough, and coagulant on the RO membrane surfaces [54].

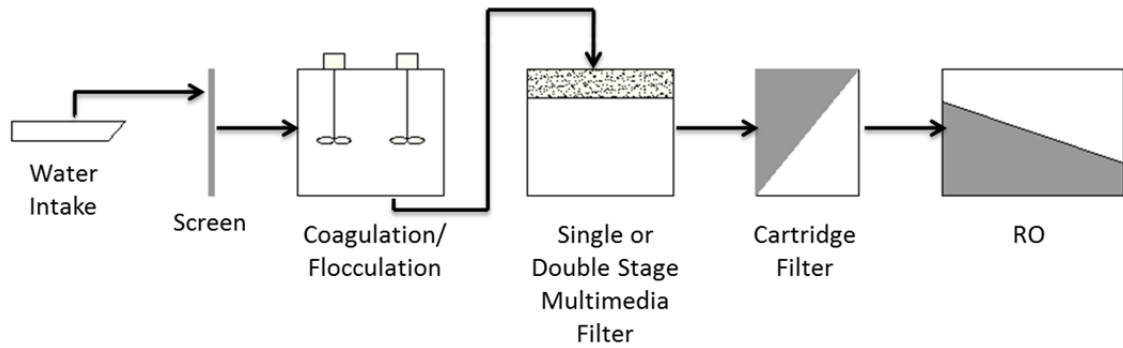


Figure 1-6 Typical Conventional Pretreatment Scheme

1.5.2 Membrane Pretreatment

Alternative pretreatment methods for RO include membrane filtration with microfiltration (MF) or ultrafiltration (UF) filters. These pretreatment methods include an intake and screening, as in conventional pretreatment. However, the other pretreatment steps are replaced with a MF or UF filter step, Figure 1-7. This replacement has a number of advantages, such as the ability to accommodate very high solids, the ability to deliver a consistent RO feed-water flow rate and quality, a significant reduction in the fouling rate of the RO membranes increasing their life expectancy, lower operational and cleaning costs, lower demand for operator control, and overall higher RO flux [50, 54, 55].

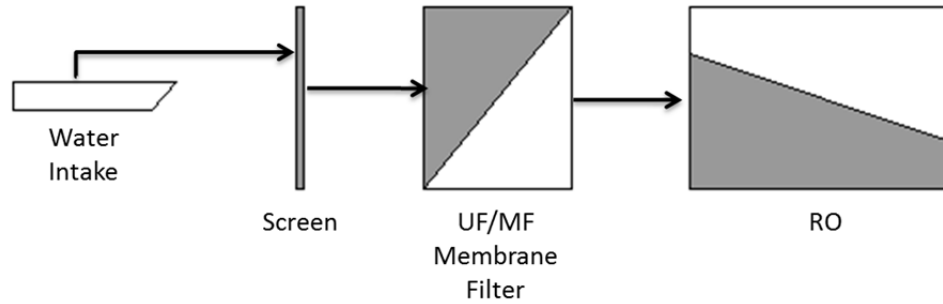


Figure 1-7 Typical Membrane Pretreatment Scheme

1.6 Biofiltration

Traditionally, due to the issues listed above, biofilm formation has been avoided in water treatment systems. The growth of microorganism in a system can lead to several unwanted effects such as odor, presence of pathogens, microbial induced corrosion, blockage of pipes increasing pumping costs, reduction of heat transfer increasing energy costs, etc. Past solutions to microbial growth in these engineered systems have involved disinfection with strong oxidants, such as chlorine or ozone; addition of biocides; or other disinfectants [56]. However, addition of oxidants to waters with high levels of microorganisms can actually lead to an increase in microbial growth by increasing the bioavailability of nutrients in that water [57]. Due to the difficulty in completely negating all microorganisms from the treatment process, and in light of research indicating that the presence of such organisms could actually be useful, interest has grown in the intentional incorporation of biofilms in filters for treatment processes [58-60]. Microbial growth and biofilm formation in engineered systems are topics of growing interest in the fields of water and wastewater treatment, water distribution, water resources, as well as myriad other systems.

Biofilters use microorganisms, and in particular their enzymes and metabolic reactions, to chemically oxidize materials in water (or gas) to inert and/or desirable forms. For example, biofilters are used to remove volatile organic compounds (VOCs), hydrogen sulfide, and other mercaptans from the off-gas of wastewater treatments plant by oxidizing these materials to relatively inert forms [61-63]. This method effectively reduces the odor of the off-gas from the wastewater treatment process. Additionally, biofilters have been used to reduce biofouling in cooling systems and in fish farms [64, 65].

The removal of organic carbon from source waters for drinking water treatment applications is of particular interest. This can be achieved of various methods, including oxidative reaction, biofiltration, and to some extent, conventional treatment methods [19, 66-70]. As stated above, biofilters make use of a fixed film of microorganisms on a surface for the biological oxidative removal contaminants as the treatment water passes over/through the filter, Figure1-8. For drinking water the presence of organic carbon can lead to the formation of disinfection byproducts, colloidal fouling, and biofouling of treatment and distribution systems. The removal of organic carbon from the treatment water by a biofilter causes the treatment water to become nutrient deprived. This phenomenon leads to the formation of a distinct microbial flora in the biofilter that is unique from the treatment water as well as microorganisms found downstream [71].

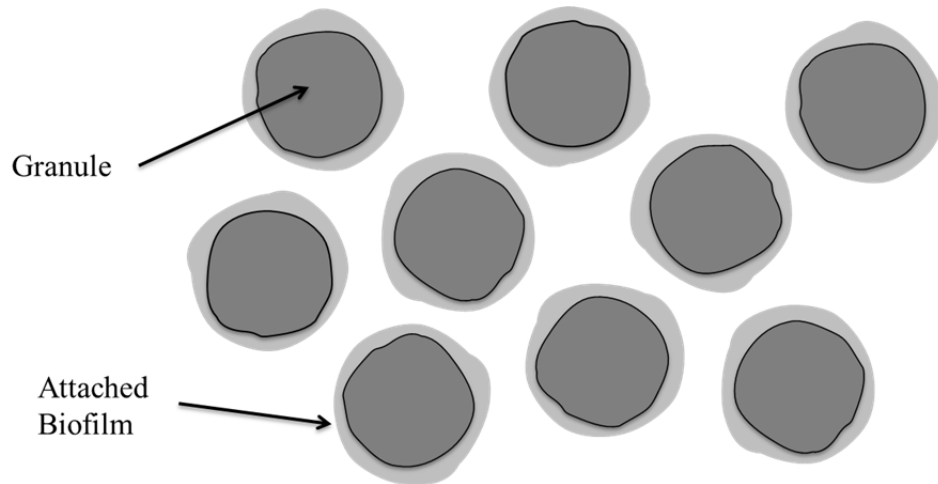


Figure 1-8 Diagram showing biofilm growth on fixed media in a biofilter

Research has shown that there is a correlation between the level of DOC, and more precisely AOC, in a system and the rate of microbial growth [72, 73]. Therefore, the removal of AOC from water is a method of reducing the biofouling potential of treatment waters. It has been widely reported that biological processes are able to effectively remove AOC [74], which has led to the application of biological processes to engineered systems in various forms such as biofiltration.

As stated above, research into the methods traditionally used for potable water treatment has shown that disinfection techniques such as chlorination and ozonation actually lead to increases in the amount of AOC in a system through the degradation and oxidation of more complex organic compounds [64, 74, 75]. The biological stability of water at various stages of treatment were investigated by monitoring the amount and change in AOC [74]. It was determined that granular activated carbon and biological treatment lead to large decreases in the amount of AOC present in the water. However, advanced

oxidation considerably increased the AOC in water. It was therefore concluded that ozonation, if used, should be combined with other treatments such as granular activated carbon or biofiltration. This treatment scheme leads to greatly increased biological stability of the potable water in the water distribution system and greatly decreased levels of AOC in the finished water. Otherwise, the level of AOC would be greatly increased and the biological stability of the water would be greatly decreased, resulting in regrowth in the distribution systems.

Removal of AOC and biodegradable organic matter (BOM) from a water system by biological processes has effects on the bacteriological populations and community structure [76-79]. In one study, a pilot system was used to investigate the effect of biofiltration and pipe material on the amount of biofilm in the distribution pipes and its rate of formation [76]. It was demonstrated that chlorination did not effectively reduce the total number of bacteria in the water, although it did reduce the cultivatable portion and shifted the population of the bacteria present. It was also reported that planktonic bacteria had little effect on biofilm in the systems. The conventionally treated system had higher levels of BOM and a higher rate of biofouling in the distribution system. On the other hand, the system treated with biofiltration had a much lower rate of biofouling in the distribution system. However, it was pointed out that the final level of biofouling was approximately the same for both systems even though the rate of biofouling was drastically different. Another difference that was readily apparent upon investigation was the community structure of the biofilms between the two treatment schemes.

The growth of biofilm in water reuse processes as a function of carbon concentration was explored by analyzing the amount of biofilm formed and its community structure [77]. The biomass and biovolume of the biofilm formed in the secondary effluent without biofiltration were consistently greater than the biomass and biovolume of the biofilm formed when biofiltration was used. It was pointed out that higher carbon concentration conditions are conducive to higher growth rates of microorganisms and hence a higher level of biofilm formation is seen. Differences in the morphology between the biofilms formed under these different conditions were also noted. Biofilms that were formed in low carbon concentrations, i.e. those formed in the system where a biofilter was used generally had a higher porosity and a higher surface to volume ratio than biofilms that were formed in high carbon concentrations. It was proposed that this is an adaptation by the microorganisms present to enable them to acquire more nutrients. When differences in the biofilms were examined using molecular tools, differences in their community structure were observed. It was concluded that biofiltration is an effective method of reducing the mass of biofilm generated; however, this method preferentially selects for organisms that are adapted to thrive in nutrient limiting conditions.

1.6.1 Biofilters for Membrane Pretreatment

Biofiltration has been investigated as a promising pretreatment method for reducing downstream membrane biofouling [80-82]. Typical biofiltration processes utilize attached-growth microorganisms, or biofilms, in a stand-alone step to remove AOC as well as colloidal material which can serve as precursor for fouling. This removal of particulate matter and dissolved nutrients significantly increases effective run time of

membrane filtration processes and extends time between required cleanings. Biofilters traditionally require a separate unit containing the filter media (e.g. sand, granular activated carbon, etc.) with the biofilm growth on the surface of that media, Figure 1-8. This design allows for relatively low pressure units and can accommodate a variety of filter media.

Membrane filtration is susceptible to fouling by various means as described above. In order to reduce the impact of biofouling on membrane filtration processes, biofiltration has been investigated as a possible pretreatment for membrane filtration [53, 81, 83]. In one study, the effect of biofiltration as a pretreatment process for reverse osmosis membrane filtration of drinking water was investigated on a pilot scale [83]. In this study, a reference system with coagulation, sedimentation, rapid sand filtration, and slow sand filtration as a pretreatment regime was used. The test system consisted of the reference system with the addition of ozonation and biofiltration using granular activated carbon. Although only a slight increase in productivity and stability of the test system was observed over the reference system, the chlorine demand for the test system was half that of the reference system. Additionally, the biofouling of the test system was also approximately half that of the reference system.

In another study, biofiltration was investigated as a pretreatment for membrane filtration of waters containing soil-derived humic substances [53]. This was a laboratory scale experiment where a pretreatment scheme consisted of a biological filter that contained biologically active carbon or iron oxide coated sand. The results of this study indicated

that biofiltration was capable of significantly reducing fouling downstream in the membrane filtration process. Using biofiltration as a pretreatment reduced the fouling layer on the membrane by approximately half, and it reduced the cell counts on the membrane surface four to five-fold. Although AOC was not a parameter measured in this experiment, the reduction of AOC by the biofilter can be inferred based on the reduction on bacteria on the membrane surface.

In an additional lab-scale study, a reverse osmosis membrane filtration system was set up at a water reclamation plant to investigate the effect of biofiltration on the filtration performance [81]. A biofilter was used as a pretreatment process to remove AOC from the feed water before it entered the membrane. The results from this study indicate that the biofilters are capable of decreasing the amount of AOC and DOC with a removal efficiency of 40-49% and 35-45% respectively. This removal efficiency translated to an increase of the operation time from 72h without biofiltration to 300h with biofiltration before a significant impact on the membrane performance due to microbial growth was observed. This can easily be translated to a decrease in cleaning requirements, an extended the life of the membrane, and decreased cost overall.

Although a separate biofiltration step is effective for organic carbon reduction and reducing biofouling issues downstream, there are upfront capital expenses, increased monitoring and operation, and additional land requirements for the footprint of the additional pretreatment process. Additionally, for a water treatment plant that is looking

to implement a pretreatment biofiltration step, the minimum required footprint of land must be available on site.

For RO processes, conventional wisdom still dictates that biofouling be eliminated or minimized to the fullest extent possible. While the above approaches are important, a third unexplored approach has the potential to dramatically alter our perception and approach toward fouling control. This approach is an *in situ* biofiltration unit in the membrane skids. This would be comprised of a lead element or lead elements in the membrane skid that contain a biofilm layer, Figure 1-9. This layer would remove AOC from solution, thereby depleting the treatment water of AOC. This would potentially have a protective effect on downstream membrane material by reducing the potential for biofilm formation and extend the time between membrane cleanings.

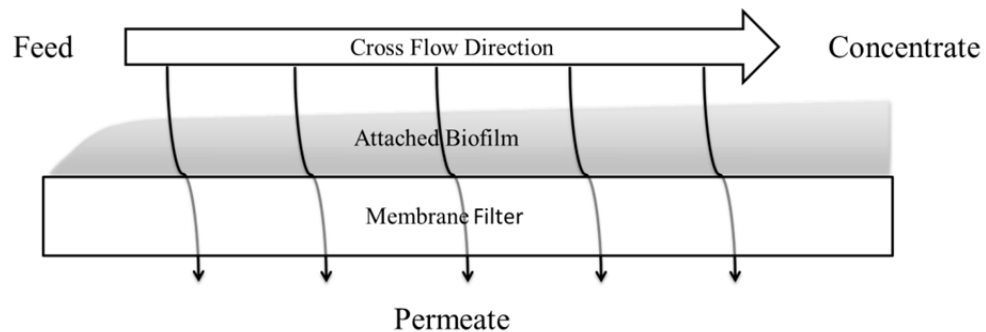


Figure 1-9 Diagram showing biofilm growth on membrane filter surface

It has been shown that fouling is not uniform throughout the treatment train, and there is a general lack of understanding on the spatial variation of fouling with changes in feed-water characteristics [84]. To improve RO system operations, an understanding of how

the microbial and chemical ecology of the feed-water and membrane foulants changes from the beginning to the end of the treatment train is needed.

1.7 Research Objectives

The goals of this research include developing a better understanding of the fouling profile throughout a membrane treatment system and developing a better understanding of the role of the biofilm present on the membrane surfaces on the reduction of organic carbon in the system. The objectives under these goals are:

- to characterize the quantity and chemical and microbial composition of the foulant layer throughout a membrane treatment plant using available analytical tools and microbiology methods
- to determine if there is a net removal of organic carbon in a RO treatment system
- to test whether the microorganisms in the foulant layer are responsible for removing organic carbon from the feed water
- to determine the extent to which *in situ* biofiltration protects downstream membranes
- To test the effects of carbon loading rate on biofilm formation and the protective effect of the biofilm on the downstream membrane performance and biofilm growth

1.7.1 Experimental Phases

To achieve the objectives listed above, the research presented here was broken into specific phases.

1.7.1.1 Phase I: Literature Investigation and Equipment Setup

A background literature investigation on related topics and studies was performed and lead to the equipment setup and experimental designs as well as the background information presented in this dissertation.

1.7.1.2 Phase II: Membrane Autopsies at Three Points of Skid

An autopsy was performed in 2006 under the guidance and with the cooperation of the scientists at Orange County Water District in Orange County California. This autopsy was performed to ascertain the types and patterns of fouling present on the membrane surfaces. Three additional membrane autopsies were performed on the lead element of the first stage, the lead element of the second stage, and the tail element of the second stage. This beginning, middle, end approach of autopsy analysis is unique in that it gives an overall picture of the fouling profile within the treatment plant.

1.7.1.3 Phase III: Plant Analysis of Carbon Mass Balance

It is believed that the biofilm is responsible for the removal of organic carbon from the treatment water, thereby making the treatment water nutrient deprived. In order to test this hypothesis, a carbon mass balance was performed on the Dunedin water treatment plant and on individual skids of the treatment plant. If carbon is indeed being removed from the treatment water, this finding would support the hypothesis that the biofilm is responsible its removal.

1.7.1.4 Phase IV: Flat Sheet Module Pilot Testing with Fouled Membrane Element

The information gathered in Phase II was used to set the experimental conditions for the pilot testing. During Phase III, a lead element with the foulant layer already present was taken from the skid simultaneous to the autopsy. This element was placed into a pilot system with eight flat sheet modules (four on the feed portion and four on the concentrate portion). The pilot was designed to operate under plant conditions and monitor the effect of flow rate and carbon loading on membrane fouling and performance before and after the membrane element. This phase was aimed to confirm the biofilm's responsibility for a protective effect of fouling and performance of downstream membrane material.

The results of this research have implications for using biofilm on membrane surfaces as an *in situ* biofilter to protect downstream membrane material. This research was carried out at the Dunedin RO water treatment plant with the full cooperation of the City of Dunedin, FL.

Chapter 2 Background

2.1 Dunedin Reverse Osmosis Water Treatment Plant

Located on the central west coast of Florida on the Gulf of Mexico, the City of Dunedin has a population of approximately 37,000 residents and an area of approximately 10 sq. mi. Due to complaints of hardness and rust discoloration from the tap water, in the late 1980's the city researched options for eliminating these issues. The options investigated included lime softening and membrane softening. The option chosen was membrane softening, and the city currently owns and operates a reverse osmosis water softening plant (9.5 MGD design capacity, 3.2 MGD typical flow) that draws groundwater from the Floridan aquifer which began operation in 1992.

2.1.1 Dunedin Pretreatment Process

The city of Dunedin owns and operates a well field with 26 wells at locations throughout the city. The well operation is alternated to avoid over pumping at any given location. The water drawn from this well field is pumped to the Dunedin water treatment plant to undergo the treatment process. Prior to filtration through the reverse osmosis membranes, the water is subjected to a pretreatment process. The plant pre-chlorinates the raw water as it is entering the plant to oxidize sulfides and iron, extend the life of the green sand filters, and reduce the KMnO_4 addition. After pre-chlorination, KMnO_4 is added to the water at a 3 ppm dosage to oxidize iron, sulfides and help regenerate the

oxidative surface of the green sand (next step of pretreatment process). The water is then passed through five mixed-media pressurized horizontal multimedia filter units (10.2 MGD total capacity). A cross-section of one of these filter units shows the composition of the various layers, Figure 2-1. The base of the filter unit is a 21.5" layer of concrete, upon which a layer of support gravel rests. Additionally, a 16" under-drain header lies between the two layers. The support gravel consists of four separate layers itself: the base layer is 8" thick and contains 1.5" x 3/4" gravel; the next layer is 4" thick and contains 1/2" x 1/4" gravel; the top layer is 4" thick and contains 1/4" x 1/8" gravel; and the top layer is 4" thick and contains 0.5" x 3/4" gravel. A 6" layer of #6 x #9 silica gravel rests on the support gravel. The next layer is a 15" layer of manganese green sand. The top layer of the filter unit is a 30" layer of anthracite. The filter unit itself has a 12' diameter, is 31' long, and has a 16" inlet. The manganese green sand portion of the filters has an oxidizing surface and oxidizes the soluble ferrous ion (Fe^{2+}) to the insoluble ferric ion (Fe^{3+}), which precipitates and is subsequently removed. Additionally, the $KMnO_4$ added to the water is absorbed by this layer reactivating the oxidative properties of its surface. Thus, it is removed from the treatment water.

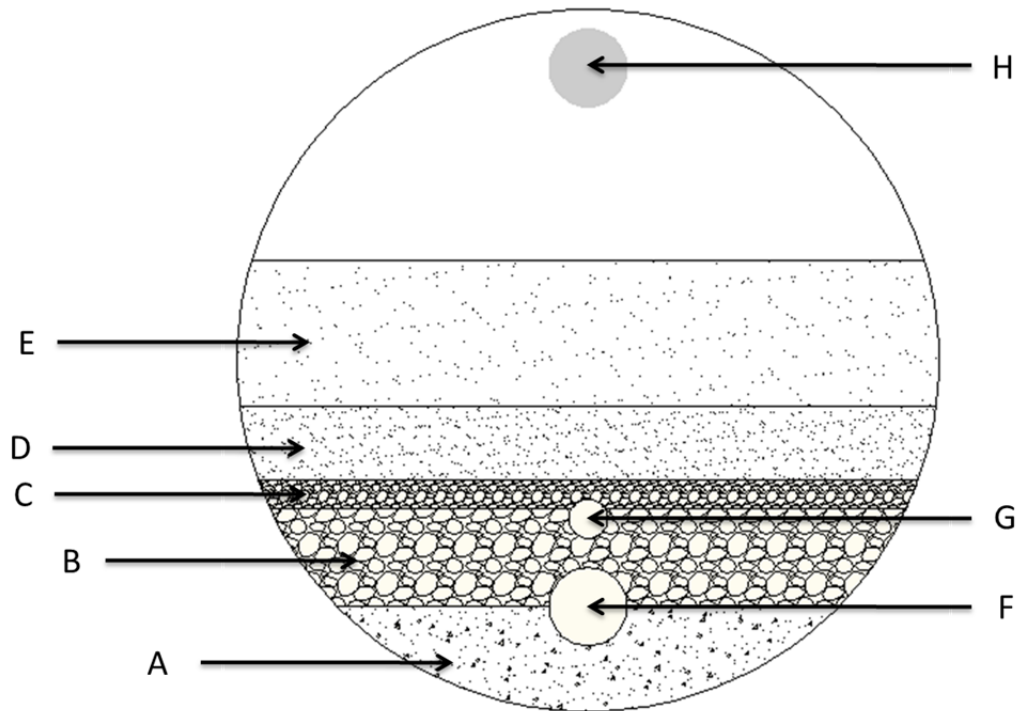


Figure 2-1 Cross section of a horizontal green sand filter unit: A) 21.5" concrete base, B) 20" support gravel, C) 6" silica gravel, D) 15" manganese green sand, E) 30" Anthracite, F) 16" underdrain header, G) air scour header, and H) 16" inlet

After green sand filtration, the water is passed through seven cartridge filtration units containing 5 μm polypropylene cartridge filters to remove particulate matter not removed in the green sand filters. A proprietary antiscalant purchased from American Water Chemicals, Inc. is added to the filtrate from four of the cartridge filter units, after which, high pressure pumps pressurize the water to 100-120 psig for the membrane filtration skids. The effluent from three cartridge filter units bypasses further treatment for subsequent blending with permeate water from the membrane treatment train.

2.1.2 Dunedin Reverse Osmosis Process

The plant has four reverse osmosis skids, each composed of two stages arranged in the concentrate staging configuration. The first stage contains twenty six pressure vessels, the concentrate streams from which feeds thirteen pressure vessels in the second stage, Figure 2-2. Each pressure vessel contains seven 8½” x 40” membrane elements containing 400 ft² (37.2 m²) of polyamide thin-film composite TFC 9921-S (Koch Membrane Systems, Inc.) with 31 mil (0.79 mm) feed spacer. Due to the high purity and aggressive nature of the permeate water, the plant’s finish water is an approximate blend of 80% permeate with 20% water from the three cartridge filter units bypassing further treatment and the membrane softening stage. A schematic of the treatment process is available in Appendix A.

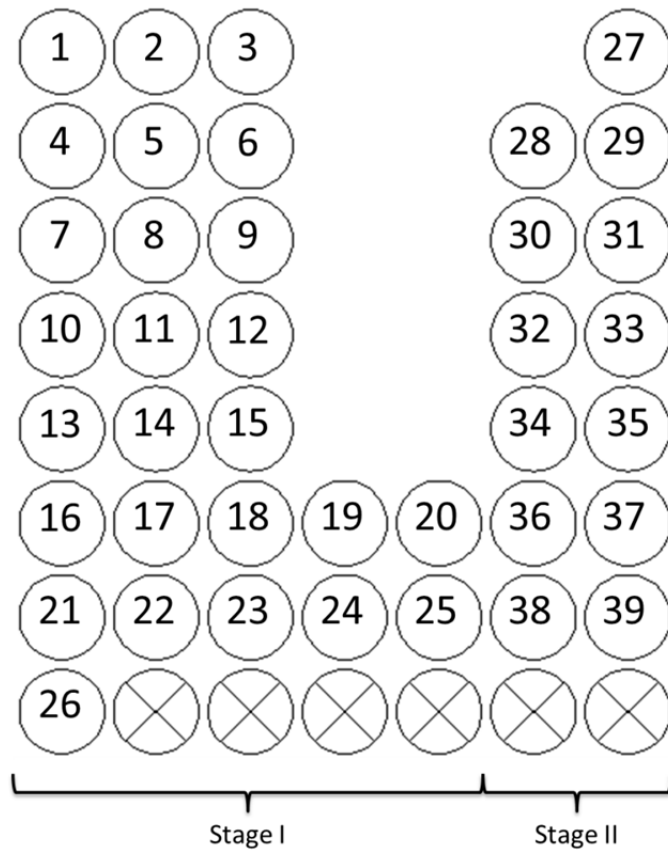


Figure 2-2 Product side of skid detailing the numbering convention for pressure vessels

Historically, the Dunedin water treatment plant has experienced problems with fouling of their reverse osmosis membranes, leading to frequent cleanings. Prior plant evaluations and membrane autopsies have indicated the fouling problems at the Dunedin water plant originate from biofouling [85, 86].

Chapter 3 Materials and Methods

3.1 Experimental Objectives

The overall research objectives of this project are delineated in Chapter 1. In order to reach these objectives, the project was divided into phases. The experimental designs and analytical methods described in this chapter were implemented and/or developed to carry out these experimental phases, and ultimately meet the research objectives.

3.2 Design of Experiments

There are several possible parameters that have an effect on the results of experimentation. In order to better understand the results and provide more appropriate insight to the questions raised, the effect of the following variables on the formation of the biofilm were explored:

- Operational conditions (cross flow velocity, trans-membrane pressure)
- Feed water characteristics (oxidation/reduction potential, pH, dissolved oxygen, TC/TN, UV₂₅₄ absorption)
- membrane surface properties (roughness)

The above variables were tested and/or monitored during specified research phases. The Plant level evaluation of carbon mass balance required the analysis of organic carbon and nitrogen concentration and carbon character (UV₂₅₄ absorption), Chapter 6. The Pilot

system evaluation of the effect of biofilm on downstream membranes required more intensive evaluation of operational conditions, characteristics of the water streams, and membrane surface properties, Chapter 7.

3.3 Experimental Protocols and Analytical Methods

This section delineates the details of the procedures used to collect data for further analysis in this research.

3.3.1 Carbohydrate Assay

The carbohydrate assay is designed to quantify the amount of carbohydrates in a sample. It was originally designed for the analysis of carbohydrates in seawater, but has been adapted for the analysis of carbohydrates in water samples and on membrane surfaces [87-89]. To apply this method to biofilms on membrane surfaces, the biofilm must first be removed by sonicating a measured area in deionized water for 10 minutes (additional sonication times of 5 minutes may be added if biofilm is not completely removed from the surface). The reagents required are a phenol reagent and a sulfuric acid reagent. The phenol reagent is 5% wt/V phenol/deionized water. This reagent can be prepared by dissolving a 25g aliquot of ultra-pure phenol in 500mL deionized water (can be scaled up or down according to amount required/ number of samples). The phenol reagent is stored in an all-glass container that will prevent exposure to light. The sulfuric acid reagent is 0.5% wt/V hydrazine sulfate/sulfuric acid. This reagent is prepared by dissolving 2.5g of hydrazine sulfate in 500mL concentrated sulfuric acid (can be scaled up or down according to amount required/ number of samples).

Large test tubes (e.g. 100x15mm) with loose fitting caps are used for this reaction. A 0.5mL aliquot of each sample is added to separate test tubes (triplicates should be run if sample volume allows). Next, a 0.5mL aliquot of the Phenol Reagent is added to each sample. In a fume hood, a 2.5mL aliquot of the Sulfuric Acid Reagent is rapidly added to the sample from a pipette while vortex mixing. A pipette pump that will allow complete rapid delivery of sulfuric acid reagent should be used, taking care not to break the tube with the pipette tip. The sulfuric acid reagent generates excessive amounts of heat so care should be taken with the acid addition. The tubes are then covered with aluminum foil and allowed to cool at room temperature in a dark place for one hour (color is stable for 24 hours). Prior to measuring optical density, the samples should be vortex mixed due to some heterogeneity of the sample (allow sample to sit to remove bubbles). The optical density of the samples are measured at 490nm using a UV-VIS spectrophotometer.

In order to calculate the carbohydrate concentration of the prepared samples, a calibration curve must be generated. This is done by preparing a 100 mg/L stock solution of dextrose (glucose) by dissolving 0.1g dextrose in 1000mL deionized water. Dilutions of the stock solution are performed as per Table 3-1. The calibration samples are run using the same method as delineated above. Micro-pipettors are used to make the dilutions, and polystyrene cuvettes are used to measure absorption spectra. Calibration samples are run in triplicate to ensure reproducibility of the data.

Table 3-1 Typical dilution series for carbohydrate calibration curve

mg/mL Concentration Sugars (Dextrose)	μ L Dextrose Stock Solution	μ L DI Water
100	500	0
70	350	150
50	250	250
30	150	350
10	50	450
0	0	500

An example of the samples generated from calibration are shown in order of most concentrated to least concentrated from left to right respectively in Figure 3-1.

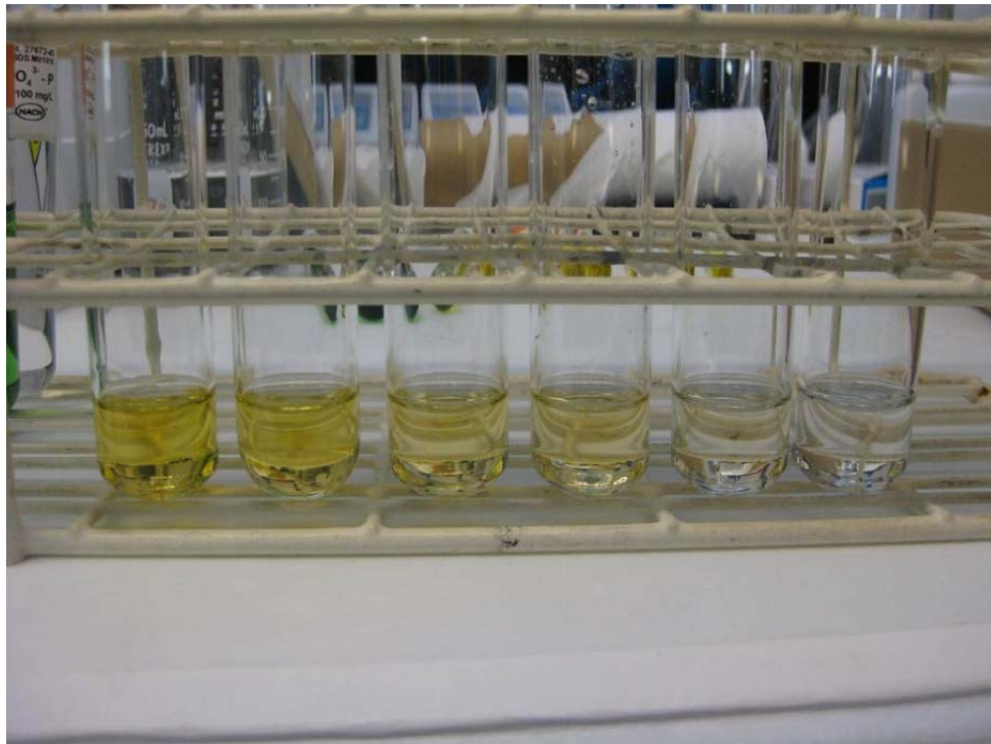


Figure 3-1 Dilution series from calibration curve from most concentrated to least concentrated, left to right

3.3.2 Total Direct Count

The purpose of the total direct count is to measure the total microorganisms present per unit area of membrane surface (mass may also be used). The method presented here is modified from Standard Methods [90]. In order to complete this analysis, the biofilm must first be removed from the membrane surface. A phosphate buffer is used to remove the biofilm and is prepared by dissolving 6.8 g potassium phosphate monobasic and 50 mg of sodium pyruvate in 500mL deionized water and adjusted to pH 7 with potassium phosphate dibasic. The solution is prepared in a 1000mL autoclavable bottle and sterilized by autoclaving at 121°C for 30 minutes. In order to visualize the microorganisms, they are treated with the fluorescent stain 4',6-diamidino-2-phenylindole (DAPI) prior to excitation at 350 nm with an epifluorescent microscope. A stock solution of DAPI is prepared by dissolving 10mg in 10mL ultrapure water. A working stock is then prepared by diluting 100µL of the stock to 1000µL with ultrapure water.

A measured area of membrane sample is placed into a 20mL scintillation vial and 10mL phosphate buffer is added. The sample is then sonicated for 10 minutes (additional sonication times of 5 minutes may be added if biofilm is not completely removed from the surface). A 5mL aliquot of the resulting suspension is placed into a vial, ensuring to vortex mix prior to removal of any sample, and a 5µL aliquot of DAPI working stock is added to vial with sample and vortex mixed. The sample is allowed to sit in dark for approximately 5 minutes. A 10^{-1} dilution of the sample is prepared by diluting 1mL sample to 10mL with phosphate buffer and vortex mixed. A 1mL aliquot of the 10^{-1} sample is filtered through a 0.2µm polycarbonate filter disk and washed with an

additional 2mL phosphate buffer. A black filter disk can be used to reduce the fluorescent background for analysis. The filter disk is mounted on a microscope slide by immersing in a 10%PBS/glycerin solution and covered with a cover slip. Additional and/or different dilutions may be prepared as needed.

The samples were taken to FCoE-BITT and visualized with a Leica DM2000 compound microscope with bright field and fluorescence (with EL6000 external light source); 5/10/20/40X, 100X long working distance (dry), 100X (oil) objectives, Figure 3-2. The 100x oil objective was used for image capture and analysis. A Canon 35 mm digital camera (8 megapixel; Powershot S5 IS, with Martin Microscope MM99 adapter) was C-mounted to the microscope for image capture. ImageJ 1.43u software was used for the numerical determination.



Figure 3-2 Microscope setup in FCoE-BITT used for total direct count

3.3.3 Fourier-Transform Infrared Spectroscopy (FTIR)

The Fourier Transform Infrared Spectroscopy (FTIR) is a useful tool for measuring the vibrational modes of compounds and their functional groups. These data give chemical information on the material being analyzed. For membrane material, it can give bonding information of the polymer and give evidence on whether the material is being degraded. Additionally, it will also yield information on the material that is adsorbed to the surface of the membrane, i.e. membrane foulants [91]. The instrument used in this study is a Bio-Rad Excalibur Series Model FTS-3000 fitted with a Pike MLRacle diamond press attenuated total reflectance (ATR) attachment, Figure 3-3. The range of data collection is $4000-400\text{ cm}^{-1}$ with a resolution of 4 cm^{-1} and a total of 256 scans. Triplicate spectra were captured for each sample.

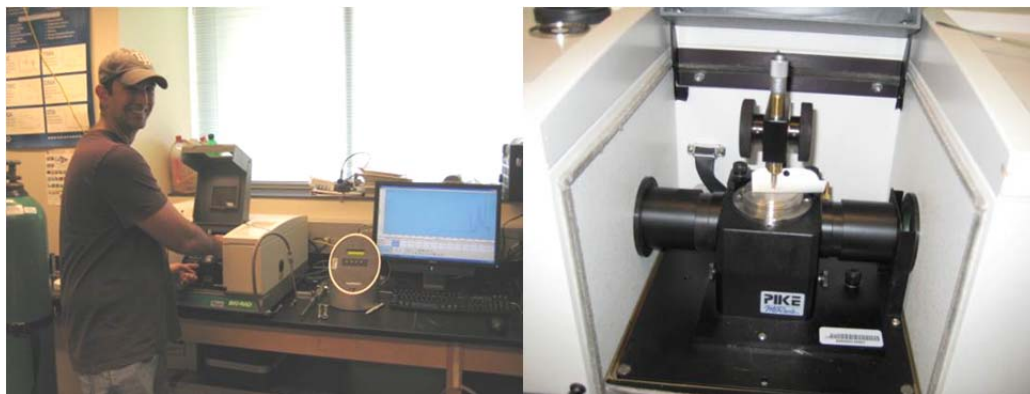


Figure 3-3 Russell Ferlita loading sample in FTIR (left) and sample in ATR-FTIR (right)

3.3.4 Heterotrophic Plate Count

The purpose of the heterotrophic plate count is to measure the total number of viable heterotrophic microorganisms present per unit area (mass may also be used) of membrane surface. R2A agar plates are used to plate the bacteria for counting. This media is

designed for heterotrophic microorganisms in drinking water applications [90]. A volume of 700mL R2A agar suspension is prepared in a 1000mL autoclavable bottle as per manufacturer's specifications. The suspension is dissolved by heating in an autoclave at 121°C for 20 minutes, allowed to cool to approximately 70°C, and mixed thoroughly. The agar is then sterilized by autoclaving at 121°C for 30 minutes and allowed to cool to 50-70°C. A volume of approximately 25-30mL agar solution is poured in each sterile petri dish (volume prepared should be enough to prepare an entire sleeve of 25). Bubbles are commonly formed when pouring agar plates and can be mistaken for colonies during analysis. To remove the bubbles, a flame is quickly passed over the hot agar pre-solidification using a torch. The petri dishes are covered to prevent contamination and allowed to cool and solidify. Excess condensate can be removed from the tops of the petri dishes by quickly removing the top, tapping it on the counter, and flicking moisture off. This should be performed in such a way as to prevent contamination of the agar (i.e. in hood under UV light). Excess petri dishes can be stored in a refrigerator.

A Phosphate Buffer is used to remove the biofilm from the membrane surface and is prepared by dissolving 6.8 g potassium phosphate monobasic and 50 mg of sodium pyruvate in 500mL deionized water and adjusted to pH 7 with potassium phosphate dibasic. The solution is prepared in a 1000mL autoclavable bottle and sterilized by autoclaving at 121°C for 30 minutes.

In order to remove the microorganisms from the membrane surface for analysis, a measured area of membrane sample is placed into a 20mL scintillation vial with 10mL

phosphate buffer solution and sonicated for 10 minutes (additional sonication times of 5 minutes may be added if biofilm is not completely removed from the surface). The sample is vortex mixed prior to removal of any sample. The suspension is diluted to obtain solutions with countable numbers of microorganisms. The following is an example of dilutions used for analysis: A 10 μ L aliquot of sample is diluted to 10mL with phosphate buffer to obtain a solution that is a 10⁻³ dilution. A 1000 μ L aliquot of the resulting solution is diluted to 10mL with phosphate buffer to obtain a solution that is a 10⁻⁴ dilution. A 1000 μ L aliquot of the resulting solution is diluted to 10mL with phosphate buffer to obtain a solution that is a 10⁻⁵ dilution.

The dilutions prepared above are plated on the R2A agar plates prepared above to achieve countable levels of microorganisms from the membrane surface. A 10 μ L aliquot of the 10⁻³ dilution solution is placed on a R2A agar plate, spreading the sample throughout using an L-shaped glass rod and a Lazy Suzan resulting in a 10⁻⁵ dilution. The L-shaped rod is dipped in ethanol and flame sterilized prior to spreading each plate. A 10 μ L aliquot of the 10⁻⁴ dilution solution is placed on a R2A agar plate, spreading the sample using an L-shaped glass rod and a Lazy Suzan resulting in a 10⁻⁶ dilution. A 10 μ L aliquot of the 10⁻⁵ dilution solution is placed on a R2A agar plate, spreading the sample with an L-shaped glass rod and a Lazy Suzan resulting in a 10⁻⁷ dilution. The above dilutions and plating is an example of an actual analysis and additional and/or different dilutions may be prepared as needed. An example of an agar plate with countable colonies is in Figure 3-4.



Figure 3-4 R2A agar plate with countable microbial colonies

3.3.5 Protein Assay

The Lowry Protein Assay is designed to quantify the amount of proteins in a sample. It has a wide spectrum of applicability, such as bulk tissue samples, enzyme digestion, and antigen-antibody precipitates. The method has been adapted for the analysis of proteins in water samples and on membrane surfaces [88, 89, 92]. To apply this method to biofilms on membrane surfaces, the biofilm must first be removed by sonicating a measured area in deionized water for 10 minutes (additional sonication times of 5 minutes may be added if the biofilm is not completely removed from the surface).

Five reagents are required for the Lowry Protein Assay. Reagent A is a 4% Sodium Carbonate in 0.2N Sodium Hydroxide solution and is prepared by first dissolving 0.8g NaOH in 100mL water, then dissolving 4.0g Na_2CO_3 in 96mL NaOH solution. Reagent B is a 2% Copper Sulfate solution and is prepared by dissolving 0.5g CuSO_4 in 24.5mL deionized water. Reagent C is a 4% Sodium Tartrate solution. It is prepared by

dissolving 2.0g Sodium Tartrate in 48mL deionized water (potassium tartrate may also be used). Reagent D is prepared by mixing Reagents A, B, and C in a 100:1:1 ratio. Reagent E is a 1:1 mixture of Folin's Reagent and deionized water. The volumes of reagents can be scaled up or down according to amount required/ number of samples to be analyzed.

Small vials, such as 20mL scintillation vials, are used to complete the reaction. A 2.0mL aliquot of sample is added to individual vials, and a 2.0mL aliquot of Reagent D is added to each sample (triplicates should be run if sample volume allows). The mixture is vortex mixed and allowed to sit capped and covered for 10 minutes. A 0.4mL aliquot of Reagent E is added to each mixture, vortex mixed, and allowed to sit capped and covered for 30 minutes. The optical density of the samples is measured at 550nm using a UV-VIS spectrophotometer.

In order to calculate the protein concentration of the prepared samples, a calibration curve must be generated. This is done by preparing a 100 mg/L stock solution of Bovine Serum Albumin (BSA) by dissolving 0.1g BSA in 1000mL deionized water. Dilutions of the stock solution are performed using micro-pipettors as per Table 3-2. A new pipette tip should be used for each aliquot to prevent cross contamination and due to the soapy nature of the BSA solution. The calibration samples are run using the same method as delineated above. Cuvettes are used to measure absorption of the samples. Calibration samples are run in triplicate to ensure reproducibility of the data.

Table 3-2 Typical dilution series for protein calibration curve

mg/L Concentration Protein (BSA)	mL BSA Stock Solution	mL DI Water
100	10.0	0.0
75	7.5	2.5
50	5.0	5.0
25	2.5	7.5
10	1.0	9.0
0	0.0	10.00

An example of the samples from calibration are shown in order of most concentrated to least concentrated from left to right respectively in Figure 3-5.

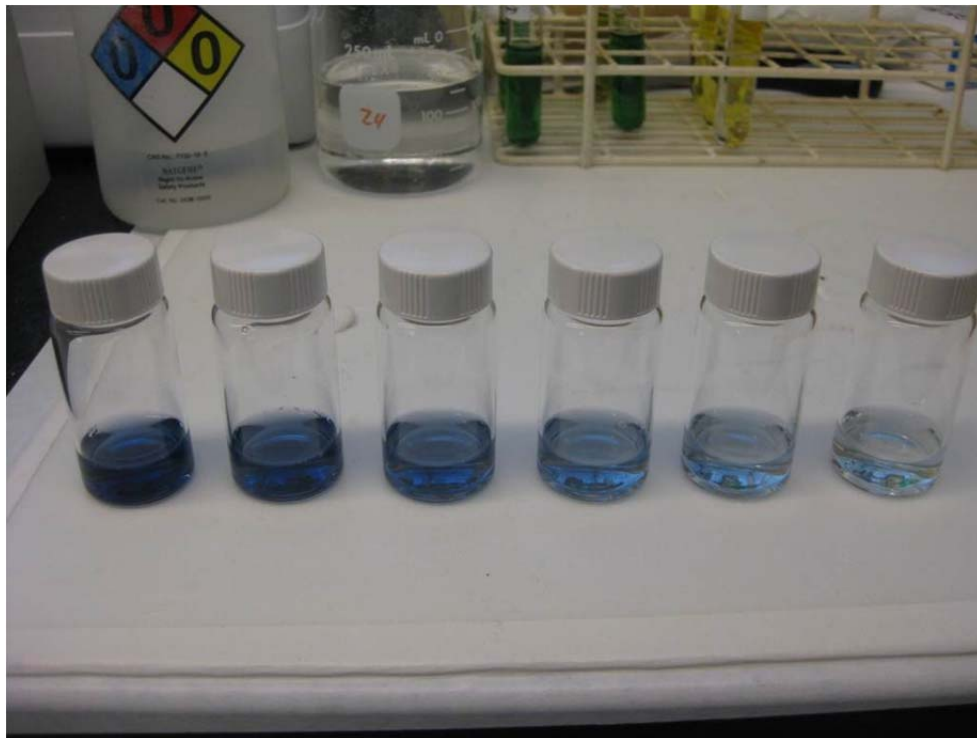


Figure 3-5 Dilution series from a protein calibration curve from most concentrated to least concentrated, left to right

3.3.6 Total Dry Mass

The total dry mass of material deposited on the membrane surface throughout the membrane elements is analyzed by scraping the fouled material from a measured area of the membrane surface with a straight razor. The scrapings are placed into a pre-weighed weighing dish, then heating it at 105°C overnight before re-weighing. Triplicates should be run to ensure reproducibility of the data.

3.3.7 Total Organic Carbon/Total Nitrogen Analysis

The concentration of total organic carbon and nitrogen are analyzed using a total organic carbon analyzer. The samples were prepared by adding 1mL 2N HCl to 49mL sample to acidify and mixed. The samples are sparged with ultrazero grade air (Air Gas) in the instrument for 90 seconds, which removes volatile compounds and the carbonates as carbon dioxide (due to acidification). Acidification may also be performed in the instrument automatically negating the need to pre-acidify the samples. The concentrations of non-purgable organic carbon (NPOC) and total nitrogen (TN) were then measured in triplicate using a Shimadzu TOC-V TOC analyzer fitted with an auto-sampler (ASI-V) (Shimadzu Scientific Instruments, Columbia, MD). The results from the instrument are analyzed against a calibration curve prepared from potassium hydrogen phthalate and potassium nitrate for determining carbon and nitrogen concentrations respectively.

3.3.8 UV₂₅₄ Absorption

The UV absorbance of the samples was measured at 254 nm in quartz cuvettes using a Hach UV/4000U UV/vis laboratory spectrophotometer (Hach Company, Loveland, CO).

3.3.9 Specific UV Absorbance (SUVA)

The specific UV absorbance (SUVA) of each sample was calculated by dividing the UV absorbance at 254 nm (section 3.3.8) by the NPOC concentration (section 3.3.7) using Equation 3.1.

$$SUVA = \frac{UV_{254nm}}{NPOC} \quad (3.1)$$

3.3.10 Microscopic Evaluation

Qualitative analyses of the membrane surface, cross-section, and foulants were performed using scanning electron microscopy (SEM) with energy dispersive spectroscopy (EDS). The electron microscope used was a Hitachi S-800 field emission high vacuum electron microscope fitted with an EDAX energy dispersive spectroscope (EDS). The SEM was used for visual analysis while EDS was used for elemental analysis. Cross sections of membrane material were also prepared for analysis by SEM and EDS using the cryosnap method, chapter 4 [93, 94].

A Digital Instruments Dimension 3100 Atomic Force Microscope (AFM) was used for surface visualization and qualitative analysis of clean and fouled membranes. This instrument was also used for quantitative measurements of the surface roughness of clean

and fouled membrane samples. Roughness values were measured as root mean squared (RMS) roughness and average (Ra) roughness.

Chapter 4 Cryo-Snap: A Simple Modified Freeze-Fracture Method for SEM Imaging of Membrane Cross-Sections

4.1 Introduction

Modern commercial water purification technologies heavily rely on the use of membranes for removal of contaminants. Microscale and nanoscale suspended matter is removed using microfiltration (MF) or ultrafiltration (UF), while large organic molecules and divalent mineral cations removed using nanofiltration membranes (NF). Reverse osmosis (RO) membranes are used to remove monovalent cations. Membrane fouling, the gradual accumulation of contaminants on a membrane surface or within a porous membrane structure that inhibits the passage of water, is an issue of great concern during membrane operations. Contaminants that lead to membrane fouling include precipitated salts (scaling), bacterial colonization (biofouling), and deposited organic materials (colloidal fouling). Fouling leads to higher energy use, greater cleaning frequency and a reduction of membrane lifetime which decreases overall productivity [95]. Many researchers have focused on improving membrane materials, surface properties, and system manipulation to manage or mitigate fouling [96-98]. A detailed understanding of the interaction between membranes and foulants is essential to improve membrane efficiency and design. There has also been much work in understanding the various types of fouling through detailed characterization of foulants [99-106]. The exact location and spatial relationships of the various types of foulants to each other and to the membrane is

crucial to appropriately diagnose fouling problems. Much of this information can be obtained if an appropriate cross-section of the membrane material is examined using scanning electron microscopy (SEM). If the sample is carefully prepared, the cross-sectional view can offer much information in terms of the micro- and nano-scale internal structures of the membrane, as well as the spatial relationship of foulants with respect to the membrane.

Membranes used for water purification may be isotropic (a single matrix) or anisotropic (a composite of polymer layers), and may be applied to a support backing. In the latter case, the dissimilarity in material properties and mechanical strengths of the layers can lead to differential deformation when a shearing force is applied, thereby distorting the structure. Polymers used for membranes may be relatively elastic and thus resist sharp force cleavage. Mechanical cuts using sharp force devices (razor blades or knives) create compression, tearing and localized heating which can severely distort the fine structures of the membrane. Relatively clean cross-sections may be obtained using special equipment such as a focused ion beam or an ultramicrotome [107, 108]; however, these methods require laborious sample preparation and expensive equipment. A commonly used approach is the direct freeze fracture method, where the membrane sample is frozen in liquid nitrogen to make it brittle and quickly broken [105]. In many cases, the resulting fracture plane can be very uneven, yielding poor results. Furthermore, some membrane polymers such as polypropylene are difficult to fracture because they do not become sufficiently brittle even when submerged in liquid nitrogen. Finally, the direct freeze fracture method is difficult to apply to membranes with a support backing such as

reverse osmosis membranes. In these instances, the membrane merely bends or rips, but does not cleave cleanly. Because the method is unable to break the tough RO membrane backing, some researchers have suggested manual removal of the backing prior to freeze fracture. Such excessive manipulation invariably distorts the membrane and likely significantly modifies or damages the foulant layer.

Biologists have employed a variation of the freeze fracture method for the preparation of biological samples and cellular membranes for cross-sectional analyses in which the sample is first embedded in a medium which is subsequently frozen and fractured with a sharp knife. A replica preserving nanoscopic detail is then made from the frozen surface which is examined by SEM [109]. Though producing clean cross-sections that preserve sample detail, this procedure is rather lengthy and requires special equipment for sample preparation. Since membrane materials are typically more dimensionally stable than individual cell membranes, we investigated a more simplified approach by dispensing with replica manufacture and directly preparing the cleaved membrane surface for SEM observation. Here, we present a modified freeze fracture approach (termed *Cryo-snap*), for production of membrane cross-sections. This method involves embedding the membrane sample in a liquid medium (water) contained in a glass tube, cryogenically freezing the medium, then cleaving the sample by manually breaking the tube and frozen cylinder of embedding medium. Following removal of the medium by vacuum sublimation, the cleaved membrane surface is prepared for examination by SEM. The method was tested on a variety of membrane types of both isotropic compositions (polypropylene hollow fibre MF) and anisotropic compositions (thin film composite RO

membranes) with materials of dissimilar mechanical properties. The effect of hydration on cleavage of a hollow fibre MF membrane was also investigated.

4.2 Experimental

4.2.1 Materials and Sample Preparation

Three membrane types were used for this study: 1) an uncoated PVDF UF membrane prepared by Membrane Technologies Research, Inc. (Menlo Park, CA); 2) a Koch TFC 9921-S thin film composite polyamide RO membrane (Koch Membrane Systems, Inc., Wilmington, Massachusetts); and 3) a Siemens CMF-S 0.2um polypropylene hollow fiber MF membrane (Siemens Water Technologies, Warrendale, PA). Membrane samples that were expected to have biological material present (biofoulants) were fixed with a 2.5% glutaraldehyde solution to prevent distortion of the biological sample and loss of information [109]. In the case of microporous membrane materials, we also examined the impact of pore hydration on the quality of the membrane cross-section. Pore spaces of virgin MF hollow fiber membrane material were fully hydrated by pulling ethanol through to the fiber lumen, followed by water, using syringe and needle.

4.2.1.1 Razor Sectioning

Samples of membrane materials obtained from bulk flat sheets or from fibers were manually cross-sectioned using a clean, sharp razor blade, and the edge of the cut section was directly examined perpendicular to the cut plane by SEM.

4.2.1.2 Direct Freeze Fracture

A small membrane sample was submerged in liquid nitrogen for approximately 5 minutes to ensure it was completely frozen. It was then removed from the liquid nitrogen and immediately snapped with two pairs of tweezers. The cleaved sample was dried under vacuum to remove any excess ice and water from the freeze fracture process, and the cleaved edge examined perpendicular to the cut plane by SEM.

4.2.1.3 Cryo-Snap

For flat sheet membrane materials, a thin sample strip (maximum dimensions 6mm x 50mm) was obtained at the location of interest using a sharp razor blade or scissors. Hollow fiber membrane samples were cut to length (maximum of 50mm) from bulk fiber in a similar fashion. The sample was submerged in an aqueous medium in a glass tube (6 x 50 mm Fisher brand flint glass test tube) previously scored using a carbide knife or glass file to permit easy manual fracturing. The tube was slowly submerged in liquid nitrogen over approximately a one minute period (freezing the sample too quickly tends to cause premature fracturing of the tube) and left in liquid nitrogen for an additional two minutes to ensure thorough freezing. Following freezing, the glass tube was removed from liquid nitrogen and immediately fractured at the score by manually snapping it in two. Insulated gloves or paper towels were used to hold the tube to prevent injury and prevent thawing. Snapping the glass tube and ice was observed to cleanly sever the membrane sample. The tube fragments containing the cleaved embedded sample were placed under vacuum to remove the ice by sublimation, which avoided the potential for damage that would otherwise be caused by capillary forces generated by the retreating

front of liquid water. Once completely dried, the membrane sample was removed from the glass tube and examined perpendicularly to the cut plane by SEM.

4.2.1.4 SEM Analysis

Prepared membrane samples were fixed to a sample mount using conductive carbon tape. The samples were coated with a layer of approximately 5 to 10 nm of gold using a Hummer X sputter coater to increase sample conductivity. A Hitachi S800 field emission scanning electron microscope fitted with an EDAX energy dispersive X-ray spectrometer (EDS) was used to examine the prepared membrane sample cross-sections.

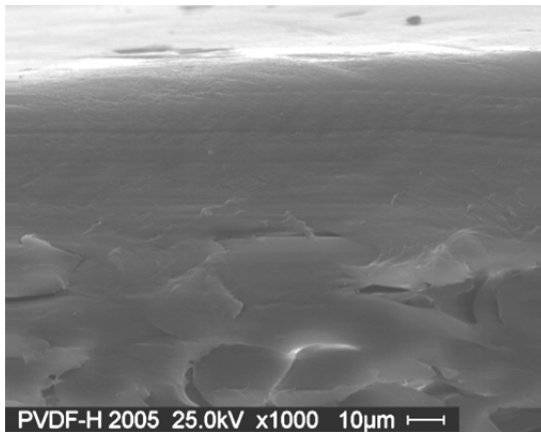
4.3 Results and Discussion

4.3.1 Ultrafiltration Membrane

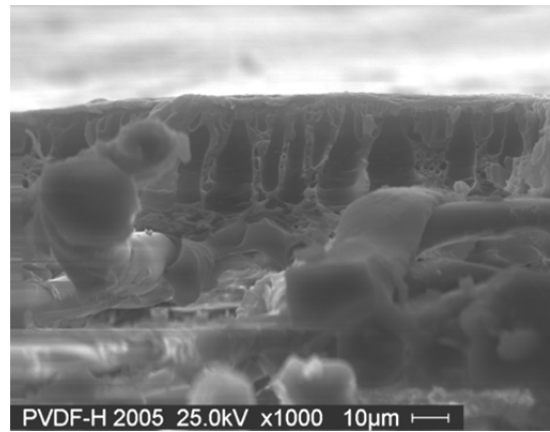
The cross-section of the UF membrane prepared using the razor sectioning method (Fig. 4-1a) shows obvious signs of deformation: the image lacks anticipated micro-structure detail. Razor sectioning apparently resulted in tearing and deformation of the micro-scale structure. Localized heating may have resulted in what appears to be micro-scale melting and loss of detailed structure. It was also observed that the top layer of the membrane folded over while sectioning, further resulting in the loss of observable detailed structure.

The direct freeze fracture method (Fig. 4-1b) produced a cross-section with much improved resolution and a significant decrease in sample deformation compared to the razor sectioning method. However, large pieces of rough membrane edges can be seen, indicating that some level of deformation occurred with this method as well.

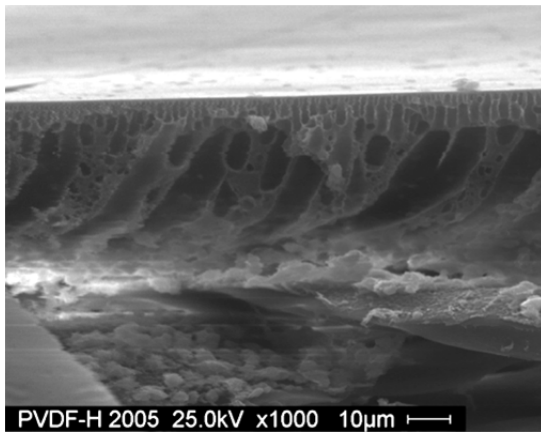
By comparison, the Cryo-snap method produced a clean fracture plane with much improved resolution of the membrane material over either of the other two methods (Fig. 4-1c). Cleavage by this method produced the least observable damage to the UF membrane material



(a)



(b)



(c)

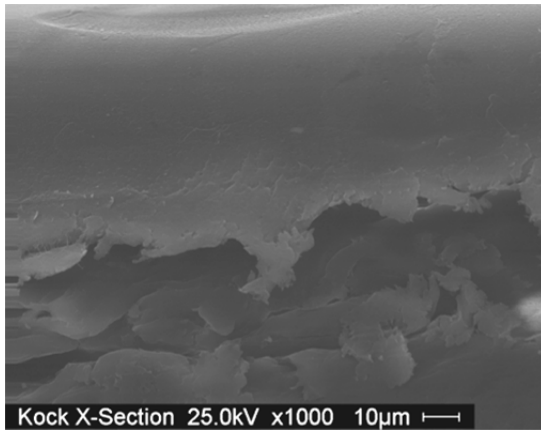
Figure 4-1 Cross-sectional SEM image of uncoated PVDF ultra-filtration membrane prepared using a) razor sectioning, b) freeze fracture, and c) Cryo-snap method.

4.3.2 Reverse Osmosis Membrane

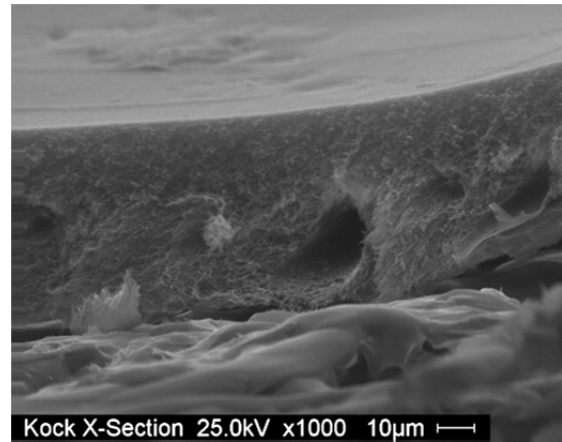
Cross-sections of thin film composite RO membranes present an especially difficult situation, as the cleavage plane extends through layers of materials with disparate mechanical properties. The SEM image obtained from the RO membrane sample cleaved using the razor sectioning method exhibited similar artifacts to those observed using this method with the ultrafiltration membrane (Fig. 4-2a), including severe mechanical deformation.

The RO membrane sample prepared by the direct freeze fracture method exhibited a significant decrease in sample deformation and increased resolution (Fig. 4-2b); however, the fracture plane was still rough and improvement would be desirable. In both cases, the non-woven backing was difficult to sever cleanly.

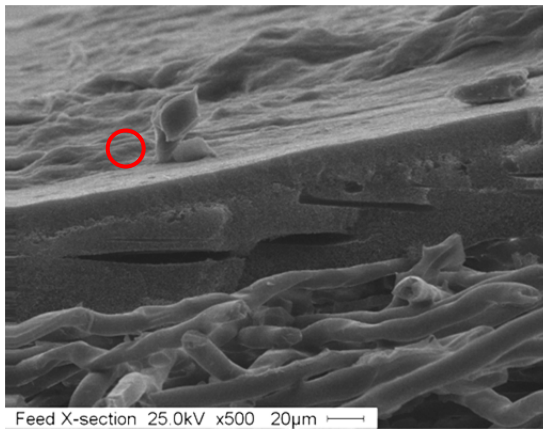
By contrast, the image of the RO membrane cleaved using the Cryo-snap method exhibited a clean fracture which preserved detailed structural information in all of the composite layers along with the foulant layer (including biofoulants) at the membrane surface (Fig. 4-2c). A clean and relatively smooth cleavage was obtained through the entire matrix despite the dissimilarity in mechanical properties of the various membrane layers and the non-woven backing. The undistorted cross-section allowed for detailed analysis with sufficient spatial resolution to determine foulant composition at specified locations, using tools such as EDS (Fig. 4-2d).



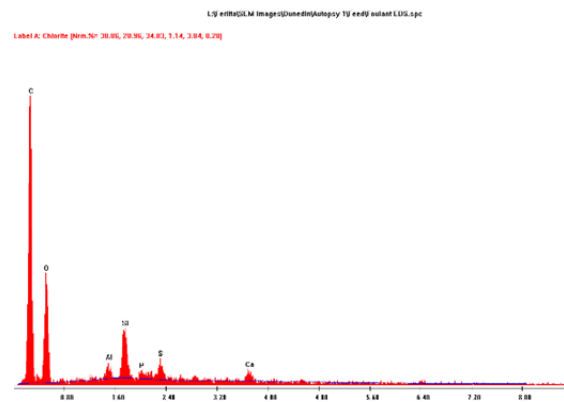
(a)



(b)



(c)



(d)

Figure 4-2 Cross-sectional SEM image of Koch polyamide reverse osmosis membrane prepared using a) razor sectioning, b) freeze fracture, c) Cryo-snap method, and d) the EDS spectrum of a portion of the foulant layer from c (indicated by circle)

4.3.3 Hollow Fiber Membrane

Razor sectioning of the isotropic hollow fiber 0.2 μm polypropylene MF membrane produced a cross-section with severe artifacts. The SEM revealed macroscopic distortion of the shape of the fiber as well as severely altered membrane microstructure (Fig. 4-3a).

It is evident that membrane structural information, material location, and foulant-membrane interaction information has been so altered as to render it completely useless.

MF material cleaved with the direct freeze fracture method (Fig. 4-3b), though not displaying the gross macro-structure distortion observed with the razor sectioning method, appeared microscopically rough and distorted. The porous polypropylene did not solidify completely in liquid nitrogen; breaking the fiber resulted in significant mechanical stretching and tearing, producing a very ragged edge to which shredded material may be observed clinging. These severe surface distortions would preclude analysis of pore size or material deposition along the cleavage plane.

In contrast, using the Cryo-snap method to cleave the MF hollow fiber material produced a superior cleavage surface compared to the other methods (Fig. 4-3c). The fiber macroscopic structure is completely whole, and the cleaved surface exhibits considerably less roughness associated with mechanical stretching and tearing. This approach allowed for better analysis of the membrane structure and definition of potential foulant-membrane interactions.

Failure of the Cryo-snap method to achieve a completely clean cleavage of the hollow fiber membrane was hypothesized to be due to the presence of air in the virgin membrane material pore spaces. Polypropylene is highly hydrophobic; thus immersing the virgin MF fiber in water resulted in retention of air in the pore spaces. Subsequent freezing

resulted in close contact between the polypropylene and water ice at the outer and lumen surfaces; however, the pore spaces were not likely hydrated. Thus, during cleavage, the material inside the membrane would be subjected to similar stresses as during dry freeze-fracturing, resulting in similar elastic deformations and tearing.

In order to prevent this, the pore spaces of the hollow fiber MF material were thoroughly hydrated by first infusing with ethanol to wet the polypropylene followed by water to fill the pore spaces.

When the membrane was fully hydrated and the fiber again sectioned using the Cryo-snap method, a nearly perfect cleavage surface was obtained (Fig. 4-3d). It is believed that in this case, the water in the filled pore spaces in the membrane matrix and water external to the fiber froze in a continuous matrix into which the polypropylene polymer was embedded. When the ice matrix was snapped, the fracture plane began on the outside portion of the sample and extended through the lattice plane formed by the pore ice, resulting in a very clean cleavage surface. With air in the pore space, the fracture plane was interrupted when it met the “dry” membrane material, resulting in more mechanical tearing and roughness at the cut surface.

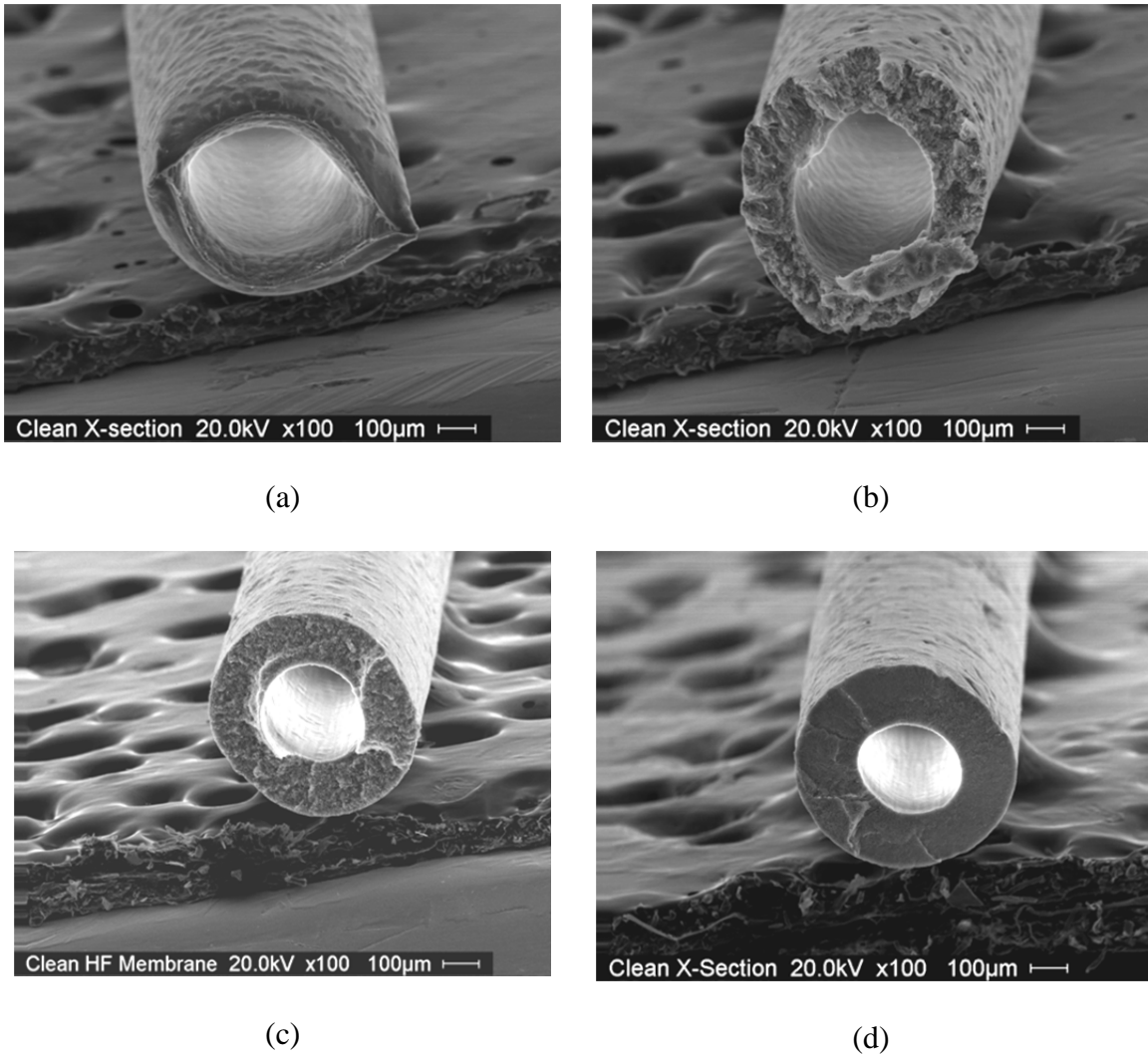


Figure 4-3 Cross-sectional SEM image of virgin polypropylene hollow fiber MF membrane material prepared via a) razor sectioning, b) freeze fracture, c) Cryo-snap method without membrane pore hydration, and d) Cryo-snap method with membrane pore hydration.

4.4 Conclusions

The Cryo-snap modified freeze-fracture method is a quick, easy means by which clean cross-sections of a wide variety of water processing membrane materials may be obtained

for SEM analysis without expensive equipment or extensive sample preparation. The method minimizes the number of introduced artifacts compared to traditional means of sample cleavage and because it involves minimal sample handling to obtain the cross-section, it is extremely useful when it is desirable to preserve delicate fouling layers. Due to the nature of the method, there is a practical limit to the size of the sample that can be prepared (less than 6mm wide), but this is not particularly objectionable when working with membrane details at the micro to nanoscale.

Chapter 5 Characterization of Membrane Fouling by Autopsies: A Plant Scale Evaluation

5.1 Introduction

The City of Dunedin water treatment plant has historically suffered from biofouling issues on their membrane surfaces [85, 86]. To diagnose the extent and type of fouling present on the membrane surface, a membrane autopsy was performed in 2006 on the lead element of skid IV from the treatment process by Micromem of Orange County Water District (OCWD) in Orange County, California [84]. At a later date, three additional membrane autopsies were performed on elements taken from three different portions of the Dunedin Water Treatment plant to determine the extent and type of fouling present at three different portions of the treatment train. The first membrane autopsy was performed on 31 Mar 2010, and the element (Serial# SE24421) was taken from the lead position of Skid IV, Stage I, pressure vessel 24. The second membrane autopsy was performed on 07 Apr 2010, and the element (Serial# SE24426) was taken from the lead position of Skid IV, Stage II, pressure vessel 38. The third membrane autopsy was performed on 14 Apr 2010, and the element (Serial# SE23890) was taken from the tail position of Skid IV, Stage II, pressure vessel 39.

5.2 Autopsy Procedure

The membrane element for autopsy was removed by the operating staff at the Dunedin water treatment plant. External evaluations were performed on site. The membrane element was then wrapped in a large garbage bag and placed on ice in a cooler for transport to the University of South Florida Tampa campus. The external fibreglass shell and plastic end caps were removed using an angle grinder fitted with a diamond blade.

Once the casing and end caps were removed from the membrane element, it was unrolled to expose the leaves and samples were taken in triplicate using a razor blade from the front, middle, and end portions of the membrane element. The analyses performed on the samples taken were protein and carbohydrate concentration, total dry mass, heterotrophic plate count, total direct count, Fourier transform infrared spectroscopy, and microscopic analysis (scanning electron microscopy and atomic force microscopy). These techniques are further described in section 3.3.

5.3 Autopsy Results From Orange County

The first autopsy performed for this study was done in Orange County in California in 2006 [84]. The autopsy was performed by the author (Russell Ferlita) and Joshua Goldman in conjunction with and under the supervision of the scientists at OCWD. The results of this autopsy are presented here. Differences in analysis procedures from section 3.3 are noted where appropriate. This autopsy was performed both for an evaluation of fouling for the Dunedin water treatment plant and as a training for the proper procedures and methods for membrane autopsy and surface foulant evaluation.

5.3.1 External Evaluation

The membrane autopsied was a KOCH TFCS 9921S (Serial number KM813295-1021) and was removed from the lead position of skid IV, stage I, pressure vessel 1. Visual inspection of the membrane element revealed some deposition of foulant material on the feed channel of the element, Figure 5-1.



Figure 5-1 Membrane element autopsied in Orange County showing the feed channel with debris deposited

The fiberglass shell and plastic end caps were removed using a circular power saw. The leaves were unrolled and measured samples were taken from areas corresponding to the front, middle, and end sections of the membrane element. Visual inspection of the membrane surface revealed a slight buildup of foulant. This buildup appeared most

pronounced to least pronounced from front to end respectively. Additionally, the pattern of the feed spacer was discernable on the surface of the membrane material, Figure 5-2.

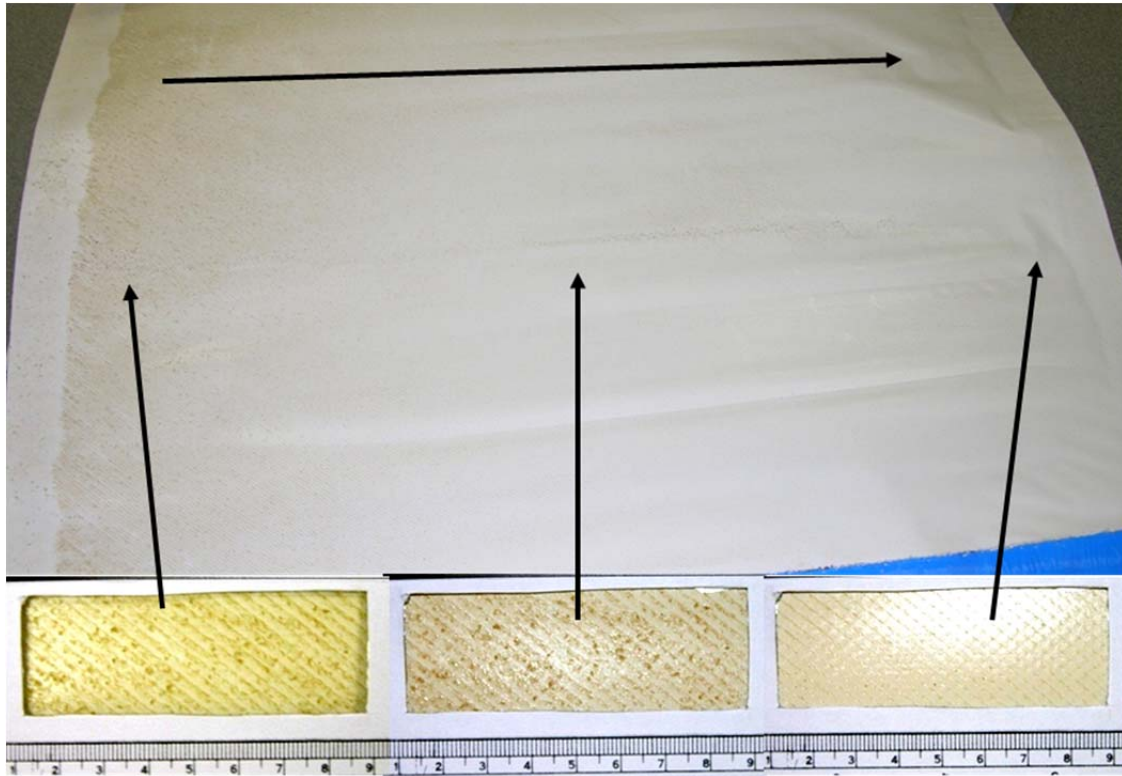


Figure 5-2 Membrane leaf surface indicating flow direction (top) and areas of the membrane sampled, front (bottom left), middle (bottom center), and end (bottom right)(scale in cm)

5.3.2 Protein and Carbohydrate Analysis

Proteins and carbohydrates indicate the presence biological debris and/or living microorganisms. Their concentrations in the foulant material on the membrane surfaces were measured, and the results are in Table 5-1.

Table 5-1 Concentrations with standard deviations of protein and carbohydrate and the ratio of carbohydrate to protein for indicated sample area

Section	Protein ($\mu\text{g}/\text{cm}^2$)		Carbohydrate ($\mu\text{g}/\text{cm}^2$)		Carbohydrate/Protein	
	Average	Stdev	Average	Stdev	Average	Stdev
Front	32.2	4.3	42.3	13.3	1.32	0.5
Middle	17.1	4.0	15.6	1.5	0.92	0.2
End	14.2	2.3	21.0	2.8	1.48	0.3

The data in Table 5-1 indicate approximately a 2-fold decrease in protein from the feed to the end portions of the membrane surface. Statistical analysis of this decrease indicates the decrease observed is significant. However, the decrease seen from the front to middle section of the membrane surface is not statistically significant. Additionally the pattern of carbohydrate concentration resembled that of the protein concentration on the membrane surface, indicating a decrease of carbohydrate concentration from the front to end sections of the membrane surface. However, due to the variability observed in the test, the results are not statistically significant at the 95% confidence interval from the front to end and the middle to end sections. The carbohydrate/protein ratio did not exhibit a clear trend from the front to end portions of the membrane surface. The protein and carbohydrate concentrations per unit area for the membrane sections are represented graphically, Figures 5-3 and 5-4 respectively. Additionally, the carbohydrate/protein ratio for each section of the autopsied membrane is represented, Figure 5-5.

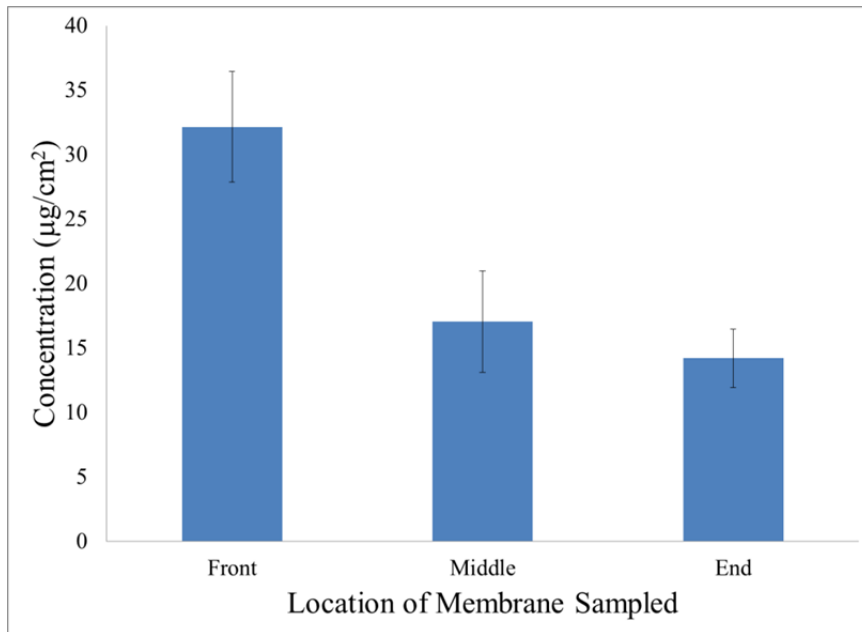


Figure 5-3 Concentration of protein per unit area as a function of membrane section sampled (error bars indicate standard deviation)

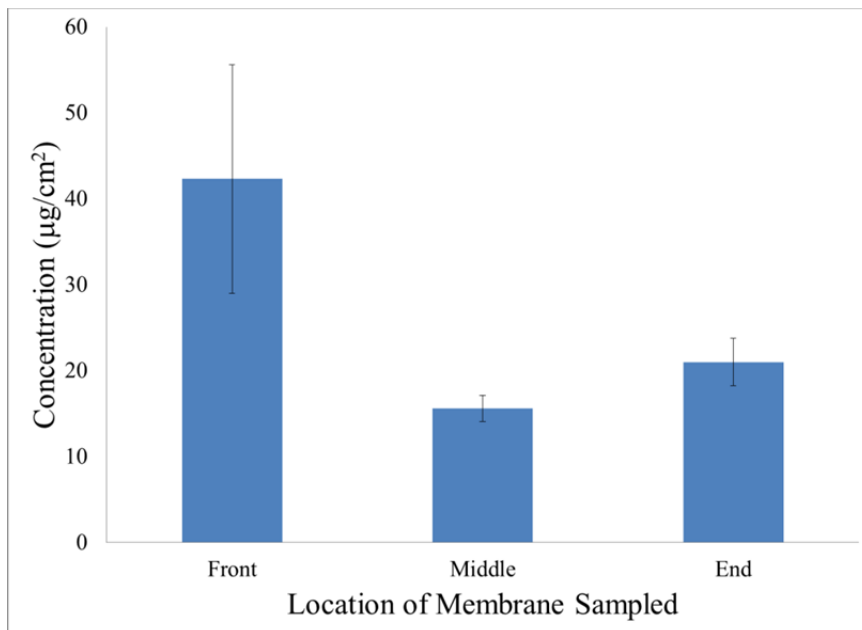


Figure 5-4 Carbohydrate concentration per unit area for each section of membrane sampled (error bars indicate standard deviation)

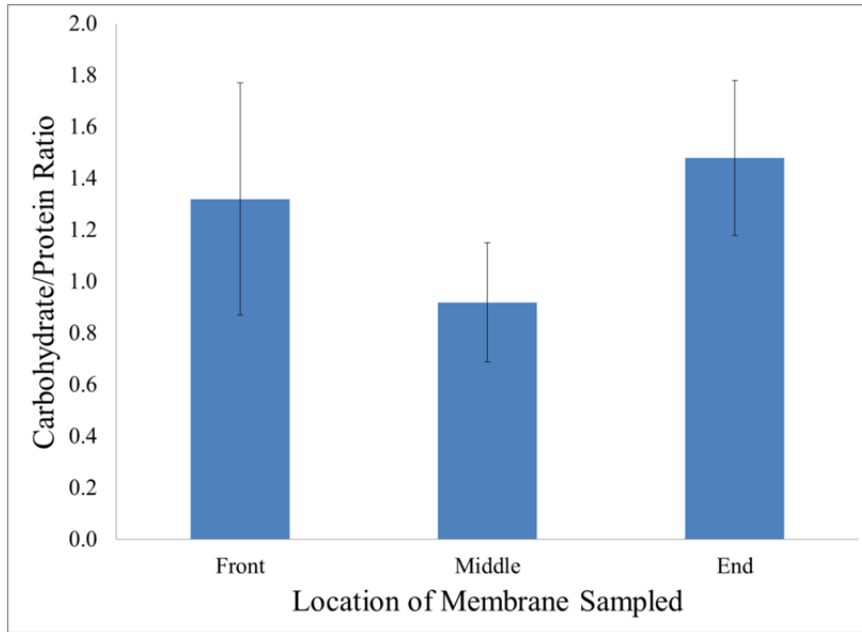


Figure 5-5 The carbohydrate/protein ratio for each section of the membrane sampled (error bars indicate standard deviation)

5.3.3 Total Direct Count and Heterotrophic Plate Count

The total number of microorganisms (total direct count) and the total culturable microorganisms (HPC) on each membrane section were measured as per the method in section 3.3. The results from these analyses are in Table 5-2.

Table 5-2 Number of total bacteria ($\# \times 10^6/\text{cm}^2$) and heterotrophic bacteria ($\# \times 10^4/\text{cm}^2$) on indicated sample area

Section	Total Bacteria		Total Aerobic Heterotrophs	
	Average	Stdev	Average	Stdev
Front	2.98	0.431	1.16	0.461
Middle	1.51	0.273	4.80	0.295
End	2.43	0.359	0.0132	0.0229

The determination of the number of total bacteria on the feed and end portions of the membrane element indicated approximately the same number present by statistical analysis. However, the middle portion of the membrane element had a significantly lower number of bacteria present. The lack of a gradient of bacterial numbers across the surface suggests deposition of microorganisms on the surface rather than growth.

The determination of the total aerobic heterotrophs (HPC) present revealed a much lower number of culturable microorganisms present on the membrane surface than the total direct count revealed. The front section of the membrane element had a significantly higher concentration of heterotrophic bacteria than the end section of the membrane surface. Additionally, the middle section of the membrane surface had a significantly higher concentration of culturable bacteria than the end section. Assuming the number of bacteria in the feed-water is constant, the number of heterotrophic microorganisms across the leaf should be approximately constant. The gradient observed could be caused by the growth of microorganisms on AOC with a concentration low enough to be significantly reduced or removed by the biofilm at the front section of the membrane.

The pattern of total aerobic heterotrophic microorganisms observed on the membrane surface is consistent with the pattern of protein and carbohydrate concentrations observed on the respective sections with higher concentration at the front section and lower concentration at the end section. The number of total bacteria and heterotrophic bacteria present on the membrane surface is represented graphically in Figure 5-6.

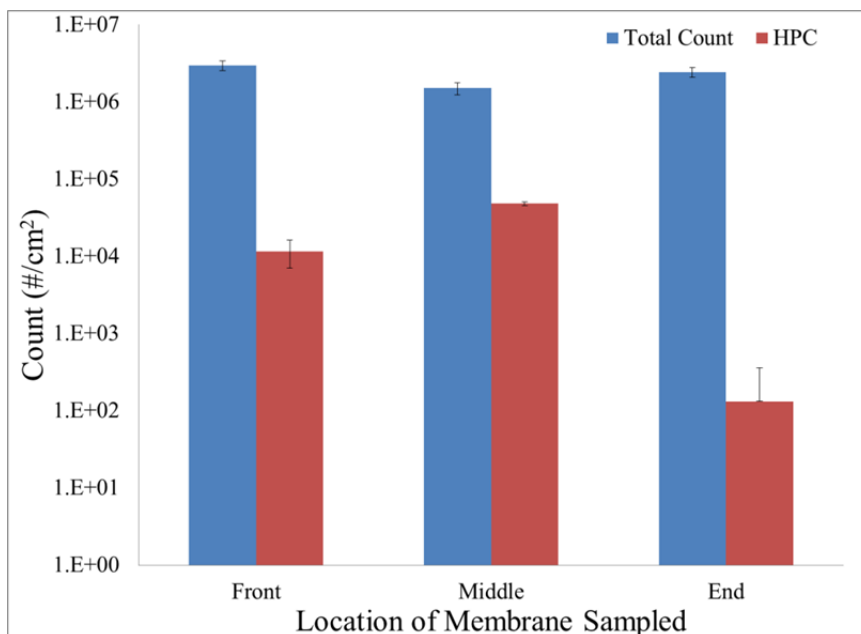


Figure 5-6 The number of total microorganisms and heterotrophic microorganisms on the indicated sections of membrane surface (error bars indicate standard deviation)

5.3.4 ATR-FTIR

The membrane samples collected were dried with compressed air passed through a Balston drier prior to analysis by Fourier transform infrared spectroscopy (Magna 550, Thermo Electron, Madison, WI). Virgin membrane material was sonicated for 30 min in 1 mM NaCl (solution was changed after 15 min). The spectra were obtained using attenuated total reflectance using a 45° single reflection germanium (Ge) ThunderDome internal reflection element (IRE) (Thermo Spectra-Tech).

The ATR/FTIR spectra of each section of membrane surface were taken in triplicate. These spectra are displayed between 4000 cm⁻¹ and 650 cm⁻¹ along with a reference spectrum of virgin membrane material in Figure 5-7. When comparing the spectra from

the fouled sections of the membrane surface to that of the virgin membrane material, it is apparent that the fouled spectra are dominated by protein and carbohydrate. Vibrational bands at 1650 cm^{-1} and 1550 cm^{-1} are visible for each section and correspond to protein vibrational bands for the amide I (C=O stretch) and amide II (N-H bend). There is also a peak associated with the C-O and C-O-C stretch of polysaccharides visible at approximately 1060 cm^{-1} for each of the membrane sections. Additionally, there is a broad O-H stretching band (or possible N-H stretch from secondary amines) at approximately 3350 cm^{-1} and aliphatic CH_2 and CH_3 bands visible below 3000 cm^{-1} for each of the membrane sections. Analysis of the spectra from each section revealed no indication of aluminum silicate, silica, calcium carbonate or calcium sulfate on the membrane surface.

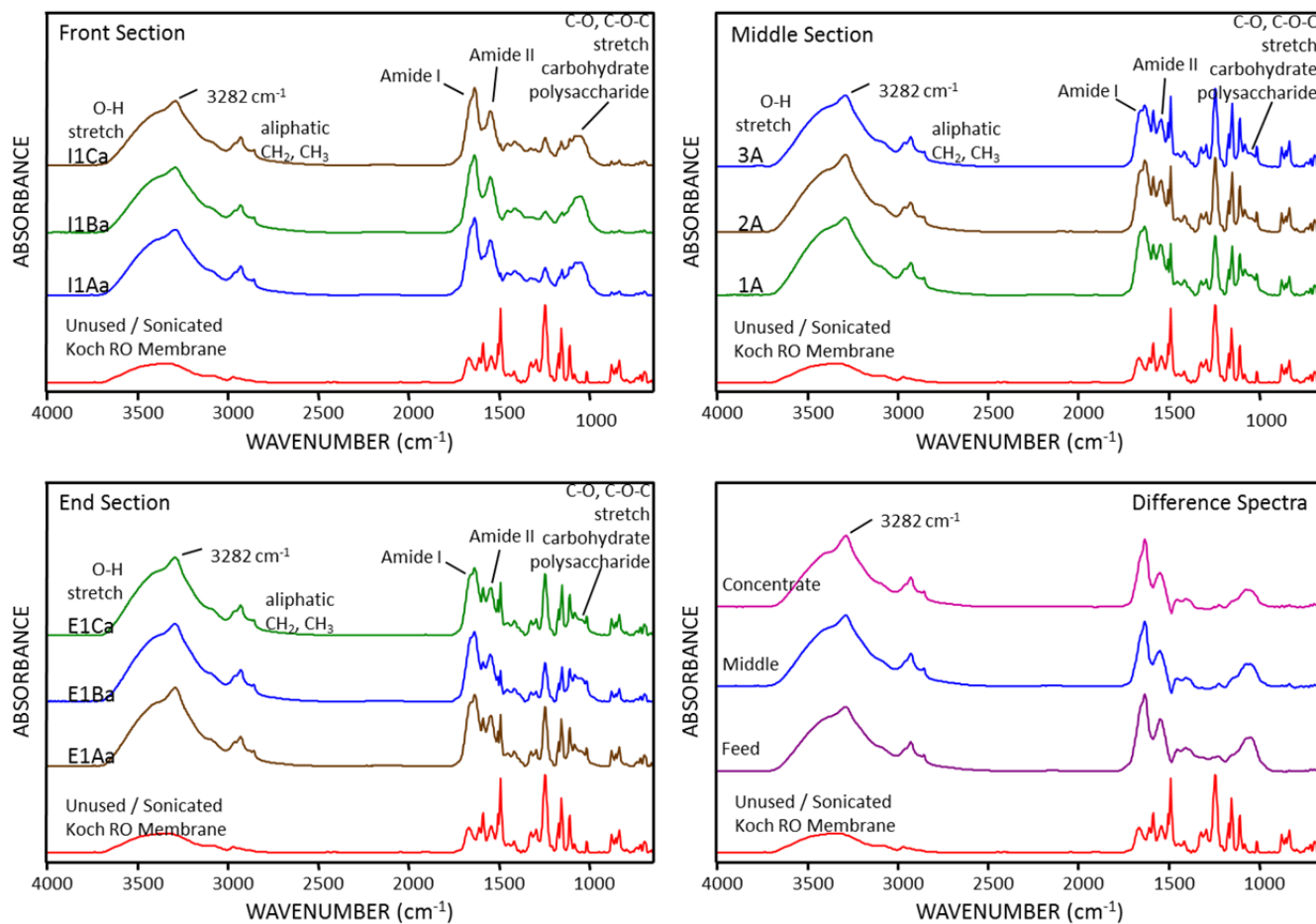


Figure 5-7 ATR-FTIR spectra for A) front, B) middle, and C) end sections; D) difference spectra for each section with the reference spectrum

The difference spectra (obtained by subtracting reference spectrum from membrane section spectrum) for each of the membrane sections along with a reference spectrum from the virgin membrane material are displayed between 2000 cm^{-1} and 650 cm^{-1} in Figure 5-8. These spectra display differences in the peak at approximately 1060 cm^{-1} , which corresponds to the presence of polysaccharides. The differences observed suggest the highest level of fouling at the front section, and similar levels of fouling at the middle and end sections of the membrane surface. These results compliment the protein, carbohydrate, and microbial results reported above.

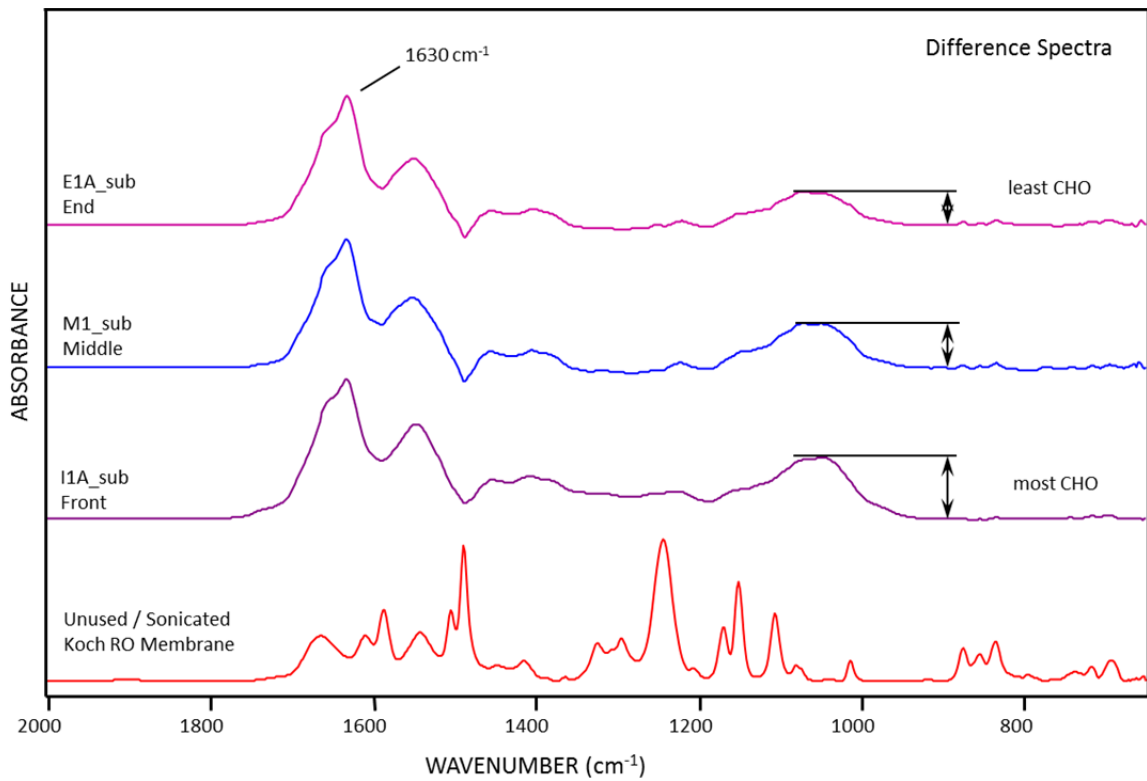


Figure 5-8 Difference spectra for each membrane section and reference spectrum

5.3.5 Microbial Community Profile

A MoBio Soil DNA extraction kit was used to recover DNA from feed-water, green sand filter backwash, and membrane samples from the front, middle, and end sections of the membrane element. Extracts were amplified using a fluorescent tagged Universal 16S rRNA PCR primer, then cut with *DdeI* endonuclease. The fragments from digestion were separated using capillary electrophoresis with fluorescent detection. This analysis is known as terminal restriction fragment length polymorphism (TRFLP).

Since this method yields fragment length information only, the number of fragments yields the minimum number of organisms present and no information as to the type or species of the organisms. The restriction enzyme is specific in its digestion site so the information yielded gives differences in the microbial communities of the samples analyzed.

The fragment lengths present for the backwash water, feed-water, and each section of membrane surface are shown from base pair lengths 34 through 215 in Figure 5-9 and base pair lengths 216 through 270 in Figure 5-10.

The green sand filter backwash and feed-water samples have only 2 fragments in common, indicating there is a different community structure in the filter and feed-water. Among the membrane sections, there are 14 fragments that occurred in common between the feed-water and one or more membrane sections, suggesting the feed-water could be a source of microorganisms observed in the analysis.

Further analysis of the capillary electrophoresis results indicate 24 front section fragments, 13 middle section fragments, and 12 end section fragments were absent from the feed-water. These results suggest that organisms present at the front section of the membrane element arose from growth of specific organisms rather than by simple deposition from the feed-water. Additionally, the microbial community structure of the feed-water is most related to that of the middle and end sections and least to that of the front section of the membrane element. Also, the microbial community structures of the middle and end sections are closely related to each other and are different from that of the front section.

Fragment BP	Membrane Samples				
	Backwash	Feed Water	Front	Middle	End
34				Shaded	
37				Shaded	
53			Shaded		
54			Shaded		
55	Shaded	Shaded		Shaded	Shaded
56		Shaded			
62		Shaded			Shaded
86	Shaded				
89	Shaded	Shaded			
90			Shaded		
96					Shaded
116			Shaded		
117			Shaded		
127			Shaded	Shaded	Shaded
128			Shaded		Shaded
129			Shaded		
130		Shaded	Shaded		Shaded
131			Shaded	Shaded	Shaded
132		Shaded	Shaded	Shaded	
133			Shaded	Shaded	Shaded
134		Shaded	Shaded		
135			Shaded	Shaded	
136		Shaded	Shaded	Shaded	Shaded
137			Shaded	Shaded	Shaded
143	Shaded				
146	Shaded				
208	Shaded				
215					Shaded

Figure 5-9 Capillary electrophoresis results of base pair lengths 34 through 215 (shaded regions indicate presence of fragment of specified length in sample indicated)

Fragment BP	Membrane Samples				
	Backwash	Feed Water	Front	Middle	End
216					
217					
218					
219					
221					
230					
232					
233					
234					
235					
236					
238					
239					
240					
241					
242					
243					
244					
246					
247					
251					
252					
253					
254					
256					
258					
259					
260					
270					

Figure 5-10 Capillary electrophoresis results of base pair lengths 216 through 270 (shaded regions indicate presence of a fragment of specified length in sample indicated)

The microbial community on the front section of the membrane element displayed fragments that were distinct from the feed-water and the other membrane sections. This suggests the microorganisms on the front section have grown and become specialized. This combined with the result that the communities on the middle and end sections are

similar to the feed-water suggests the community on the front section is growing off of and depleting nutrients in the feed-water, whereas the microorganisms on the middle and end sections result from deposition from the feed-water.

5.3.6 SEM/EDS

The surface and cross-section of the membrane sections were viewed and analyzed by scanning electron microscopy and energy dispersive spectroscopy, section 3.3 and chapter 4. The surface and cross-section of each membrane section as well as the EDS spectrum of the foulant on the front section are shown in Figure 5-11.

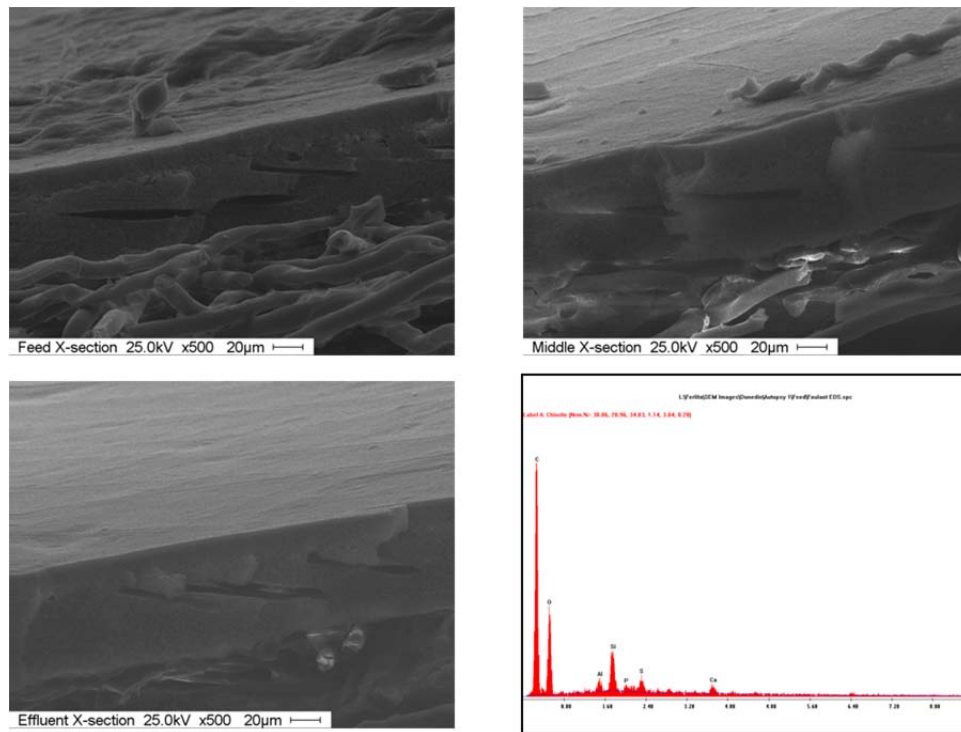


Figure 5-11 Cryosnap images of front (top left), middle (top right), and end (bottom left) sections; and EDS spectrum for foulant on front section (bottom right)

5.3.7 AFM

The surface morphologies and roughness of the fouled sections of the membrane element as well as the virgin membrane material were characterized by tapping mode AFM using a TM Microscopes CP AutoProbe (Sunnyvale, CA). A representative AFM image from each section is shown in Figure 5-12.

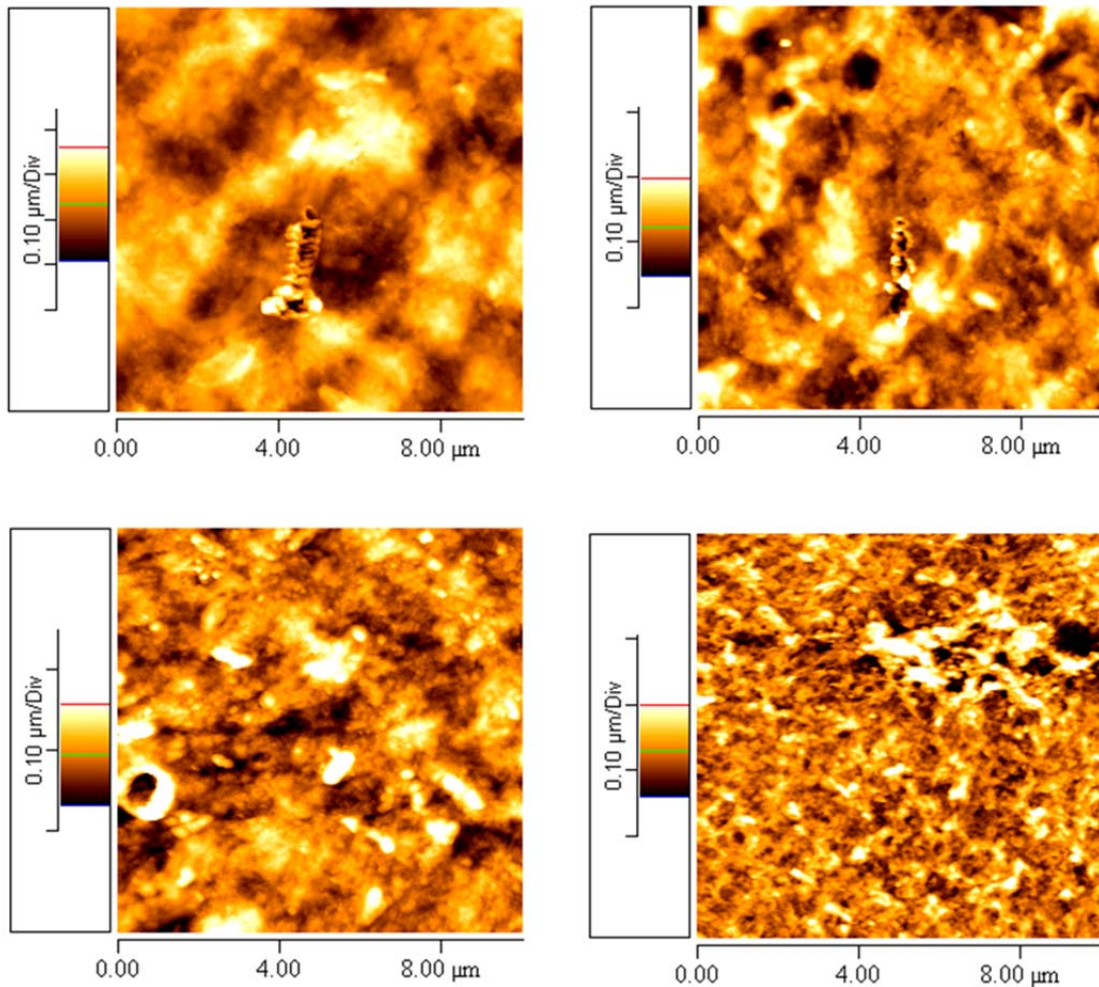


Figure 5-12 AFM top view images for autopsied membrane front (top left), middle (top right), and end (bottom left) sections as well as virgin membrane material (bottom right)

The AFM images of the front, middle, and end sections appear visually smoother than the virgin membrane material. The surface roughness of the membrane sections and virgin membrane material were analyzed and the results are in Table 5-3.

Table 5-3 Roughness data for indicated membrane samples

Membrane	RMS (nm)	Stdev	Ra (nm)	Stdev
Front	52.1	21.4	38.7	13.9
Middle	41.2	15.4	30.8	10.7
End	30.3	4.4	23.4	3.1
Virgin	31.8	22.2	23.7	17.5

The data in Table 5-3 indicate the root mean squared (RMS) and average (Ra) roughness values for the membrane samples. The roughness values were the largest for the front section and smallest (and most similar to virgin membrane material) for the end section. However, statistical comparison of the data revealed no difference in these values at the 95% confidence interval due to the variability of the data. The samples do appear visually different, but these differences could not be confirmed through roughness analysis.

5.4 Plant-Wide Autopsies

Three membranes were taken for autopsy from the Dunedin water treatment plant on three separate dates. The first membrane (membrane 1) was taken on March 31, 2010 from the lead position of Skid IV, Stage I, pressure vessel number 24, serial number SE24421. The second element (membrane 2) was taken on April 7, 2010 from the lead position of Skid IV, Stage II, pressure vessel number 38, serial number SE24426. The

final element (membrane 3) was taken on April 14, 2010 from the tail position of Skid IV, Stage II, pressure vessel number 39, serial number SE23890. A map of the pressure vessel numbering is in Figure 2-2.

The analyses performed on the samples collected include carbohydrate and protein concentration, total direct count, heterotrophic plate count, Fourier transform infrared spectroscopy, and microscopic evaluation (scanning electron microscopy with EDS and atomic force microscopy). Details of these analyses are available in section 3.3.

5.4.1 External Evaluation

The external fiberglass shell and the feed channel of the membrane elements were inspected upon removal for autopsy. Images of the feed channel for each of the autopsied membranes are in Figure 5-13.

Visual inspection of the feed channel for each of the autopsied membranes revealed deposition of debris for membrane 1 and no discernable deposition of debris for membranes 2 and 3.

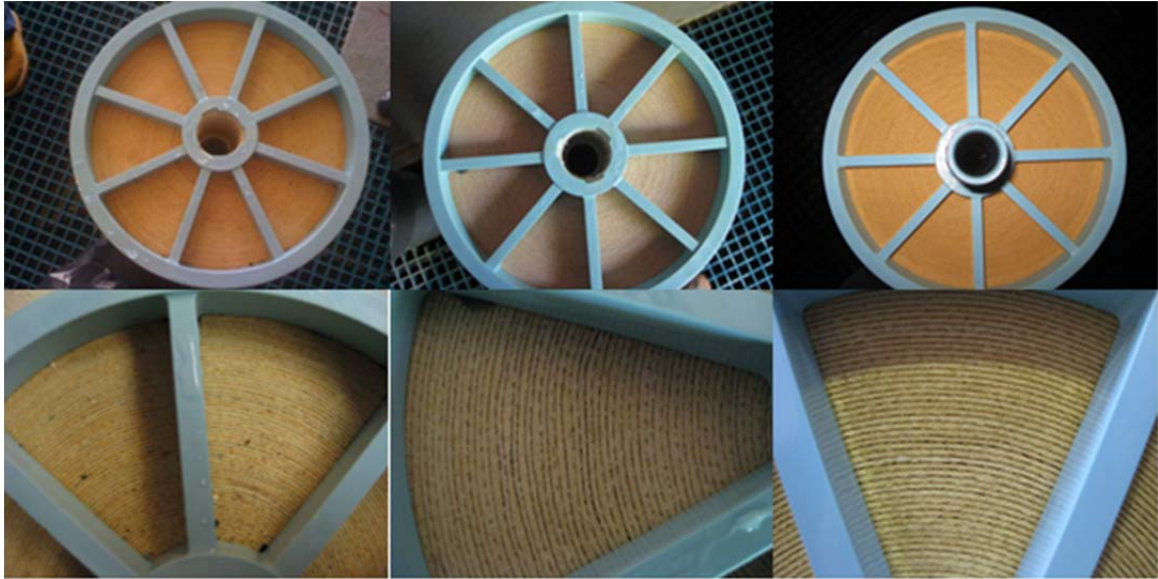


Figure 5-13 Feed channel for membrane 1 (left), membrane 2 (middle), and membrane 3 (right)

5.4.2 Dry Mass Analysis

The total dry mass of the foulants on the surface of the three autopsied membranes were characterized with the methods as per section 3.3. The results of the total dry mass for each of the membranes are available in Table 5-4.

The total dry mass for membrane 1 displayed a decreasing trend from the front to end sections. This result indicates the level of fouling decreases from the front to end membrane surfaces. The results from membrane 1 displayed a similar trend to membrane 1, indicating a decrease in total mass from the front to end surfaces. The results from membrane 3 displayed the opposite trend from membranes 1 and 2. This membrane displayed an increase in the total mass of foulant from the front to the end sections of the membrane surface. These analyses portray a general picture of the membrane surfaces

throughout the skid and indicate a general decrease in foulant concentration for at least the first half of the membrane surfaces and an increase in the foulant concentration for up to the second half of the membrane surface of the skid. The data presented in Table 5-4 are represented graphically in Figure 5-14. This graph allows for easy visualization of the trends discussed above.

The total dry mass data obtained for the foulants on the membrane surfaces only give a total amount of material present and does not give additional information on what types of materials are present.

Table 5-4 The dry mass concentrations on the surface of the membranes

Section	Date	Concentration ($\mu\text{g}/\text{cm}^2$)	Stdev
Front 1	3/31/2010	67.0	5.5
Middle 1	3/31/2010	51.5	2.5
End 1	3/31/2010	39.0	0.8
Front 2	4/7/2010	44.8	1.2
Middle 2	4/7/2010	38.6	1.6
End 2	4/7/2010	24.1	6.6
Front 3	4/14/2010	43.8	0.8
Middle 3	4/14/2010	49.3	0.7
End 3	4/14/2010	71.1	2.2

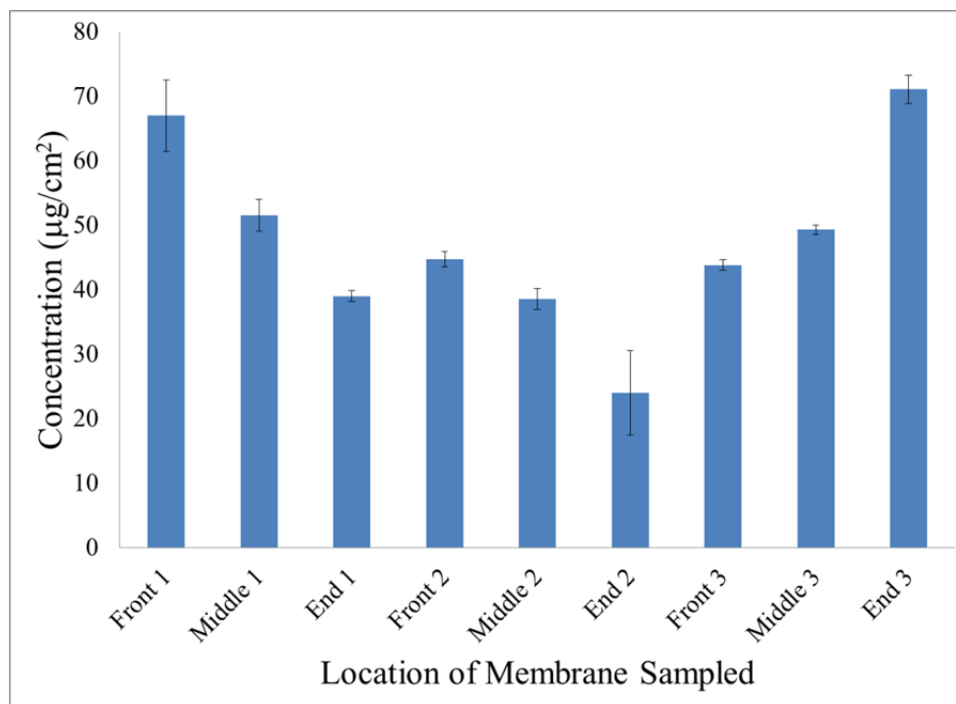


Figure 5-14 The concentration of dry mass measured for each section of membrane area autopsied (error bars indicate standard deviation)

5.4.3 Protein and Carbohydrate Analysis

To delve further into what types of materials are present in the foulant layer, additional analytical testing was performed on the membrane surfaces from each autopsy. Among these tests were the measurement of protein and carbohydrate concentrations in this foulant layer (details on the procedures of these tests are available in section 3.3). These tests give insight to how much of the foulant layer measured from the dry mass measurement could be attributed to protein and how much could be attributed to carbohydrates, Table 5-5.

Table 5-5 The protein and carbohydrate concentrations on the surface of the membranes and the carbohydrate/protein ratio

Section	Date	Protein ($\mu\text{g}/\text{cm}^2$)		Carbohydrate ($\mu\text{g}/\text{cm}^2$)		Carbohydrate/Protein	
		Average	Stdev	Average	Stdev	Average	Stdev
Front 1	3/31/2010	37.6	1.3	12.9	8.2	0.34	0.22
Middle 1	3/31/2010	32.2	2.0	5.3	2.0	0.16	0.06
End 1	3/31/2010	23.7	1.2	6.6	2.0	0.28	0.08
Front 2	4/7/2010	30.2	2.1	3.7	1.2	0.12	0.04
Middle 2	4/7/2010	23.4	1.4	3.9	1.3	0.17	0.05
End 2	4/7/2010	16.7	1.4	0.6	1.5	0.03	0.09
Front 3	4/14/2010	16.8	1.9	3.0	0.8	0.18	0.05
Middle 3	4/14/2010	24.6	2.8	3.4	1.9	0.13	0.07
End 3	4/14/2010	35.8	3.0	5.0	1.4	0.14	0.04

The third and fourth columns reported in Table 5-5 gives the protein concentration with standard deviation respectively of the foulant material for each of the membrane sections listed. From the data, it can be seen that membranes 1 and 2 displayed the same decreasing trend in protein concentration as described in the dry mass concentration above (section 5.4.2). Additionally, membrane 3 showed an increasing trend in protein concentration, which coincides with the dry mass result above. These data are represented graphically in Figure 5-15.

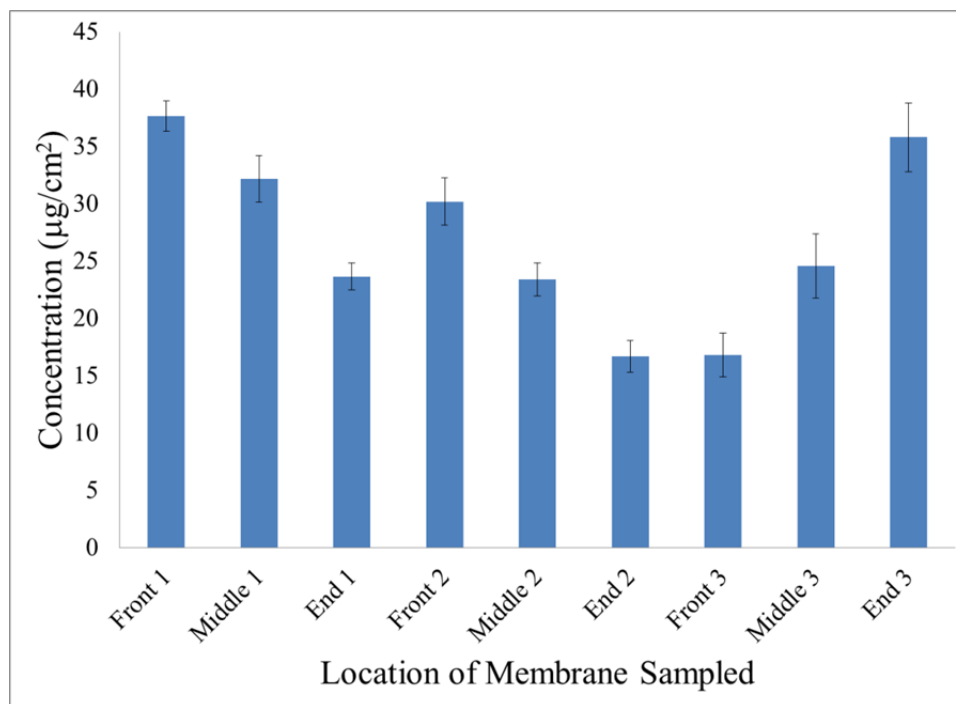


Figure 5-15 The protein concentration measured for each section of membrane area autopsied (error bars indicate standard deviation)

The carbohydrate concentration and associated standard deviation on the surfaces of the membranes autopsied are reported in columns five and six respectively of Table 5-5. These data give further insight to the content of the foulant material on the membrane surfaces. The data indicate a decreasing trend of carbohydrate concentration present for membranes 1 and 2. However, the carbohydrate concentration on membrane 3 appeared to stay approximately constant and may have a slight increase in concentration. This trend is similar to that seen in the dry mass test and protein concentration. These data are represented graphically in Figure 5-16.

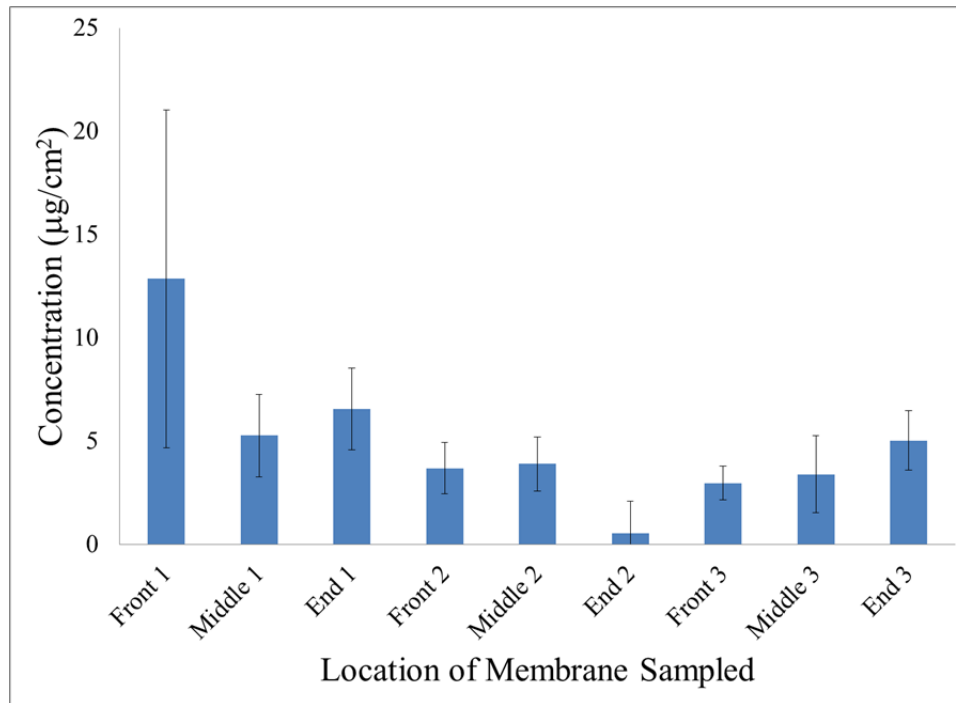


Figure 5-16 The carbohydrate concentration measured for each section of membrane area autopsied (error bars indicate standard deviation)

5.4.4 Total Direct Count and Heterotrophic Plate Count

The total number of microorganisms and the total number of culturable microorganisms (HPC) were analyzed for each section of each membrane autopsied, Table 5-6. The data indicate low levels of culturable microorganisms on all membrane surfaces for all the autopsied membranes. The surfaces for membrane 1 had especially low levels of culturable microorganisms. This is likely due to the residual chlorine in the feed-water to the membrane skids, which is an effective secondary disinfectant [110]. Additionally, the number of culturable microorganisms increases as the membrane material is further from the lead element. This could be from the gradual reduction in chlorine residual in the treatment water as it passes along the membrane surfaces.

Table 5-6 Number of culturable microorganisms for each section of each autopsied membrane

Section	Total Bacteria (#/cm ²)		Total Aerobic Heterotrphs (#/cm ²)	
	Average	Stdev	Average	Stdev
Front 1	-	-	1.6	1.5
Middle 1	-	-	10.2	7.8
End 1	-	-	1	0.7
Front 2	-	-	69	32
Middle 2	-	-	25	28
End 2	-	-	49	53
Front 3	6.54E+07	1.4E+07	870	39
Middle 3	7.54E+07	1.6E+07	669	132
End 3	3.26E+07	2.0E+07	7358	1135

The data in Table 5-6 are plotted as the total number of microorganisms and the number of culturable microorganisms per unit area as a function of membrane section and autopsied element, Figure 5-17. This graph portrays the increasing trend in culturable microorganisms as the feed-water passes along the membrane surface; giving evidence the residual chlorine has a disinfectant effect on the surfaces closest to the front of the skid.

The total number of microorganisms was not countable for membranes 1 and 2 using the method in section 3.3. It is believed this is due to the lysing of dead bacteria and a high level of genetic material in the foulant layer. This gives a high fluorescent background and makes counting with this method difficult.

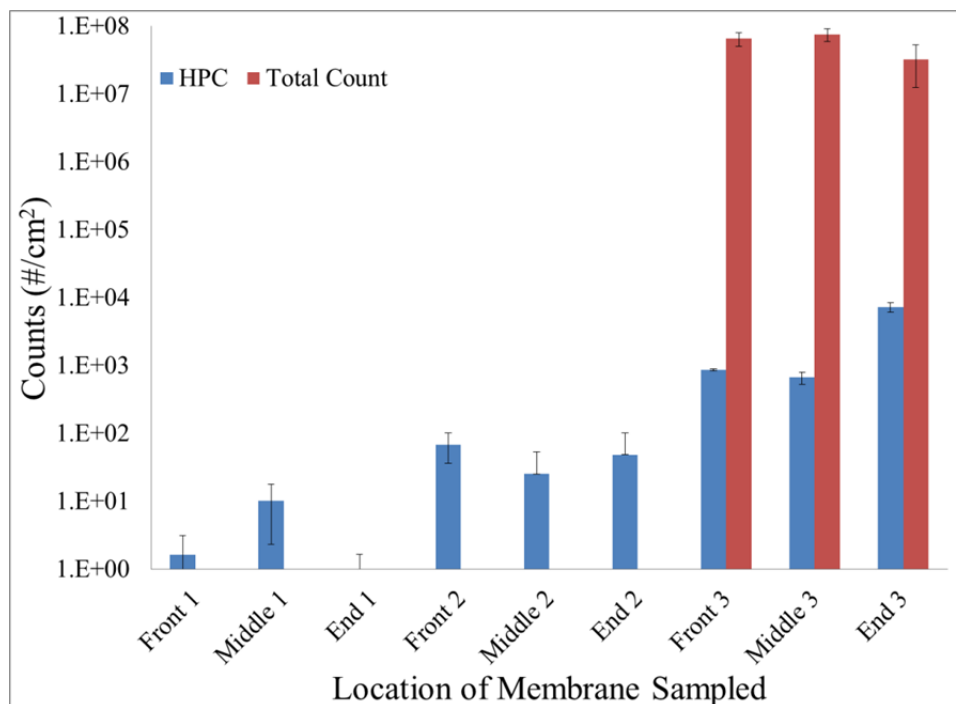


Figure 5-17 Number of culturable microorganisms per unit area on each section of each autopsied membrane element (error bars indicate standard deviation)

5.4.5 ATR-FTIR

The membrane samples collected were placed in a desiccator for at least 24 hours prior to ATR-FTIR analysis as per the methods in section 3.3. The front, middle, and end sections of each membrane element were analyzed to investigate the type and relative amount of foulant material on the surfaces throughout the plant. Spectra from each membrane section for all three autopsied membrane elements along with virgin membrane material are displayed from 4000-600 cm^{-1} , Figure 5-18. Figure 5-18 also displays difference spectra between a representative spectrum from each autopsied membrane element and virgin membrane material (from 4000-600 cm^{-1}). These spectra do not display foulant layers as thick as the autopsy from 2006 in Orange County. This is

likely due to alteration in the plant operation since that autopsy, especially chlorination of the raw water prior to pretreatment. The spectra were also analyzed for signs of degradation of the polyamide surface by chlorine, and no signs were readily apparent, suggesting chlorine may not be attacking the membrane surface. [111].

When qualitatively analyzing the peaks observed for foulant material in the range of 4000-600 cm^{-1} , the same trend is observed as with the protein and carbohydrate concentration analyses. Namely, the foulant layer is thickest to thinnest from front to end on membranes 1 and 2, and the foulant layer gets thicker from front to end for membrane 3. A general idea of the types of foulants can be ascertained by the location of the peaks present in the fouled membrane material. The exaggeration of the broad peak at approximately 3350 cm^{-1} indicates the presents of hydroxyl and/or amine groups in the foulant on all membrane element surfaces. The peak at 2900 cm^{-1} is also present on all membrane element surfaces and is consistent with aliphatic carbon. The peaks at approximately 2300 cm^{-1} is from carbon dioxide in the atmosphere of the sample chamber.

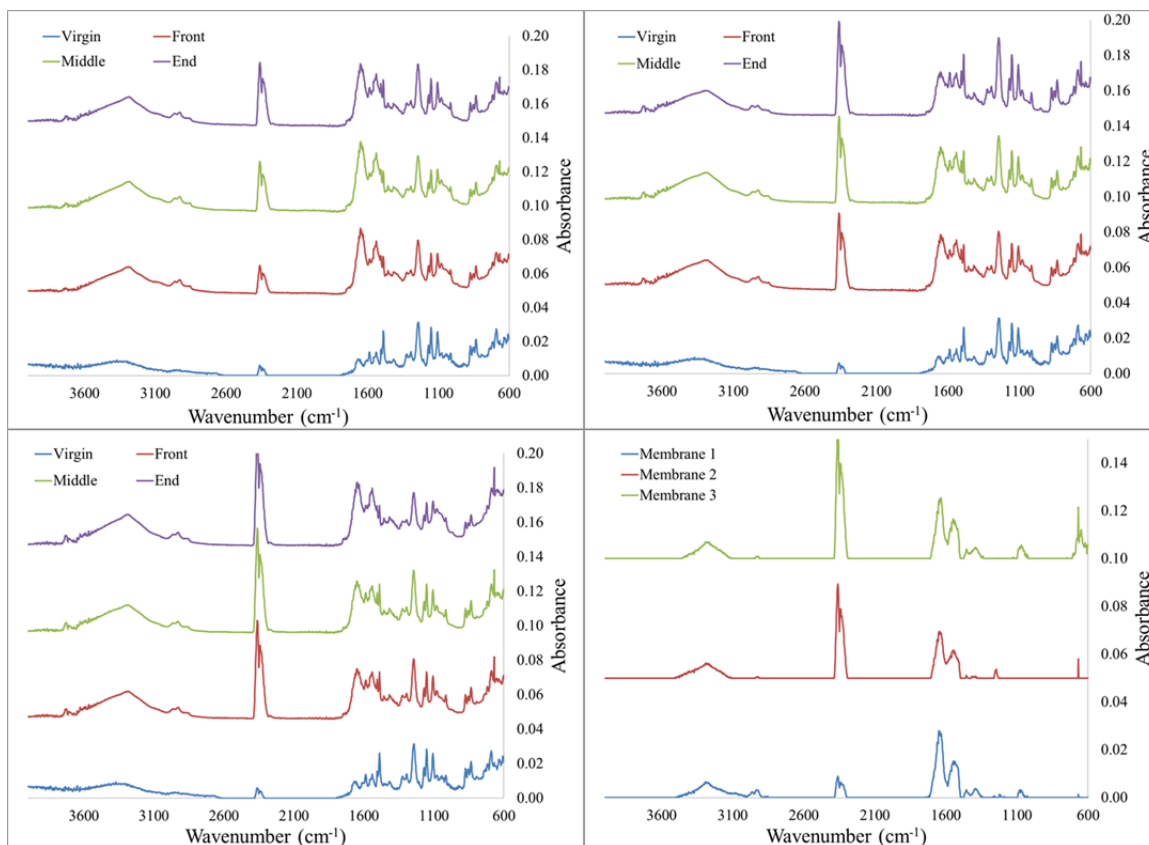


Figure 5-18 FTIR spectra for the front, middle, and end sections of the autopsied membranes for membrane 1 (top left), membrane 2 (top right), and membrane 3 (bottom left); and difference spectra for a representative spectrum from each autopsied membrane (bottom right)

The difference spectra between a representative sample for each autopsied membrane and the virgin membrane is displayed from 2000-600 cm⁻¹, Figure 5-19. When analyzing these difference spectra, the foulant layer appears thickest for membrane 1 and thinnest for membrane 2. Identification of some of these peaks reveals the amide I and amide II bonds at approximately 1650 cm⁻¹ and 1550 cm⁻¹ respectively. The peak associated with the CHO carbohydrate component of biofilm is present at 1060cm⁻¹, however this peak is

small and barely visible for membrane 2. This observation is consistent with the low levels of carbohydrates observed in the carbohydrate concentration analysis.

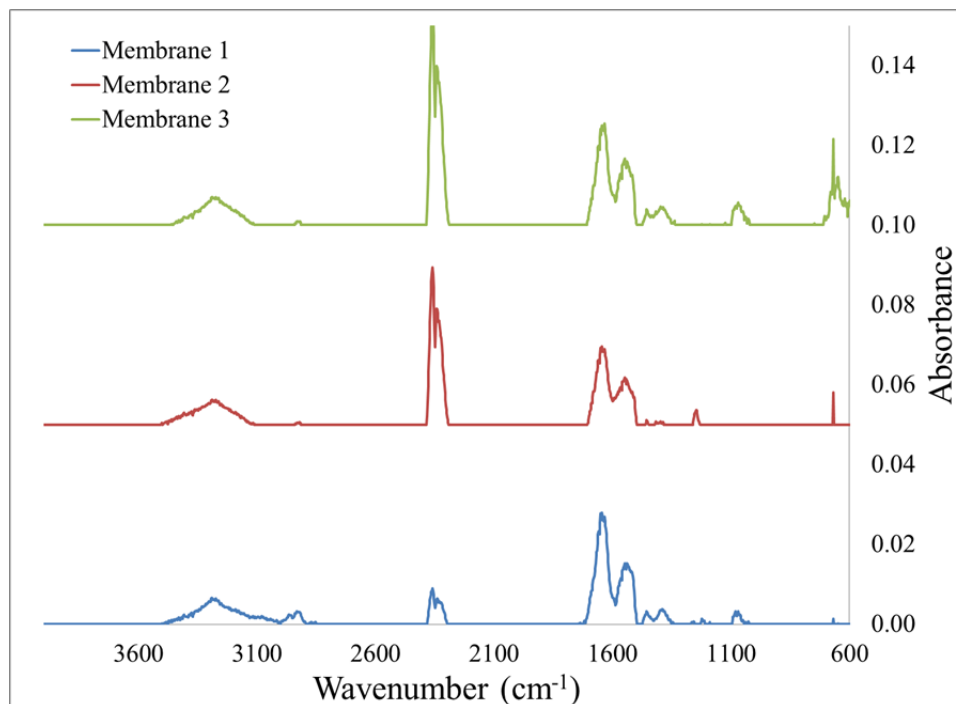


Figure 5-19 ATR-FTIR spectra from a representative sample from each autopsied membrane and virgin membrane material displayed from 2000-600 cm^{-1}

5.4.6 SEM/EDS

Analysis of the debris sampled from the feed channel of membrane 1, section 5.3.1, by SEM showed irregular shaped particles of heterogeneous composition. An example of one of these particles displaying heterogeneous composition (indicated by different reflective intensities in the SEM image) is shown in Figure 5-20.

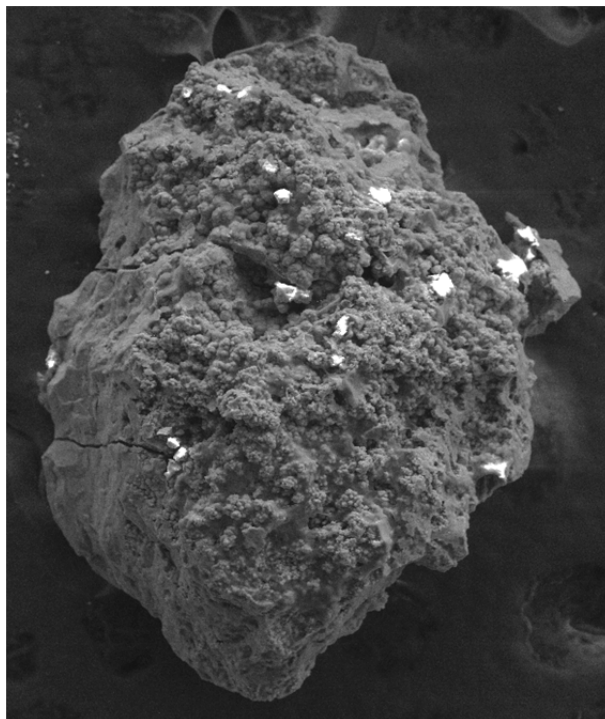


Figure 5-20 Debris particle deposited on feed channel of membrane 1

Further analysis of the particle using EDS revealed the heterogeneous composition of the particle as observed in the SEM image, Figure 5-21. The particle contained material consistent with organic and/or scale in composition, carbon, oxygen, and calcium; components of steel, chromium and molybdenum; and material possibly from the green sand filters that made it through pretreatment, silicon and manganese.

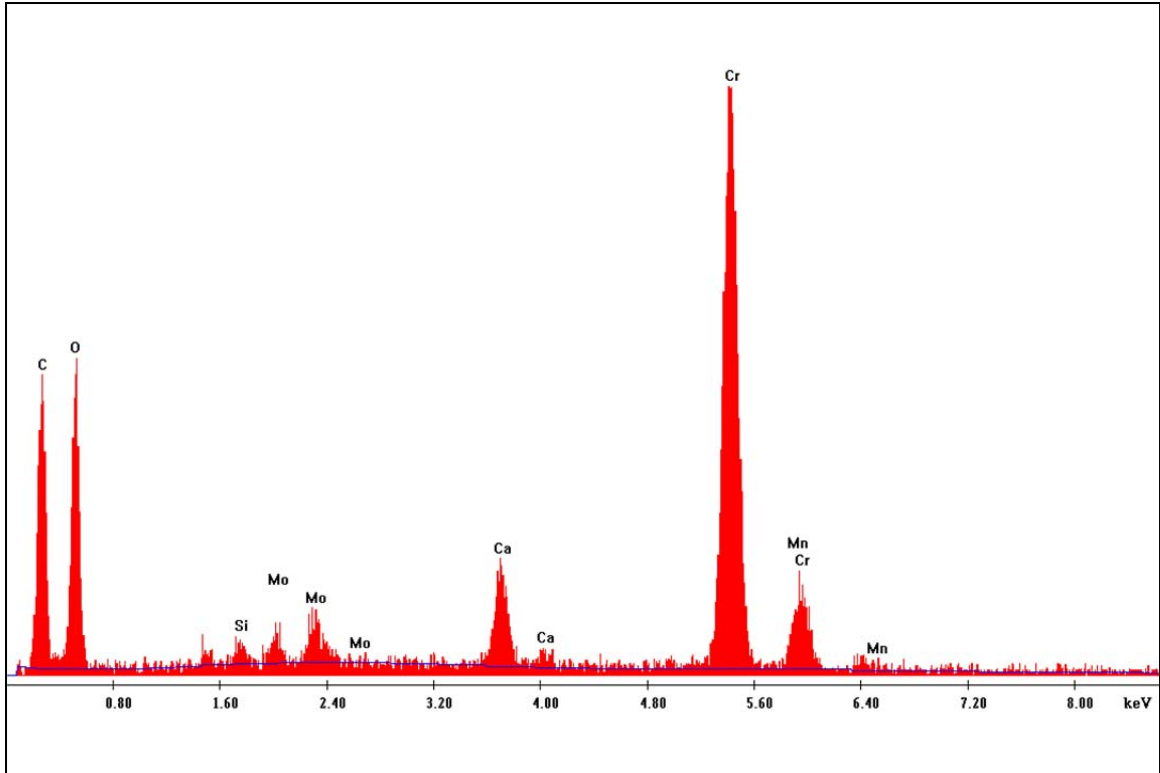


Figure 5-21 EDS spectrum of a particle lodged in feed channel of membrane 1

The front, middle and end sections of the membrane surface from each of the autopsied membrane elements were imaged, Figure 5-22. Qualitative observation of the membrane surfaces indicated relatively low levels of foulant material when compared to the autopsy performed at Orange County in 2006. The foulant material present was sparse and feathery appearance on all of the membrane surfaces. Additionally, particles of a different composition appeared on the surface of each of the membrane elements and sections with increasing frequency as the surface material approached the tail of the plant.

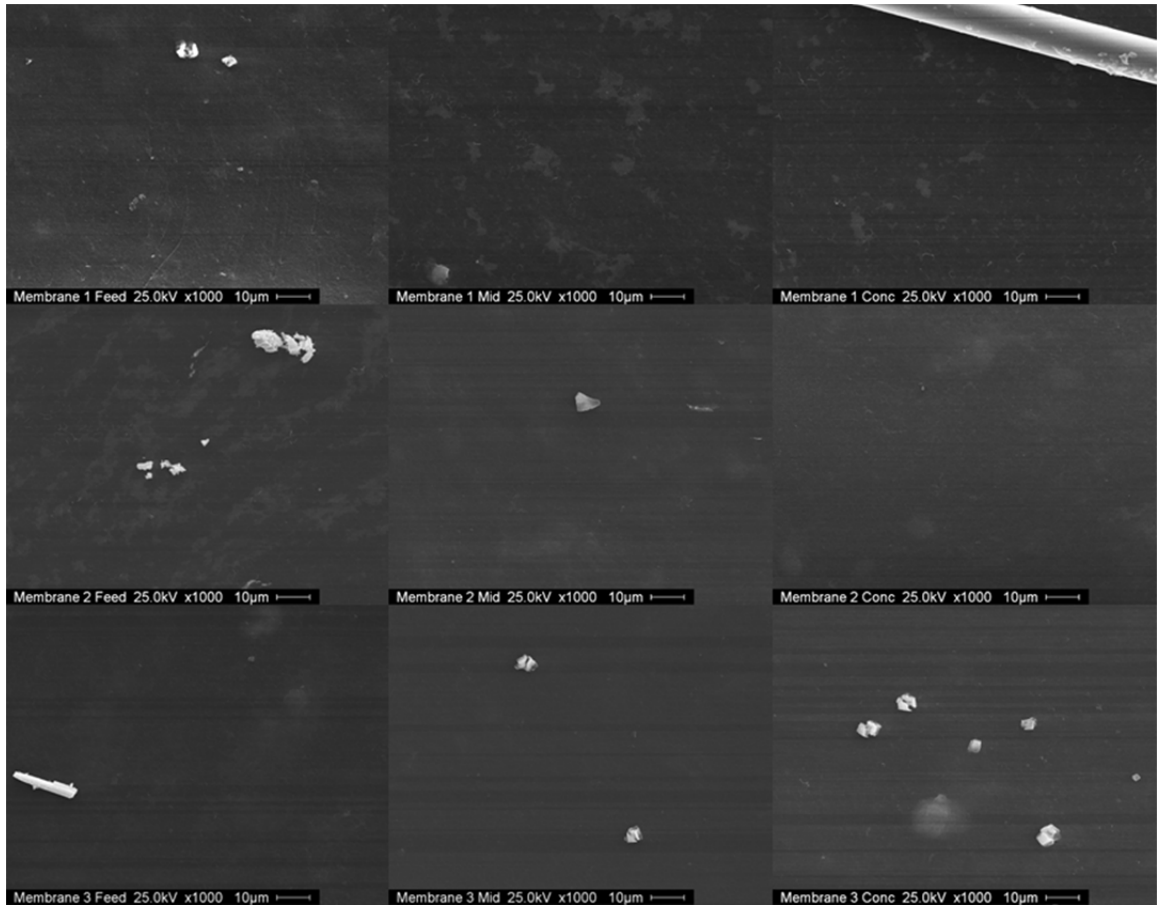


Figure 5-22 SEM images of the surface for membrane 1 front (Top left), membrane 1 middle (top center), membrane 1 end (top right), membrane 2 front (middle left), membrane 2 middle (middle center), membrane 2 end (middle right), membrane 3 front (bottom left), membrane 3 middle (bottom center), and membrane 3 end (bottom right)

The elemental composition of the foulant material present on the surface of the membrane element sections was investigated using EDS. The results of these analyses indicate the primary composition of the spectra is organic in nature, which is consistent with biofilm and/or the membrane material itself. Low levels of calcium, silicon, and aluminum was observed for the surface of membrane 1. This is likely from low levels of precipitated scalant materials and some small particles from the green sand filters making

it through the pretreatment process. EDS analysis of the surface of membrane 2 indicated similar foulant composition as membrane 1. When the surface of membrane 3 was analyzed, the same components seen on the surface of membrane 1 and 2 were observed. However, the level of calcium present on the surface was higher, especially on the end section of the element. Additionally, a low level of iron was also observed in some of the spectra, Figure 5-23. No presence of chlorine was observed on any section of the three membrane elements, suggesting the total chlorine residual in the feed-water may not be reacting with the polyamide surface of the membranes.

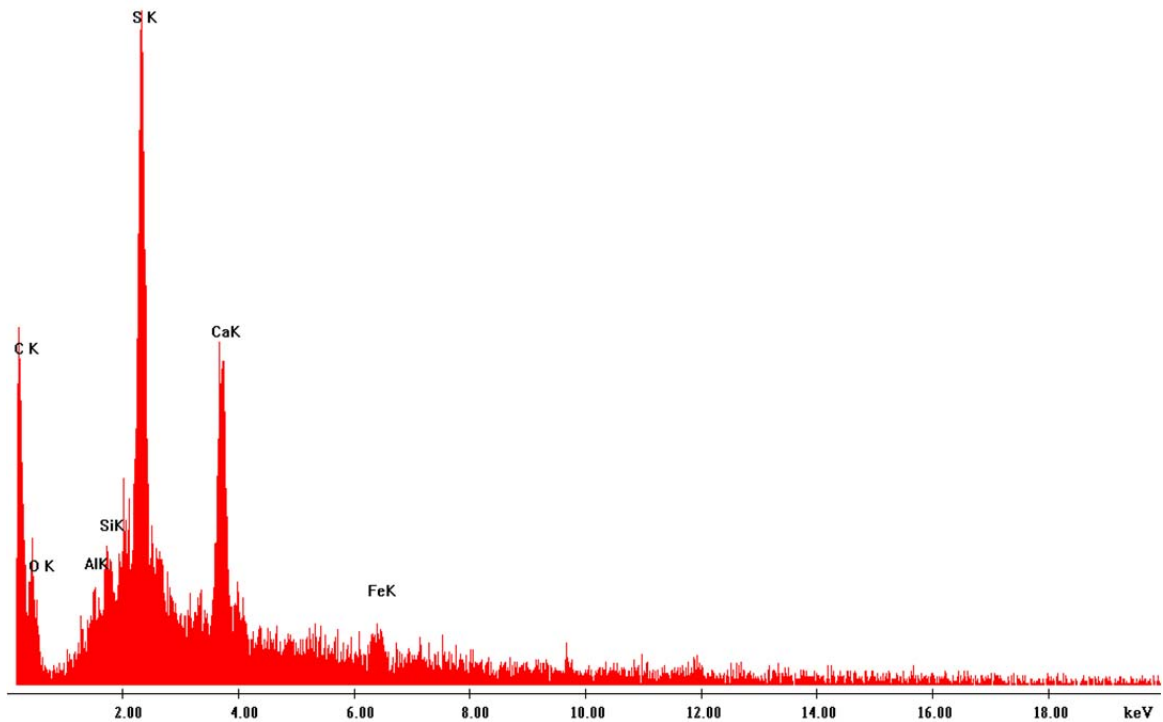


Figure 5-23 EDS spectrum from the end section of membrane 3

5.4.7 AFM

The surface morphologies and roughness of the front, middle, and end sections of the three autopsied membrane elements were characterized by tapping mode AFM using the methodologies in section 3.3. The averaged data for each section is in Table 5-7, and a representative AFM image from each section are shown in Figure 5-24. Using a t-test to statistically analyze the data in Table 5-7, there is no significant difference observed for the roughness of the membrane surfaces within each of the elements autopsies or between each of the elements. This analysis was performed for both RMS and Ra roughness values.

Table 5-7 AFM Roughness data for front middle and end sections of all three autopsied membrane elements

Section	Date	RMS (nm)	Stdev	Ra (nm)	Stdev
Front 1	3/31/2010	53.7	11.5	42.1	9.5
Middle 1	3/31/2010	43.6	3.0	34.5	1.8
End 1	3/31/2010	37.8	1.4	30.1	1.1
Front 2	4/7/2010	53.1	24.4	40.9	16.8
Middle 2	4/7/2010	36.3	1.0	28.5	0.5
End 2	4/7/2010	29.2	3.4	22.3	2.4
Front 3	4/14/2010	42.9	12.7	33.7	9.0
Middle 3	4/14/2010	37.5	6.7	29.3	4.8
End 3	4/14/2010	45.0	9.9	35.0	7.3

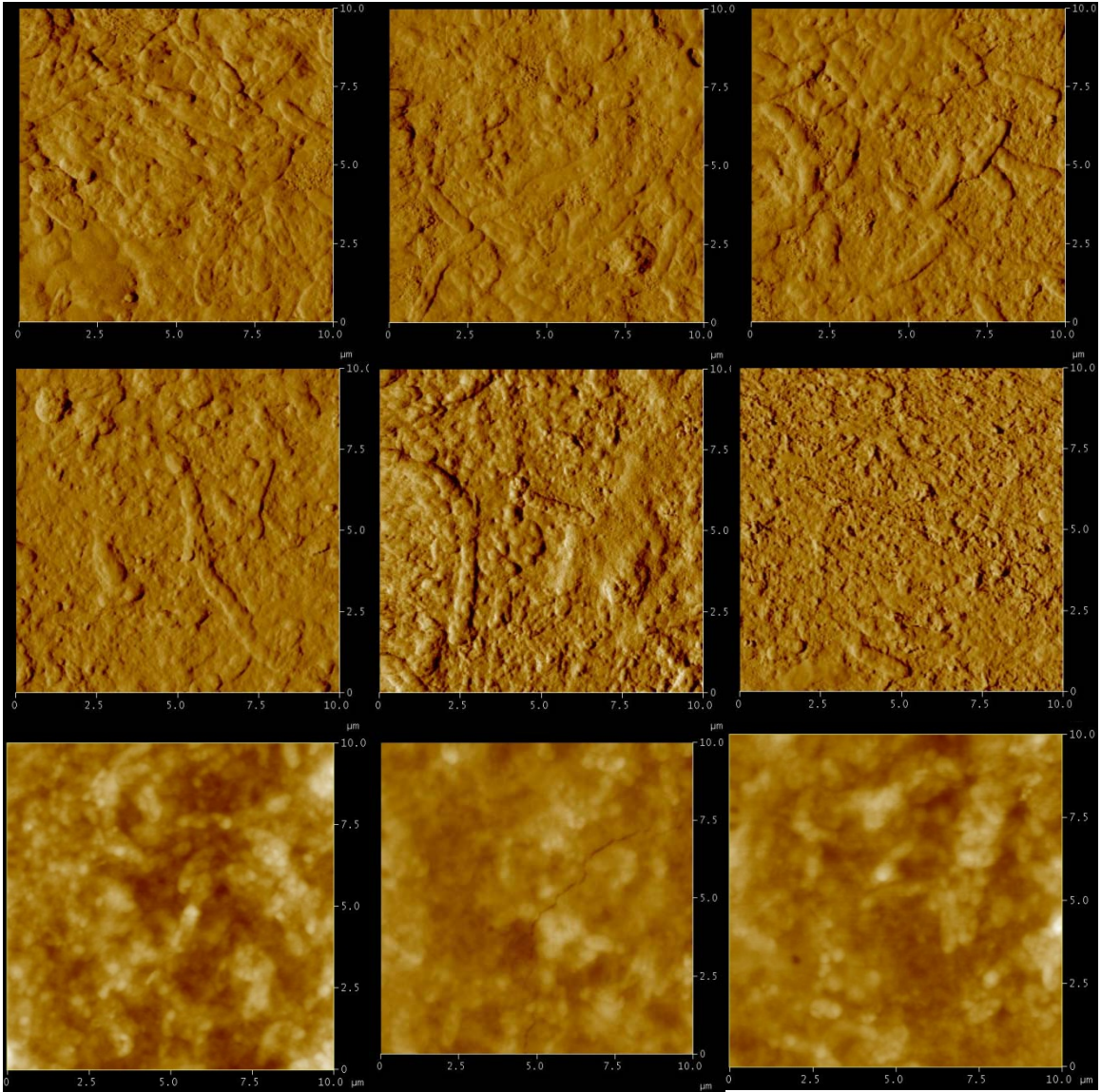


Figure 5-24 AFM images of the membrane sections from membrane 1 front (top left), membrane 1 middle (top center), membrane 1 end (top right), membrane 2 front (middle left), membrane 2 middle (middle center), membrane 2 end (middle right), membrane 3 front (bottom left), membrane 3 middle (bottom center), and membrane 3 end (bottom right)

5.5 Conclusions

5.5.1 Orange County Autopsy

The distribution of fouling material on the membrane surface exhibited a decreasing trend from the front section to the end section. Visual and microscopic observation suggested this trend, and the trend was observed quantitatively in the protein and carbohydrate concentrations and the number of culturable organisms (although total direct count is inconclusive). The HPC distribution and community profile data reveal the organisms at the front section of the membrane element are dominant, and are different from those in the feed-water as well as the middle and end sections of the membrane.

The results from the autopsy lead to the hypothesis that biofilm on the front section of the element act as a biological filter, removing AOC and nutrients from the feed-water, thereby making the feed-water nutrient deprived and preventing/reducing biological growth on downstream membrane surfaces.

5.5.2 Plant-Wide Autopsies

The autopsy results from membrane 1 and 2 revealed a decreasing trend in the distribution of fouling material on the membrane surfaces from the front section to the end section, and an increasing trend from front to end for membrane 3. This trend was observed quantitatively in the total dry mass, protein concentration, and carbohydrate concentration. However, the number of culturable organisms increased as the treatment water traveled along the membrane surface (although total direct count is inconclusive). The microbial data suggest a possible disinfectant effect of the residual total chlorine in

the feed-water, which could be consumed and become ineffective as the water travels toward the concentrate. However, the HPC only measures microorganisms that are culturable using the R2A media, so a large portion of viable microorganisms could be neglected in the assessment.

The protein, carbohydrate, and dry mass results from the three autopsies support the hypothesis that biofilm on the front section of the element act as a biological filter, removing AOC and nutrients from the feed-water and preventing biological growth on downstream membrane surfaces. However, the tail element does have increased foulant (especially scalant) concentrations and an increased number of culturable microorganisms is observed. This increase could be due to increased deposition of materials that have exceeded their solubility limit and an increased deposition of colloidal matter due to its higher concentration in solution.

5.5.3 Overall Autopsy Conclusions

The results from the plant-wide membrane autopsies revealed much lower levels of fouling than the original autopsy performed in Orange County in 2006. The reduction in the overall levels of fouling is believed to be caused by differences in the treatment process that have occurred since 2006. The most notable change in the process is the addition of chlorine to the raw water prior to pretreatment. This was done to help oxidize iron and sulfides in the hopes of reducing potassium permanganate addition to the green sand filters and extend their life. A total chlorine (not free chlorine) residual does remain in the treatment water and is fed to the membrane skids. The secondary disinfectant

effect of the chlorine residual is what is believed to be causing this reduction in fouling on the membrane surfaces, namely the reduction of biofilm formation. Additionally, it is believed the chlorine residual is responsible for the reduced number of culturable microorganisms observed at the head of the membrane treatment process.

Chapter 6 Mass Balance Analysis of Dissolved Organic Carbon in a Reverse Osmosis Membrane Water Treatment Plant: Implications for Biofouling Control

6.1 Introduction

Natural organic matter (NOM) is a mixture of organic compounds from diverse biological origins and is commonly found in the source water of water treatment plants. For surface water, NOM can be present in concentrations as high as 30 mg C/L (1). For groundwater, the typical NOM concentration is around 2 mg/L, although concentrations can be as high as 15 mg C/L [112]. The presence of NOM in treatment plant feed-water can lead to a number of problems, such as formation of disinfection by-products, biofilm growth at the treatment plant, and re-growth in the distribution system [31, 78, 112-115]. For drinking water treatment systems, the source and type of organic matter in the feed-water has been shown to greatly impact the treatment process [116]. For systems implementing reverse osmosis membrane filtration, the presence of NOM in the membrane feed-water can lead to severe impact on the membrane surfaces, such as colloidal fouling and/or biofilm growth [20, 26, 117, 118], which lead to decreased performance and increased costs.

A technique commonly used for the characterization of organic material in natural waters is the specific UV absorbance (SUVA), which is UV_{254} (the absorbance of the sample at 254nm, corresponding to aromatic structures) normalized to the concentration of DOC

(section 3.3). Higher values SUVA indicate that a greater fraction of the organic carbon is hydrophobic (due to aromatic groups), relative to the more hydrophilic aliphatic groups. High SUVA can also mean greater resistance to biodegradation, as aromatic materials are generally more difficult to degrade than aliphatic materials. Values for SUVA for natural systems have been reported from around $1 \text{ L mg}^{-1} \text{ m}^{-1}$ up to around $5 \text{ L mg}^{-1} \text{ m}^{-1}$ [69, 119-121].

The removal of organic carbon from plant feed-water can be achieved by various methods. Traditional methods use coagulation, flocculation, and filtration to achieve removal [19, 122, 123]. Advanced treatment methods, such as advanced oxidation, activated carbon adsorption, and biologically activated carbon, and biofiltration may also be used for removal [66, 124, 125]. Biofiltration is effective for removing a significant fraction of NOM, and unique microbial community structures have been noted in these systems [67, 71]. Removal efficiencies of 5-45% for dissolved organic carbon (DOC) in biofiltration as a pretreatment for RO has been reported, although removal is highly dependent on source and type of organic carbon present [77, 81, 126]. The use of biofiltration as pretreatment has been shown to greatly decrease the formation of biofilm on membrane surfaces and decrease the rate of flux decline, thereby extending system runtime [81, 127].

Located on the central west coast of Florida on the Gulf of Mexico, the City of Dunedin has a population of approximately 37,000 residents and an area of approximately 10 sq. mi. The city owns and operates a reverse osmosis water softening plant, the details of

which are in chapter 2. Prior plant evaluations and membrane autopsies have indicated problems with membrane biofouling at the Dunedin water plant [85, 86]. Autopsy results indicate the highest concentration of biofilm on the front portion of the first-stage lead element of the plant, with a rapidly declining biomass profile along the element in the direction of flow. Further spatial analysis of the microbial community structure (based on DNA fragment comparisons) of the lead element biofilm indicate that the front portion of the membrane contained a unique microbial community (more growth, less diversity) that was statistically distinct from the planktonic microbial communities present in the feed-water to the membrane skids, whereas the middle and end portions of the same element had microbial communities (less growth, more diversity) that were statistically similar to that in the feed-water [84]. This spatial differentiation suggests that the biofilm on different portions of the element had developed under different selection pressure, likely due to differences in the availability of organic carbon in the feed-water. It is believed that the heterotrophic biofilm on the front portion of the element developed by actively assimilating the DOC, whereas the biofilm on the remaining portions were mainly deposited from the feed-water. This chapter explores the hypothesis that feed-water organic carbon is removed (through assimilation and degradation) as it flows over the length of the membrane element, by conducting a plant-wide mass balance analysis on DOC total nitrogen at the Dunedin Water Treatment Plant.

6.2 Sample Collection

For the plant-wide carbon and nitrogen mass balance, water samples were collected from locations representative of the feed, permeate, and concentrate streams of the membrane

system. A simple schematic of the plant and the respective sampling points are shown in Figure 6-1. Prior to sampling, each sampling port was flushed for five minutes and the sample bottles were double rinsed with the sample water. Water samples were collected in dark brown glass bottles (Fisher Scientific) without headspace and brought back the University of South Florida water quality lab for immediate analysis. The actual flow rate of water at each of the sample points was obtained from the plant's SCADA system. The DOC concentrations on the plant level were collected and evaluated over a 20 month period, and the TN concentrations were collected and evaluated over an 11 month period.

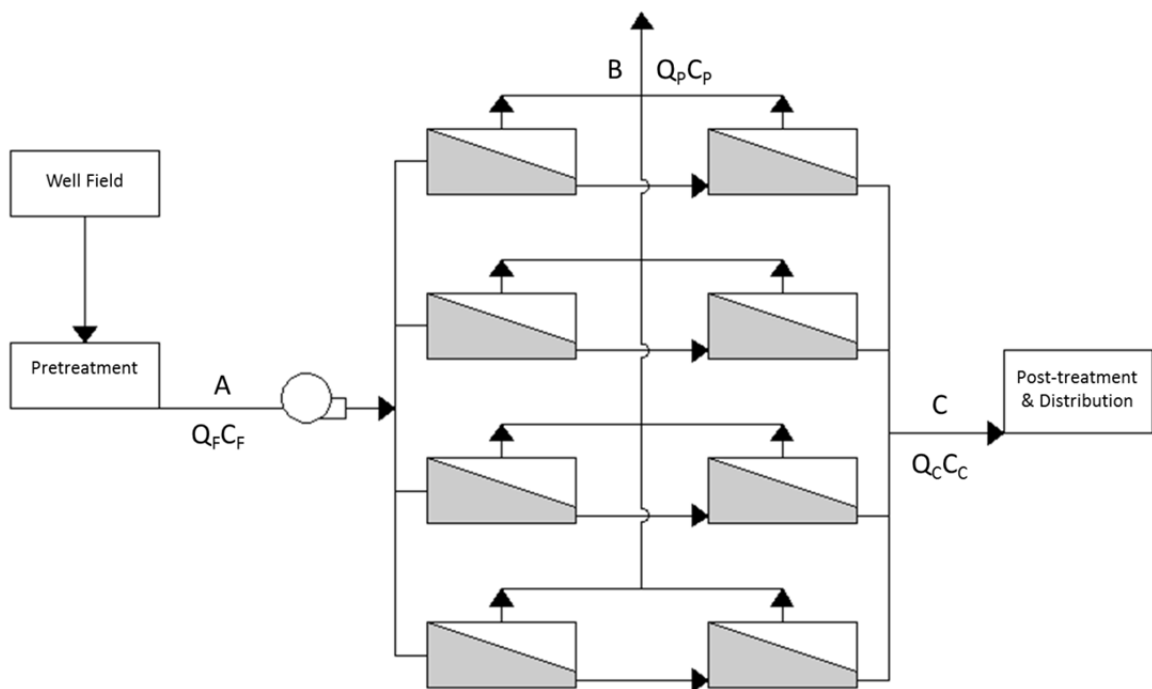


Figure 6-1 Representation of plant sampling points: A) plant feed, B) plant permeate, and C) plant concentrate

The concentration of DOC and TN and the UV254 absorption were measured and the SUVA was calculated for the samples collected. These measurements were performed as per the procedures delineated in section 3.3.

6.3 Mass Balance Calculation

The data presented here are from the analyses of DOC and TN taken on the plant level. The mass flow rate of DOC and TN at each of the sample points was determined using the measured concentration of DOC and TN respectively, multiplied by the recorded volumetric flow rates at each sample point from the SCADA system. A mass balance equation for these systems can be written as follows:

$$Q_F \cdot C_F = Q_P \cdot C_P + Q_C \cdot C_C + M_R \quad (6.1)$$

where Q_F , Q_P , and Q_C are the volumetric flow rates for the feed, permeate and concentrate respectively; C_F , C_P , C_C , are the DOC (or TN) concentrations for the feed, permeate and concentrate respectively; and M_R represents the mass of organic carbon removed from the system through assimilation or degradation. The percent removal of organic carbon (or total nitrogen) from the system can be determined using the following equation:

$$\% \text{Removal} = \frac{\text{mass removed}}{\text{mass input}} \times 100 = \frac{Q_F C_F - (Q_P C_P + Q_C C_C)}{Q_F C_F} \times 100 \quad (6.2)$$

6.4 Results and Discussion

Temporal profiles of DOC and TN concentrations and the associated value of SUVA for the plant feed-water are shown in Figures 6-2 and 6-3 respectively. The SUVA of the plant feed water is also plotted as a function of the DOC concentration of the feed-water (Figure 6-5). Temporal profiles of the percent removal of DOC and TN (along with the average removal percentage of each) are shown in Figure 6-6. The percent removal and unit removal of DOC plotted as a function of the unit loading of DOC are shown in Figure 6-7. Temporal profile of the percent change of SUVA ($(\text{SUVA}_{\text{feed}} - \text{SUVA}_{\text{conc}})/\text{SUVA}_{\text{feed}} \times 100$) during the monitoring is shown in Figure 6-8.

The DOC concentration in the plant feed-water (Figure 6-2) is typically around 20mg/L, which is high for a groundwater source [112]. However, the source water is drawn from a relatively shallow aquifer in an urban well field, so may be more exposed to surface input of organic carbon. Interestingly, there is a period of approximately 6 months (April – October 2009) when the DOC concentration in the feed-water dropped by approximately an order of magnitude, to about 2.5 mg/L. However, the TN concentration remained relatively constant, between 0.25 and 0.4 mg/L. Consequently, the C:N ratio for the feed-water, typically around 60, dropped to approximately 7 during this 6 month period.

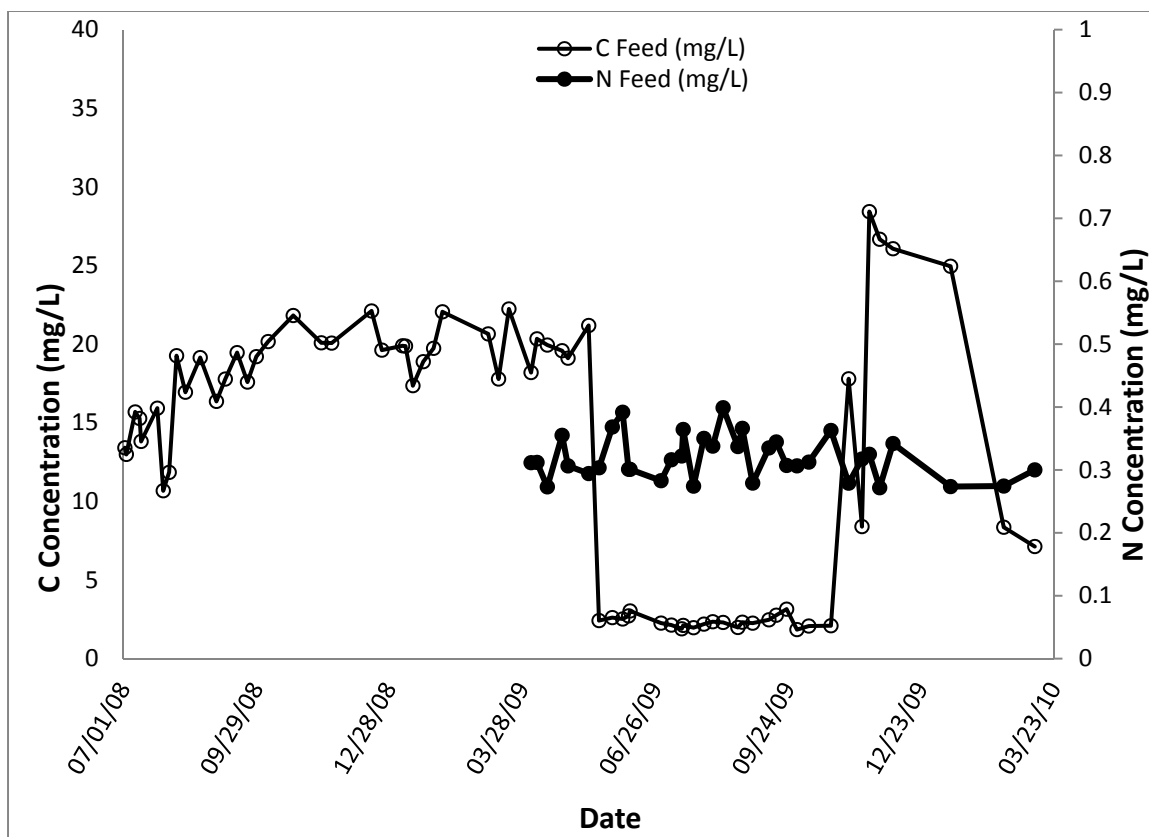


Figure 6-2 Temporal profile of the concentration of DOC and TN in the plant feed-water

Upon closer examination, it was found that the period of low DOC concentration correlates well with a period of high rain fall (Figure6- 4). The monthly precipitation data, measured in Dunedin, were provided by the water plant. From the temporal profile of the SUVA of the plant feed-water (Figure 6-3), it can be seen that the SUVA for the feed-water was low, with the exception of the 6 month period where the feed-water DOC dropped. The high SUVA values suggest that the ratio of aliphatic carbon to aromatic carbon decreased during this time period, with a corresponding decrease in biodegradability [113, 121].

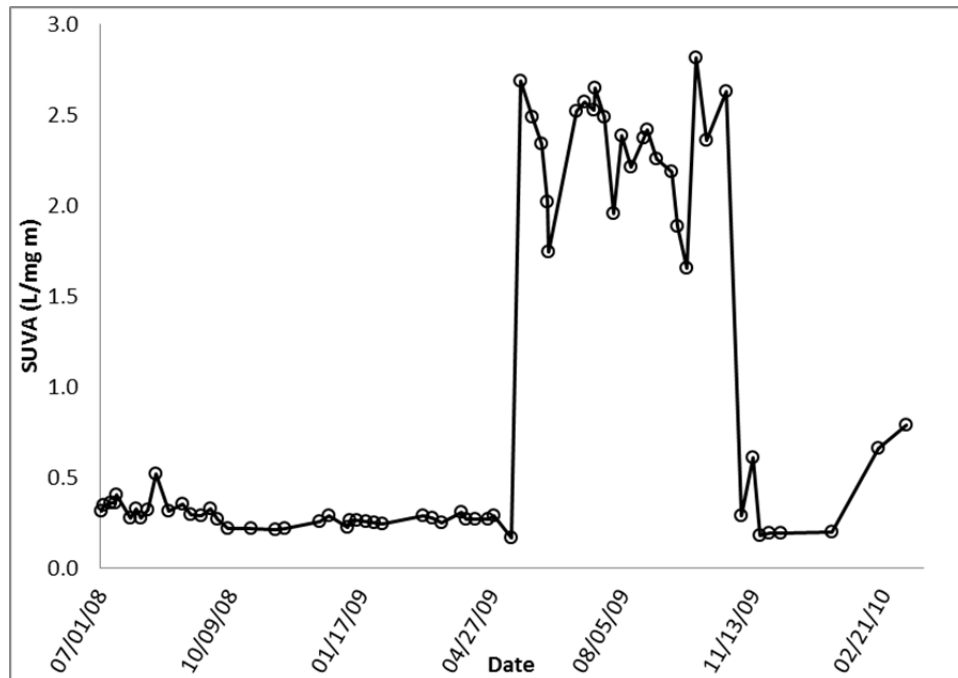


Figure 6-3 Temporal profile of calculated SUVA of the plant feed-water

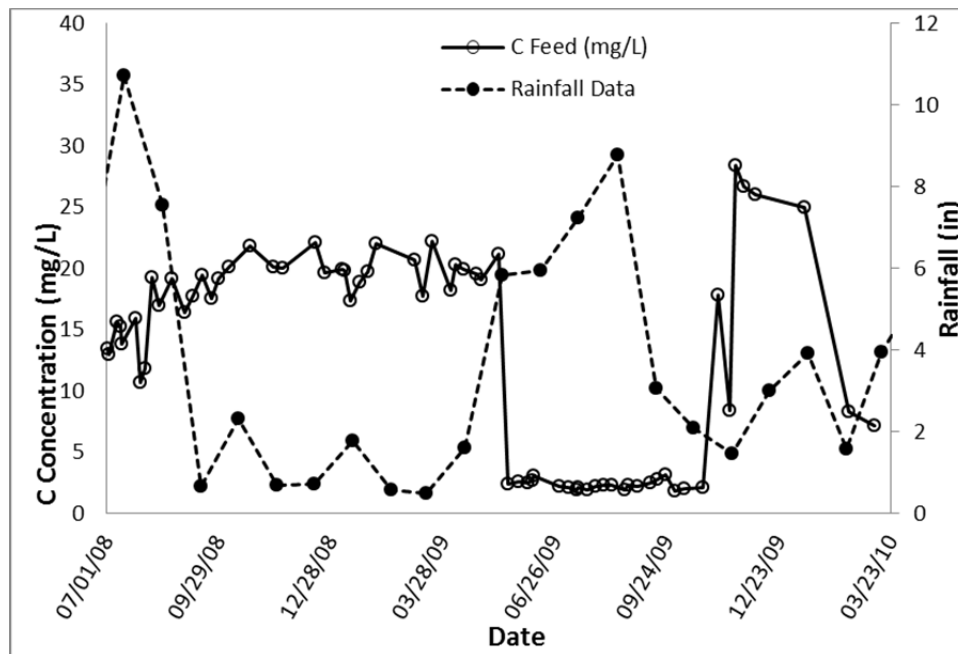


Figure 6-4 Temporal profiles of the concentration of DOC in the plant feed-water and monthly precipitation

When the feed SUVA is plotted as a function of feed DOC (Figure 6-5), it can be seen that SUVA decreases with increasing DOC concentration, with high SUVA associated with DOC concentrations less than 5 mg/L and a stable region of low SUVA values of 0.2 – 0.5 L/mg-m above a DOC concentration of 10 mg/L. The above correlation, coupled with the rainfall data, give rise to a possible explanation that this period of high rainfall triggered increased microbial activity in the aquifer, thereby degrading the organic carbon and preferentially removing the more labile aliphatic portions. The result is lower DOC concentration coupled with higher SUVA for this 6 month period.

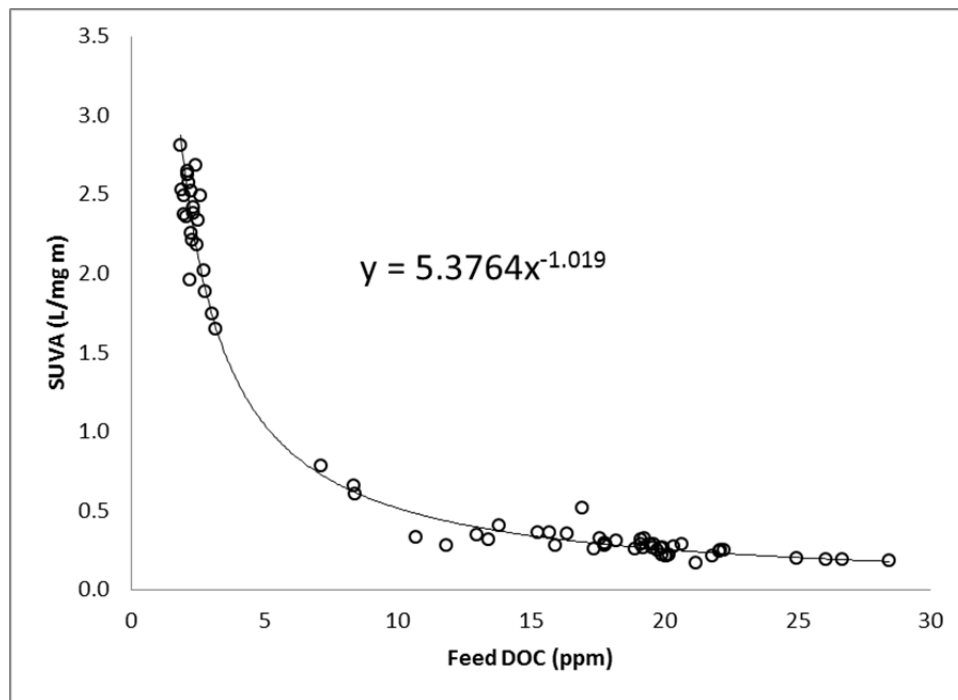


Figure 6-5 SUVA of the plant feed-water plotted as a function of plant feed-water DOC

The percent DOC removed from the system was consistently positive (Figure 6-6), although a few data points do fall below into the negative range. These negative data

points are likely due to contamination of the concentrate sample, possibly from sloughing of material from the membrane surfaces or plumbing. The majority of the data show positive removal of DOC from the system, indicating a likely sink for the organic carbon. The average removal of DOC from the RO process was $12.5 \pm 10\%$. The high variability of the data was likely due to variability in the RO system as well as variability in feed-water DOC composition and concentration coming into the plant.

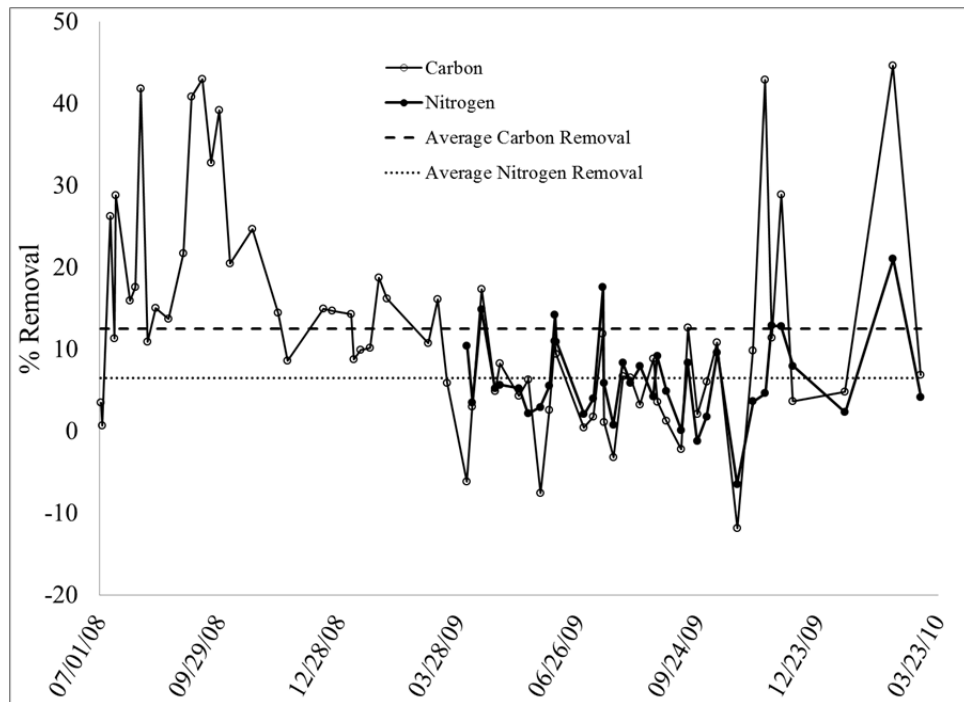


Figure 6-6 Temporal profiles of percent removal of DOC and TN from RO treatment train

When the percent removal of DOC was plotted against unit loading (in g DOC per m² membrane in operation per day, based on actual number of skids in operation that day), two distinct regions of the graph are observed (Figure 6-7 top). The first region coincides

with low carbon loading, and little to no removal is seen in this region. The second region displays a trend of decreasing removal percentage with increasing loading, with a maximum removal around a unit loading of $40 \text{ g/m}^2 \text{ day}$. When the mass of DOC removed per unit area is plotted against unit loading (Figure 6-7 bottom), the same two regions are apparent. The region of low unit loading of DOC displays little removal of DOC, while the second region of higher unit loading of DOC displays a consistent removal range of approximately $1\text{-}4 \text{ g C/m}^2 \text{ day}$ which did not correlate with increasing unit carbon loading. When a one-tailed t test was performed on this region of the graph, it resulted in a statistically significant positive removal of DOC during the treatment process with greater than 99.5% confidence. The graphs in Figure 6-7 assume that biofilm is present on the entire membrane surface throughout the treatment train, equally contributing to the removal of DOC. If only the lead element of the first stage were active in DOC removal (as suggested by previous autopsy results), then the range of carbon mass removal could be as high as $10\text{-}40 \text{ g C/m}^2 \text{ day}$. Since the actual mass of biofilm on the membrane surface throughout the entire treatment plant is not known, the actual removal range of DOC per unit area is only known to fall somewhere between these extremes (from $1\text{-}4 \text{ g C/ m}^2$ to $10\text{-}40 \text{ g C/m}^2 \text{ day}$).

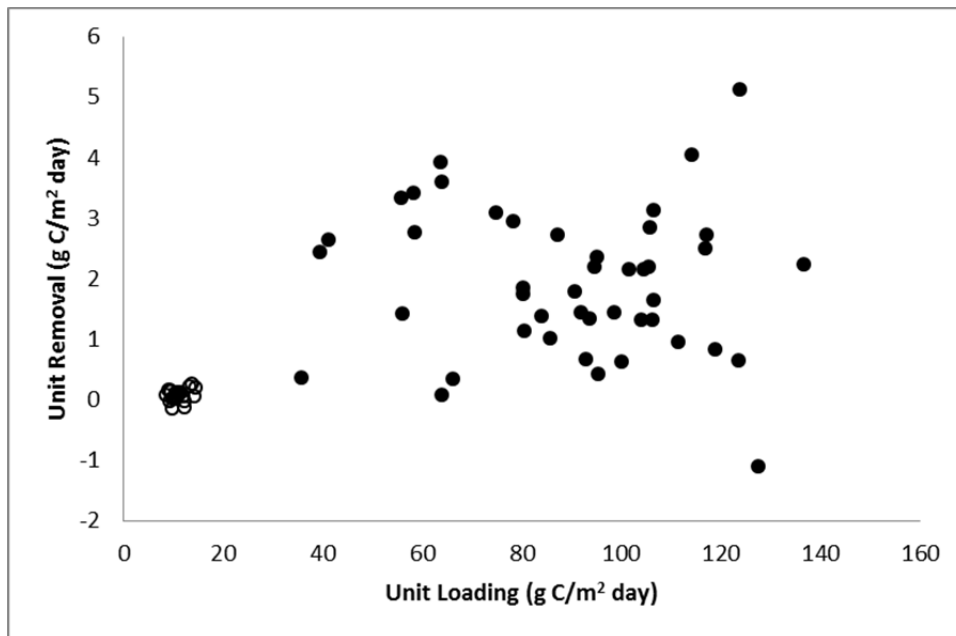
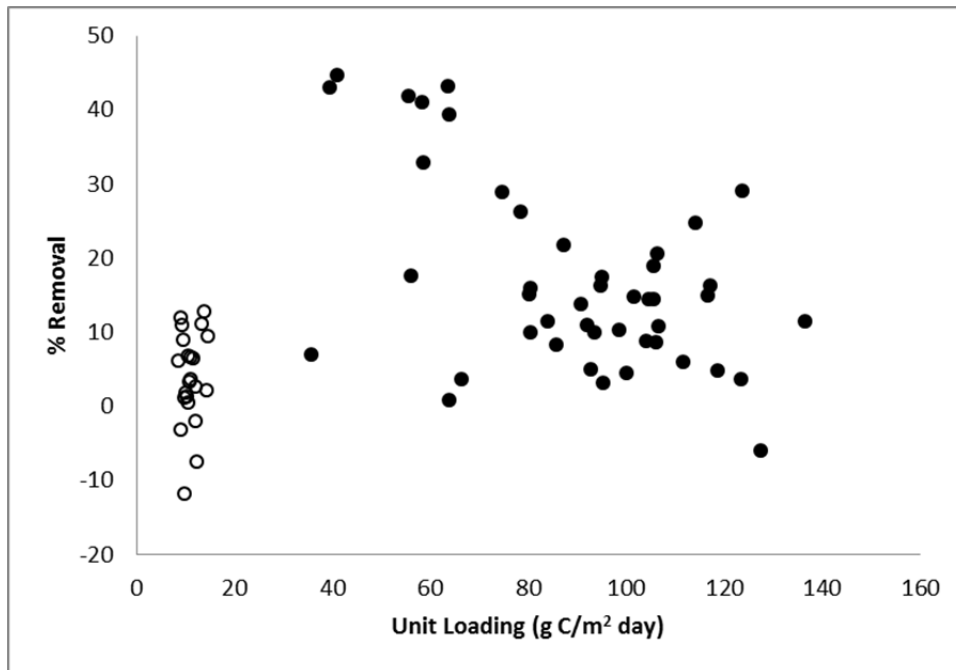


Figure 6-7 Removal of DOC within the RO treatment train plotted against the unit DOC loading based on the total membrane area in operation at the time of sampling top) percent removal of DOC and bottom) unit removal of DOC

The percent change in SUVA was also consistently positive (Figure 6-8). A one tailed t test of these data indicates this positive increase observed graphically is statistically significant with greater than 99.5% confidence.

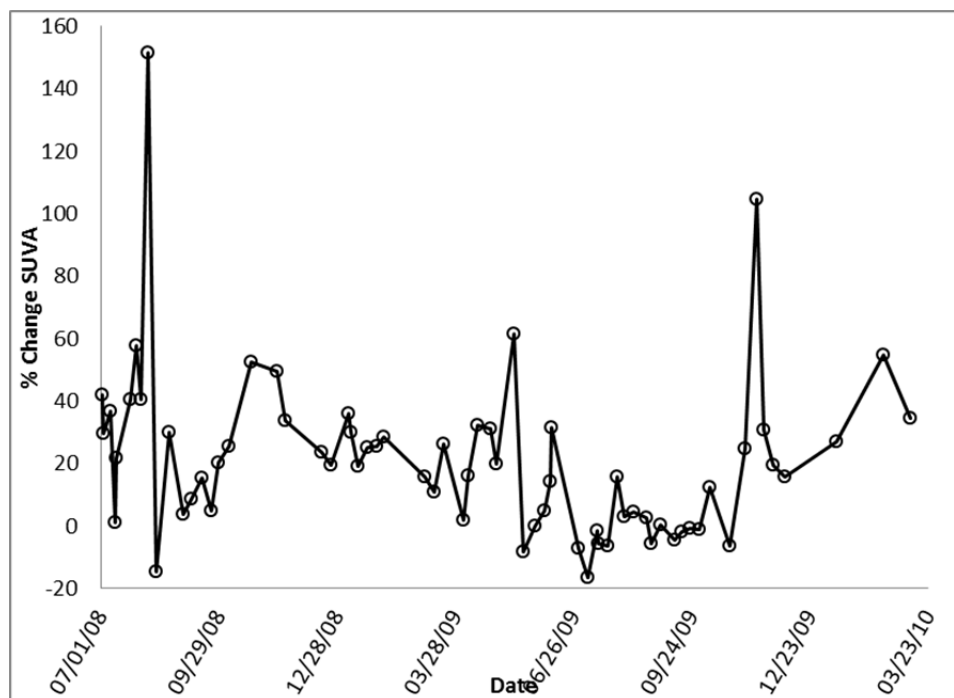


Figure 6-8 Temporal profile of the percent change in SUVA from feed-water to concentrate

This observed increase in SUVA suggest an increase in the aromatic character of the organic carbon dissolved in the water. This change in character of the organic carbon, as measured by SUVA, is seen in systems where biodegradation plays a role [113, 121]. Likely, the smaller molecular weight aliphatic and more biodegradable carbon molecules were removed from the system [112]. Some of the data points show no change or a small decrease in the SUVA during treatment. Many of these points coincide with the region of

relatively low influent DOC concentration (Figure 6-2), and relatively high values of SUVA for the influent water (Figure 6-3). These data suggest that the smaller aliphatic carbon molecules, and thus more easily assimilable or biodegradable matter, are being removed from the treatment water during the RO process. Additionally, when the concentration of easily assimilable or biodegradable organic carbon is low, the removal was also low. Examining Figures 6-3 and 6-6 together, it can be seen that the periods of high feed-water SUVA (hence aromaticity) correlated with periods of low DOC removal.

The percent removal of TN from the plant was also monitored over time. The TN concentration in the feed-water remains relatively unchanged at concentration of approximately 0.3mg/L (Figure 6-2). Additionally, the percent removal of TN in the plant was also consistently positive (Figure 6-6). The average removal of TN from the RO process was $6.5 \pm 5\%$. Variability was also seen with the removal of TN; however, the TN concentration in the plant feed-water did not exhibit the same variability as did the DOC concentration. These data indicate a sink for TN in the system in addition to or in conjunction with DOC removal.

The results of prior autopsies performed on membrane elements from the City of Dunedin indicated that there is significant growth of bacterial biofilm on the membrane surfaces [85, 86]. This growth exists as a gradient, with a much higher concentration of biofilm and a distinct community structure (less diverse, more growth, statistically different from feed-water microbial community) at the front portion of the lead membrane element [84]. The data discussed above indicate a sink for the organic carbon

and nitrogen in the treatment plant. This data, paired with the SUVA data, which denote the smaller aliphatic carbon is being removed and the remaining carbon has an increased aromatic character, suggest the biofilm present on the membrane surfaces was responsible for the removal of the DOC and TN observed. Based on these observations, the following hypothesis was made. The organic carbon and nitrogen removed from the system functions as a food source for heterotrophic bacteria, thus resulting in an overall reduction in the mass of organic carbon and nitrogen from the system. Since the organic carbon removed is likely the smaller aliphatic carbon, and thus the more easily biodegraded carbon, the biofilm on the surface of the membranes may indeed be functioning as an *in situ* biofilter which may have a protective effect against fouling for downstream membrane surfaces. This is observed in the relatively high biofilm concentration at the front portion of the membrane element and the relatively low biofilm concentration at the end portion of the lead membrane element[84]. Furthermore, the removal efficiency ranges of approximately 5-45% DOC observed in the membrane system is comparable to reported ranges of 5-15% [77], 16-33% [126], and 35-45% [81]. Additional carbon balance information on the plant level and on the individual skid level is in Appendix D.

6.5 Conclusions

From the plant-wide mass balance of DOC and TN, there is an observed reduction in the total mass of organic carbon ($12.5 \pm 10\%$) and nitrogen ($6.5 \pm 5\%$) from the system. There is also an increase of SUVA (20-30%) in the feed-water after traveling through the pressure vessels and exiting as concentrate, thus an increase in aromatic character of the

organic carbon remaining. These data indicate a sink for the organic carbon and nitrogen in the system, possibly by the biofilm growing on the surface of the membranes. Previous autopsy results indicated a gradient of biofilm growth on the membrane surface, with higher concentrations of biofilm at the front end. In order to further elucidate the role of membrane-associated biofilm in removing organic carbon from the feed-water, a single-element pilot system has been built at the Dunedin water treatment plant. The system is capable of complete data acquisition to monitor system conditions. The pilot system uses the same 8½” elements used for water production at the Dunedin plant, as well as flat sheet modules for non-invasive testing of the membranes. This system will allow for more detailed carbon mass balance and direct test of the role of lead element biofilm in reducing downstream fouling propensity.

Chapter 7 Pilot System Analysis of Biofilm Effect on Downstream Membrane Material

7.1 Introduction

The gradient pattern of foulant formation observed (Chapter 5) and the removal of organic carbon in a RO treatment plant (Chapter 6) suggest the potential of biofilm on the surface of the membrane to act as an *in situ* biofilter to protect downstream membrane surfaces. If the biofilm on the lead membrane surface can be used as an *in situ* biofilter, differences in fouling should be observed between the front and end portions of the membrane. Additionally, the protective effect should be quantifiable and be dependent on carbon concentration in the treatment water. This protective effect should be visible in both fouling characteristics, including quantity on the membrane surface, and in the performance of the membranes themselves. A pilot system was built to study the effects of biofilm on the surface of a membrane element on membrane surfaces downstream. The details of the pilot system are in Section 7.2 and Appendix C.

7.2 Pilot Design and Testing

A pilot system was designed to test the effect of the membrane and the foulant on its surface on membrane material downstream. This was accomplished by building a pump-driven system fed by a 150 gallon feed tank with an 8½” single element pressure vessel (from Department of Reclamation, AZ), Figure 7-1 (details of system diagram and pilot

operation are available in Appendix C). An actual fouled element (serial number SE24427) was taken from Skid IV, Stage I, pressure vessel 21 at the same time as the first membrane autopsy (31 Mar 2010) and placed into single element pressure vessel so the approximate initial conditions of the biofilm on the membrane surface would be known for the pilot system (Chapter 5). Operation of the pilot system under zero external carbon loading conditions commenced from this time. Additionally, the flow rate and carbon loading rate to the system were varied to investigate their effects on performance and fouling.

The feed, permeate, and concentrate pressures of the system were monitored using pressure transducers. The Feed flow rate was kept constant and set using an analog flow meter. The concentrate flow was monitored using a GPI industrial grade digital flow meter (model# G2S15N09), and the permeate flow was calculated by subtracting the concentrate flow rate from the feed flow rate. The temperature of the system was kept constant at 25°C using a TempTek CF Series 1.5 ton air cooled portable chiller. The data collected from the detectors above were recorded using HOBO U30 data loggers. The data were exported into Excel spreadsheets for analysis.

The pilot system was operated for a 35 week period. In order to better understand the effect of carbon concentration in the feed water on the biofilm growth, the pilot system evaluation was divided into two distinct sub-phases, no carbon addition to pilot system and carbon addition. This length of time encompassing the period of zero external carbon loading to the pilot system was 17 weeks long and extended from 31 Mar 2010 to

26 Jul 2010. The pump malfunctioned at the end of this portion of the study and had to be rebuilt, causing the system to be down for approximately one month. The carbon loading portion of the study was 18 weeks long and extended from 23 August 2010 to 03 Jan 2011. This portion of the study encompassed periods of carbon loading of 0.1, 0.5, and 2 g/m²day. Each period of carbon loading was 6 weeks long, with 3 weeks performed at a flow rate of 50 GPM and 3 weeks at a flow rate of 25 GPM (the concentration of carbon loading increases chronologically).

The foulant deposition and formation on the surface of the membrane swatches for the pilot system were monitored for the feed and concentrate flat sheet modules for the entire duration of operation. In addition to characterizing the foulant material deposited and/or formed on the membrane surfaces, the performance of the membrane swatches was also characterized by monitoring the transmembrane pressure and the permeate flux. Comparison of these measurements between the feed and concentrate sides of the pilot membrane pressure vessel allow for an evaluation of the effect of the biofilm on the performance of downstream membrane material. The results from the foulant analyses as well as the performance characterization of the flat sheet modules are presented in the following sections.

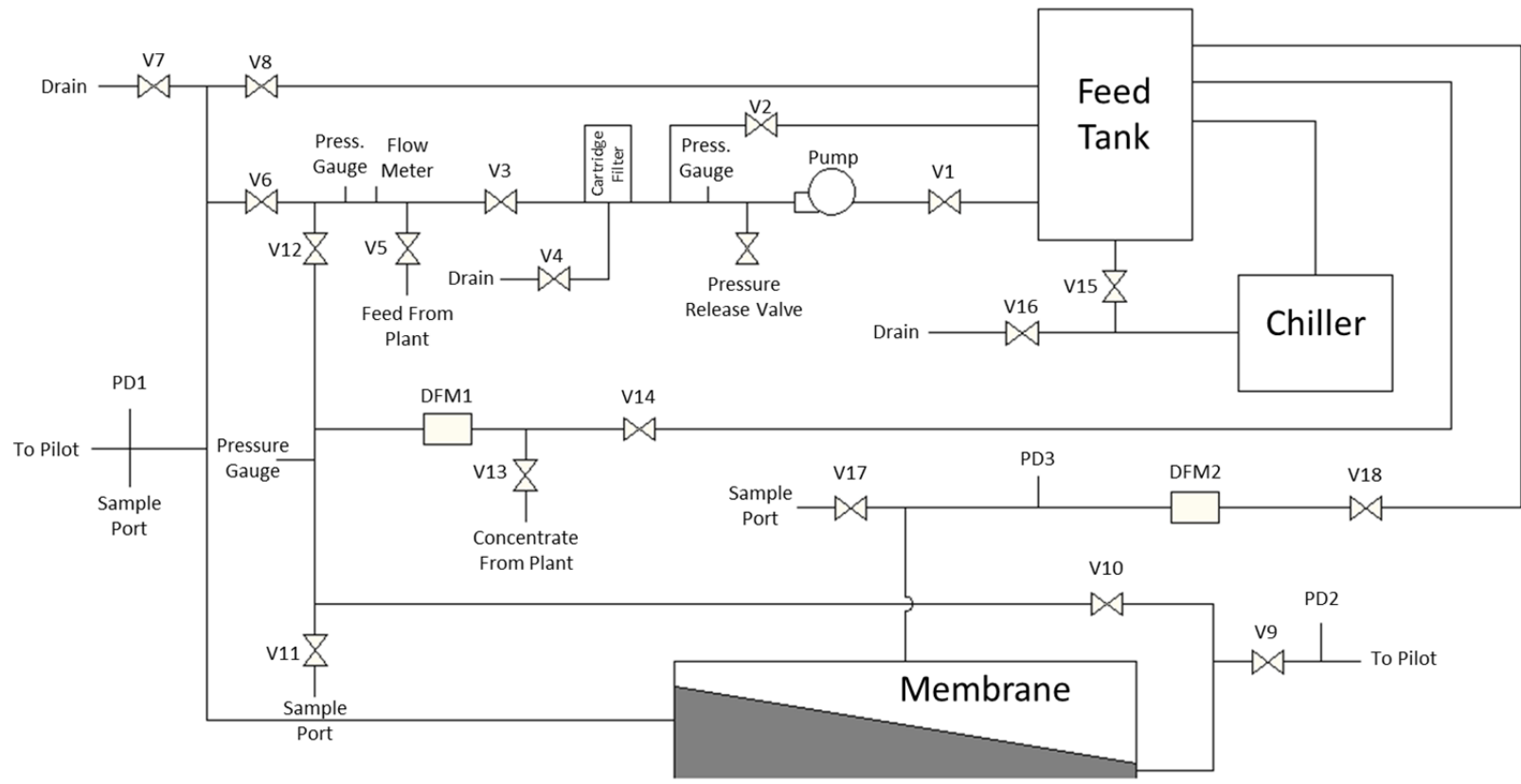


Figure 7-1 Schematic of pilot system

In order to non-destructively sample the membrane surface to determine what the effect of the pilot element biofilm is on the downstream membrane material, water from the pilot feed and the pilot concentrate was passed over four flat sheet modules each. The flat sheet modules are from Sterlitech, model number CF042, containing a 1.800" x 3.625" (42cm²) active area of membrane material, Figure 7-2. These membrane swatches are easily removed for destructive analysis without disturbing the 8½" membrane element.

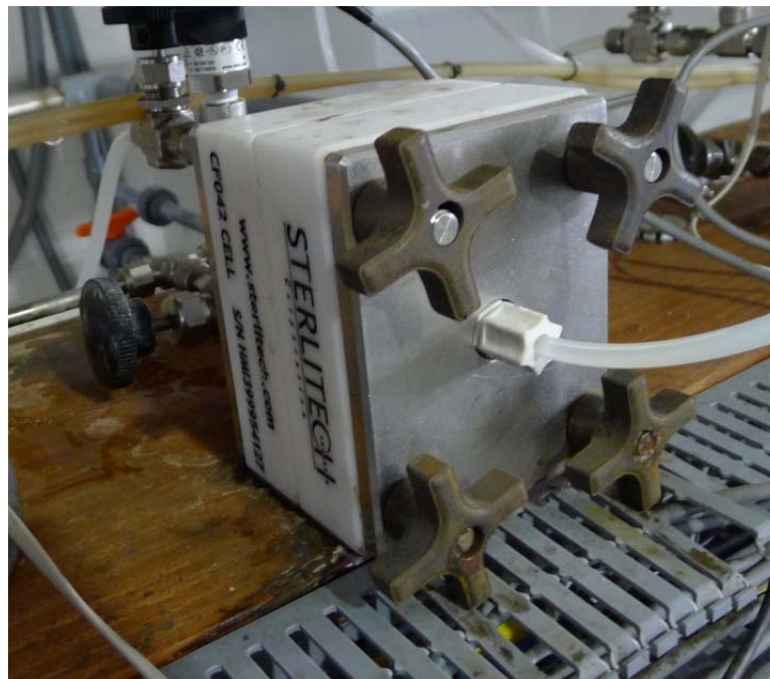


Figure 7-2 Sterlitech Flat Sheet Module

The flat sheet modules at the feed and concentrate portion of the 8½" membrane element were arranged identically as four parallel units with a pressure transducer and an analog flow meter on the concentrate portion of each flat sheet module, a La Crosse (model number WS-2310-16 or TX32U-IT) rain gage was used to collect permeate flow data.

Valves were used to regulate flow, Figure 7-3. Details of the flat sheet module portion of the pilot system are in Appendix C.

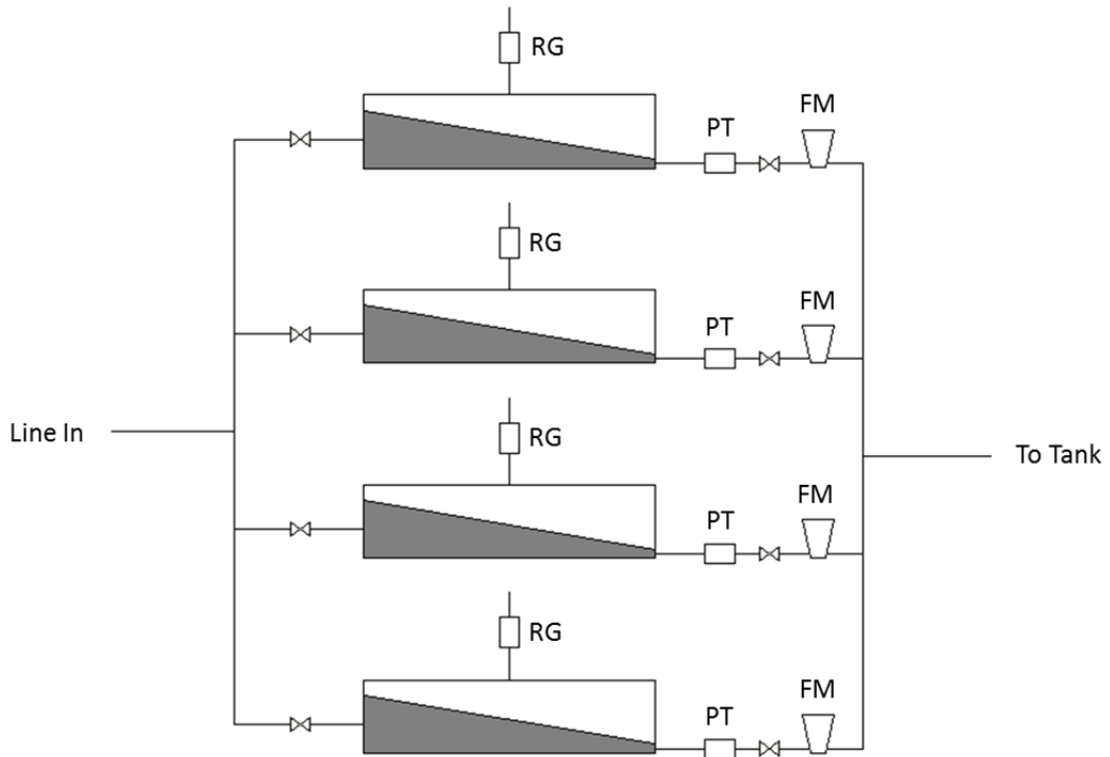


Figure 7-3 FSM portion of pilot system

7.2.1 Membrane Sampling

The pilot system was shut down and membrane swatches in specified flat sheet modules were removed and replaced. The membrane swatches were taken for analysis from each of the feed and the concentrate pilot streams once per week. The analyses performed on the membrane swatches include protein and carbohydrate concentration, total direct count, heterotrophic plate count, Fourier transform infrared spectroscopy, and microscopic evaluation (scanning electron microscopy and atomic force microscopy). Details of these analyses are in section 3.3.

7.2.2 Zero External Carbon Loading

In order to simulate actual treatment conditions at the Dunedin RO treatment plant as closely as possible, the feed tank was filled to approximately 145 gallons with feed water and refreshed biweekly. The flow rate and pressure of the system were set to 50 GPM and approximately 120psig respectively. One membrane swatch was taken from the feed portion of the pilot and one swatch was taken from the concentrate portion of the pilot for analysis weekly from 07 April 2010 to 26 July 2010.

7.2.3 Carbon Loading

In order to reliably pump a known concentration of carbon into the pilot system feed tank, a peristaltic pump (Cole Palmer Masterflex model number 7553-79) was used to pump a glycerin solution from a 5 gallon bucket into the feed tank. The flow rate of the peristaltic pump was determined by pumping water over a known period of time and measuring the volume pumped. The volume pumped was 790mL over a 270 minute time, giving a flow rate of 2.93 mL/min (1.11 gal/day). The contents of the bucket containing the glycerin solution for carbon loading were refreshed biweekly. The amount of glycerin required to give the desired carbon loading was calculated for each point.

The glycerin concentration in the bucket to give a carbon feed rate of 0.1 g C/m²day was determined as follows:

$$\text{glycerin concentration} = \left(\frac{0.1 \text{ g C}}{\text{m}^2 \text{ day}} \right) \left(\frac{37.2 \text{ m}^2}{\text{membrane}} \right) \left(\frac{1 \text{ day}}{1.11 \text{ gal}} \right) \left(\frac{1 \text{ g glycerin}}{0.3913 \text{ g C}} \right)$$

This gives a glycerin concentration of 8.56 g/gallon, or 42.8g glycerin in 5 gallons. To determine the glycerin concentration for a carbon feed rate of 0.5 g C/m²day, the following calculation was performed:

$$\text{glycerin concentration} = \left(\frac{0.5 \text{ g C}}{\text{m}^2 \text{ day}} \right) \left(\frac{37.2 \text{ m}^2}{\text{membrane}} \right) \left(\frac{1 \text{ day}}{1.11 \text{ gal}} \right) \left(\frac{1 \text{ g glycerin}}{0.3913 \text{ g C}} \right)$$

This gives a glycerin concentration of 42.8 g/gallon, or 214.1g glycerin in 5 gallons. To determine the glycerin concentration for a carbon feed rate of 2.0 g C/m²day, the following calculation was performed:

$$\text{glycerin concentration} = \left(\frac{2.0 \text{ g C}}{\text{m}^2 \text{ day}} \right) \left(\frac{37.2 \text{ m}^2}{\text{membrane}} \right) \left(\frac{1 \text{ day}}{1.11 \text{ gal}} \right) \left(\frac{1 \text{ g glycerin}}{0.3913 \text{ g C}} \right)$$

This gives a glycerin concentration of 171.3 g/gallon, or 856.5 g glycerin in 5 gallons. Two membrane swatches were taken weekly from each the feed portion and the concentrate portion of the pilot from 30 August 2010 to 03 January 2011. The flow rate for the pilot system was alternated between 25 and 50 GPM for each carbon loading condition. This was done to test if flow rate has an effect on the relative fouling and performance between the feed and concentrate membrane swatches.

7.3 Results

7.3.1 Surface Fouling Characterization

The amount and type of foulant on the membrane surface is an essential part of this study. Additionally, the relative amount of foulant on the feed and concentrate membrane surfaces yields important information on the effect of the pilot element biofilm on downstream membrane surfaces.

7.3.1.1 Zero External Carbon Loading

The pilot system was initially operated with plant feed-water only, refreshing the feed tank on a biweekly basis. This was performed in order to simulate plant treatment conditions as closely as possible. A feed tank was used for recirculation in order to run the pilot continuously, since the plant staggers operation hours. Details on the operation of the pilot system from the period of zero external carbon loading are in Appendix C.

The composition of the foulant material was characterized by measuring protein and carbohydrate concentrations, total direct count, and total culturable microorganisms (HPC) per unit area of membrane surface. The foulant and membrane surface was further characterized using energy dispersive spectroscopy and attenuated total reflectance Fourier Transform infrared spectroscopy. Additionally, the membrane surface was visualized through SEM and AFM, which allowed for qualitative evaluation of the membrane surface and any foulant material present. AFM also yields a quantitative measurement of surface roughness. Details on the methods and procedures for these characterization techniques are in section 3.3. These analyses were performed

on a weekly basis for selected membrane swatches. The results for the swatches taken from the feed side modules were compared to the swatches from the concentrate to evaluate differences in the foulant material. The results for the fouling characterization and the performance analysis of the zero external carbon loading portion of the pilot study are reported in this section.

7.3.1.1.1 Protein and Carbohydrate Data

The concentration of proteins and carbohydrates on the feed and concentrate membrane swatches were measured as per the methods in section 3.3. The results of these analyses along with their respective standard deviations are in Table 7-1. This table also contains the carbohydrate/protein ratio data for the feed and concentrate swatches.

Table 7-1 The protein and carbohydrate concentrations of the pilot feed and concentrate swatches for the zero external carbon loading portion of the study

Date	Protein concentration ($\mu\text{g}/\text{cm}^2$)				Carbohydrate concentration ($\mu\text{g}/\text{cm}^2$)			
	Feed		Concentrate		Feed		Concentrate	
	Avg	Stdev	Avg	Stdev	Avg	Stdev	Avg	Stdev
4/7/2010	45.2	0.3	35.0	1.6	2.9	1.5	6.6	1.8
4/14/2010	63.1	2.6	62.9	2.9	20.5	4.5	25.7	2.7
4/20/2010	55.9	3.4	60.7	5.6	17.4	1.7	23.2	2.1
4/27/2010	56.8	3.6	56.7	3.5	17.8	4.4	18.7	2.9
5/4/2010	89.3	0.4	75.1	0.4	27.9	1.4	23.1	1.0
5/11/2010	75.7	0.3	74.3	0.3	27.6	2.5	30.4	1.8
5/18/2010	45.8	0.2	43.0	0.1	13.0	1.2	12.4	1.5
5/25/2010	10.5	1.4	12.9	1.2	8.3	0.1	9.5	0.3
6/1/2010	80.6	5.1	73.0	1.6	22.6	2.1	22.3	0.7
6/7/2010	60.3	1.0	60.6	2.2	31.2	0.7	27.8	0.8
6/14/2010	59.1	2.9	72.7	1.5	26.3	1.9	29.9	0.6
6/21/2010	70.9	1.2	32.6	2.1	29.7	2.3	10.3	0.1
6/28/2010	31.4	2.8	46.1	2.4	11.2	0.7	16.5	0.7
7/5/2010	54.0	1.6	47.9	2.8	21.6	1.7	20.3	2.3
7/12/2010	46.1	0.8	70.4	1.8	20.1	0.9	29.8	1.4
7/19/2010	61.2	0.6	63.4	1.5	32.6	3.9	29.3	1.2
7/26/2010	47.6	4.2	41.5	4.6	18.2	1.3	16.6	1.6

The temporal profile of protein concentration on the feed and the concentrate membrane swatches listed in Table 7-1 above is graphed in Figure 7-4. This graph displays fluctuation in the protein concentration on the membrane surfaces, but no trend is evident over time. The carbohydrate concentration on the feed and concentrate membrane swatches listed in Table 7-1 above are graphed as a function of sampling date in Figure 7-5. As with the protein concentration, there is a fluctuation apparent in the data, but there is no discernible trend.

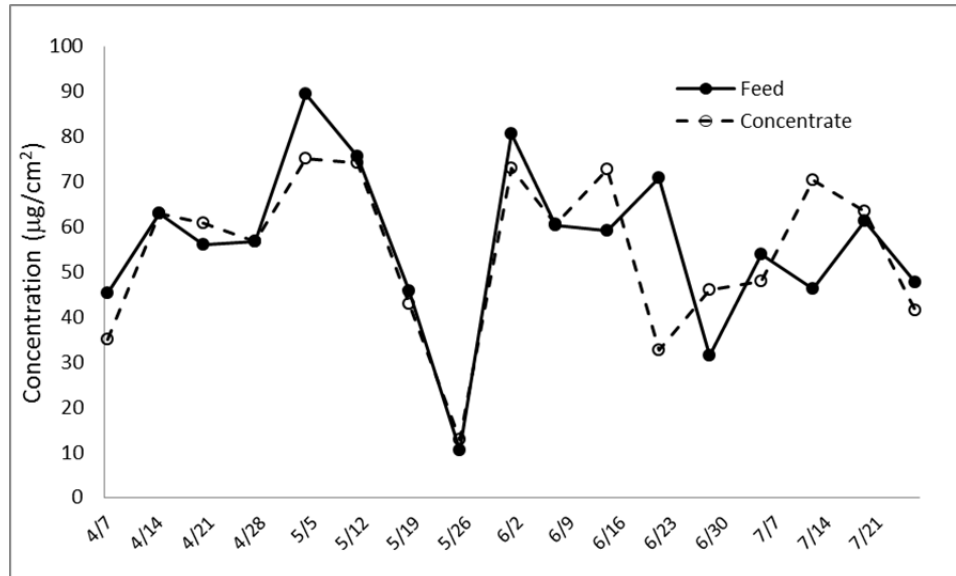


Figure 7-4 Time function of protein concentration on pilot feed and concentrate swatches

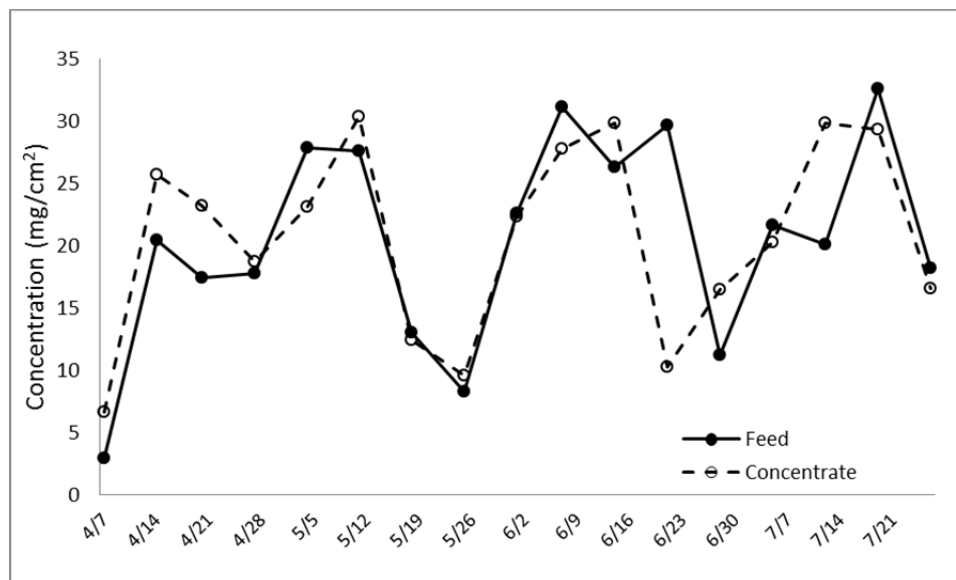


Figure 7-5 Carbohydrate concentration on pilot feed and concentrate swatches as a function of sampling date

Although the total amount of proteins and carbohydrates displayed no discernible trend as a function of sampling date when visually inspecting the curves, the overall

feed/concentrate ratio of these concentrations is of interest. A ratio greater than 1 indicates a larger proportion of that material on the feed, indicating the feed is experiencing more severe fouling. However, a ratio less than 1 indicates a larger proportion of that material on the concentrate, indicating more severe fouling for the concentrate. The feed/concentrate ratio data for protein and carbohydrate concentrations are in Table 7-2.

Table 7-2 The carbohydrate/protein for the feed and concentrate swatches and the feed/concentrate ratio data for protein and carbohydrate concentrations

Date	Carb/Protein		Feed/Concentrate		Feed/Concentrate	
	Feed	Concentrate	Protein	Carb	Protein	Carb
	Average	Stdev	Average	Stdev		
4/7/2010	0.06	0.03	0.19	0.04	1.3	0.4
4/14/2010	0.33	0.08	0.41	0.03	1.0	0.8
4/20/2010	0.31	0.03	0.38	0.04	0.9	0.8
4/27/2010	0.31	0.06	0.33	0.07	1.0	0.9
5/4/2010	0.31	0.02	0.31	0.01	1.2	1.2
5/11/2010	0.37	0.03	0.41	0.02	1.0	0.9
5/18/2010	0.28	0.03	0.29	0.04	1.1	1.0
5/25/2010	0.80	0.11	0.74	0.07	0.8	0.9
6/1/2010	0.28	0.04	0.31	0.01	1.1	1.0
6/7/2010	0.52	0.02	0.46	0.01	1.0	1.1
6/14/2010	0.45	0.01	0.41	0.02	0.8	0.9
6/21/2010	0.42	0.04	0.32	0.02	2.2	2.9
6/28/2010	0.36	0.03	0.36	0.03	0.7	0.7
7/5/2010	0.40	0.04	0.43	0.07	1.1	1.1
7/12/2010	0.44	0.03	0.42	0.03	0.7	0.7
7/19/2010	0.53	0.06	0.46	0.03	1.0	1.1
7/26/2010	0.39	0.06	0.41	0.08	1.1	1.1

A statistical analysis was performed on the data in Table 7-2 to see if they indicate a significant difference in the amount of protein or carbohydrate for the feed and

concentrate swatches. This was accomplished by using a t-test on the average value of the feed concentrate ratio to see if it is significantly different than 1. The results of this test indicate no significant difference in the concentration of protein or carbohydrate on the feed and concentrate surfaces with a 95% confidence level (i.e. the value is not significantly different from 1), see Appendix E. The feed/concentrate ratio data from Table 7-2 are plotted as a function of sampling date for the protein and carbohydrate concentrations, Figure 7-6.

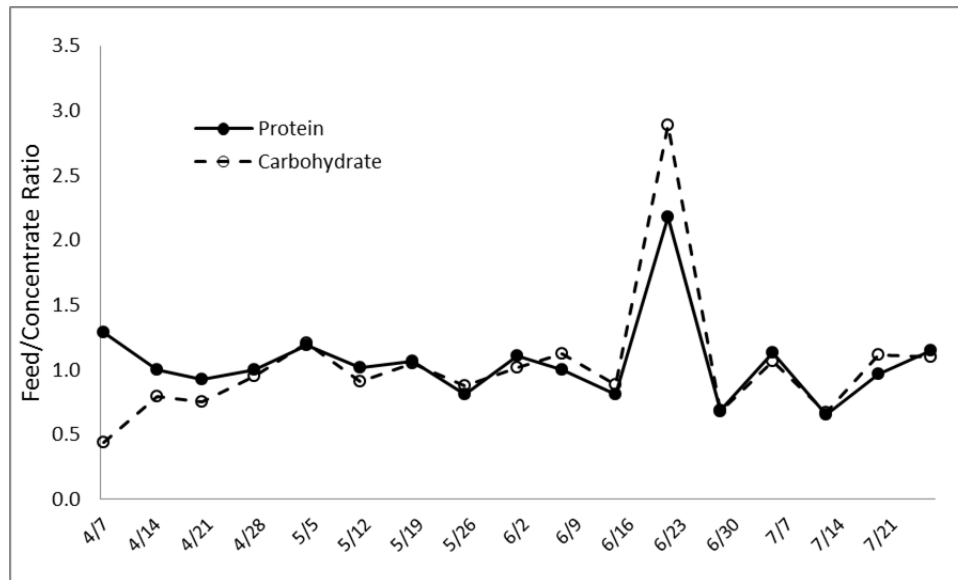


Figure 7-6 The feed/concentrate ratio for protein and carbohydrate concentrations plotted as a function of date sampled

The carbohydrate/protein ratio data for the feed and the concentrate pilot swatches are also in Table 7-2. These data indicate a carbohydrate/protein ratio of 0.4 ± 0.2 for the zero external carbon loading portion of the study. These data are represented graphically in Figure 7-7.

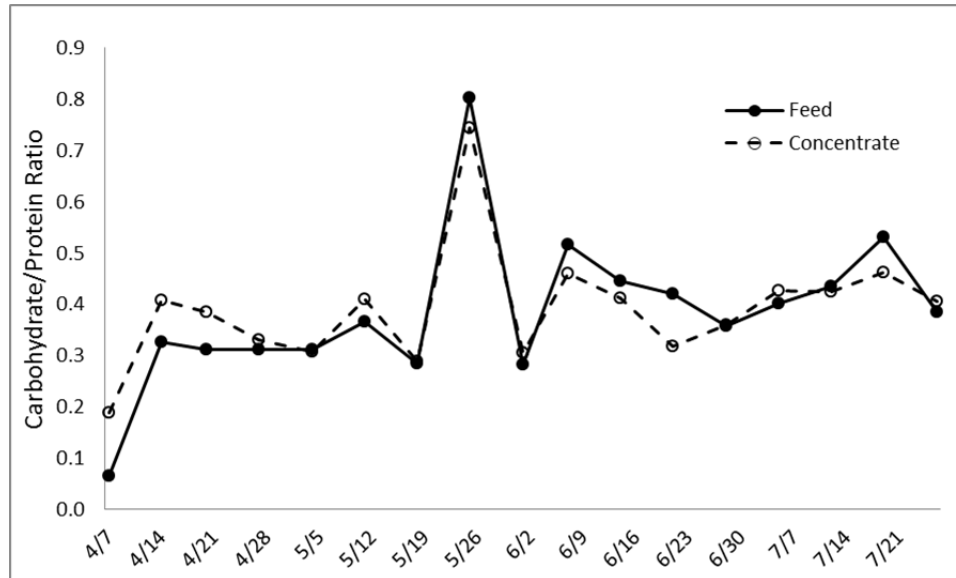


Figure 7-7 The carbohydrate/protein ratio for the feed an concentrate swatches of the pilot system

7.3.1.1.2 Microbiological Data

The total number of microorganisms (total direct count) was measured per unit area for the feed and concentrate swatches from the pilot system for the zero external carbon loading portion of the study, Table 7-3.

Table 7-3 Total direct count for feed and concentrate swatches and feed/concentrate ratio

Date	Feed (# x 10 ⁷ /cm ²)		Concentrate (# x 10 ⁷ /cm ²)		Feed/Conc
	Avg	Stdev	Avg	Stdev	
4/7/2010	2.40	1.0	1.13	0.53	2.1
4/14/2010	1.53	0.49	1.79	0.21	0.9
4/20/2010	3.17	0.72	2.71	0.40	1.2
4/27/2010	4.59	0.68	1.17	0.12	3.9
5/4/2010	8.76	0.65	5.85	0.76	1.5
5/11/2010	6.50	0.57	5.76	0.47	1.1
5/18/2010	3.88	0.69	2.79	0.54	1.4
5/25/2010	1.41	0.13	1.44	0.29	1.0
6/1/2010	9.16	2.5	7.41	0.60	1.2
6/7/2010	13.3	0.91	4.91	1.9	2.7
7/26/2010	9.94	1.5	8.83	1.1	1.1

The feed/concentrate ratio of microorganisms was 1.6±0.9. When analyzing this ratio using a t-test, there are significantly more microorganisms on the feed swatch than the concentrate with a 95% level of confidence, Appendix E.

The total number of culturable microorganisms (HPC) per unit area were measured on the feed and concentrate swatches of the pilot system. These data along with the feed/concentrate ratio are in Table 7-4.

Table 7-4 HPC data for the feed and concentrate swatches as well as feed/concentrate ratio data for these counts

Date	Feed (# x 10 ⁵ /cm ²)		Concentrate (# x 10 ⁵ /cm ²)		Feed/Concentrate
	Average	Stdev	Average	Stdev	
4/7/2010	-	-	-	-	-
4/14/2010	6.9	1.3	8.8	3.8	0.78
4/20/2010	1.1	0.44	1.2	0.12	0.95
4/27/2010	2.1	0.21	11	0.82	0.20
5/4/2010	14	1.5	18	4.5	0.77
5/11/2010	0.57	0.27	0.30	0.031	1.90
5/18/2010	2.5	0.11	2.4	0.17	1.05
5/25/2010	1.1	0.27	1.1	0.046	0.96
6/1/2010	12	1.4	7.6	0.51	1.57
6/7/2010	11	0.52	10	0.88	1.07
6/14/2010	18	1.6	25	1.8	0.72
6/21/2010	21	3.3	4.1	1.6	5.22
6/28/2010	0.32	0.070	4.8	0.36	0.07
7/5/2010	0.93	0.34	2.0	0.11	0.48
7/12/2010	2.5	1.1	7.8	5.5	0.32
7/19/2010	18	3.8	11	1.6	1.55
7/26/2010	-	-	-	-	-

The number of culturable bacteria per unit area on the feed and concentrate pilot swatches are represented graphically in Figure 7-8.

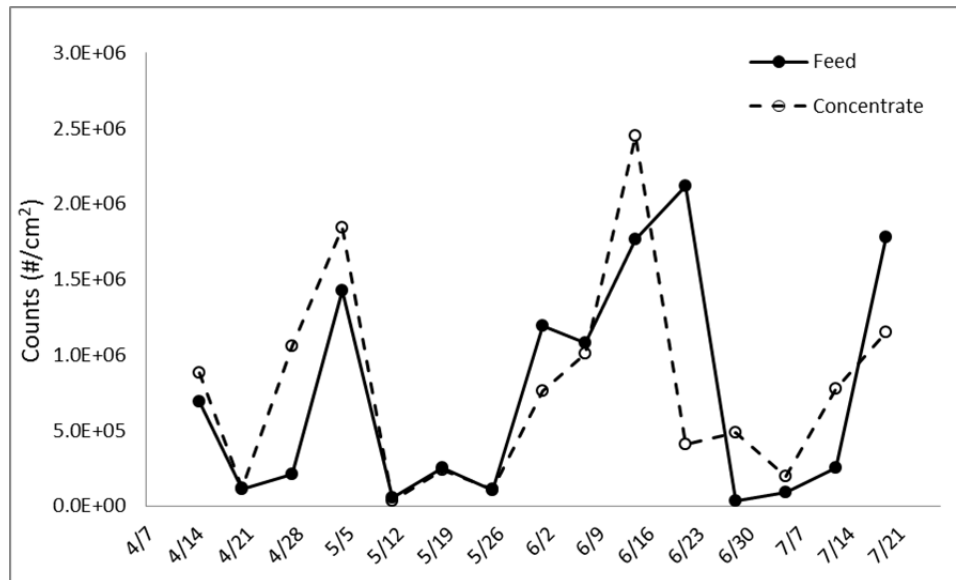


Figure 7-8 The number of culturable bacteria per unit area on the feed and concentrate pilot swatches

The graph in Figure 7-8 displays fluctuation in the number of culturable bacteria on the membrane surfaces for both the feed and the concentrate. As with the protein and carbohydrate, there is no trend evident over time. The feed/concentrate ratio data for HPC during the zero external carbon loading portion of the study were calculated, Table 7-4. This gives an indication of the relative number of culturable bacteria present on the membrane surfaces. Ratios greater than 1 indicate more culturable microorganisms on the feed surface, while ratios less than 1 indicate more culturable microorganisms on the concentrate surface. A t-test was performed on the data in Table 7-4, and the results indicate no significant difference with a 95% confidence level in the number of culturable bacteria present on the feed and concentrate surfaces from the zero external carbon loading portion of the study, Appendix E. The ratio data from Table 7-4 are plotted as a function of sampling date in Figure 7-9.

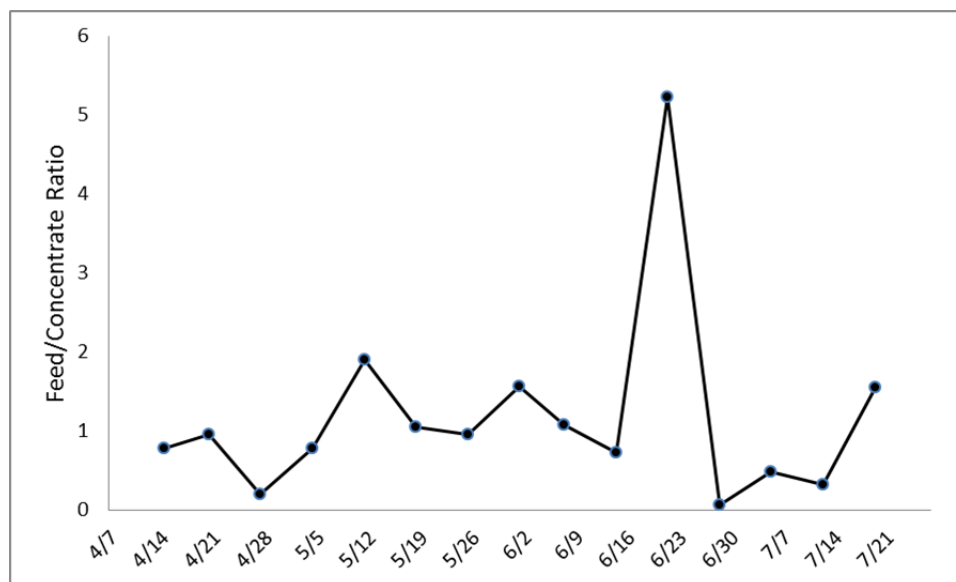


Figure 7-9 The feed/concentrate ratio of the number of culturable bacteria on the membrane surface

7.3.1.1.3 ATR-FTIR

Infrared spectra of the feed and concentrate membrane swatches from the zero external carbon loading portion of the study were obtained as per the methods in section 3.3. This analysis gives chemical information of the materials deposited on and/or grown on the surface of the membrane as well as the membrane material itself (assuming the foulant layer is thin enough). Example spectra of the feed and concentrate pilot swatches from this portion of the study are plotted from 4000-600 cm^{-1} along with virgin membrane material, Figure 7-10 (spectra from 01 Jun 2010). The foulant layer is apparent in these spectra, indicated by the amine and/or hydroxyl stretch at approximately 3300 cm^{-1} and the aliphatic stretch at approximately 2900 cm^{-1} .

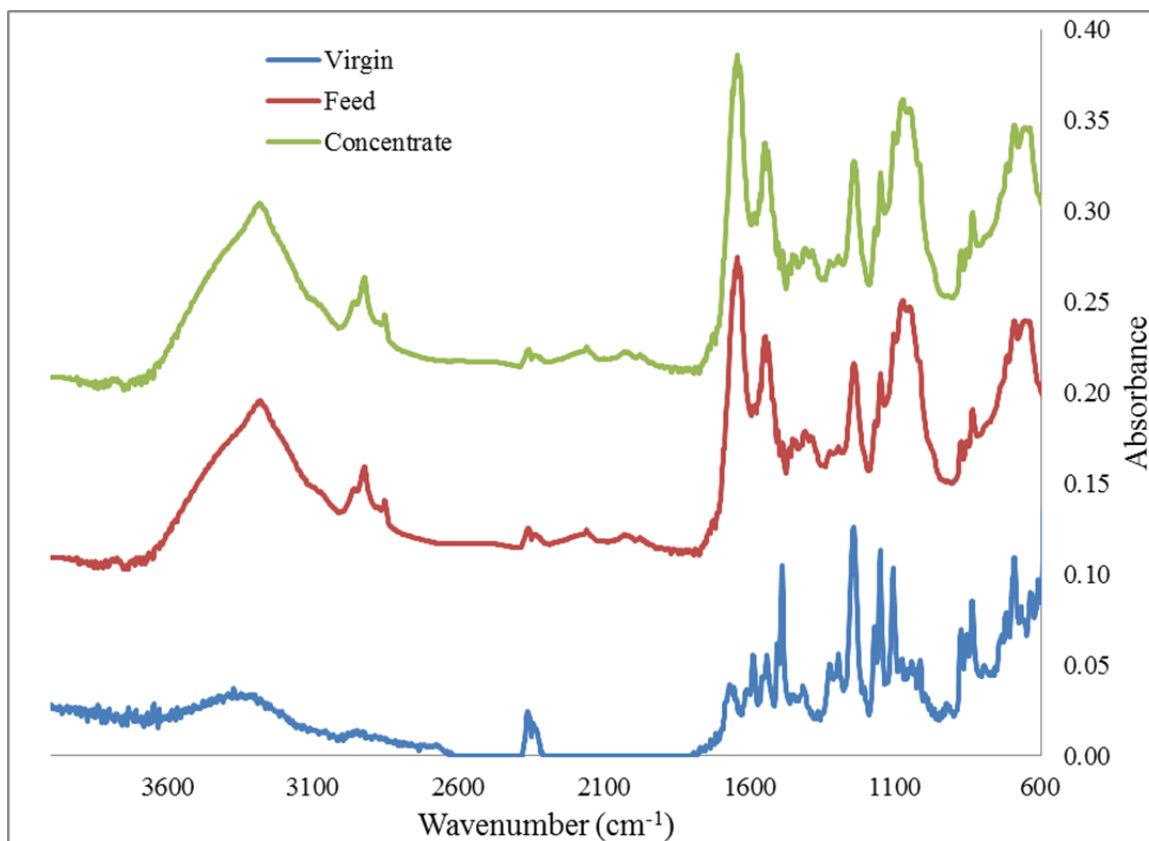


Figure 7-10 ATR-FTIR spectra for virgin membrane material and pilot feed and concentrate membrane swatches from the zero external carbon loading portion of the study

In order to more closely analyze the peaks from the 2000-600 cm^{-1} region, that area is expanded and the difference between the pilot sample spectrum and the virgin membrane material was taken, Figure 7-11. This method makes foulant peaks more readily apparent. The peaks that are visible in these spectra are the Amide I and Amide II peaks, approximately 1630 and 1530 cm^{-1} respectively, and carbohydrate CHO peak, approximately 1050 cm^{-1} . Differences in peak intensity indicating differences in concentration of foulant material are not readily apparent, indicating the foulant materials

either have approximately the same amounts of these foulants, or the foulant layer is too thick to indicate differences.

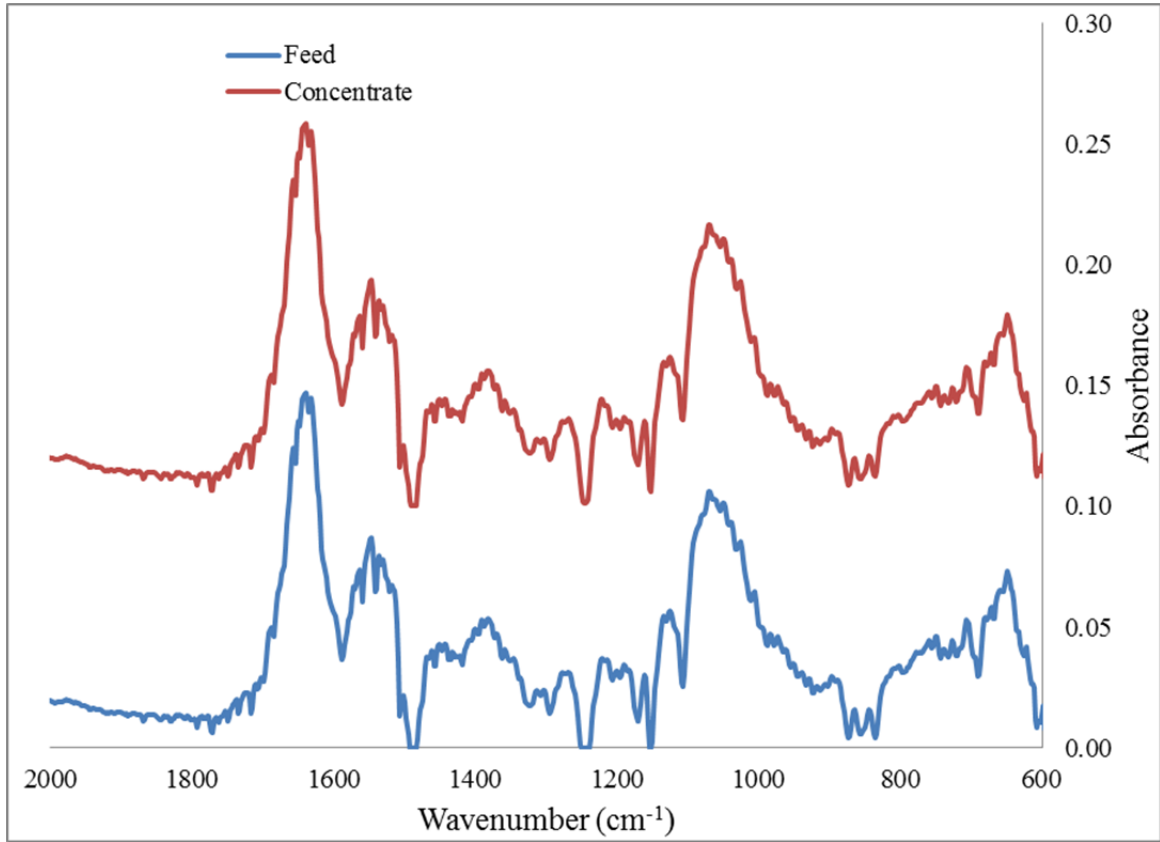


Figure 7-11 Difference spectra for pilot feed and concentrate

7.3.1.1.4 SEM-EDS

The surface of the membrane swatches were qualitatively analyzed using scanning electron microscopy with energy dispersive spectroscopy (SEM-EDS). Details on these analyses are available in section 3.3. The surface of the membrane swatches did not display a high level of fouling, although signs of biofilm formation were commonly observed on the surfaces of both the feed and concentrate swatches from the pilot system. Additionally, the EDS spectra for the samples displayed organic content and sulfur,

which is consistent with biofilm formation as well as the membrane material itself. No sign of scale formation was observed on the membrane surfaces by SEM or EDS. Example SEM images and EDS spectra of a feed and concentrate membrane swatch are displayed in Figure 7-12 (images and spectra from 20 April 2010).

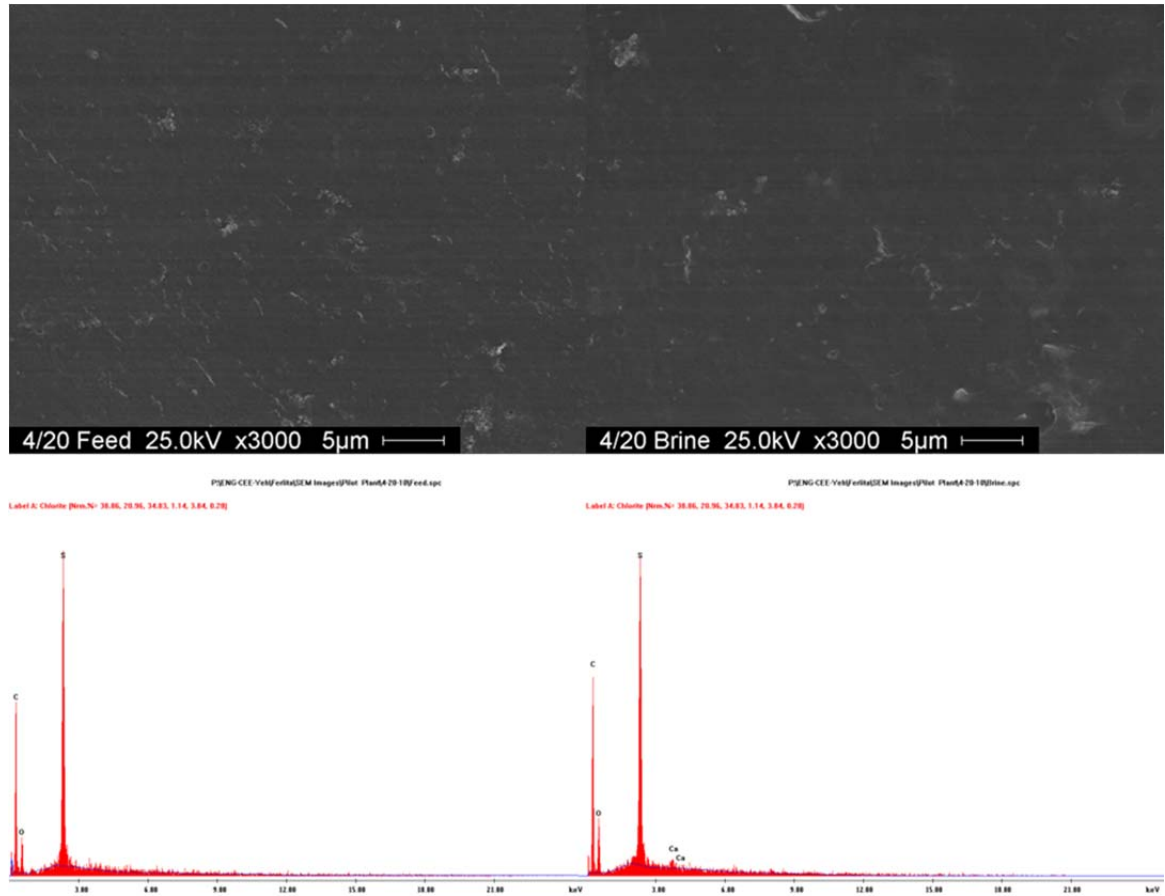


Figure 7-12 SEM images of feed (top left) and concentrate (top right) and EDS images of feed (bottom left) and concentrate (bottom right)

7.3.1.1.5 AFM

The membrane surface was imaged using an AFM as per the procedure in section 3.3, which allows for qualitative analysis of materials deposited on or grown on the surface of the membrane. This analysis gives a three-dimensional image of the membrane surface, so the roughness of the surface can be calculated. Example AFM images of the pilot membrane swatches are in Figure 7-13 (images from 20 April 2010 sampling). Additionally, the roughness values for the surface are reported as root mean squared roughness (RMS) and average roughness (Ra). The roughness data for the zero external carbon loading portion of the study are in Table 7-5.

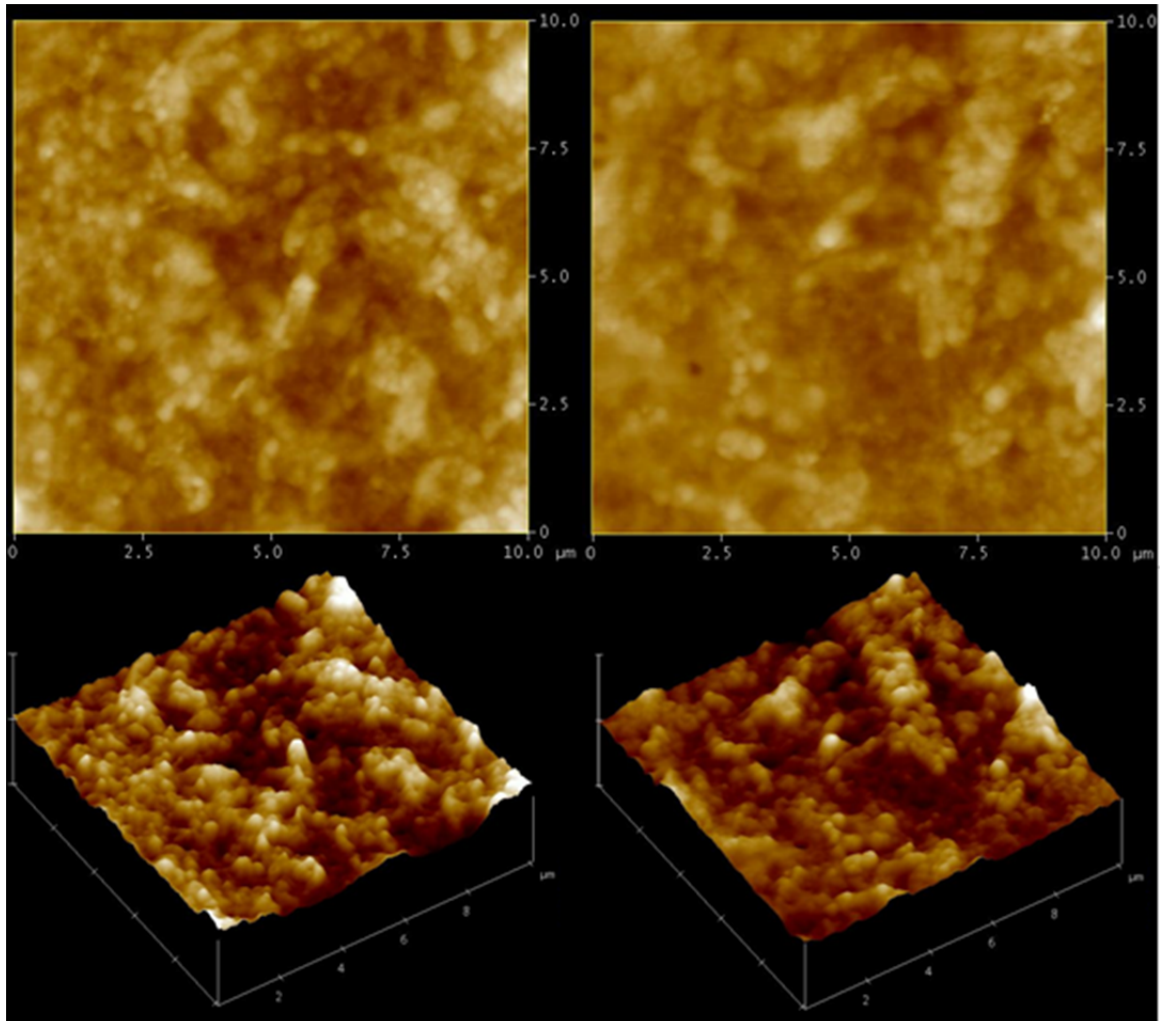


Figure 7-13 AFM images of the pilot membrane surface swatches: top view for feed (top left), top view for concentrate (top right), surface view for feed (bottom left), and surface view for concentrate (bottom right)

Table 7-5 The AFM roughness data for the feed and concentrate membrane swatches as a function of sampling date

Date	Feed		Concentrate				Feed/concentrate RMS	Feed/Concentrate Ra		
	Avg RMS (nm)	Stdev	AVG Ra (nm)	Stdev	AVG RMS (nm)	Stdev				
4/7/2010	47.8	17.9	34.5	9.6	49.1	1.5	36.2	1.2	1.0	1.0
4/14/2010	70.4	12.7	48.8	7.1	59.8	25.6	45.4	17.8	1.2	1.1
4/20/2010	50.0	2.3	38.3	0.3	55.1	7.3	42.0	4.1	0.9	0.9
4/27/2010	55.1	2.5	43.6	1.7	69.1	29.1	54.2	23.2	0.8	0.8
5/4/2010	63.1	15.3	48.1	11.2	52.5	18.2	39.9	13.5	1.2	1.2
5/11/2010	141.8	76.1	113.7	64.0	104.5	51.6	84.5	44.0	1.4	1.3
5/18/2010	73.6	18.4	56.4	13.3	65.3	13.5	47.8	7.4	1.1	1.2
5/25/2010	44.9	8.2	32.8	4.7	36.1	7.0	28.4	4.9	1.2	1.2
6/1/2010	55.1	17.2	41.9	10.7	42.6	3.9	33.8	3.3	1.3	1.2
6/7/2010	45.5	3.9	35.4	2.5	46.7	5.3	35.6	2.9	1.0	1.0
6/14/2010	36.6	5.5	29.1	5.1	45.7	14.6	36.2	12.3	0.8	0.8
6/21/2010	41.7	7.2	30.7	2.1	43.2	2.2	33.2	2.2	1.0	0.9
6/28/2010	45.4	14.8	35.5	11.4	43.1	5.4	34.0	5.3	1.1	1.0
7/5/2010	48.7	6.7	38.6	4.8	42.9	5.1	33.1	3.8	1.1	1.2
7/12/2010	45.2	4.1	35.0	2.5	49.7	4.9	38.6	3.7	0.9	0.9
7/19/2010	66.7	13.3	53.9	10.0	53.4	10.1	39.7	6.8	1.2	1.4
7/26/2010	47.9	9.4	37.3	8.3	56.1	7.5	44.3	5.5	0.9	0.8

Statistical analyses using a t-test were performed on the feed/concentrate ratio for the RMS and Ra roughness values to determine if there is a significant difference in the surface roughness for these membrane swatches. The results of these analyses for the RMS and Ra roughness ratio data indicate no significant difference between feed and ratio with a 95% level of confidence (i.e. the ratio is not significantly different from 1), Appendix E.

7.3.1.2 Carbon Loading

The results from the zero external carbon loading portion of the study did not indicate significantly higher foulant on the either membrane swatch. It is believed the lack of constant AOC exposure to the membrane surface is responsible for the lack of difference observed on the feed and concentrate swatches. In order to simulate constant exposure of organic carbon to the membrane surface, a carbon loading portion of the study was performed. The source of organic carbon chosen for the carbon loading portion of the pilot study was glycerin; since it more closely resembles natural organic matter than other carbon sources (e.g. dextrose, acetate). This was achieved by adding a solution of known glycerin concentration to the feed tank at a known flow rate using a peristaltic pump (see section 7.3 and Appendix C for details).

The feed and concentrate membrane swatches from the pilot system were characterized using the same techniques used in the carbon loading portion of the study. The concentration of organic carbon added to the system was varied to determine its effect of the growth of biofilm on the membrane surfaces.

7.3.1.2.1 Protein and Carbohydrate Data

The concentration of proteins and carbohydrates on the feed and concentrate membrane swatches of the pilot system were measured as per the methods in section 3.3. The results of these analyses with their respective standard deviations for the period of 0.1 g C/m²day carbon addition are in Table 7-6.

Table 7-6 Protein and carbohydrate concentration on pilot membrane swatches from the 0.1 g/m²day portion of study

Date	Flow (GPM)	Protein concentration (µg/cm ²)				Carbohydrate concentration (µg/cm ²)			
		Feed		Concentrate		Feed		Concentrate	
		Avg	Stdev	Avg	Stdev	Avg	Stdev	Avg	Stdev
08/30/10	50	26.2	0.3	39.6	0.5	14.6	2.8	15.3	0.9
08/30/10	50	20.7	0.1	20.6	0.2	10.6	0.9	9.4	0.8
09/06/10	50	27.7	0.3	28.6	0.2	2.2	0.7	2.0	0.5
09/06/10	50	26.7	0.4	34.1	0.2	3.0	1.8	5.0	1.1
09/13/10	50	13.6	0.2	13.5	0.1	6.3	0.4	6.6	0.3
09/13/10	50	15.2	0.3	14.9	0.3	8.7	1.8	7.7	0.8
09/20/10	25	8.7	0.1	10.1	0.2	6.8	0.3	5.5	0.3
09/20/10	25	10.6	0.2	10.1	0.1	6.3	1.7	5.7	0.4
09/27/10	25	5.9	0.4	5.3	0.1	5.8	1.6	5.6	0.2
09/27/10	25	7.0	0.1	6.9	0.0	6.9	2.2	6.0	0.3
10/04/10	25	6.9	0.1	6.0	0.6	6.0	0.4	4.2	0.2
10/04/10	25	6.7	0.1	6.6	0.1	4.2	0.7	5.9	0.7

The data in Table 7-7 can be analyzed to determine the carbohydrate/protein ratio for the feed and concentrate membrane swatches. The feed/concentrate ratio of protein and carbohydrates for the pilot system can be calculated as well. These calculations for the 0.1 g C/m²day portion of the carbon loading study are in Table 7-7.

Table 7-7 The carbohydrate/protein ratio data for the feed and concentrate swatches and feed/concentrate ratio data for protein and carbohydrates from the 0.1 g/m²day portion of study

Date	Flow (GPM)	Carb/Protein Feed		Concentrate		Feed/concentrate	
		Avg	Stdev	Avg	Stdev	Protein	Carb
8/30/2010	50	0.6	0.1	0.4	0.0	0.7	1.0
8/30/2010	50	0.5	0.0	0.5	0.0	1.0	1.1
9/6/2010	50	0.1	0.0	0.1	0.0	1.0	1.1
9/6/2010	50	0.1	0.1	0.1	0.0	0.8	0.6
9/13/2010	50	0.5	0.0	0.5	0.0	1.0	0.9
9/13/2010	50	0.6	0.1	0.5	0.1	1.0	1.1
9/20/2010	25	0.8	0.0	0.5	0.0	0.9	1.2
9/20/2010	25	0.6	0.2	0.6	0.0	1.0	1.1
9/27/2010	25	1.0	0.3	1.0	0.0	1.1	1.0
9/27/2010	25	1.0	0.3	0.9	0.0	1.0	1.2
10/4/2010	25	0.9	0.1	0.7	0.1	1.1	1.4
10/4/2010	25	0.6	0.1	0.9	0.1	1.0	0.7

The data in Table 7-6 indicate an average carbohydrate/protein ratio of 0.6 ± 0.3 for the feed swatch and 0.6 ± 0.3 for the concentrate swatch. The feed/concentrate ratios for protein and carbohydrate concentrations are 1.0 ± 0.1 and 1.0 ± 0.2 respectively for the 0.1 g C/m²day portion of the carbon loading study. A t-test performed on the feed/concentrate ratio data indicates no significant difference between the feed and concentrate membrane swatches for the protein and carbohydrate concentrations with a 95% confidence level. However, when the carbohydrate/protein ratio data from the 0.1 g C/m²day were compared to the zero external carbon loading data, there was a significant increase in the ratio with greater than a 95% level of confidence for the feed and concentrate membrane swatches, Appendix E.

The next portion of the carbon loading study is the addition of 0.5 g C/m²day. The data for the protein and carbohydrate concentrations on the surface of the feed and concentrate membrane swatches are in Table 7-8.

Table 7-8 Protein and carbohydrate concentrations on pilot membrane swatches from the 0.5 g/m²day portion of study

Date	Flow (GPM)	Protein concentration (µg/cm ²)				Carbohydrate concentration (µg/cm ²)			
		Feed		Concentrate		Feed		Concentrate	
		Avg	Stdev	Avg	Stdev	Avg	Stdev	Avg	Stdev
10/11/10	25	18.2	0.5	14.1	0.1	24.6	1.9	14.4	0.8
10/11/10	25	15.7	0.8	14.1	0.6	23.4	0.4	16.1	1.2
10/18/10	25	12.4	1.1	10.6	0.1	16.6	0.7	15.4	0.5
10/18/10	25	12.3	0.4	11.1	1.2	16.3	1.3	13.8	0.0
10/25/10	25	3.6	0.2	5.7	0.2	0.5	0.3	2.1	0.2
10/25/10	25	4.5	0.1	5.4	0.2	1.1	0.3	1.1	0.3
11/08/10	50	19.3	0.9	10.4	0.8	18.2	2.4	14.0	1.4
11/08/10	50	19.1	1.2	8.3	0.3	20.6	0.8	10.3	0.8
11/15/10	50	20.2	0.6	9.3	0.3	25.4	0.1	14.2	0.5
11/15/10	50	15.2	0.4	10.0	0.1	19.3	1.4	19.0	1.3
11/22/10	50	25.4	0.9	13.6	0.4	24.7	3.3	14.1	0.8
11/22/10	50	19.5	1.2	17.0	0.5	19.4	3.0	16.8	0.4

The data in Table 7-8 were further analyzed to determine the carbohydrate/protein ratio for the feed and the concentrate swatches, Table 7-9. This table also contains the feed/concentrate ratio for both the protein and carbohydrate concentrations.

Table 7-9 The carbohydrate/protein ratio data for the feed and concentrate swatches and feed/concentrate ratio data for protein and carbohydrates from the 0.5 g/m²day portion of study

Date	Flow (GPM)	Carb/Protein Feed		Concentrate		Feed/Concentrate	
		Avg	Stdev	Avg	Stdev	Protein	Carb
10/11/2010	25	1.4	0.1	1.0	0.1	1.3	1.7
10/11/2010	25	1.5	0.1	1.1	0.1	1.1	1.4
10/18/2010	25	1.4	0.1	1.4	0.0	1.2	1.1
10/18/2010	25	1.3	0.1	1.2	0.1	1.1	1.2
10/25/2010	25	0.1	0.1	0.4	0.0	0.6	0.2
10/25/2010	25	0.2	0.1	0.2	0.1	0.8	0.9
11/8/2010	50	0.9	0.2	1.3	0.2	1.9	1.3
11/8/2010	50	1.1	0.1	1.2	0.1	2.3	2.0
11/15/2010	50	1.3	0.0	1.5	0.1	2.2	1.8
11/15/2010	50	1.3	0.1	1.9	0.1	1.5	1.0
11/22/2010	50	1.0	0.1	1.0	0.1	1.9	1.8
11/22/2010	50	1.0	0.2	1.0	0.0	1.1	1.2

The data in Table 7-9 indicate an average carbohydrate/protein ratio of 1.0±0.4 for the feed swatch and 1.1±0.5 for the concentrate swatch. The feed/concentrate ratios for protein and carbohydrate concentration are 1.4±0.5 and 1.3±0.5 respectively for the 0.5 g C/m²day portion of the carbon loading study. A t-test reveals a significant difference in both the protein and carbohydrate concentrations between the feed and concentrate membrane swatches. A t-test was also performed on the carbohydrate/protein ratio data, indicating a significant increase over the 0.1 g C/m²day portion of the study with a 95% confidence level, Appendix E.

The final portion of the carbon loading study is the addition of 2.0 g C/m²day. The data for the protein and carbohydrate concentrations on the surface of the feed and concentrate membrane swatches are in Table 7-10.

Table 7-10 Protein and carbohydrate concentration on pilot membrane swatches from the 2.0 g/m²day portion of study

Date	Flow (GPM)	Protein concentration (µg/cm ²)				Carbohydrate concentration (µg/cm ²)			
		Feed		Concentrate		Feed		Concentrate	
		Avg	Stdev	Avg	Stdev	Avg	Stdev	Avg	Stdev
11/29/10	50	13.8	0.9	10.9	0.5	15.1	2.2	11.6	0.6
11/29/10	50	14.0	0.3	10.4	0.2	12.9	0.8	9.9	0.4
12/06/10	50	10.4	0.5	8.9	0.1	15.2	1.3	10.7	0.6
12/06/10	50	10.0	0.3	7.4	0.2	16.8	0.9	10.4	1.4
12/13/10	50	9.9	0.3	6.6	0.2	13.6	4.7	3.6	0.9
12/13/10	50	9.7	0.3	6.8	0.4	9.1	0.5	2.9	1.5
12/20/10	25	11.3	0.7	7.6	1.7	11.2	0.8	8.4	1.5
12/20/10	25	12.3	0.9	11.8	0.6	9.9	0.9	5.4	1.0
12/27/10	25	14.2	0.3	11.2	0.7	9.0	0.9	6.9	0.9
12/27/10	25	13.0	0.7	11.5	0.5	10.9	1.0	9.2	0.1
01/03/11	25	9.1	0.2	7.8	0.2	8.2	0.7	5.2	0.1
01/03/11	25	9.1	0.1	7.3	0.2	9.0	0.9	7.0	0.9

The data in Table 7-10 are used to calculate the carbohydrate/protein ratio for the feed and the concentrate swatches. The feed/concentrate ratio for the protein and carbohydrate concentrations are also calculated using these data, Table 7-11.

Table 7-11 The carbohydrate/protein ratio data for the feed and concentrate swatches and feed/concentrate ratio data for protein and carbohydrates from the 2.0 g/m²/day portion of study

Date	Flow (GPM)	Carb/Protein		Feed/Concentrate			
		Feed	Concentrate	Protein	Carb		
11/29/2010	50	1.1	0.1	1.1	0.1	1.3	1.3
11/29/2010	50	0.9	0.1	0.9	0.0	1.3	1.3
12/6/2010	50	1.5	0.2	1.2	0.1	1.2	1.4
12/6/2010	50	1.7	0.1	1.4	0.2	1.3	1.6
12/13/2010	50	1.4	0.5	0.5	0.1	1.5	3.8
12/13/2010	50	0.9	0.1	0.4	0.2	1.4	3.1
12/20/2010	25	1.0	0.0	1.1	0.3	1.5	1.3
12/20/2010	25	0.8	0.1	0.5	0.1	1.0	1.8
12/27/2010	25	0.6	0.1	0.6	0.1	1.3	1.3
12/27/2010	25	0.8	0.1	0.8	0.0	1.1	1.2
1/3/2011	25	0.9	0.1	0.7	0.0	1.2	1.6
1/3/2011	25	1.0	0.1	0.9	0.1	1.2	1.3

The data in Table 7-11 reveal an average carbohydrate/protein ratio of 1.0±0.3 and 0.9±0.3 for the feed and concentrate swatches respectively. The feed/concentrate ratios for protein and carbohydrate concentrations are 1.3±0.1 and 1.8±0.8 respectively. Analysis of the feed/concentrate ratio data revealed a significant difference with a 95% confidence level using a t-test for both protein and carbohydrate concentrations. However, when compared to the 0.5 g C/m²/day portion of the study, the feed/concentrate ratio data are not significantly different, indicating no additional protective effect with the additional carbon loading. Analysis of the carbohydrate/protein ratio indicated a significant difference between the 2.0 g C/m²/day data and the zero external carbon

loading data with a 95% confidence level. However, the data for the 2.0 g C/m²day and 0.5 g C/m²day carbon loading portions are not significantly different, Appendix E.

The protein concentration on the feed and concentrate membrane swatches for the carbon loading portion of the study is displayed graphically as a function of sampling date, Figure 7-14. The initial decrease observed for carbon concentration on the surface of the membrane swatches is likely due to equilibration from carbon addition and from startup after the pump rebuild (see above).

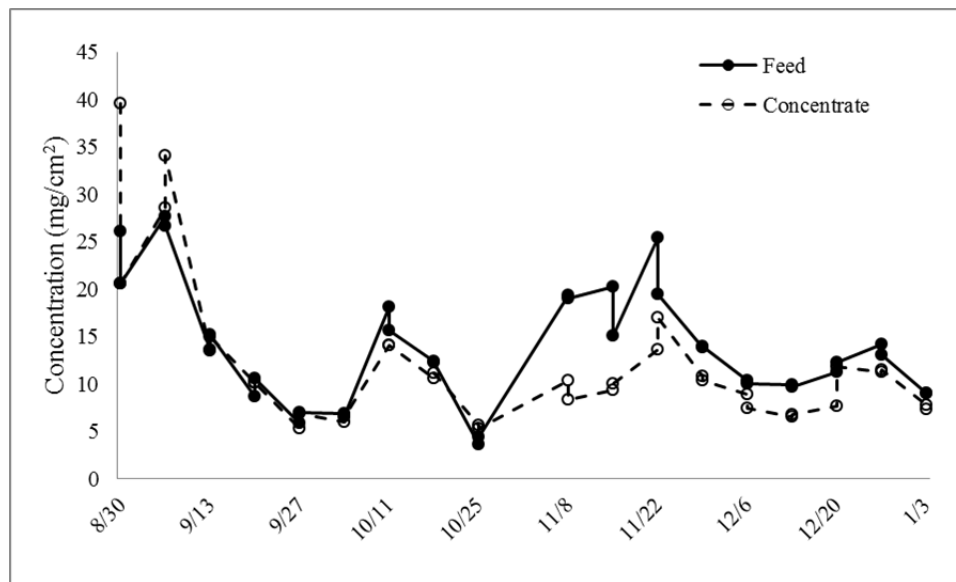


Figure 7-14 Protein concentration on the feed and concentrate pilot swatches for the carbon loading portion of the study

The carbohydrate concentration on the feed and concentrate membrane swatches for the carbon loading portion of the study is represented graphically in Figure 7-15. In order to find a trend in the data for the protein and carbohydrate concentrations on the pilot

membrane surfaces, the feed/concentrate ratio of these concentrations for the membrane swatches are calculated as a function of sampling date, Figure 7-16. Qualitatively, the feed/concentrate ratio appears to be both greater than one and increasing. This would indicate a protective effect for the membrane material downstream from the membrane element. The statistical analysis performed above also indicates an increasing trend for the feed/concentrate ratio of protein and carbohydrate concentrate as the concentration of carbon addition increases. The carbohydrate/protein ratio also appears to increase with increasing carbon addition for the carbon loading portion of the study, and a t-test revealed a statistically significant increasing trend as the concentration of carbon addition increases, Figure 7-17.

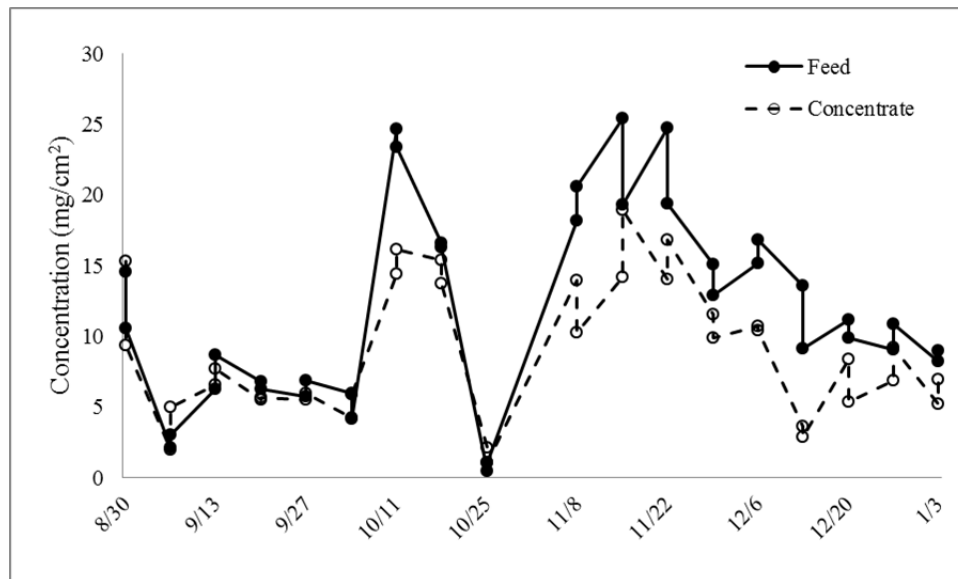


Figure 7-15 Carbohydrate concentration on the feed and concentrate swatches from the pilot system during the carbon loading portion of the study

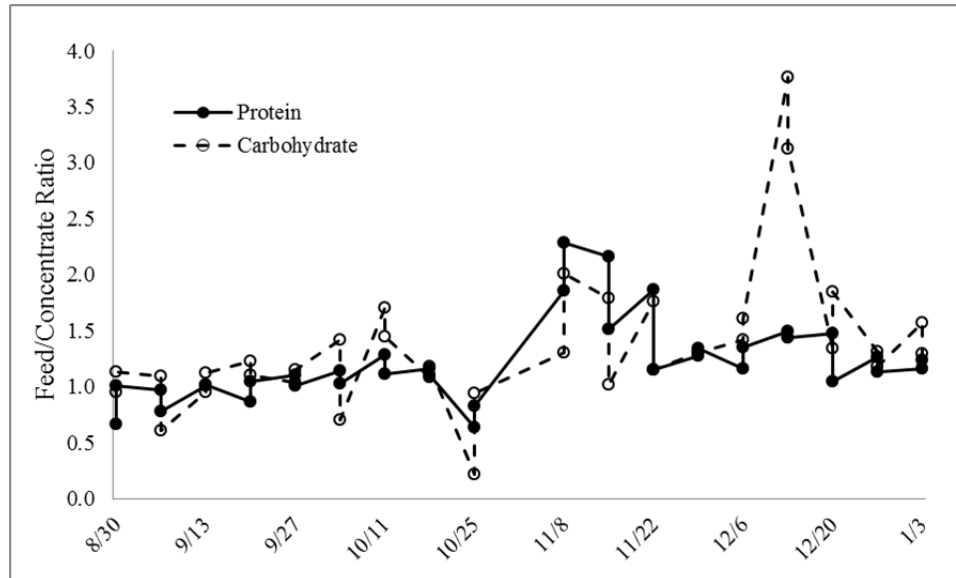


Figure 7-16 The feed/concentrate ratio for protein and carbohydrate concentrations on the pilot membrane surfaces

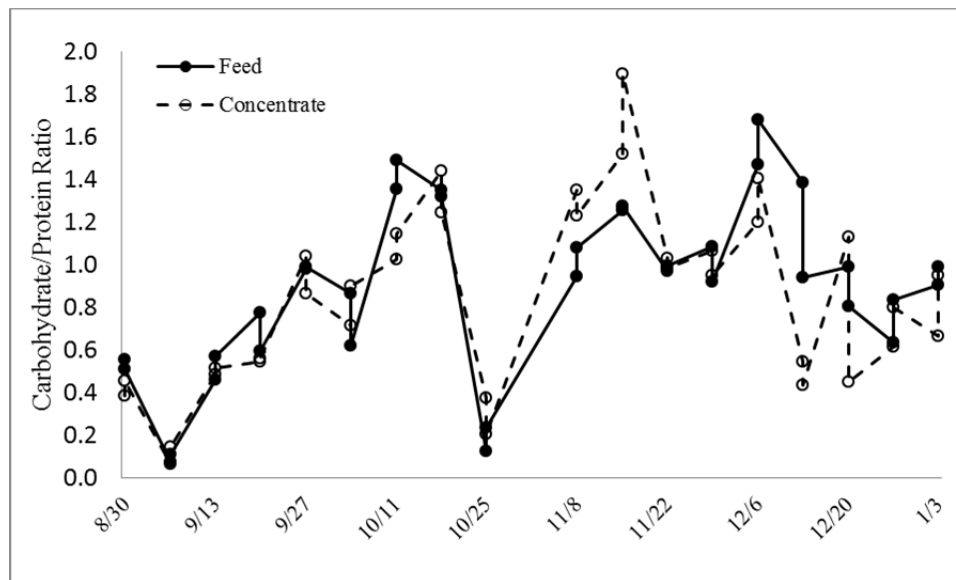


Figure 7-17 The carbohydrate/protein ratio for the pilot feed and concentrate membrane surfaces during the carbon loading portion of the study

7.3.1.2.2 Microbiological Data

The total number of microorganisms on the membrane surfaces for the carbon loading portion of the study is in Appendix E. The feed/concentrate ratio of total microorganisms was 1.4 ± 0.4 from the $0.1 \text{ g/m}^2\text{day}$ portion of the study. Analysis of the data reveals no significant difference between the feed and concentrate swatches at a 95% confidence level. For the $0.5 \text{ g/m}^2\text{day}$ portion of the study, the feed/concentrate ratio was 1.8 ± 0.6 . This result indicates a significantly higher number of total microorganisms on the feed swatch to a 95% level of confidence. Finally, the feed/concentrate ratio for the $2.0 \text{ g/m}^2\text{day}$ is 1.8 ± 0.5 , which yields a significantly higher number on the feed swatch as compared to the concentrate swatch, Appendix E.

The data from each of the carbon loading concentrations were further analyzed to determine if there was a significant difference between the points using a t-test. Although the results from the carbon loading levels of 0.5 and $2.0 \text{ g/m}^2\text{day}$ indicated significantly higher numbers of total bacteria on the feed swatch, analysis of the data indicated no significant difference between any of the ratio data. Thus, the total direct count data are inconclusive as far as a relationship to carbon loading levels.

The total number of culturable microorganisms on the surface of the feed and concentrate membrane swatches for the carbon loading portion of the study as well as the feed/concentrate ratio data are displayed in Tables 7-12, 13, and 14 for the 0.1 , 0.5 , and the $2.0 \text{ g C/m}^2\text{day}$ carbon loading rates respectively. The ratio of culturable microorganisms for the feed to concentrate membrane swatches for the $0.1 \text{ g C/m}^2\text{day}$

portion of the study is 1.3 ± 0.8 . However, there was not a significant difference in the number of culturable bacteria on the feed and concentrate swatches at a 95% confidence level, Appendix E.

The feed/concentrate ratio of culturable microorganisms for the $0.5 \text{ g C/m}^2\text{day}$ portion of the study was 2.6 ± 2 . A t-test analysis reveals a significant difference in the number of culturable microorganisms on the feed and concentrate swatches, i.e. the ratio was statistically different than 1. When the ratio of culturable microorganisms from the $0.1 \text{ g C/m}^2\text{day}$ and the $0.5 \text{ g C/m}^2\text{day}$ portions of the study were compared, there is not a significant difference at a 95% confidence level (although there is a significant difference at a 90% confidence level), Appendix E.

The culturable microorganisms from the $2.0 \text{ g C/m}^2\text{day}$ had a feed/concentrate ratio of 2.5 ± 1.5 . Analysis of these data using a t-test indicates a significant difference in the number of culturable microorganisms for the feed and concentrate membrane swatches. Additionally, when comparing the feed/concentrate ratio of culturable microorganisms from the $0.1 \text{ g C/m}^2\text{day}$ and $2.0 \text{ g C/m}^2\text{day}$ carbon loading portions of the study, there is a significant difference, but when comparing the $0.5 \text{ g C/m}^2\text{day}$ and $2.0 \text{ g C/m}^2\text{day}$ carbon loading portions of the study, no significant difference is observed, Appendix E.

Table 7-12 Total culturable microorganisms on the feed and concentrate membrane swatches from the 0.1 g C/m²day portion of the study and the feed/concentrate ratio

Date	Feed (# x 10 ⁴ /cm ²)		Concentrate (# x 10 ⁴ /cm ²)		Feed/Conc
	Average	Stdev	Average	Stdev	
8/30/2010	15	3.4	12	3.5	1.2
8/30/2010	29	15	8.9	0.84	3.3
9/6/2010	16	5.6	9.2	4.3	1.7
9/6/2010	12	1.6	16	2.5	0.8
9/13/2010	7.0	1.9	11	0.80	0.7
9/13/2010	20	6.6	9.6	2.8	2.1
9/20/2010	5.6	4.2	8.2	5.8	0.7
9/20/2010	3.7	1.7	13	2.9	0.3
9/27/2010	5.9	0.93	5.9	1.7	1.0
9/27/2010	9.2	2.6	6.3	2.3	1.5
10/4/2010	7.6	1.7	5.2	0.069	1.5
10/4/2010	5.9	1.5	4.8	0.82	1.2

Table 7-13 Total culturable microorganisms on the feed and concentrate membrane swatches from the 0.5 g C/m²day portion of the study and the feed/concentrate ratio

Date	Feed (# x 10 ⁴ /cm ²)		Concentrate (# x 10 ⁴ /cm ²)		Feed/Conc
	Average	Stdev	Average	Stdev	
10/11/2010	5.3	0.59	3.9	0.17	1.3
10/11/2010	3.3	0.072	4.6	2.7	0.7
10/18/2010	31	6.4	4.0	2.5	7.7
10/18/2010	27	4.7	7.0	3.5	3.9
10/25/2010	6.0	2.1	3.6	1.2	1.7
10/25/2010	6.3	5.4	5.4	1.3	1.2
11/8/2010	33	8.1	33	13	1.0
11/8/2010	42	9.9	19	9.0	2.2
11/15/2010	83	6.2	16	9.9	5.1
11/15/2010	63	16	26	5.2	2.5
11/22/2010	18	1.5	7.2	2.8	2.5
11/22/2010	16	4.9	10	1.5	1.5

Table 7-14 Total culturable microorganisms on the feed and concentrate membrane swatches from the 2.0 g C/m²day portion of the study and the feed/concentrate ratio

Date	Feed (# x 10 ⁴ /cm ²)		Concentrate (# x 10 ⁴ /cm ²)		Feed/Conc
	Average	Stdev	Average	Stdev	
11/29/2010	1.9	0.67	1.5	1.3	1.3
11/29/2010	1.4	1.3	1.1	1.1	1.3
12/6/2010	17	4.8	9.4	5.8	1.8
12/6/2010	22	10	4.6	2.7	4.8
12/13/2010	13	5.8	9.3	4.1	1.4
12/13/2010	27	31	10	3.9	2.6
12/20/2010	30	23	5.5	6.3	5.4
12/20/2010	16	20	4.7	7.2	3.4
12/27/2010	1.2	1.2	1.2	1.9	1.0
12/27/2010	2.7	2.4	2.3	2.0	1.2
1/3/2011	15	11	4.2	0.84	3.5
1/3/2011	10	1.8	3.5	4.2	2.9

The total number of culturable microorganisms from all phases of the carbon loading portion of the study is plotted as a function of sampling date in Figure 7-18. Additionally, the feed/concentrate ratio of culturable microorganisms on the pilot membrane swatches is represented graphically, Figure 7-19.

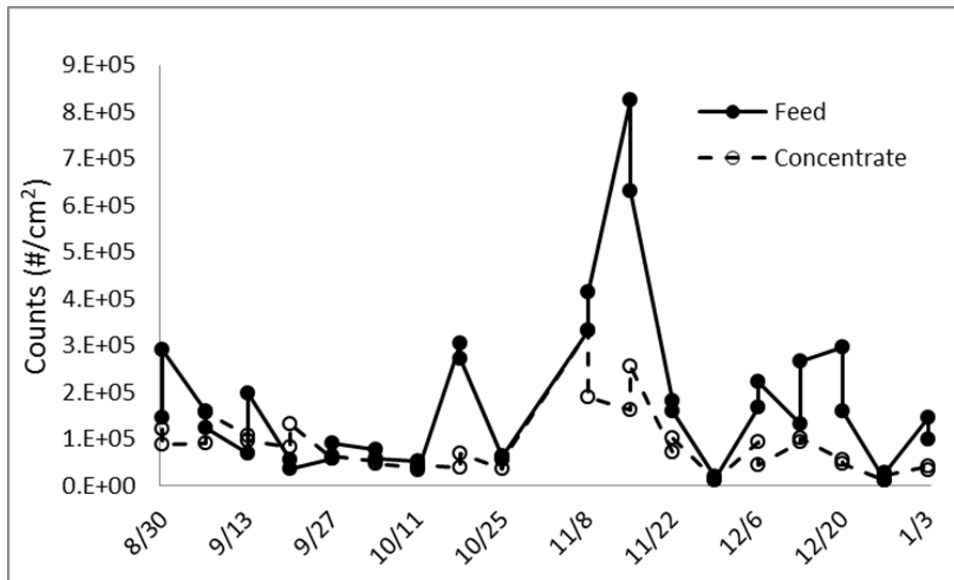


Figure 7-18 The total number of culturable microorganisms as a function of sampling date for the carbon loading portion of the study

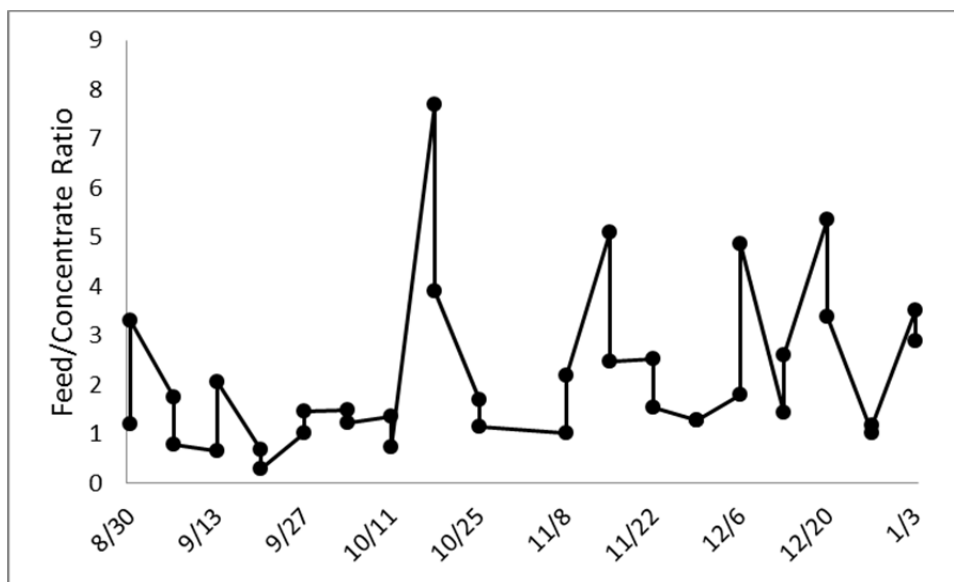


Figure 7-19 The feed/concentrate ratio of culturable microorganisms as a function of sampling date for the carbon loading portion of the study

7.3.1.2.3 ATR-FTIR

Infrared spectra of the feed and concentrate membrane swatches from the carbon loading portion of the study were obtained as per the methods in section 3.3. Example spectra of the feed and concentrate pilot swatches from the carbon loading portion of the study along with virgin membrane material are plotted from 4000-600 cm^{-1} , Figure 7-20 (spectra from 11 Oct 2011). Signs of foulant material are apparent in these spectra, indicated by the amine and/or hydroxyl stretch at approximately 3300 cm^{-1} and the aliphatic stretch at approximately 2900 cm^{-1} .

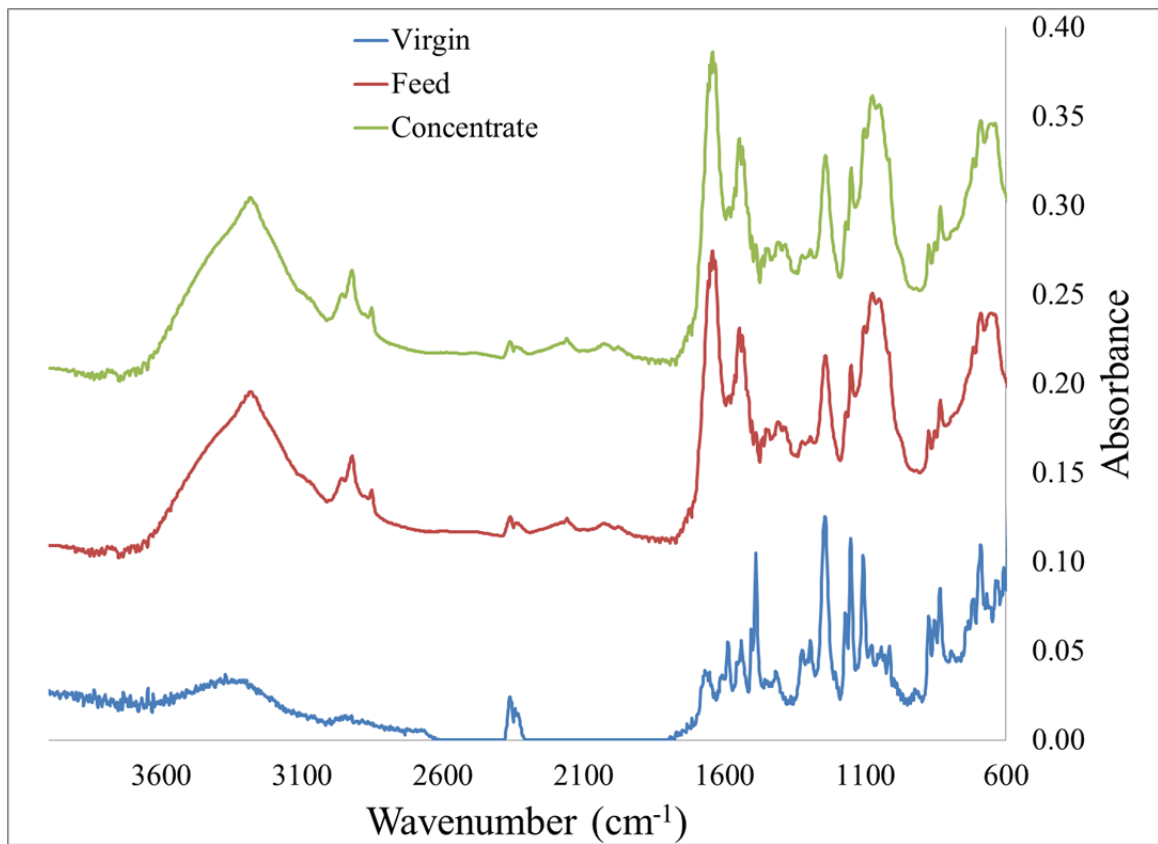


Figure 7-20 FTIR spectra of feed and concentrate membrane swatches from the carbon loading portion of the study along with virgin membrane material

The region of the spectra from 2000-600 cm^{-1} was expanded and the difference between the pilot sample spectrum and virgin membrane material was taken, Figure 7-21. The notable peaks that are visible in these spectra are a carboxyl group peak at approximately 1730 cm^{-1} , an amide peak at approximately 1630 cm^{-1} , and a carbohydrate CHO peak at approximately 1050 cm^{-1} . There appears to be slightly more foulant material on the concentrate membrane swatch, although this difference may be due to sampling location on the membrane swatch. There are no notable differences in peak location, indicating the same type of foulant material is present on the feed and concentrate membrane swatches.

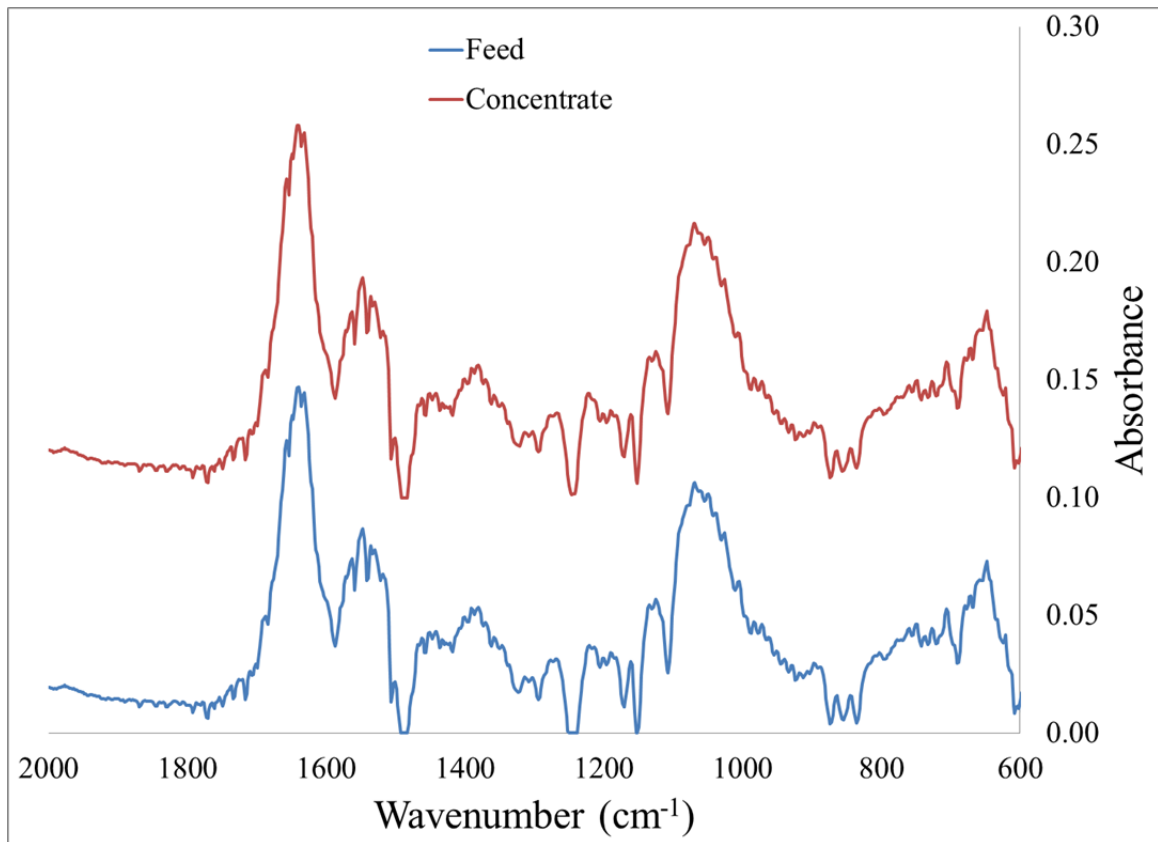


Figure 7-21 FTIR difference spectra for feed and concentrate membrane swatches

7.3.1.2.4 SEM-EDS

The surface of the membrane swatches from the carbon loading portion of the study were qualitatively analyzed using scanning electron microscopy with energy dispersive spectroscopy (SEM-EDS). Details on these analyses are available in section 3.3. The surface of the membrane swatches displayed signs of biofilm on both the feed and concentrate swatches of the pilot system. Example SEM images of a feed and concentrate membrane swatches are displayed in Figure 7-22 (images and spectra from 18 October 2010). Additionally, the EDS spectra for the samples displayed organic content and sulfur, which is consistent with biofilm formation as well as the membrane material itself. No sign of scale formation is observed on the membrane surfaces by SEM or EDS.

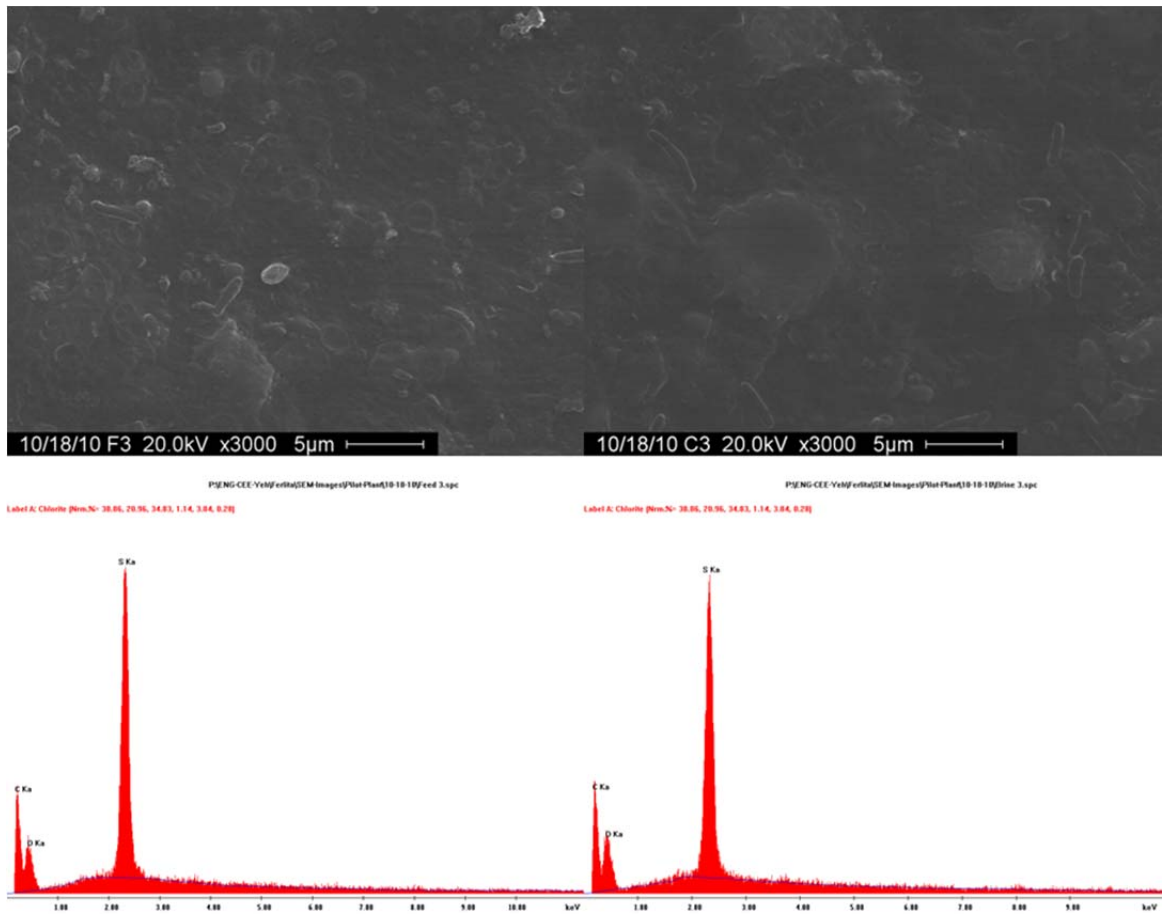


Figure 7-22 SEM images of pilot membrane swatch surface for feed (top left) and concentrate (top right) and EDS spectra for feed (bottom left) and concentrate (bottom right)

7.3.1.2.5 AFM

The membrane surface was imaged and qualitatively analyzed using an AFM as per the procedure in section 3.3. Example AFM images of the pilot membrane swatch top and surface views from the carbon loading portion of the study are in Figure 7-23 (images from 18 October 2010). Additionally, the roughness values for the surface are reported as root mean squared roughness (RMS) and average roughness (Ra). The roughness data

for the carbon loading portion of the study are in Appendix E. Analysis of these data using a t-test indicates no difference in the roughness of the feed and concentrate membrane swatches for the carbon loading portion of the study as well as the zero external carbon loading portion of the study.

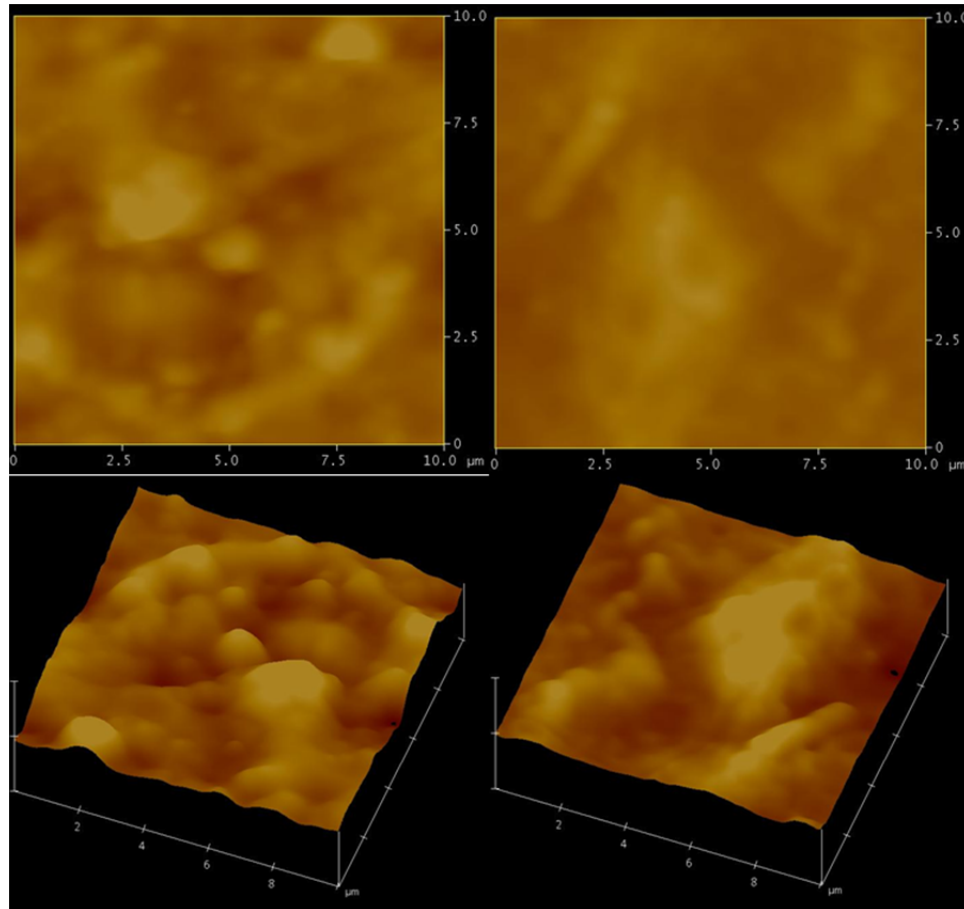


Figure 7-23 AFM images of the pilot membrane swatch surfaces: top view for feed (top left), top view for concentrate (top right), surface view for feed (bottom left), and surface view for concentrate (bottom right)

7.3.1.3 Overall Foulant Trends

The foulant characterization data for the zero external carbon loading and the carbon loading portions of the pilot study give insight to the effect of carbon concentration on the relative deposition/growth of the foulant layer on the feed and concentrate membrane surfaces. At zero external carbon loading and $0.1 \text{ g C/m}^2\text{day}$, no significant difference was observed between the feed and concentrate pilot membrane swatches for either the protein or carbohydrate concentrations. Additionally, the number of culturable microorganisms on the feed and concentrate surfaces was statistically the same for the zero external carbon loading portion of the study. However, there was a statistically significant difference for the $0.1 \text{ g C/m}^2\text{day}$ portion of the study, indicating a greater number of culturable microorganisms for the feed membrane swatches. This suggests that even though there was no observable difference in the amount of biofilm (protein and carbohydrate concentrations) between the feed and concentrate membrane swatches, the microorganisms are more active at the feed portion with the small amount of carbon addition. Given a longer time of operation, differences in biofilm formation for the feed and concentrate surfaces may be observed for the $0.1 \text{ g C/m}^2\text{day}$ carbon addition rate.

The $0.5 \text{ g C/m}^2\text{day}$ carbon loading rate portion of the study provided more significant results for the differences in biofilm growth. Not only is there a significant increase in the feed/concentrate ratio of culturable microorganisms, there also is a significant increase in the feed/concentrate ratio of biofilm on the surfaces (protein and carbohydrate concentrations).

The highest carbon loading portion of the study was 2.0 g C/m²day. This rate of carbon addition did lead to a significantly higher feed/concentrate ratio of protein concentration, carbohydrate concentration, and culturable microorganisms over the 0.1 g C/m²day portion of the study. However, when compared to the 0.5 g C/m²day carbon loading rate portion of the study, there was no significant difference observed.

The Feed/concentrate ratios for protein concentration, carbohydrate concentration, and culturable microorganisms (HPC) are displayed graphically, Figure 7-24. This plot displays the increased difference in concentrations for feed and concentrate surfaces with increased carbon loading conditions.

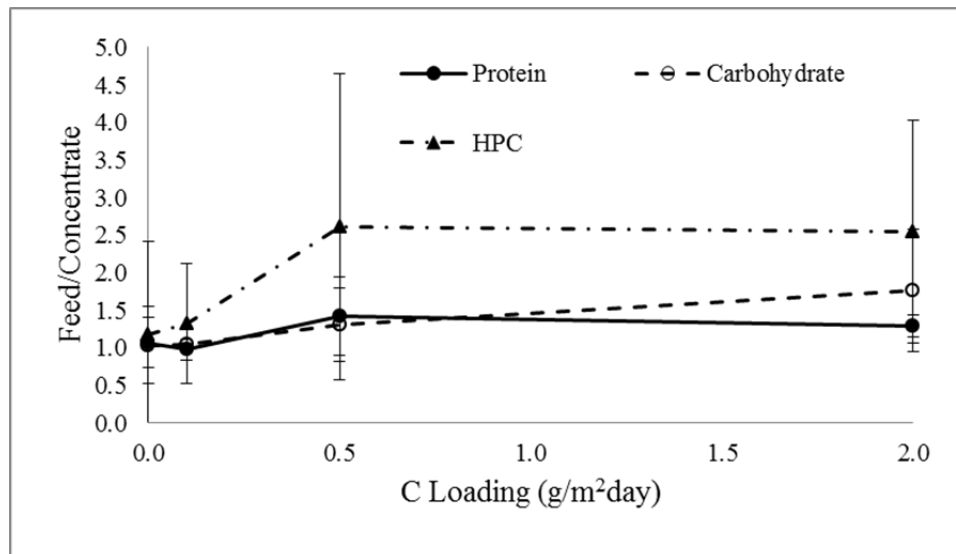


Figure 7-24 The feed/concentrate ratio of protein concentration, carbohydrate concentration, HPC (error bars indicate standard deviation)

As stated above, the feed/concentrate ratio of foulant on the pilot surfaces increases as the carbon loading rate increases. This indicates the feed membrane surfaces are fouling more severely than the concentrate. Thus, the membrane element has a protective effect on the fouling of downstream membrane material. Additionally, the carbohydrate/protein ratio increases as the rate of carbon loading increases, Figure 7-25. This indicates the formation of more biofilm (excretion of EPS by microorganisms) with higher levels of carbon present. These data, paired with the gradient pattern of formation seen in the membrane autopsies (Chapter 5) and the removal of organic carbon in the Dunedin water treatment plant (Chapter 6), indicate the biofilm on the membrane element surface has a protective effect on downstream membrane material by removal of organic carbon from the treatment water and making it nutrient deprived.

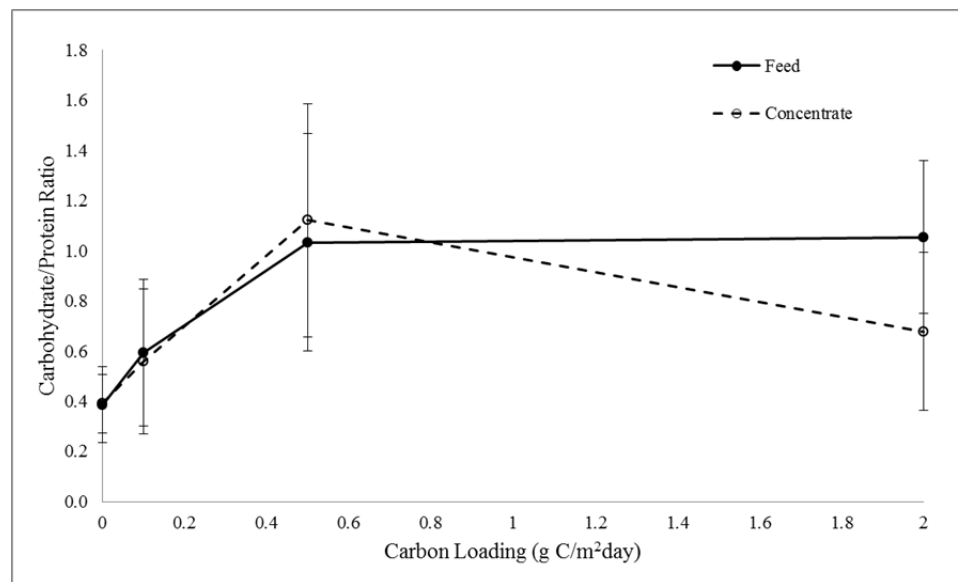


Figure 7-25 Carbohydrate/protein ratio for the pilot feed and concentrate membrane swatches plotted against carbon loading rate (error bars indicate standard deviation)

The data for surface roughness (measured by AFM) displayed no significant difference between the feed and concentrate swatches for any portion of the study. There was also no significant difference in roughness for the different carbon loading rates. Additionally, no differences were observed using SEM-EDS or ATR-FTIR in the types of foulant material deposited for any portion of the study.

7.3.2 Flat Sheet Module Performance Characterization

In addition to analyzing the content and concentration of the foulant material deposited on the membrane surface, the performance of the membrane swatches was analyzed throughout the study. The performance variables that were monitored were the permeate flux for the membrane swatches and the transmembrane pressure. These variables were chosen for performance characterization due to their importance to the costs of operation of a membrane treatment plant.

7.3.2.1 Flux Characterization

The first performance variable analyzed and presented here is the permeate flux. As the membrane swatch begins to foul, the permeate flux decreases proportionally. This trend tends to happen quickly as the foulant layer begins to form/deposit. After the initial flux decline, this decrease begins to level off. The initial rapid flux decline of the membrane swatch can be characterized using a linear approximation. This allows for the comparison of the feed and concentrate portions of the pilot system.

In order to compare flux data for each flat sheet module over the entire study, the permeate flux of each module is normalized to its own initial flux, since the initial flux approximately represents the maximum flux for the unfouled membrane. Thus, the loss of normalized flux represents a percentage loss of flux. As stated above, the initial flux decline due to the membrane fouling can be approximated linearly, and the slope of that curve would represent the normalized initial rate of fouling, m , for that membrane, Equation 7.1.

$$m = \frac{\Delta \left(J/J_o \right)}{\Delta t} \quad (7.1)$$

In Equation 7.1, J is instantaneous flux at time t , J_o is initial flux, and t is time. In order to obtain the slope of the line for the initial loss of flux, the normalized flux for each membrane module must first be plotted as a function of time. These data must then be truncated to obtain the initial linear portion of the curve and the artifact points (points from pump shut down, tank refilling, etc.) removed. An example of a curve prepared to obtain the initial flux decline data is in Figure 7-26 (flux graphs for all carbon loading levels and all flat sheet modules are in Appendix E). This graph displays the initial flux decline data for flat sheet module 4 during the 2 g C/m²day portion of the study.

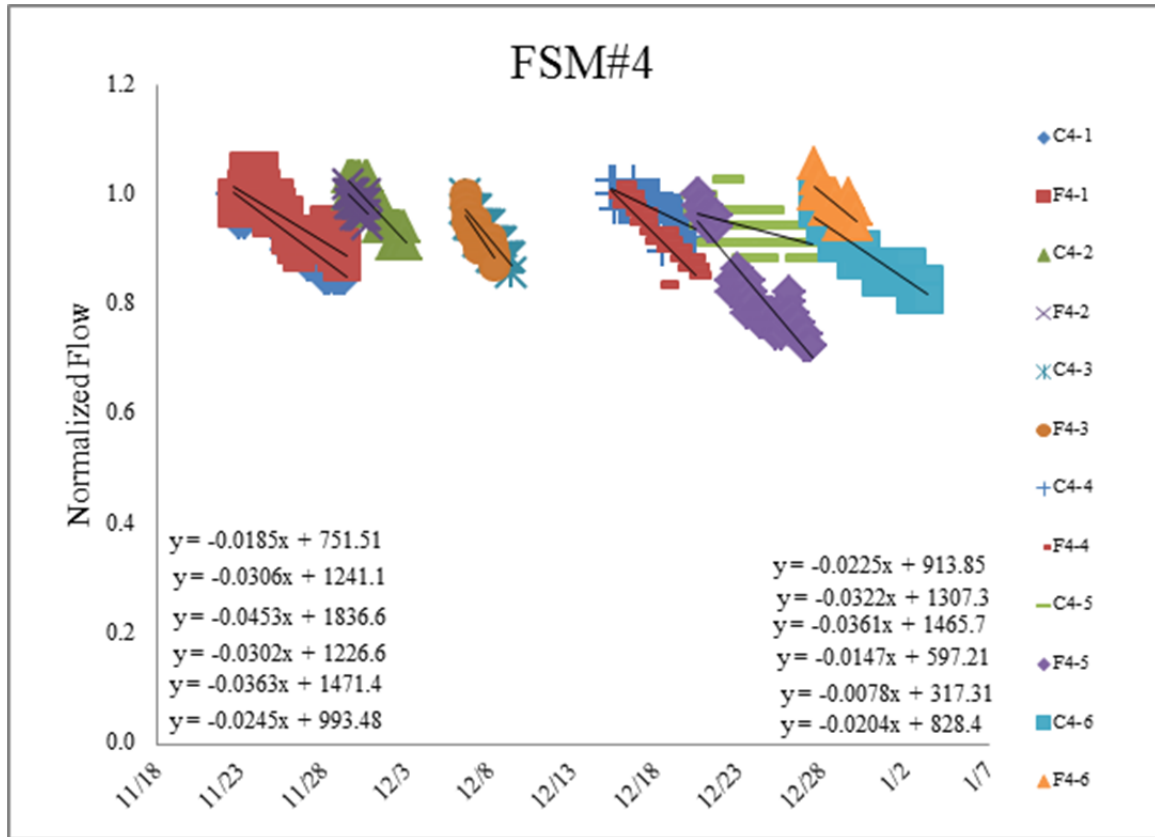


Figure 7-26 Initial flux decline data for FSM#4 during the 2 g C/m²day portion of the study

The initial flux decline for the feed and concentrate membrane swatches of the pilot system can be compared by taking the ratio of the feed to concentrate normalized initial rates of flux decline, Equation 7.2. This ratio is represented by the variable M.

$$M = \frac{m_{feed}}{m_{concentrate}} \quad (7.2)$$

where M is the fouling rate ratio, m_{feed} is the normalized initial rate of fouling for the feed, and $m_{concentrate}$ is the normalized initial rate of fouling for the concentrate. This

variable was calculated for corresponding flat sheet modules (i.e. Feed 1 to Concentrate 1, etc.) each week, see Appendix E. The ratio data for each carbon loading condition were then averaged to determine the trend of the fouling ratio with respect to carbon loading, Table 7-15. These data are represented graphically in Figure 7-27. Additionally, the first two weeks for each data point were deleted. This was done to reduce the effect of the equilibration time for each new condition.

Table 7-15 Ratio of initial flux decline for feed to concentrate with their standard deviations at each carbon loading condition as well as the number of samples used and the t-value for the difference from M=1

C Loading	Avg M	Stdev	n	t-value	Significant
0	1.232	0.480	23	2.32	Yes
0.1	0.968	0.542	11	0.20	No
0.5	1.187	0.240	12	2.70	Yes
2	1.384	0.621	16	2.48	Yes

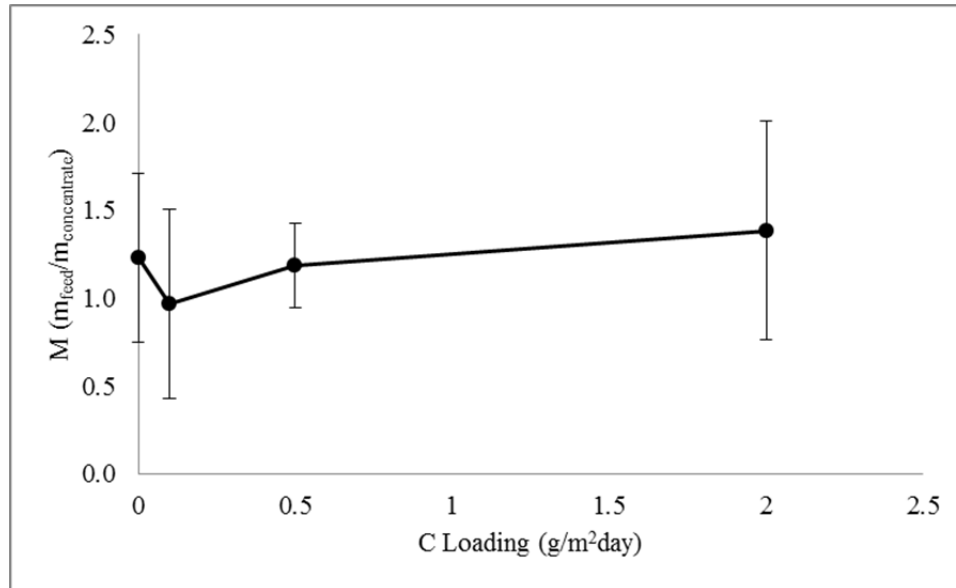


Figure 7-27 Relationship of fouling rate ratio, M, to carbon loading rate (error bars indicate standard deviation)

The data in Figure 7-27 indicate an increasing trend for the fouling rate ratio with increasing carbon loading. This indicates the biofilm on the surface of the pilot membrane element has a greater protective effect on downstream membrane material as the concentration of organic carbon in the feed water increases. The data do have a high level of variability due to slightly different conditions for each flat sheet module. Statistical analysis of each data point indicates an M value greater than 1 for the carbon loading rates of 0, 0.5, and 2.0 g C/m²day with a 95% level of confidence (see t-values in Table 7-15). Additionally, a two tailed t-test analysis was performed for each data point of increasing carbon loading to test if there was an increase in M value. Although the degradation in performance of the feed membrane swatches was significantly higher than the concentrate, the results of this two tailed t-test analysis failed to show a significant

difference in the value of M as the rate of carbon loading increases to a 95% level of confidence, Table 16.

Table 7-16 Two-tailed t-test results between each carbon loading condition showing degrees of freedom (df), t-value, and indication of significance at 0.05

C Loading 1	C Loading 2	df	t-value	Significant
0.0	0.1	32	1.44	No
0.0	0.5	33	0.31	No
0.0	2.0	37	0.86	No
0.1	0.5	21	1.27	No
0.1	2.0	25	1.80	No
0.5	2.0	26	1.04	No

7.3.2.2 Transmembrane Pressure Characterization

The pressure of each flat sheet module was monitored throughout the study. The trend commonly observed was a slight increase in pressure for the feed module with respect to the concentrate, Figure 7-28. This trend indicates an increase in resistance by the pilot membrane element, suggesting an increase in foulant material on the pilot element.

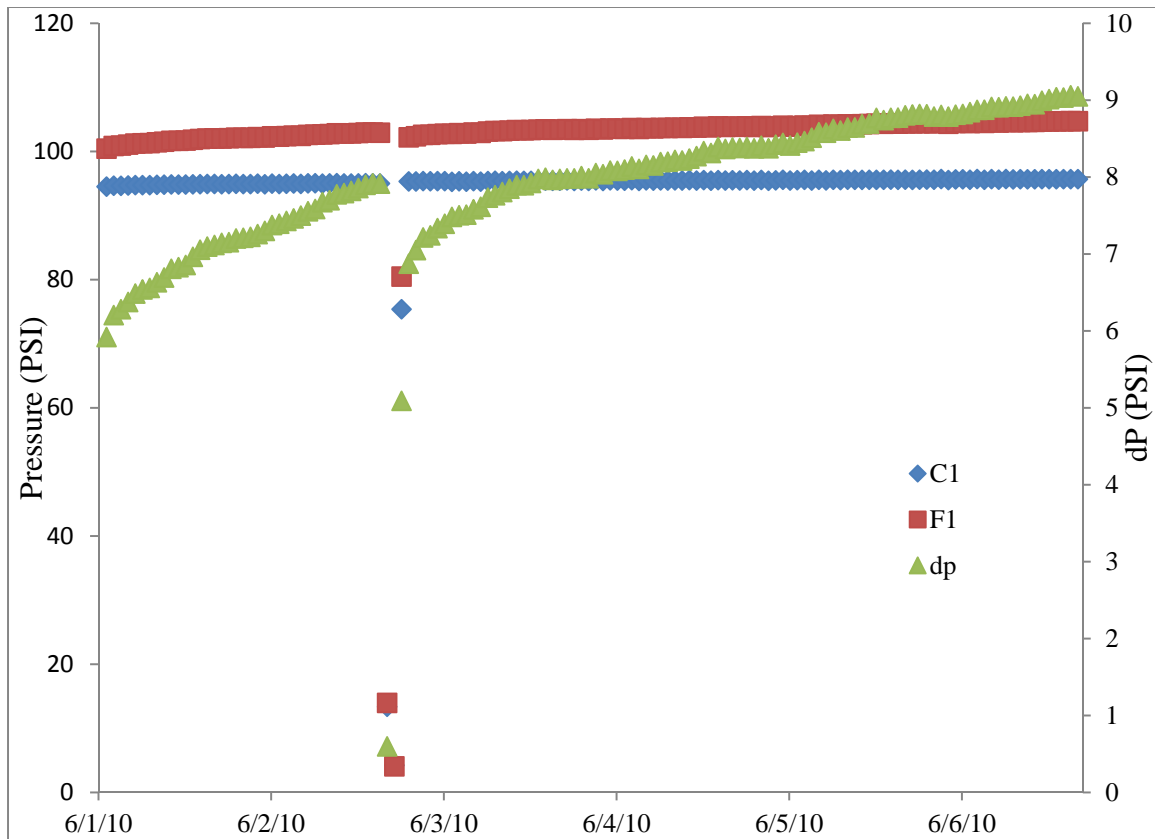


Figure 7-28 The pressure for FSM#1 feed and concentrate membrane swatches and their differential pressure

7.3.3 Flow Rate

The flow rate to the pilot system was altered between 50GPM and 25GPM for each of the carbon loading conditions (except the zero external carbon loading portion). This was performed to see if the flow rate for the system would have an effect on the relative rates of fouling for the feed and concentrate membrane material. The feed/concentrate ratio data for the 50GPM and 25GPM flow rates are in Tables 7-17 and 7-18 respectively. A two tailed t-test analysis of the data indicates no significant difference in the quantity of foulant material on the surface for the two flow rates at each carbon loading condition (except for protein at 0.5 g C/m²day). Additionally, no difference in membrane

performance was observed for each carbon loading condition at the two flow rates, Appendix E.

Table 7-17 Feed/concentrate ratio of foulants for each carbon loading level at 50GPM

Carbon Loading (g/m ² day)	Protein	Stdev	Carbohydrate	Stdev	HPC	Stdev
0	1.06	0.3	1.03	0.5	1.17	1.2
0.1	0.91	0.1	0.98	0.2	1.62	1.0
0.5	1.81	0.4	1.50	0.4	2.47	1.4
2	1.34	0.1	2.09	1.1	2.21	1.4

Table 7-18 Feed/concentrate ratio of foulants for each carbon loading level at 25GPM

Carbon Loading (g/m ² day)	Protein	Stdev	Carbohydrate	Stdev	HPC	Stdev
0	-	-	-	-	-	-
0.1	1.03	0.1	1.11	0.2	1.02	0.5
0.5	1.02	0.2	1.10	0.5	2.75	2.7
2	1.22	0.1	1.42	0.2	2.88	1.6

7.3.4 Carbon and Nitrogen Mass Balance

The procedures from Chapter 6 were followed on the pilot system to calculate the mass balance of carbon and nitrogen for the pilot system along with the change in SUVA. The percent removal of each species was calculated using Equation 6.2. The statistical analysis used to determine significance to a 95% confidence level for the mass balance and SUVA change was a t-test. Results are not available for the individual phases of external carbon loading due to problems with the instrument preventing full analyses. Thus, the available results are combined to give an overall picture, Table 7-19.

Table 7-19 The percent removal of carbon and nitrogen and percent increase in SUVA along with statistical results for the pilot system

Variable	Mean	Stdev	n	t-value	Significant
C	12.3	8.5	14	5.380	Yes
SUVA	6.2	9.6	12	2.231	Yes
N	12.7	14.7	14	3.241	Yes

The results from the analyses indicate a significant removal of carbon and nitrogen as well as a significant increase in SUVA. These results agree with the results of the mass balance analysis presented in Chapter 6. Paired with the results of the autopsies, Chapter 5, the ratio of foulant deposition/formation on the feed and concentrate surfaces of the pilot system and the performance of the feed and concentrate membrane swatches of the pilot, the data suggest the biofilm on the membrane surface is removing nutrients from the treatment water and protecting downstream membrane surfaces.

7.4 Discussion

The data and statistical analyses presented above give insight to the effect of the biofilm on downstream membrane surfaces. No relative difference in the level of fouling between the feed and concentrate membrane swatches was observed for the zero external carbon loading portion of the study. However, the carbon loading portion of the study indicated a protective effect of the pilot membrane element biofilm on downstream membrane material for both membrane foulant deposition/formation and performance.

The membrane swatches that were exposed to initial feed water stream (pilot treatment water before the pilot membrane element) exhibited an overall higher level of fouling

than the membrane swatches exposed the concentrate water stream (pilot treatment water after the pilot membrane element). Additionally, the difference in fouling seen was greater as the level of carbon loading increased, although a maximum protective effect was observed for carbon loading rate of approximately 0.5 g C/m²day. Low levels of carbon loading (including zero external carbon loading) did not reveal a significant difference in fouling between the feed and concentrate. These trends were observed with all the constituents investigated, including proteins, carbohydrates, and total culturable microorganisms (although HPC numbers were significantly different at low carbon loading levels). Parallel to the increase of protective effect (and carbon loading), the carbohydrate/protein ratio increased as well. This is likely due to the formation of more biofilm, and subsequently the excretion of more EPS. The formation of more biofilm would have the ability to remove a higher level of organic carbon, and thus have a higher protective effect on downstream membrane material.

The surface properties (i.e. roughness) and the types of foulant material deposited/formed on the feed and concentrate membrane surfaces did not change with respect to each other throughout the study. These properties were observed qualitatively with the use of SEM, EDS and AFM, and the roughness of the membrane surfaces was quantitatively measured with an AFM.

In addition to measuring the deposition/formation of foulant material on the membrane surfaces and membrane surface properties, the performance of the feed and concentrate membrane swatches was monitored in terms of permeate flux production. It was found

that the feed performance degrades faster than the concentrate in all the cases tested (except the 0.1 g C/m²day carbon loading portion). This degradation in performance agrees with the higher levels of foulant material observed on the feed test swatches. The disparity in membrane performance between the feed and concentrate also increased as the level of carbon loading to the system increased. Additionally, the pressure for the feed membrane swatches increased at a higher rate than the concentrate membrane swatches. This increase in pressure is likely the result of increased fouling on the surface of the pilot membrane element.

The carbon and nitrogen mass balance analysis on the pilot system indicated significantly positive removal from the pilot system. Additionally, there was a significant increase in SUVA (aromatic character of carbon) in the pilot system. These results agree with the analysis presented in Chapter 6, suggesting the biofilm formed in the system is responsible for the changes observed.

7.5 Conclusions

The biofilm on the membrane surface was found to have a protective effect on downstream membrane material. This protective effect manifested itself in both the deposition/formation of foulant material on the membrane surfaces and the overall performance of the membrane swatches. In both cases, this protective effect was found to be dependent on the level of carbon loading to the system. Additionally, there was a significant removal of nutrients (carbon and nitrogen) as well as a change in carbon character (SUVA increase). Although there was no observed difference for the type of

foulant material present on the feed and concentrate membrane surfaces, the difference in quantity of foulant present suggests the biofilm on the pilot membrane surface is performing as an *in situ* biofilter.

No difference in the surface roughness between the feed and concentrate swatches was observed for any portion of the study. Additionally, no differences were observed between portions of carbon loading. This suggests surface roughness is not a good indicator of relative fouling levels. The flow rate of treatment water did not appear to have an effect on the performance of the pilot system and the relative fouling and performance of the feed and concentrate membrane swatches.

Chapter 8 Conclusions

8.1 Summary of Work

The autopsy performed in OCWD revealed a gradient distribution of fouling material on the membrane surface from the highest concentration on the front section to the lowest concentration on the end section. This trend was qualitatively observed microscopically, and it was quantitatively reinforced in the measurement of protein and carbohydrate concentrations and the number of culturable organisms (HPC), although total direct count was inconclusive. The results of the HPC distribution and community profile analysis revealed the organisms at the front section of the membrane are different from those in the feed-water and other membrane sections, and they are more numerous than the other membrane sections. The results from the OCWD autopsy suggest that the biofilm on the front section of the element acts as a biological filter, removing AOC and nutrients from the feed-water, thereby making the feed-water nutrient deprived and preventing/reducing biological growth on downstream membrane surfaces.

A plant-wide autopsy results revealed an overall decreasing trend in the distribution of fouling material on the membrane surfaces for at least the first half of the membrane treatment train. Additionally, an increasing trend was observed for up to the second half of the treatment train. However, HPC increased as the treatment water traveled along the membrane surface. These results do support the hypothesis that biofilm at the lead of the

treatment train act as a biological filter, removing AOC and nutrients from the feed-water and preventing the formation of biological debris on downstream membrane surfaces. However, the tail element does have increased foulant concentrations and an increased number of culturable microorganisms are observed. This increase could be due to increased deposition of materials that have exceeded their solubility limit and an increased deposition of colloidal matter due to its higher concentration in solution.

The overall levels of foulant material on the membrane surfaces from the plant-wide membrane autopsies revealed much lower levels of fouling than the OCWD autopsy. This difference in the levels of fouling are believed to be caused by differences in the treatment process that have occurred since the OCWD autopsy. The most notable change in the process is the addition of chlorine to the raw water. A residual of total chlorine does remain in the feed water to the membrane skids. The secondary disinfectant effect of the chlorine residual is what is believed to cause this reduction in fouling on the membrane surfaces, and namely the reduction of biofilm formation observed. The chlorine residual in the treatment water is likely consumed as the water travels toward the concentrate, enabling biofilm growth at the tail of the plant

The gradient patten of fouling observed in the membrane autopsies was believed to be due to biofilm removing AOC from treatment water as it passes, making it nutrient deprived. To further investigate the idea that the biofilm on the membrane surfaces is acting as a biological filter, a carbon mass balance was performed at the Dunedin water treatment plant. These analyses revealed a reduction in the total mass of organic carbon and

nitrogen from the system as well as an increase in the aromatic character (SUVA) of the carbon in the treatment water after traveling through the membrane treatment process. This indicates a sink for the organic carbon and nitrogen in the system, likely by the biofilm growing on the surface of the membranes.

To test the level of protection afforded by the biofilm on downstream membrane surfaces, a pilot system was built and operated. The results of the pilot operation indicated a protective effect on downstream membrane material in terms of quantity of foulant deposited/formed on the membrane surface and in the flux performance. In both cases, this protective effect was found to be dependent on the level of external carbon loading to the system. The level of external carbon loading to the system also had an effect on the carbohydrate/protein ratio, suggesting to formation of higher levels of biofilm with higher levels of external carbon loading. Although there was no significant difference observed for the type of foulant between the feed and concentrate membrane surfaces and their surface roughness, the difference in quantity of foulant present suggested the biofilm on the pilot surface is performing as an *in situ* biofilter.

8.2 Impacts of Proposed Activities

Membrane fouling has traditionally been avoided and membranes cleaned thoroughly. The research goes against this convention by embracing biofouling in a limited fashion. This parallels the shift in view on biological growth on sand or media in water filtration, which was initially viewed as a nuisance. Due to the extreme difficulty with fighting the microbial growth, research was undertaken into possible advantages of the biofilms,

leading to the innovation of biofiltration. Biofiltration is currently an accepted and practiced process for reducing AOC and microbial instability in distribution water. This research could have a similar impact on spiral-wound RO systems, which commonly experience biofouling. By intentionally allowing the formation of biofilm on the lead element or a portion thereof, a more sustainable approach than the currently accepted guidelines of biofouling prevention may be achieved. The overall performance of this passive strategy of manipulating and employing biofouling could be better than the current strategy of trying to keep it from happening altogether. The development of an *in situ* biofilter will utilize existing pressure vessels, negating the need for additional capital and O&M requirements of a separate pretreatment biofiltration step.

8.3 Recommendations for Future Work

The results of this research indicate the biofilm on the membrane surfaces are performing as an *in situ* biofilter, protecting downstream membranes in terms of foulant deposition/formation and membrane performance. In order to increase the protective effect of the biofilm, different membrane materials should be tested to see if membrane surface properties could lead to higher levels of biofilm formation, increasing the protective effect on downstream membrane materials. Additionally, smoother membrane surfaces could be implemented downstream, which could lead to lower levels of fouling and higher overall performance. This could lead to a hybrid system with different membrane materials. An additional advantage of hybrid systems for a plant like the one in the City of Dunedin is tuning the salt rejection of the membranes. The aggressive

nature of the permeate water forces Dunedin to blend their treatment water. A hybrid system could reduce, or potentially eliminate this necessity.

Along the lines of a hybrid membrane treatment train, the lead RO element can be turned into a UF element by oxidation with KMnO_4 [128]. The optimal treatment time (oxidation level of the RO surface) would need to be investigated. Further, the performance of the membrane would need to be tested and tuned for the application. As with the hybrid system stated above, this method has the potential to reduce, or even eliminate the need for blending permeate water to reduce its aggressive nature.

In addition to testing the effect of carbon loading to the pilot system, a study investigating pairing carbon loading with nitrogen loading could be performed. This would give additional insight to the properties of the nutrient loading on the formation of biofilm and the protective effect that biofilm would have on downstream membrane material.

To gain a better understanding of the behavior of biofilm formation throughout the treatment plant as a function of location and membrane material, flat sheet modules could be placed at various points in the treatment train. This would allow for determinations of the protective effect of the biofilm on downstream membrane material in terms of foulant level and performance under actual treatment conditions. It would also allow for a better understanding of the behavior of the different types of membrane material tested.

It is likely the behavior of the biofilm as a biofilter is not exclusive to RO systems. Thus, this concept could be applied to other membrane types and systems. Examples include forward osmosis and nanofiltration systems.

References

1. Shannon, M.A., et al., *Science and technology for water purification in the coming decades*. Nature, 2008. 452(7185): p. 301-310.
2. Van der Bruggen, B. and Vandecasteele, C., *Removal of pollutants from surface water and groundwater by nanofiltration: overview of possible applications in the drinking water industry*. Environmental Pollution, 2003. 122(3): p. 435-445.
3. Jacangelo, J.G., Trussell, Rhodes R., and Watson, M., *Role of membrane technology in drinking water treatment in the United States*. Desalination, 1997. 113(2-3): p. 119-127.
4. Van Der Bruggen, B., et al., *A review of pressure-driven membrane processes in wastewater treatment and drinking water production*. 2003, American Institute of Chemical Engineers. p. 46-56.
5. Baker, R.W., *Membrane Technology and Applications*. 2 ed. 2004, West Sussex: John Wiley & Sons Ltd. 538.
6. Ultrapure and Industrial Services, LLT.; Available from: <http://www.ultrapure.com/equipment/filtration.php>.
7. Loeb, S. and Sourirajan, S., *Sea Water Demineralization by Means of an Osmotic Membrane*. Advances in Chemistry. Vol. 38. 1963: American Chemical Society.
8. So, M.T., et al., *Preparation of asymmetric loeb-sourirajan membranes*. Journal of Polymer Science: Polymer Letters Edition, 1973. 11(3): p. 201-205.
9. Sourirajan, S. and Agrawal, J.P., *REVERSE OSMOSIS*. Industrial & Engineering Chemistry, 1969. 61(11): p. 62-89.
10. Elimelech, M., et al., *Role of membrane surface morphology in colloidal fouling of cellulose acetate and composite aromatic polyamide reverse osmosis membranes*. Journal of Membrane Science, 1997. 127(1): p. 101-109.
11. Cadotte, J.E., et al., *A new thin-film composite seawater reverse osmosis membrane*. Desalination, 1980. 32: p. 25-31.

12. Dickson, J.M., et al., *Reverse osmosis separations of some organic and inorganic solutes in aqueous solutions using aromatic polyamide membranes*. Journal of Applied Polymer Science, 1975. 19(3): p. 801-819.
13. McKinney, R. and Rhodes, J.H., *Aromatic Polyamide Membranes for Reverse Osmosis Separations*. Macromolecules, 1971. 4(5): p. 633-637.
14. Matsuura, et al. (2010) *Thin Film Composite Membrane Preparation and Surface Modification*. SciTopics.
15. Suthanthararajan, R., et al., *Membrane application for recovery and reuse of water from treated tannery wastewater*. Desalination, 2004. 164(2): p. 151-156.
16. Wilf, M. and Alt, S., *Application of low fouling RO membrane elements for reclamation of municipal wastewater*. Desalination, 2000. 132(1-3): p. 11-19.
17. Ciardelli, G., Corsi, L., and Marcucci, M., *Membrane separation for wastewater reuse in the textile industry*. Resources, Conservation and Recycling, 2001. 31(2): p. 189-197.
18. Wintgens, T., et al., *The role of membrane processes in municipal wastewater reclamation and reuse*. Desalination, 2005. 178(1-3): p. 1-11.
19. Crittenden, J.C., et al., *Water Treatment Principles and Design*. 2 ed. 2005, Hoboken, New Jersey: MWH.
20. Allgeier, S., Alspach, B., and Vickers, J., *MEMBRANE FILTRATION GUIDANCE MANUAL*, E.P. Agency, Editor. 2005, Environmental Protection Agency. p. 332.
21. Weishaar, J.L., et al., *Evaluation of Specific Ultraviolet Absorbance as an Indicator of the Chemical Composition and Reactivity of Dissolved Organic Carbon*. Environmental Science & Technology, 2003. 37(20): p. 4702-4708.
22. Zhang, M., et al., *Fouling and Natural Organic Matter Removal in Adsorbent/Membrane Systems for Drinking Water Treatment*. Environmental Science & Technology, 2003. 37(8): p. 1663-1669.
23. Liu, C., et al. *Membrane Chemical Cleaning: From Art to Science*. in *AWWA Water Quality Technology Conference*. 2000. Denver, CO: Pall.
24. Liu, W., et al., *Investigation of assimilable organic carbon (AOC) and bacterial regrowth in drinking water distribution system*. Water Research, 2002. 36(4): p. 891-898.

25. Liang, Y., et al., *Sources and Properties of Natural Organic Matter (NOM) in Water Along the Dongjiang River (the Source of Hong Kong's Drinking Water) and Toxicological Assay of Its Chlorination By-Products*. Archives of Environmental Contamination and Toxicology, 2008. 54(4): p. 597-605.
26. Hong, S. and Elimelech, M., *Chemical and physical aspects of natural organic matter (NOM) fouling of nanofiltration membranes*. Journal of Membrane Science, 1997. 132(2): p. 159-181.
27. Allgeier, S.C. and Summers, R.S., *Evaluating NF for DBP Control with the RBSMT*. Journal AWWA, 1995. 87(3): p. 87-99.
28. Fu, P., et al., *Selecting Membranes for Removing NOM and DBP Precursors*. Journal AWWA, 1994. 86(12): p. 18.
29. Zularisam, A.W., Ismail, A.F., and Salim, R., *Behaviours of natural organic matter in membrane filtration for surface water treatment -- a review*. Desalination, 2006. 194(1-3): p. 211-231.
30. Bratby, J., *Coagulation and Flocculation in Water and Wastewater Treatment*. 2 ed. 2006: International Water Association (IWA).
31. Escobar, I.C. and Randall, A.A., *Assimilable organic carbon (AOC) and biodegradable dissolved organic carbon (BDOC):: complementary measurements*. Water Research, 2001. 35(18): p. 4444-4454.
32. Charnock, C. and Kjønne, O., *Assimilable organic carbon and biodegradable dissolved organic carbon in Norwegian raw and drinking waters*. Water Research, 2000. 34(10): p. 2629-2642.
33. Frías, J., Ribas, F., and Lucena, F., *Comparison of methods for the measurement of biodegradable organic carbon and assimilable organic carbon in water*. Water Research, 1995. 29(12): p. 2785-2788.
34. He, F., et al., *Potential for scaling by sparingly soluble salts in crossflow DCMD*. Journal of Membrane Science, 2008. 311(1-2): p. 68-80.
35. Semiat, R., Sutzkover, I., and Hasson, D., *Scaling of RO membranes from silica supersaturated solutions*. Desalination, 2003. 157(1-3): p. 169-191.
36. Boerlage, S.F.E., et al., *The scaling potential of barium sulphate in reverse osmosis systems*. Journal of Membrane Science, 2002. 197(1-2): p. 251-268.
37. Gilron, J. and Hasson, D., *Calcium sulphate fouling of reverse osmosis membranes: Flux decline mechanism*. Chemical Engineering Science, 1987. 42(10): p. 2351-2360.

38. Lee, S., Kim, J., and Lee, C.-H., *Analysis of CaSO₄ scale formation mechanism in various nanofiltration modules*. Journal of Membrane Science, 1999. 163(1): p. 63-74.
39. van de Lisdonk, C.A.C., van Paassen, J.A.M., and Schippers, J.C., *Monitoring scaling in nanofiltration and reverse osmosis membrane systems*. Desalination, 2000. 132(1-3): p. 101-108.
40. Cho, J., et al., *Characterization of clean and natural organic matter (NOM) fouled NF and UF membranes, and foulants characterization*. Desalination, 1998. 118(1-3): p. 101-108.
41. Ghosh, K. and Schnitzer, M.; *Macromolecular Structures of Humic Substances*. Soil Science, 1980. 129(5): p. 266-276.
42. Bremere, I., et al., *Controlling scaling in membrane filtration systems using a desupersaturation unit*. Desalination, 1999. 124(1-3): p. 51-62.
43. Flemming, H.C., *Biofouling in water systems – cases, causes and countermeasures*. Applied Microbiology and Biotechnology, 2002. 59(6): p. 629-640.
44. Flemming, H.C. and Wingender, J., *Relevance of microbial extracellular polymeric substances (EPSs) – Part I: Structural and ecological aspects*. Water Science and Technology: Water Supply, 2001. 43(6): p. 1-8.
45. Flemming, H.C. and Wingender, J., *Relevance of microbial extracellular polymeric substances (EPSs) – Part II: Technical aspects*. Water Science and Technology: Water Supply, 2001. 43(6): p. 9-16.
46. LeChevallier, M.W., Cawthon, C.D., and Lee, R.G., *Inactivation of Biofilm Bacteria*. Appl. Environ. Microbiol., 1988. 54(10): p. 2492-2499.
47. Mallevaille, J., Odendaal, P.E., and Wiesner, M.R., *Water Treatment Membrane Processes* 1ed. 1996: McGraw-Hill.
48. Ridgway, H.F., Rigby, M.G., and Argo, D.G., *Bacterial Adhesion and Biofouling of Reverse Osmosis Membranes*. Journal AWWA, 1985. 77(7): p. 97-106.
49. Darton, E.G. and Fazel. M., *A Statistical Review of 150 Membrane Autopsies*. 2002; Available from: <http://www.derwentwatersystems.co.uk/chemical-treatments/paper-four.pdf>.
50. Durham, B. and Walton, A., *Membrane pretreatment of reverse osmosis: long-term experience on difficult waters*. Desalination, 1999. 122(2-3): p. 157-170.

51. Kim, S.H., et al., *Design of TiO₂ nanoparticle self-assembled aromatic polyamide thin-film-composite (TFC) membrane as an approach to solve biofouling problem*. Journal of Membrane Science, 2003. 211(1): p. 157-165.
52. Song, W., et al., *Nanofiltration of natural organic matter with H₂O₂/UV pretreatment: fouling mitigation and membrane surface characterization*. Journal of Membrane Science, 2004. 241(1): p. 143-160.
53. Wend, C.F., et al., *Pretreatment for membrane water treatment systems: a laboratory study*. Water Research, 2003. 37(14): p. 3367-3378.
54. Wolf, P.H., Siverns, S., and Monti, S., *UF membranes for RO desalination pretreatment*. Desalination, 2005. 182(1-3): p. 293-300.
55. Brehant, A., Bonnelye, V., and Perez, M., *Comparison of MF/UF pretreatment with conventional filtration prior to RO membranes for surface seawater desalination*. Desalination, 2002. 144(1-3): p. 353-360.
56. Freese, S.D., Noziac, D. J., *Chlorine: is it really so bad and what are the alternatives?* Water SA, 2004. 30(5): p. 4.
57. Applegate, L.E., Erkenbrecher, C.W., and Winters, H., *New chloroamine process to control aftergrowth and biofouling in permasepR B-10 RO surface seawater plants*. Desalination, 1989. 74: p. 51-67.
58. Bouwer, E.J. and Crowe, P.B., *Biological Processes in Drinking Water Treatment*. Journal AWWA, 1988. 80(9): p. 12.
59. Scott, J.P. and Ollis, D.F., *Integration of chemical and biological oxidation processes for water treatment: Review and recommendations*. 1995, American Institute of Chemical Engineers. p. 88-103.
60. Huck, P.M., Fedorak, P.M., and Anderson, W.B., *Formation and Removal of Assimilable Organic Carbon During Biological Treatment*. Journal AWWA, 1991. 83(12): p. 12.
61. *PRACTICAL EXPERIENCES WITH BIOLOGICAL TREATMENT OF ODOR AND VOCS AT POTWS IN USA*. Proceedings of the Water Environment Federation, 2002. 2002: p. 705-726.
62. Leson, G. and Winer, A.M., *Biofiltration: An innovative air pollution control technology for VOC emissions*. Journal of the Air and Waste Management Association ; Vol/Issue: 41:8, 1991: p. 1045-1054.

63. Gao, L., et al., *A technical and economic comparison of biofiltration and wet chemical oxidation (scrubbing) for odor control at wastewater treatment plants*. Environmental Engineering and Policy, 2001. 2(4): p. 203-212.
64. Meesters, K.P.H., Van Groenestijn, J.W., and Gerritse, J., *Biofouling reduction in recirculating cooling systems through biofiltration of process water*. Water Research, 2003. 37(3): p. 525-532.
65. Schuenhoff, A., et al., *A semi-recirculating, integrated system for the culture of fish and seaweed*. Aquaculture, 2003. 221(1-4): p. 167-181.
66. Chen, C., et al., *Comparison of seven kinds of drinking water treatment processes to enhance organic material removal: A pilot test*. Science of The Total Environment, 2007. 382(1): p. 93-102.
67. Chien, C.C., et al., *Application of biofiltration system on AOC removal: Column and field studies*. Chemosphere, 2008. 71(9): p. 1786-1793.
68. Huang, X., Leal, M., and Li, Q., *Degradation of natural organic matter by TiO₂ photocatalytic oxidation and its effect on fouling of low-pressure membranes*. Water Research, 2008. 42(4-5): p. 1142-1150.
69. Treguer, R., et al., *Ozonation effect on natural organic matter adsorption and biodegradation - Application to a membrane bioreactor containing activated carbon for drinking water production*. Water Research. 44(3): p. 781-788.
70. Cohen, Y., *Biofiltration - the treatment of fluids by microorganisms immobilized into the filter bedding material: a review*. Bioresource Technology, 2001. 77(3): p. 257-274.
71. Kolehmainen, R.E., Langwaldt, J.H., and Puhakka, J.A., *Natural organic matter (NOM) removal and structural changes in the bacterial community during artificial groundwater recharge with humic lake water*. Water Research, 2007. 41(12): p. 2715-2725.
72. Escobar, I.C., Hong, S., and Randall, A.A., *Removal of assimilable organic carbon and biodegradable dissolved organic carbon by reverse osmosis and nanofiltration membranes*. Journal of Membrane Science, 2000. 175(1): p. 1-17.
73. Ong S. et al., *Effect of AOC on Membrane Biofouling*. Advanced Asian Environmental Engineering, 2002. 2: p. 30-36.
74. Hu, J.Y., et al., *The effect of water treatment processes on the biological stability of potable water*. Water Research, 1999. 33(11): p. 2587-2592.

75. Yavich, A.A., et al., *Evaluation of biodegradability of NOM after ozonation*. Water Research, 2004. 38(12): p. 2839-2846.
76. Norton, C.D. and LeChevallier, M.W., *A Pilot Study of Bacteriological Population Changes through Potable Water Treatment and Distribution*. Appl. Environ. Microbiol., 2000. 66(1): p. 268-276.
77. Pang, C.M. and Liu, W.-T., *Biological Filtration Limits Carbon Availability and Affects Downstream Biofilm Formation and Community Structure*. Appl. Environ. Microbiol., 2006. 72(9): p. 5702-5712.
78. LeChevallier, M.W., Welch, N.J., and Smith, D.B., *Full-scale studies of factors related to coliform regrowth in drinking water*. Appl. Environ. Microbiol., 1996. 62(7): p. 2201-2211.
79. Camper, A.K., *Involvement of humic substances in regrowth*. International Journal of Food Microbiology, 2004. 92(3): p. 355-364.
80. Gabelich, C.J., et al., *Pilot-scale testing of reverse osmosis using conventional treatment and microfiltration*. Desalination, 2003. 154(3): p. 207-223.
81. Hu, J.Y., et al., *Biofiltration pretreatment for reverse osmosis (RO) membrane in a water reclamation system*. Chemosphere, 2005. 59(1): p. 127-133.
82. Hallé, C., et al., *Assessing the Performance of Biological Filtration As Pretreatment to Low Pressure Membranes for Drinking Water*. Environmental Science & Technology, 2009. 43(10): p. 3878-3884.
83. Nederlof, M.M., et al., *Integrated multi-objective membrane systems application of reverse osmosis at the Amsterdam Water Supply*. Desalination, 1998. 119(1-3): p. 263-273.
84. *Orange County Water District R&D, Koch TFCS 9921S Membrane Autopsy Results Prepared for the City of Dunedin*. 2006, Orange County Water District R&D Department.
85. Carnahan, R.P., Bolin, L., and Suratt, W., *Biofouling of PVD-1 reverse osmosis elements in the water treatment plant of the City of Dunedin, Florida*. Desalination, 1995. 102(1-3): p. 235-244.
86. Lovins, W.A., et al., *City of Dunedin Membrane Softening WTP Alternative Pretreatment Evaluation*. 2005, Boyle: Orlando, FL.
87. Strickland, J.D.H. and Parsons, T.R., *A Practical Handbook of Seawater Analysis*. Vol. 167. 1968: Fisheries Research Board of Canada.

88. Ridgway, H.F., et al., *Biofilm Fouling of RO Membranes - Its Nature and Effect on Treatment of Water for Reuse*. Journal AWWA, 1984. 76(6): p. 9.
89. Lazarova, V. and Manem, J., *Biofilm characterization and activity analysis in water and wastewater treatment*. Water Research, 1995. 29(10): p. 2227-2245.
90. Eaton, A.D. and Franson, M.A.H., *Standard methods for the examination of water & wastewater*. 21 ed, ed. L.S. Clesceri, A.E. Greenberg, and E.W. Rice. 2005: American Water Works Association; Water Environment Federation; American Public Health Association Publications
91. Flemming, H.C., et al., *Biofouling--the Achilles heel of membrane processes*. Desalination, 1997. 113(2-3): p. 215-225.
92. Lowry, O.H., et al., *Protein Measurement with the Folin Phenol Reagent*. Journal of Biological Chemistry, 1951. 193(1): p. 265-275.
93. Ferlita, R., et al. *A Simple Modified Freeze-Fracture Method for SEM Imaging of Membrane Cross Sections*. in *Annual Meeting of the North American Membrane Society*. 2007. Orlando, FL.
94. Ferlita, R., et al., *Cryo-snap: A simple modified freeze-fracture method for SEM imaging of membrane cross sections*. Environmental Progress, 2008.
95. *Membrane Filtration Guidance Manual*. 2003.
96. Vrijenhoek, E.M., Hong, S., and Elimelech, M., *Influence of membrane surface properties on initial rate of colloidal fouling of reverse osmosis and nanofiltration membranes*. Journal of Membrane Science, 2001. 188(1): p. 115-128.
97. Kwak, S.Y., Kim, S.H., and Kim, S.S., *Hybrid Organic/Inorganic Reverse Osmosis (RO) Membrane for Bactericidal Anti-Fouling. 1. Preparation and Characterization of TiO₂ Nanoparticle Self-Assembled Aromatic Polyamide Thin-Film-Composite (TFC) Membrane*. Environ. Sci. Technol., 2001. 35(11): p. 2388-2394.
98. Czekaj, P., Lopez, F., and Guell, C., *Membrane fouling by turbidity constituents of beer and wine: characterization and prevention by means of infrasonic pulsing*. Journal of Food Engineering, 2001. 49(1): p. 25-36.
99. Wang, S., Guillen, G., and Hoek, E.M.V., *Direct Observation of Microbial Adhesion to Membranes*. Environ. Sci. Technol., 2005. 39(17): p. 6461-6469.
100. Chang, I.S., et al., *Membrane fouling in membrane bioreactors for wastewater treatment*. Journal of Environmental Engineering-Asce, 2002. 128(11): p. 1018-1029.

101. Ho, C.-C. and Zydney, A.L., *Effect of membrane morphology on the initial rate of protein fouling during microfiltration*. Journal of Membrane Science, 1999. 155(2): p. 261-275.
102. Kang, S.-T., et al., *Direct observation of biofouling in cross-flow microfiltration: mechanisms of deposition and release*. Journal of Membrane Science, 2004. 244(1-2): p. 151-165.
103. Kim, S. and Hoek, E.M.V., *Interactions controlling biopolymer fouling of reverse osmosis membranes*. Desalination, 2007. 202(1-3): p. 333-342.
104. Lee, S., et al., *Natural organic matter fouling due to foulant-membrane physicochemical interactions*. Desalination, 2007. 202(1-3): p. 377-384.
105. Li, Q. and Elimelech, M., *Synergistic effects in combined fouling of a loose nanofiltration membrane by colloidal materials and natural organic matter*. Journal of Membrane Science, 2006. 278(1-2): p. 72-82.
106. Liang, S. and Song, L.F., *Characteristics and fouling behaviors of dissolved organic matter in submerged membrane bioreactor systems*. Environmental Engineering Science, 2007. 24(5): p. 652-662.
107. F. A. Stevie, et al., *Application of focused ion beam lift-out specimen preparation to TEM, SEM, STEM, AES and SIMS analysis*. Surface and Interface Analysis, 2001. 31(5): p. 345-351.
108. Lo, Horace Ho-Kei, et al., *Characterization of the lubricant layer formed at the interface between the extrudate and the die wall during the extrusion of high density polyethylene and fluoroelastomer blends by XPS, SIMS and SEM*. Polymer Engineering & Science, 1999. 39(4): p. 721-732.
109. Bozzola, J.J. and Russell, L.D., *Electron Microscopy Principles and Techniques for Biologists*. 2nd ed. 1999, Sudbury, MA: Jones and Bartlett Publishers.
110. Neden, D.G., et al., *Comparing Chlorination and Chloramination for Controlling Bacterial Regrowth*. Journal AWWA, 1992. 84(7): p. 9.
111. Kwon, Y.-N. and Leckie, J.O., *Hypochlorite degradation of crosslinked polyamide membranes: I. Changes in chemical/morphological properties*. Journal of Membrane Science, 2006. 283(1-2): p. 21-26.
112. Prevost, M., et al., *Biodegradable Organic Matter in Drinking Water and Distribution*. 1 ed. 2005, Denver, CO: American Water Works Association.
113. Singer, P.C., *Humic Substances as Precursors for Potentially Harmful Disinfection By-Products*. Water Science and Technology, 1999. 40(9): p. 25-30.

114. Schwartz, T., Hoffmann, S., and Obst, U., *Formation and bacterial composition of young, natural biofilms obtained from public bank-filtered drinking water systems*. Water Research, 1998. 32(9): p. 2787-2797.
115. Siddiqui, M.S., Amy, G.L., and Murphy, B.D., *Ozone enhanced removal of natural organic matter from drinking water sources*. Water Research, 1997. 31(12): p. 3098-3106.
116. Fabris, R., et al., *Comparison of NOM character in selected Australian and Norwegian drinking waters*. Water Research, 2008. 42(15): p. 4188-4196.
117. Hörsch, P., et al., *Biofouling of ultra- and nanofiltration membranes for drinking water treatment characterized by fluorescence in situ hybridization (FISH)*. Desalination, 2005. 172(1): p. 41-52.
118. Her, N., et al., *Characterizing dissolved organic matter and evaluating associated nanofiltration membrane fouling*. Chemosphere, 2008. 70(3): p. 495-502.
119. Ates, N., et al., *Removal of disinfection by-product precursors by UF and NF membranes in low-SUVA waters*. Journal of Membrane Science, 2009. 328(1-2): p. 104-112.
120. Mladenov, N., et al., *Dissolved Organic Matter Accumulation, Reactivity, and Redox State in Ground Water of a Recharge Wetland*. Wetlands, 2008. 28(3): p. 747-759.
121. Westerhoff, P. and Pinney, M., *Dissolved organic carbon transformations during laboratory-scale groundwater recharge using lagoon-treated wastewater*. Waste Management, 2000. 20(1): p. 75-83.
122. Qin, J.-J., et al., *Impact of coagulation pH on enhanced removal of natural organic matter in treatment of reservoir water*. Separation and Purification Technology, 2006. 49(3): p. 295-298.
123. van Leeuwen, J., Daly, R., and Holmes, M., *Modeling the treatment of drinking water to maximize dissolved organic matter removal and minimize disinfection by-product formation*. Desalination, 2005. 176(1-3): p. 81-89.
124. Chin, A. and Bérubé, P.R., *Removal of disinfection by-product precursors with ozone-UV advanced oxidation process*. Water Research, 2005. 39(10): p. 2136-2144.
125. Hammes, F., et al., *Mechanistic and kinetic evaluation of organic disinfection by-product and assimilable organic carbon (AOC) formation during the ozonation of drinking water*. Water Research, 2006. 40(12): p. 2275-2286.

126. Hozalski, R.M., Goel, S., and Bouwer, E.J., *TOC Removal in Biological Filters*. Journal AWWA, 1995. 87(12): p. 15.
127. Mosqueda-Jimenez, D.B. and Huck, P.M., *Effect of biofiltration as pretreatment on the fouling of nanofiltration membranes*. Desalination, 2009. 245(1-3): p. 60-72.
128. Veza, J.M. and Rodriguez-Gonzalez, J.J., *Second use for old reverse osmosis membranes: wastewater treatment*. Desalination, 2003. 157(1-3): p. 65-72.

Appendices

Appendix A Plant Diagram

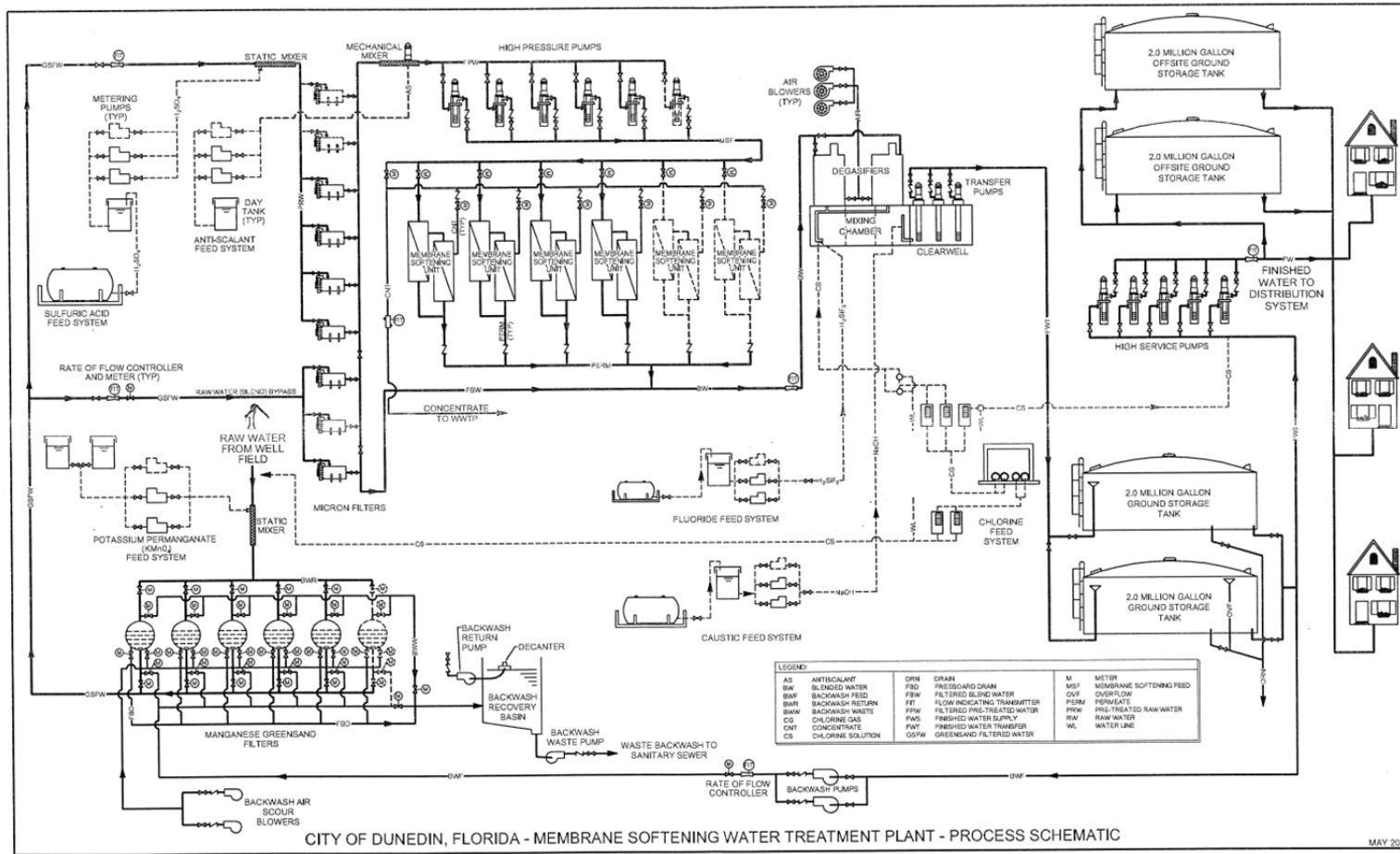


Figure A-1 Plant Diagram

Appendix B Analytical Methods SOPs

Carbohydrate Assay

Objective:

The purpose of this analysis is to measure the total carbohydrate concentration of a sample in question.

Reagents:

1. Reagent A: Phenol Reagent

A 25g aliquot of ultra-pure phenol is dissolved in 500mL DI water

Store in an all-glass container that will prevent exposure to light

2. Reagent B: Sulfuric Acid Reagent

2.5g of Hydrazine Sulfate in dissolved in 500mL Concentrated Sulfuric Acid

Sample Preparation:

1. A measured sample, mass or area depending on desired units, is placed into a 20 mL scintillation vial
2. 10mL distilled water is added to the sample
3. The sample is sonicated for 10 minutes (additional 5 minute increments can be added if sample is not completely suspended)
4. The sample is vortex mixed prior to removal of any sample

Appendix B (Continued)

Method:

1. A 0.5mL aliquot of sample is added to a 100x15mm test tube
2. A 0.5mL aliquot of the Phenol Reagent is added to sample
3. A 2.5mL aliquot of the sulfuric acid reagent is rapidly added to the sample from a pipette while rapidly vortex mixing.

Note: use a pipette pump that will allow complete rapid delivery of sulfuric acid reagent, taking care not to break tube with pipette tip.

Caution: The sulfuric acid reagent generates excessive amounts of heat. Use proper safety attire and carry out the reaction in a fume hood.

4. The tubes are then covered with aluminum foil and allowed to cool at room temperature in a dark place for one hour (color is stable for 24 hours)
5. The optical density of the sample is measured at 490nm using a UV-VIS spectrophotometer

Calibration Curve:

A stock solution of glucose (dextrose) is prepared by dissolving 0.100g in 1000mL DI water. The following table is used for the calibration curve of the concentration of carbohydrates. Micro-pipettors and cuvettes are used to make the dilutions/measure absorption spectra. Calibration samples are run in triplicate to ensure reproducibility of the data.

Appendix B (Continued)

Table B-1 Dilution series for carbohydrate calibration

mg/mL Concentration Sugars (Dextrose)	μ L Dextrose Stock Solution	μ L DI Water
100	500	0
70	350	150
50	250	250
30	150	350
10	50	450
0	0	500

Appendix B (Continued)

Total Direct Count

Objective:

The purpose of this analysis is to measure the total microorganisms present per unit area (mass may also be used).

Reagents:

1. Reagent A: DAPI

10mg DAPI is dissolved in 10mL DI water for stock solution

100 μ L diluted to 900 μ L working stock

2. Reagent B: Phosphate Buffer

A 13.6 g/L solution of potassium phosphate monobasic is prepared and adjusted to pH 7 with potassium phosphate dibasic. 100 mg sodium pyruvate is dissolved in 1L of this solution.

Method:

1. A measured sample, mass or area depending on desired units, is placed into a vial
2. 10mL phosphate buffer is added to the sample
3. The sample is then sonicated for 10 minutes (Triplicates may be taken to ensure reproducibility in the data)
4. If biofilm not completely removed, sonicate for increments of 5 additional minutes until biofilm is completely removed

Appendix B (Continued)

5. The sample is vortex mixed prior to removal of any sample
6. A 5mL aliquot of sample placed into a vial
7. A 5 μ L aliquot of DAPI working stock is added to vial with sample and vortex mixed
8. Sample is allowed to sit in dark for 5 minutes
9. A 1mL aliquot of sample is diluted to 10mL with phosphate buffer and vortex mixed
10. A 1mL aliquot of sample is filtered through a 0.2 μ m filter disk
11. Filter disk is washed with an additional 2mL phosphate buffer
12. Filter disk is analyzed with an Epifluorescent microscope

Note: additional and/or different dilutions may be prepared as needed.

Appendix B (Continued)

Heterotrophic Plate Count

Objective:

The purpose of this analysis is to measure the total number of culturable microorganisms present per unit area (mass may also be used).

Reagents:

1. Reagent A: R2A Agar

A solution of agar is prepared as per manufacturers specifications. Approximately 25-30mL agar is placed in sterile petri dish (prepare enough to perform analyses).

2. Reagent B: Phosphate Buffer

A 13.6 g/L solution of potassium phosphate monobasic is prepared and adjusted to pH 7 with potassium phosphate dibasic. 100 mg sodium pyruvate is dissolved in 1 L of this solution.

Method:

1. A measured sample, mass or area depending on desired units, is placed into a vial
2. 10mL phosphate buffer is added to the sample
3. The sample is then sonicated for 10 minutes (Triplicates may be taken to ensure reproducibility in the data)

Appendix B (Continued)

4. If biofilm not completely removed, sonicate for increments of 5 additional minutes until biofilm is completely removed
5. The sample is vortex mixed prior to removal of any sample
6. A 10 μ L aliquot of sample is diluted to 10mL with R2A broth (the resulting solution is a 10⁻³ dilution)
7. A 1000 μ L aliquot of resulting solution from step 6 is diluted to 10mL with R2A broth (the resulting solution is a 10⁻⁴ dilution)
8. A 1000 μ L aliquot of resulting solution from step 7 is diluted to 10mL with R2A broth (the resulting solution is a 10⁻⁵ dilution)
9. A 10 μ L aliquot of the 10⁻³ dilution (step 6) is placed on a R2A agar plate, spreading the sample throughout using a L-shaped glass rod and a Lazy Suzan resulting in a 10⁻⁵ dilution (L-shaped rod is dipped in ethanol and flame sterilized prior to spreading each plate)
10. A 10 μ L aliquot of the 10⁻⁴ dilution solution is placed on a R2A agar plate, spreading the sample throughout using a L-shaped glass rod and a Lazy Suzan (resulting in a 10⁻⁶ dilution)
11. A 10 μ L aliquot of the 10⁻⁵ dilution solution is placed on a R2A agar plate, spreading the sample throughout using a L-shaped glass rod and a Lazy Suzan (resulting in a 10⁻⁷ dilution)

Note: additional and/or different dilutions may be prepared as needed.

Appendix B (Continued)

Protein Assay

Objective:

The purpose of this analysis is to measure the total protein concentration of a sample in question.

Reagents:

1. Reagent A: 4% Sodium Carbonate in 0.2N Sodium Hydroxide
8g NaOH dissolved in 1000mL DI water
40g Na₂CO₃ dissolved in 960mL NaOH solution
2. Reagent B: 2% Copper Sulfate
0.5g CuSO₄ dissolved in 24.5mL DI water
3. Reagent C: 4% Sodium Tartrate
1.0g Sodium Tartrate dissolved in 24mL DI water (potassium tartrate may also be used)
4. Reagent D
100mL Reagent A, 1.0mL Reagent B, and 1.0mL Reagent C
5. Reagent E
1:1 mixture of Folin's Reagent to DI water

Appendix B (Continued)

Sample Preparation:

1. A measured sample, mass or area depending on desired units, is placed into a vial
2. 10mL DI water is added to the sample
3. The sample is then sonicated for 10 minutes (if biofilm not completely removed, sonicate for increments of 5 additional minutes until biofilm is completely removed)
4. The sample is vortex mixed prior to removal of any sample

Method:

1. 2.0mL of Reagent D is added to 2.0mL sample
2. Mixture is vortex mixed
3. Sample is allowed to sit for 10 minutes
4. 0.4mL Reagent E is added to the mixture
5. Sample is vortex mixed and allowed to sit for 30 minutes
6. The optical density of the sample is measured at 550nm using a UV-VIS spectrophotometer

Appendix B (Continued)

Calibration Curve:

A stock solution of Bovine Serum Albumin (BSA) is prepared by dissolving 0.100g in 1000mL DI water, making sure to gently agitate as to prevent foaming of sample. The following table is used for the calibration curve of the concentration of protein. Micro-pipettors and cuvettes are used to make the dilutions/measure absorption spectra. Calibration samples are run in triplicate to ensure reproducibility of the data.

Table B-2 Dilution series for protein calibration

mg/L Concentration Protein (BSA)	mL BSA Stock Solution	mL DI Water
100	10.0	0.0
75	7.5	2.5
50	5.0	5.0
25	2.5	7.5
10	1.0	9.0
0	0.0	10.0

Appendix C Pilot System Operation

The pilot system consists of two main parts, the skid with the membrane element and the flat sheet module portion with the membrane samples for analysis. This appendix lays out the operation of the skid, retrieval of the data, and operation and sampling from the flat sheet module portion.

Filling the Feed Tank

A 150 gallon feed tank is connected to the system for recirculation of fluid through the system. The feed tank can be filled with a variety of fluids; including plant feed water, plant concentrate water, or any combination thereof. To fill the tank with plant feed water, the following procedure is used (refer to Figure C-1 for identification of named devices on pilot system):

1. Ensure valves V1, V4, V6, V7, V12, and V16 are in the closed position
2. Ensure valves V2 and V3 are in the open position
3. Slowly open valve V5 and monitor the water level in the feed tank
4. Slowly close valve V5 when the feed tank is at approximately 145 gal

To fill the feed tank with plant concentrate, the following procedure is used (refer to Figure C-1 for identification of named devices on skid):

1. Ensure valves V1, V4, V10, V12, and V16 are on the closed position
2. Ensure valve V14 is in the open position
3. Slowly open valve V13 and monitor the water level in the feed tank

Appendix C (Continued)

4. Slowly close valve V13 when the feed tank is at approximately 145 gal

The pilot system is currently not designed to be filled with plant permeate water. However, simple modification to the system can be undertaken to accommodate this.

Pilot Skid Operation

The pilot skid is designed to operate under actual plant conditions. Additionally, the pilot skid has been built to allow flexibility in feed flow and pressure, allowing for a wide range of potential studies. Once the tank has been filled with the desired feed-water, the operation of the skid is outlined as follows (refer to Figure C-1 for identification of named devices on pilot system):

1. Ensure valves V1, V2, V3, V6, V9, V10, V14, V15, and V18 are in the open position
2. Ensure valves V4, V5, V7, V8, V11, V12, V13, V16, and V17 are in the closed position
3. Turn on the chiller and set the temperature to the desired set point
4. On the pump control panel, press the green FWD button (Figure C-3), press the up button to start pump, and close valve V2
5. Press the up button to increase the pump speed and partially close valve V10 (Alternate increasing pump speed and valve adjustment until desired pressure and flow rate are achieved)

Appendix C (Continued)

During pump startup, check pressure and flow rates to ensure all procedures were followed correctly. If pressure increases too rapidly, or not at all, immediately press the red STOP button (figure C-3) and check all valves. If a significant leak is detected, press the red STOP button and perform necessary repairs.

Draining the Feed Tank

The feed tank can be periodically drained for refilling as often as necessary for experimental design. Draining the feed tank is performed as follows (refer to Figure C-1 for identification of named devices on pilot system):

1. Ensure valves V5 and V13 are in the closed position
2. Ensure valves V1, V2, V3, V4, V6, V7, V12, V15 and V16 are in the open position
3. Allow tank to drain completely

Data Acquisition

The pilot system is designed to collect pressure and flow data for the pilot skid. Additionally, the pressure and flow for each flat sheet module is also collected. All data are collected and saved on two HOBO U30 weather stations (for FSM feed portion, for FSM concentrate portion).

1. A computer with HOBO software is connected to the HOBO U30 weather station via a USB cable.
2. Launch HOBO software.

Appendix C (Continued)

3. In the upper left portion of the screen, select launch weather station.
4. Pop-up screen will appear. Ensure all sensors appear in the pop-up screen. If not, check all connections, sensors and adaptors.
5. Select the desired data acquisition parameters.
6. Click launch to activate data logger.
7. Once parameters are finished loading, disconnect computer from U30 device

The data may be downloaded and exported for analysis periodically from the U30 weather stations. The following procedure is followed for data export:

1. A computer with HOBO software is connected to the HOBO U30 weather station via a USB cable.
2. Launch HOBO software
3. The Readout button is chosen on the upper left portion of the screen.
4. A file name and file location is chosen.
5. Data may be exported in .CSV format, enabling analysis in Excel.

Appendix C (Continued)

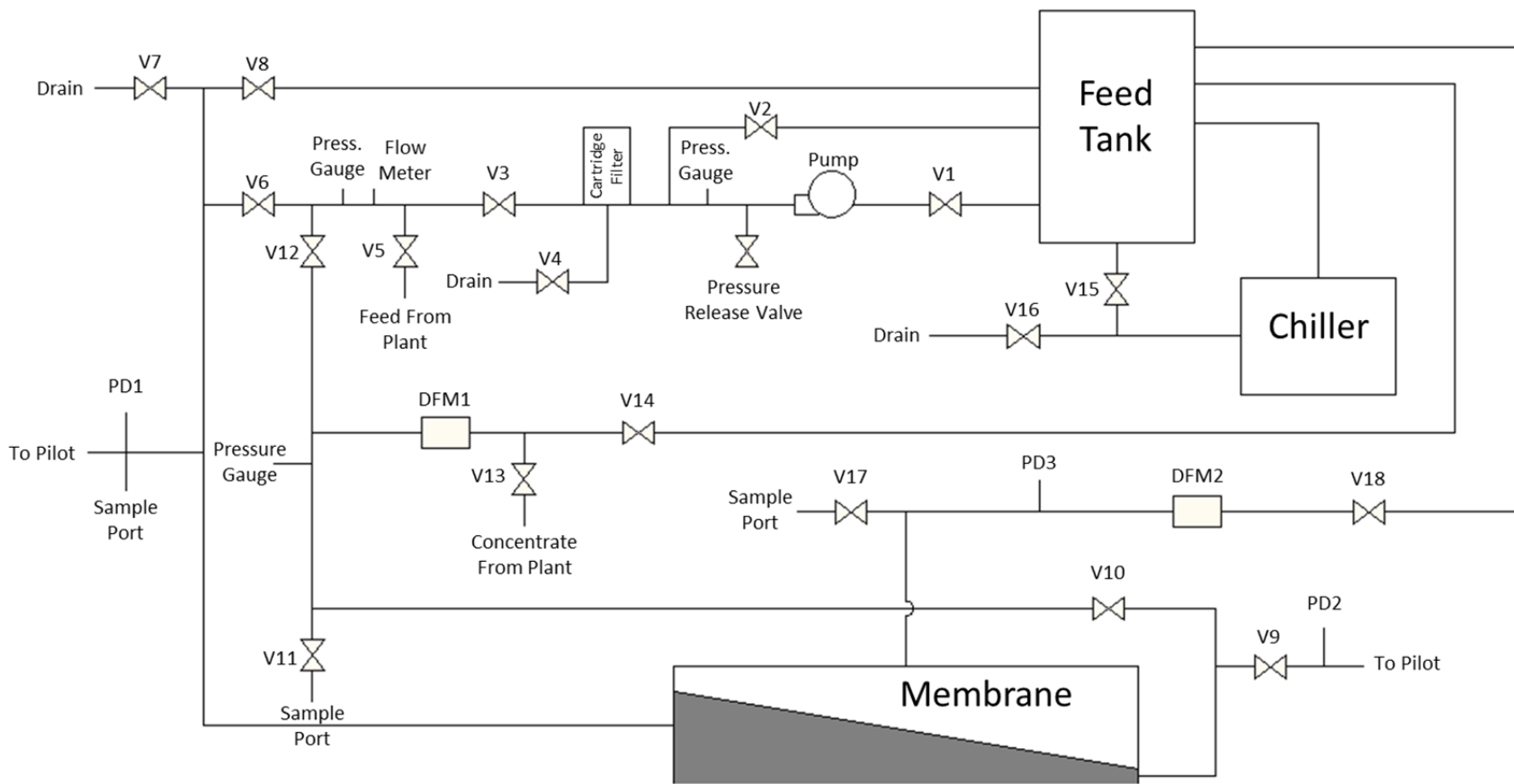


Figure C-1 Schematic of pilot system, not including flat sheet module portion

Appendix C (Continued)



Figure C-2 Pump interface for pilot system

Flat Sheet Module Pilot Operation

The flat sheet module portion of the pilot system is connected to the pilot system skid. Thus, the approximate pressure, temperature, and feed water are consistent with what is chosen for the pilot system skid. The flat sheet module portion contains 4 individual flat sheet modules, each with its own pressure transducer, variable flow meter, and rain gage (for permeate flow). The four flat sheet modules are fed with pilot water through a manifold system.

Appendix C (Continued)

The concentrate water from each flat sheet module is combined and returned to the pilot system feed tank. The permeate water from all flat sheet modules is collected in a basin, and then pumped back into the feed tank using a bilge pump. Identical flat sheet module pilot portions are connected to the feed and concentrate portions of the pilot system skid. For operation, the valves from the skid to the flat sheet modules are opened completely (Figure C-1). The flow meters on the concentrate portion of the individual flat sheet modules are variable, allowing for adjustment of cross flow velocity on each flat sheet module, Figure C-3. The flow chosen for this study was 1200 ccm, since it approximates the cross flow velocity of the Dunedin water treatment plant operational conditions.

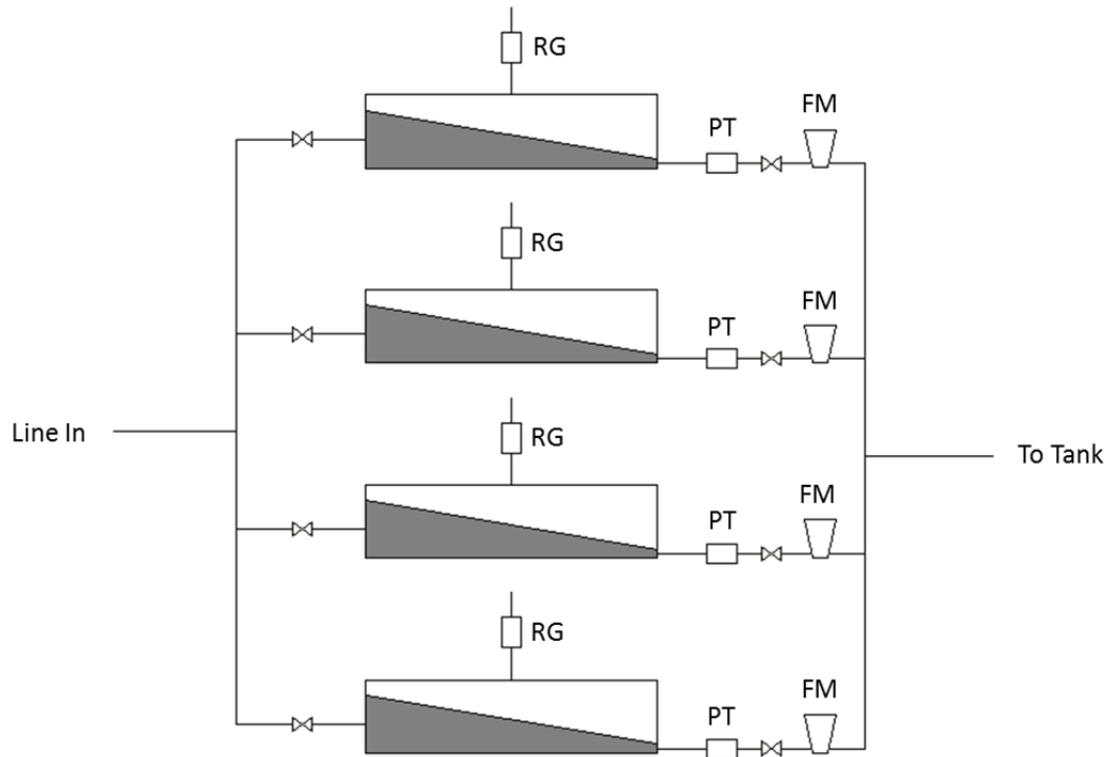


Figure C-3 Schematic of flat sheet module portion of pilot system

Appendix C (Continued)

Membrane Swatch Sample Exchange

Different membrane materials and/or types can be tested and analyzed at desired time points in the flat sheet module pilot system, Figure C-3. The individual flat sheet modules (Sterlitech CF042 cross flow cells) are used to hold and test the membrane material, Figure C-4. Prior to exchanging membrane swatches, the pilot system skid pump is turned off, and the valves to the flat sheet module portion are closed. To exchange membrane swatches, the wing nuts are removed, the two halves separate and the old membrane swatch is removed and placed into a storage container for later analysis. A new membrane swatch is cut using the template (included with the modules and in tool kit at plant), scissors, and a single hole punch. The new membrane swatch is placed into module, ensuring proper alignment, the two halves are closed together, and the wing nuts are retightened.

Appendix D Additional Carbon Balance Information

In addition to performing a carbon and nitrogen mass balance on the treatment train level, a mass balance analysis was also performed on the individual skid and the individual stage levels. This appendix contains additional information from the skid and stage level carbon and nitrogen mass balance, the SUVA analysis, the plant sampling information, and data.

Plant Sampling

Water samples were collected as per the procedures outlined in Chapter 3. In addition to collecting the membrane treatment train feed, permeate and concentrate; samples of the stage I permeate, stage II feed, stage II permeate, and stage II concentrate were taken for the skid and stage mass balance analysis, Figure D-1. The feed for the skid was assumed to be the same as the treatment train feed. Data for the flow of each sample were obtained from the plant SCADA system, except for the stage II concentrate. This flow rate was calculated by stage I permeate from stage I feed since the plant did not have a flow meter to monitor this flow. The mass balance of the individual skid can be written as in equation D.1.

$$Q_{S1F}C_{S1F} = Q_{SP}C_{SP} + Q_{S2C}C_{S2C} + M_R \quad (D.1)$$

Appendix D (Continued)

where Q_{S1F} is the flow rate of the feed to the skid, C_{S1F} is the concentration of carbon (or nitrogen) in the skid feed, Q_{SP} is the flow rate of the skid permeate, C_{SP} is the concentration in the skid permeate, Q_{S2C} is the flow rate of the skid concentrate, C_{S2C} is the concentration in the skid concentrate, and M_R represents the mass of the organic carbon (or nitrogen) removed from the system by assimilation or degradation. To calculate the percentage of carbon (or nitrogen) removed from the skid, Equation D.2 is used.

$$\% \text{Removal} = \frac{\text{mass removed}}{\text{mass input}} \times 100 = \frac{Q_{S1F} C_{S1F} - (Q_{SP} C_{SP} + Q_{S2C} C_{S2C})}{Q_{S1F} C_{S1F}} \times 100 \quad (\text{D.2})$$

The sample points coinciding with the concentrations and flows for the feed, permeate, and concentrate on the skid level are points A, B, and C respectively, Figure D-1.

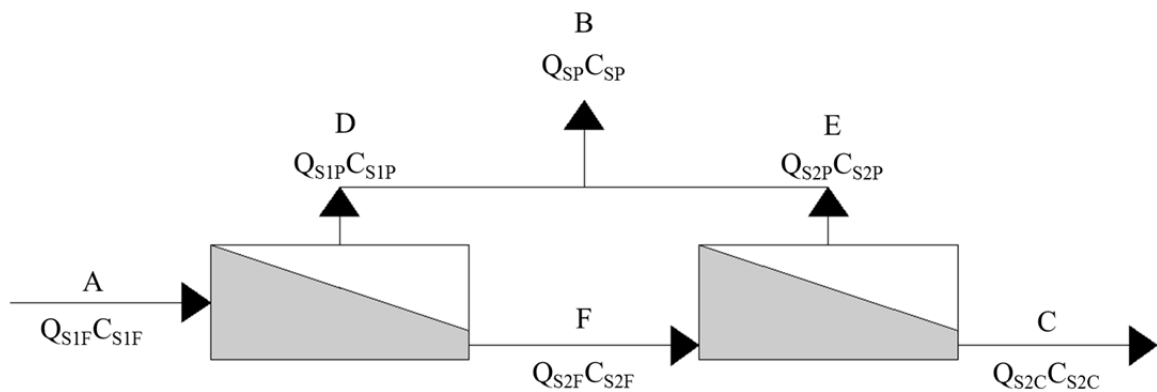


Figure D-1 Sampling scheme for individual skid and stage level

Appendix D (Continued)

For further analysis, a mass balance for carbon (or nitrogen) can be performed on the individual stage level. To perform this analysis on the first stage of the skid, Equation D.3 is used, and the analysis of the second stage requires the use of Equation D.4.

$$Q_{S1F}C_{S1F} = Q_{S1P}C_{S1P} + Q_{S2F}C_{S2F} + M_R \quad (D.3)$$

where Q_{S1F} is the flow rate of the feed to the skid (and stage 1), C_{S1F} is the concentration of carbon (or nitrogen) in the skid feed, Q_{S1P} is the flow rate of stage 1 permeate, C_{S1P} is the concentration in stage 1 permeate, Q_{S2F} is the flow rate of stage 1 concentrate, C_{S2F} is the concentration in stage 1 concentrate, and M_R represents the mass of the organic carbon (or nitrogen) removed from the system by assimilation or degradation.

$$Q_{S2F}C_{S2F} = Q_{S2P}C_{S2P} + Q_{S2C}C_{S2C} + M_R \quad (D.4)$$

where Q_{S2F} is the flow rate of stage 2 feed, C_{S2F} is the concentration of carbon (or nitrogen) in stage 2 feed, Q_{S2P} is the flow rate of stage 2 permeate, C_{S2P} is the concentration in stage 2 permeate, Q_{S2C} is the flow rate of stage 2 concentrate, C_{S2C} is the concentration in stage 2 concentrate, and M_R represents the mass of the organic carbon (or nitrogen) removed from the system by assimilation or degradation. To calculate the removal of organic carbon (or nitrogen) in stage 1 and stage 2, Equations D.5 and D.6 respectively are used.

Appendix D (Continued)

$$\% \text{Removal} = \frac{\text{mass removed}}{\text{mass input}} \times 100 = \frac{Q_{S1F}C_{S1F} - (Q_{S1P}C_{S1P} + Q_{S2F}C_{S2F})}{Q_{S1F}C_{S1F}} \times 100 \quad (\text{D.5})$$

$$\% \text{Removal} = \frac{\text{mass removed}}{\text{mass input}} \times 100 = \frac{Q_{S2F}C_{S2F} - (Q_{S2P}C_{S2P} + Q_{S2C}C_{S2C})}{Q_{S2F}C_{S2F}} \times 100 \quad (\text{D.6})$$

The sample points used for the feed, permeate, and concentrate for the stage 1 calculations were A, D and F respectively, Figure D-1. The sample points used for the feed, permeate, and concentrate for the stage 2 calculations were D, E and C respectively, Figure D-1. The data generated for the carbon mass balance for the skid level and the individual stages are in Tables D-1, D-2, D-3, and D-4. Additionally, the nitrogen balance data generated on the skid and individual stage level are in Table D-9. In addition to investigating the removal of carbon, the character of the organic carbon was analyzed for each scale of investigation. The SUVA data for the skid and individual stage levels are in Tables D-5, D-6, D-7, and D-8.

The temporal profile of organic carbon removal for the skid and individual stages is plotted for the duration of the study, Figure D-2. The organic character, plotted as SUVA, for this duration is also graphed for each sampling point, Figure D-3. Finally, the data for the removal of nitrogen for the latter part of the study were determined on the skid and stage level, Figure D-4.

Appendix D (Continued)

Table D-1 Influent carbon into membrane treatment train and % removal to 04/07/09

Date Run	NPOC Raw Water	Plant Feed (ppm)	Plant Feed (g/min)	Plant Feed (kg/day)	% C Removal Plant
07/02/08	15.4	13.4	200.5	288.7	3.5
07/03/08	15.3	13.0	193.5	278.6	0.7
07/09/08	16.8	15.7	236.9	341.2	26.2
07/12/08	14.2	15.3	169.6	244.2	11.3
07/13/08	13.4	13.8	150.7	217.0	28.9
07/24/08	14.5	15.9	243.1	350.0	15.9
07/28/08	6.3	10.7	113.1	162.9	17.6
08/01/08	2.9	11.8	168.4	242.5	41.8
08/06/08	16.0	19.3	278.2	400.7	10.9
08/12/08	16.1	16.9	242.6	349.3	15.1
08/22/08	18.2	19.1	274.6	395.4	13.7
09/02/08	18.8	16.4	176.0	253.4	21.8
09/08/08	17.3	17.8	117.5	169.2	40.9
09/16/08	18.9	19.5	128.5	185.0	43.0
09/23/08	16.1	17.6	118.1	170.1	32.8
09/29/08	19.0	19.2	128.7	185.3	39.3
10/07/08	18.8	20.2	214.7	309.1	20.5
10/24/08	17.5	21.8	230.1	331.4	24.7
11/12/08	17.4	20.1	212.9	306.6	14.5
11/19/08	15.0	20.1	214.2	308.4	8.6
12/16/08	20.1	22.1	235.5	339.1	15.0
12/23/08	19.3	19.6	204.9	295.0	14.7
01/06/09	18.1	19.9	210.8	303.5	14.3
01/08/09	19.7	19.9	209.8	302.1	8.8
01/13/09	16.9	17.4	188.5	271.5	9.9
01/20/09	16.4	18.9	198.8	286.2	10.2
01/27/09	16.9	19.7	213.2	306.9	18.8
02/02/09	20.5	22.1	236.4	340.4	16.2
03/05/09	-	20.7	214.9	309.4	10.8
03/12/09	22.0	17.8	191.0	275.0	16.1
03/19/09	20.7	22.2	224.9	323.8	5.9
04/03/09	21.5	18.2	257.1	370.2	-6.1
04/07/09	21.7	20.3	288.3	415.2	3.0

Appendix D (Continued)

Table D-2 Influent carbon into membrane treatment train and % removal from 04/14/09

Date Run	NPOC Raw Water	Plant Feed (ppm)	Plant Feed (g/min)	Plant Feed (kg/day)	% C Removal Plant
04/14/09	20.0	19.9	287.3	413.8	17.3
04/24/09	21.7	19.6	280.7	404.3	4.9
04/28/09	19.8	19.1	259.1	373.1	8.3
05/12/09	22.4	21.2	302.8	436.0	4.4
05/19/09	2.5	2.4	35.1	50.5	6.3
05/28/09	2.7	2.6	37.3	53.8	-7.5
06/04/09	2.7	2.5	36.3	52.2	2.6
06/08/09	2.8	2.7	26.9	38.8	11.0
06/09/09	2.5	3.0	43.8	63.1	9.5
06/30/09	2.6	2.3	32.1	46.2	0.43
07/07/09	2.2	2.1	30.1	43.3	1.7
07/14/09	2.1	1.9	18.2	26.2	11.9
07/15/09	2.3	2.1	29.8	42.9	1.1
07/22/09	2.4	2.0	27.7	39.9	-3.2
07/29/09	2.4	2.2	31.7	45.6	6.7
08/04/09	2.5	2.4	33.4	48.1	6.6
08/11/09	2.5	2.3	32.3	46.5	3.3
08/21/09	2.1	2.0	19.4	28.0	8.9
08/24/09	2.5	2.3	33.4	48.1	3.6
08/31/09	2.3	2.3	31.4	45.3	1.3
09/11/09	2.9	2.5	36.7	52.9	-2.1
09/16/09	2.9	2.8	27.8	40.0	12.7
09/23/09	3.3	3.1	43.2	62.1	2.1
09/30/09	1.9	1.8	26.1	37.6	6.0
10/08/09	2.2	2.1	28.1	40.5	10.9
10/23/09	2.1	2.1	29.5	42.5	-11.8
11/04/09	17.7	17.8	243.7	350.9	9.8
11/13/09	11.9	8.4	119.4	172.0	42.9
11/18/09	27.6	28.4	413.0	594.8	11.4
11/25/09	27.3	26.7	249.5	359.3	28.9
12/04/09	27.7	26.1	373.4	537.7	3.6
01/12/10	28.1	25.0	359.1	517.2	4.8
02/17/10	6.1	8.4	82.8	119.2	44.7
03/10/10	6.363	7.132	108.3	155.9	6.9

Appendix D (Continued)

Table D-3 Carbon removal on skid and individual stage levels to 04/07/09

Date Run	Skid Level	Skid Stage I	Skid Stage II
07/02/08	-0.3	-17.0	16.1
07/03/08	-1.0	-19.0	17.0
07/09/08	25.2	23.2	3.0
07/12/08	7.0	14.3	-9.4
07/13/08	-7.3	-9.8	2.5
07/24/08	87.9	6.6	96.3
07/28/08	68.7	8.9	68.7
08/01/08	16.7	-12.2	29.1
08/06/08	13.5	6.1	8.8
08/12/08	0.6	-4.6	5.6
08/22/08	13.3	3.0	11.9
09/02/08	15.7	4.0	13.7
09/08/08	8.6	8.7	-0.2
09/16/08	10.3	3.2	8.4
09/23/08	-1.4	3.3	-5.5
09/29/08	13.2	5.1	9.6
10/07/08	2.9	-11.8	13.7
10/24/08	9.7	4.9	5.5
11/12/08	14.2	3.7	12.3
11/19/08	8.6	-10.7	19.6
12/16/08	-7.4	-10.8	3.4
12/23/08	3.4	-2.7	6.6
01/06/09	11.5	-4.2	16.5
01/08/09	2.6	-20.3	20.8
01/13/09	-5.9	-7.7	1.9
01/20/09	10.9	-108.0	58.0
01/27/09	6.8	-8.1	15.3
02/02/09	6.4	-3.1	10.6
03/05/09	-7.5	-29.9	19.5
03/12/09	6.2	-15.0	20.8
03/19/09	35.2	-103.6	73.3
04/03/09	-4.3	-9.8	5.7
04/07/09		-12.4	-31.2

Appendix D (Continued)

Table D-4 Carbon removal on skid and individual stage levels from 04/14/09

Date Run	Skid Level	Skid Stage I	Skid Stage II
04/14/09	7.7	-4.4	12.9
04/24/09	-5.0	-15.1	9.9
04/28/09	3.0	-13.2	16.1
05/12/09	9.0	-4.4	14.4
05/19/09	-2.6	-21.3	16.9
05/28/09	-4.5	-21.4	15.7
06/04/09	-7.2	-26.8	17.8
06/08/09	-4.4	-14.4	10.5
06/09/09	-2.8	-14.6	12.4
06/30/09	-8.5	-15.2	6.2
07/07/09	-6.3	-8.2	1.6
07/14/09	-8.3	-14.8	5.7
07/15/09	-8.1	-22.3	11.6
07/22/09	-7.0	-18.4	9.7
07/29/09	-4.4	-24.5	16.2
08/04/09	-9.9	-13.4	3.1
08/11/09	-7.1	-16.4	8.0
08/21/09	-11.4	-1.7	-9.8
08/24/09	-4.2	-18.5	12.1
08/31/09	-3.0	-17.3	12.2
09/11/09	-0.7	-11.5	9.9
09/16/09	-8.6	-13.1	4.1
09/23/09	-3.1	-10.0	6.4
09/30/09	-3.1	-13.0	8.9
10/08/09	-3.0	-16.8	12.0
10/23/09	-0.3	-7.7	7.1
11/04/09	0.0	-5.6	5.9
11/13/09	48.9	38.3	19.5
11/18/09	5.2	-11.3	16.4
11/25/09	-5.0	-9.1	4.2
12/04/09	1.2	-4.0	5.6
01/12/10	2.6	-19.1	21.1
02/17/10	25.4	27.9	-3.7
03/10/10	4.3	-9.5	14.6

Appendix D (Continued)

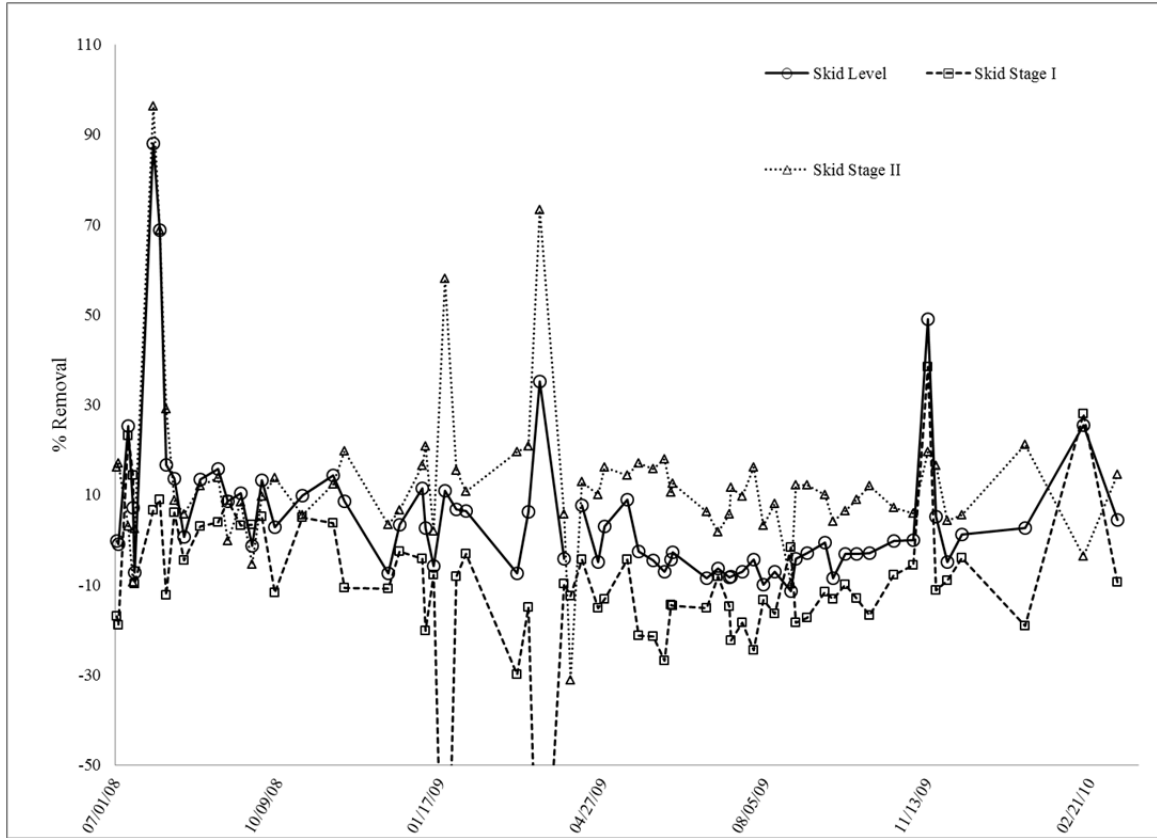


Figure D-2 Temporal profile of individual skid and stage level carbon removal

The data in Figure D-2 indicate a similar trend as seen in the plant level analysis, Chapter 6. Additionally, discrepancies are seen between the removals for stages 1 and stage 2. This discrepancy is likely due to the lack of accurate and reliable flow data for stage 2 feed. Further, the confidence level in this data is lower than the plant level due to the lack in confidence in the flow data acquired. Since these data are not required for plant operation, calibrations of the flow meters are performed infrequently.

Appendix D (Continued)

Table D-5 Feed and concentrate SUVA and % change on plant level to 04/07/09

Date Run	Feed L/mg m	Concentrate L/mg m	% Change SUVA
07/02/08	0.313	0.445	42.0
07/03/08	0.346	0.449	29.6
07/09/08	0.357	0.488	36.7
07/12/08	0.360	0.364	1.1
07/13/08	0.405	0.493	21.8
07/24/08	0.276	0.388	40.6
07/28/08	0.328	0.517	57.8
08/01/08	0.276	0.388	40.6
08/06/08	0.321	0.806	151.4
08/12/08	0.519	0.443	-14.7
08/22/08	0.313	0.407	29.9
09/02/08	0.354	0.367	3.6
09/08/08	0.292	0.317	8.5
09/16/08	0.288	0.332	15.4
09/23/08	0.324	0.340	4.8
09/29/08	0.266	0.319	20.3
10/07/08	0.218	0.274	25.6
10/24/08	0.215	0.329	52.7
11/12/08	0.209	0.312	49.3
11/19/08	0.214	0.287	33.8
12/16/08	0.253	0.313	23.6
12/23/08	0.285	0.341	19.3
01/06/09	0.221	0.300	35.8
01/08/09	0.262	0.340	30.2
01/13/09	0.259	0.309	19.2
01/20/09	0.254	0.318	25.2
01/27/09	0.248	0.312	25.7
02/02/09	0.240	0.309	28.6
03/05/09	0.286	0.330	15.7
03/12/09	0.276	0.306	11.0
03/19/09	0.252	0.318	26.2
04/03/09	0.308	0.314	1.9
04/07/09	0.270	0.314	16.1

Appendix D (Continued)

Table D-6 Feed and concentrate SUVA and % change on plant level from 04/14/09

Date Run	Feed L/mg m	Concentrate L/mg m	% Change SUVA
04/14/09	0.266	0.351	32.2
04/24/09	0.266	0.348	31.2
04/28/09	0.288	0.345	19.8
05/12/09	0.165	0.267	61.6
05/19/09	2.683	2.463	-8.2
05/28/09	2.488	2.487	-0.1
06/04/09	2.337	2.454	5.0
06/08/09	2.021	2.312	14.4
06/09/09	1.745	2.295	31.5
06/30/09	2.519	2.342	-7.0
07/07/09	2.573	2.144	-16.7
07/14/09	2.526	2.485	-1.6
07/15/09	2.648	2.498	-5.7
07/22/09	2.489	2.331	-6.4
07/29/09	1.956	2.266	15.8
08/04/09	2.383	2.455	3.1
08/11/09	2.212	2.310	4.4
08/21/09	2.369	2.431	2.6
08/24/09	2.415	2.279	-5.6
08/31/09	2.258	2.264	0.3
09/11/09	2.184	2.083	-4.6
09/16/09	1.881	1.846	-1.8
09/23/09	1.651	1.638	-0.8
09/30/09	2.812	2.775	-1.3
10/08/09	2.361	2.653	12.4
10/23/09	2.627	2.458	-6.4
11/04/09	0.287	0.358	24.8
11/13/09	0.607	1.243	104.7
11/18/09	0.179	0.235	30.7
11/25/09	0.191	0.228	19.5
12/04/09	0.192	0.222	15.7
01/12/10	0.200	0.254	26.9
02/17/10	0.658	1.018	54.6
03/10/10	0.785	1.055	34.4

Appendix D (Continued)

Table D-7 SUVA data for the skid and stage levels with % removal to 04/07/09

Date Run	Stage I Feed L/mg m	Stage II Feed L/mg m	Stage II Concentrate L/mg m	% Removal Stage I	Stage II	Skid Level
07/02/08	0.313	0.403	0.446	28.8	10.6	42.5
07/03/08	0.346	0.393	0.445	13.6	13.0	28.4
07/09/08	0.357	0.552	0.568	54.5	2.9	59.1
07/12/08	0.360	0.440	0.408	22.1	-7.2	13.3
07/13/08	0.405	0.426	0.437	5.2	2.5	7.8
07/24/08	0.276	0.421	-	52.3	-	-
07/28/08	0.328	0.511	0.838	56.1	63.8	155.7
08/01/08	0.276	0.421	-	52.3	-	-
08/06/08	0.321	0.464	0.655	44.7	41.2	104.3
08/12/08	0.519	0.733	0.266	41.1	-63.7	-48.8
08/22/08	0.313	0.384	0.420	22.6	9.3	33.9
09/02/08	0.354	0.377	0.446	6.3	18.5	25.9
09/08/08	0.292	0.353	0.347	20.8	-1.8	18.7
09/16/08	0.288	0.366	0.377	27.4	2.8	31.0
09/23/08	0.324	0.362	0.368	11.7	1.5	13.4
09/29/08	0.266	0.356	0.386	34.0	8.5	45.4
10/07/08	0.218	0.239	0.286	9.8	19.6	31.3
10/24/08	0.215	0.302	0.309	40.4	2.2	43.4
11/12/08	0.209	0.308	0.352	47.2	14.4	68.4
11/19/08	0.214	0.286	0.319	33.7	11.4	48.9
12/16/08	0.253	0.279	0.271	10.1	-2.9	6.8
12/23/08	0.285	0.333	0.339	16.5	1.8	18.6
01/06/09	0.221	0.277	0.320	25.4	15.5	44.8
01/08/09	0.262	0.308	0.309	17.7	0.4	18.2
01/13/09	0.259	0.292	0.346	12.8	18.4	33.5
01/20/09	0.254	0.308	0.324	21.1	5.3	27.6
01/27/09	0.248	0.306	0.343	23.2	12.1	38.1
02/02/09	0.240	0.274	0.308	13.9	12.5	28.2
03/05/09	0.286	0.342	0.379	19.8	10.9	32.8
03/12/09	0.276	0.300	0.355	8.9	18.4	28.8
03/19/09	0.252	0.282	0.310	11.9	9.9	23.0
04/03/09	0.308	0.333	0.352	8.1	5.8	14.4
04/07/09	0.270	0.305	0.308	12.8	0.9	13.8

Appendix D (Continued)

Table D-8 SUVA data for the skid and stage levels with % removal from 04/14/09

Date Run	Stage I Feed L/mg m	Stage II Feed L/mg m	Stage II Concentrate L/mg m	% Removal Stage I	Stage II	Skid Level
04/14/09	0.266	0.342	0.354	28.7	3.4	33.1
04/24/09	0.266	0.310	0.312	16.9	0.5	17.4
04/28/09	0.288	0.329	0.363	14.3	10.3	26.1
05/12/09	0.165	0.262	0.313	58.5	19.4	89.3
05/19/09	2.683	2.534	2.463	-5.5	-2.8	-8.2
05/28/09	2.488	2.457	2.474	-1.3	0.7	-0.6
06/04/09	2.337	2.421	2.449	3.6	1.2	4.8
06/08/09	2.021	2.258	2.361	11.7	4.6	16.8
06/09/09	1.745	2.170	2.304	24.3	6.2	32.0
06/30/09	2.519	2.470	2.373	-2.0	-3.9	-5.8
07/07/09	2.573	2.429	2.210	-5.6	-9.0	-14.1
07/14/09	2.526	2.593	2.540	2.6	-2.1	0.5
07/15/09	2.648	2.407	2.523	-9.1	4.8	-4.7
07/22/09	2.489	2.409	2.374	-3.2	-1.5	-4.6
07/29/09	1.956	2.071	2.265	5.9	9.3	15.8
08/04/09	2.383	2.482	2.415	4.1	-2.7	1.4
08/11/09	2.212	2.297	2.334	3.8	1.6	5.5
08/21/09	2.369	2.494	2.383	5.3	-4.4	0.6
08/24/09	2.415	2.325	2.282	-3.7	-1.9	-5.5
08/31/09	2.258	2.260	2.198	0.1	-2.7	-2.6
09/11/09	2.184	2.065	2.047	-5.4	-0.9	-6.3
09/16/09	1.881	1.875	1.818	-0.3	-3.0	-3.3
09/23/09	1.651	1.625	1.633	-1.6	0.5	-1.1
09/30/09	2.812	2.864	2.785	1.8	-2.8	-1.0
10/08/09	2.361	2.422	2.434	2.6	0.5	3.1
10/23/09	2.627	2.802	2.746	6.7	-2.0	4.6
11/04/09	0.287	0.351	0.348	22.4	-0.9	21.3
11/13/09	0.607	1.303	1.526	114.6	17.1	151.4
11/18/09	0.179	0.216	0.226	20.4	4.5	25.8
11/25/09	0.191	0.210	0.225	9.6	7.3	17.7
12/04/09	0.192	0.219	0.227	14.2	3.4	18.1
01/12/10	0.200	0.236	0.276	18.0	16.7	37.6
02/17/10	0.658	1.037	0.935	57.6	-9.8	42.1
03/10/10	0.785	0.960	1.039	22.2	8.3	32.3

Appendix D (Continued)

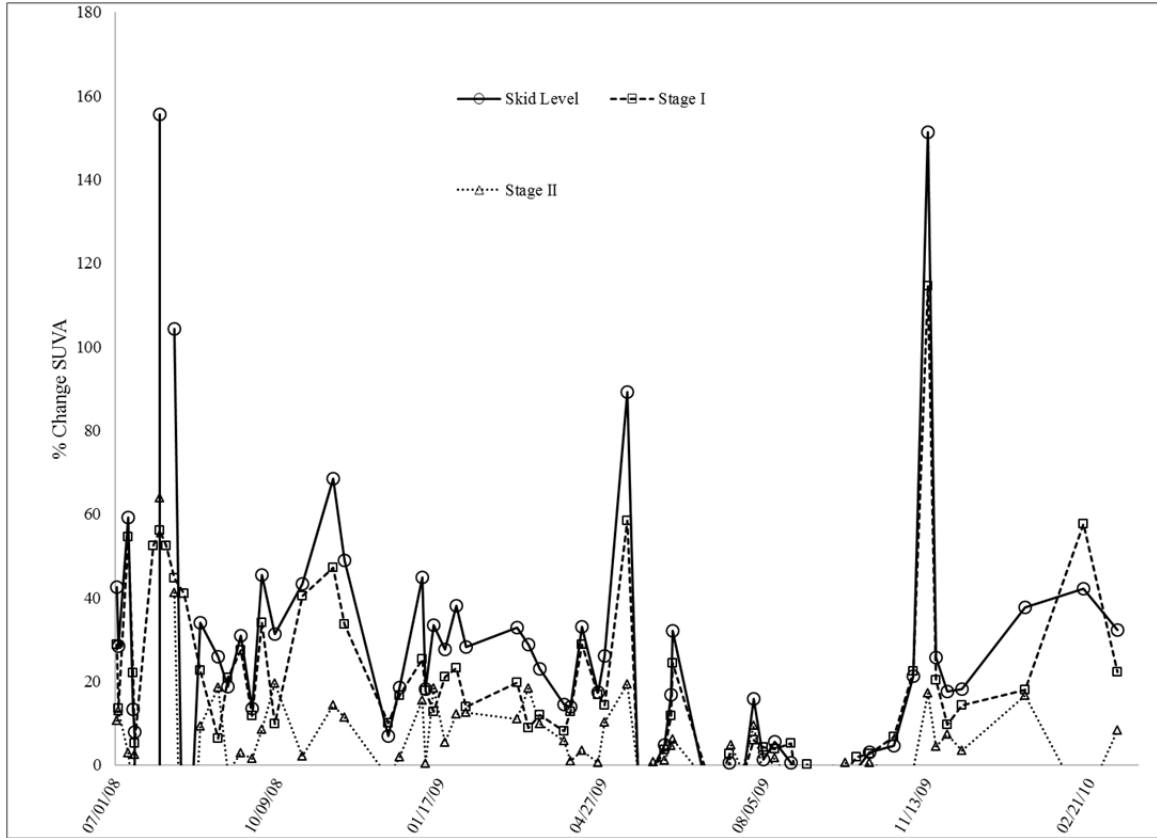


Figure D-3 Temporal profile of change in SUVA on individual skid and stage level

The temporal profile of SUVA data for the individual skid and stage levels coincides with the profile observed for the plant level analysis in Chapter 6. Figure D-3. Since the SUVA data are dependent on the concentration of organic carbon collected, the same discrepancies in the SUVA data were noted as with the % removal calculations. These discrepancies are the result from the same sources listed above.

Appendix D (Continued)

Table D-9 Influent nitrogen with removal on plant, skid and stage levels and C:N ratio

Date Run	Raw Water (ppm)	Plant Feed (ppm)	% Removal Plant	Skid Level	Stage I	Stage II	C:N Mass Ratio
04/03/09	0.379	0.312	10.4	4.9	-1.5	8.4	58.4
04/07/09	0.324	0.312	3.5	-24.9	-8.5	-19.5	65.2
04/14/09	0.333	0.273	14.9	5.8	-9.7	18.7	73.0
04/24/09	0.408	0.355	5.3	2.0	-12.2	16.3	55.1
04/28/09	0.325	0.306	5.7	1.2	-12.5	15.9	62.4
05/12/09	0.301	0.294	5.2	3.5	-3.7	9.2	72.0
05/19/09	0.359	0.304	2.2	3.0	-12.4	18.1	8.0
05/28/09	0.401	0.368	3.0	0.9	-10.5	13.2	7.1
06/04/09	0.380	0.392	5.6	2.8	-11.5	16.2	6.4
06/08/09	0.296	0.301	14.3	2.8	-7.1	11.7	9.0
06/09/09	0.304	0.301	10.9	2.1	-10.0	14.0	10.1
06/30/09	0.308	0.283	2.1	-6.5	-14.3	9.1	8.0
07/07/09	0.336	0.316	4.0	1.2	-3.2	5.7	6.8
07/14/09	0.329	0.322	17.6	6.1	-0.9	9.2	5.9
07/15/09	0.424	0.364	5.9	1.4	-7.6	10.9	5.8
07/22/09	0.340	0.274	0.8	-0.2	-9.7	11.3	7.2
07/29/09	0.444	0.350	8.3	2.7	-12.2	16.3	6.3
08/04/09	0.401	0.338	5.9	-5.8	-13.0	8.0	7.0
08/11/09	0.490	0.399	8.0	-2.0	-6.9	5.7	5.8
08/21/09	0.394	0.337	4.2	-7.3	-2.7	-5.9	5.9
08/24/09	0.443	0.366	9.2	0.5	-12.2	14.3	6.3
08/31/09	0.357	0.279	4.9	1.9	-11.4	14.7	8.1
09/11/09	0.421	0.335	0.1	1.5	-8.2	11.3	7.4
09/16/09	0.362	0.345	8.4	-3.1	-10.5	8.5	8.0
09/23/09	0.350	0.307	-1.2	0.3	-7.0	8.9	10.2
09/30/09	0.339	0.307	1.8	-0.8	-9.4	9.7	6.0
10/08/09	0.364	0.313	9.6	-2.1	-12.1	11.3	6.6
10/23/09	0.406	0.363	-6.5	-1.4	-10.3	9.9	5.8
11/04/09	0.297	0.279	3.6	-5.2	-19.0	14.4	63.8
11/18/09	0.348	0.325	12.9	8.4	-8.9	19.2	87.5
11/25/09	0.318	0.272	12.9	-11.2	-13.9	2.9	98.1
12/04/09	0.354	0.342	8.0	-1.4	-5.9	5.5	76.2
01/12/10	0.371	0.274	2.3	1.8	-14.6	16.7	91.2
02/17/10	0.272	0.274	21.1	1.7	-6.3	9.1	30.5
03/10/10	0.318	0.300	4.2	-8.1	-19.8	12.8	23.8

Appendix D (Continued)

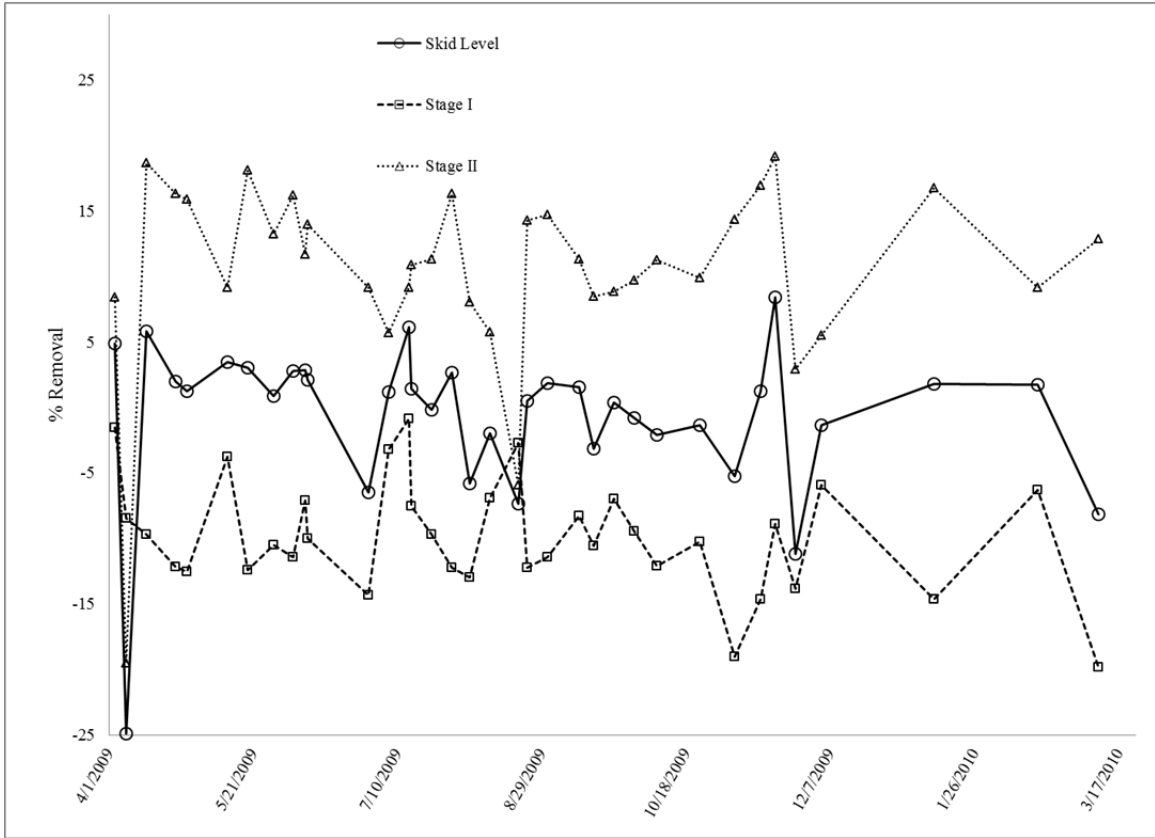


Figure D-4 Temporal profile of nitrogen removal on an individual skid and stage level

The removal of nitrogen observed on the skid level is consistent with the removal observed on the plant level, Figure D-4. However, when analyzing the individual stage level, there is a discrepancy between the stage removals. As stated, above, this is likely due to poor calibration of the flow meters on this scale. When analyzing the data from the skid and stage levels, it is apparent the skid level data are a combination of the stage 1 and 2 data, further supporting the hypothesis that the poor calibration of flow meters on this scale is responsible for these discrepancies.

Appendix E Additional Pilot Study Information

The information presented in Chapter 7 includes the highlights and key points from the pilot testing portion of this research. This appendix contains supplementary information as well as some supporting data.

Foulant Analysis

The data presented in Chapter 7 are a pretty comprehensive representation of the finished data for the pilot study. This section presents some data not presented in Chapter 7 as well as some additional data in a more raw form.

The total number of microorganisms on the surface of the membrane swatches was measured using the procedure for total direct count in Chapter 3. Additionally, the statistical analyses for the total direct count for the carbon loading portion of the study is presented in Chapter 7. The data for the total direct count from the carbon loading portion of the study along with the feed/concentrate ration are in Table E-1.

Appendix E (Continued)

Table E-1 The total number of microorganisms on the feed and concentrate pilot membrane swatches and the respective feed/concentrate ratio for the carbon loading portion of the study

Date	Carbon Loading	Feed (#/cm ²)		Concentrate (#/cm ²)		Feed/Conc
		Avg	Stdev	Avg	Stdev	
8/30/10	0.1	4.55	0.9	2.43	0.9	1.9
8/30/10	0.1	4.22	1.4	4.00	0.2	1.1
9/6/10	0.1	5.75	0.3	4.19	0.8	1.4
9/6/10	0.1	4.75	0.9	3.92	0.2	1.2
10/11/10	0.5	2.59	0.9	2.90	0.3	0.9
10/11/10	0.5	3.81	0.1	1.80	0.2	2.1
10/18/10	0.5	2.44	0.6	1.87	0.4	1.3
10/18/10	0.5	2.56	0.1	2.29	0.2	1.1
10/25/10	0.5	1.41	0.1	1.13	0.3	1.2
10/25/10	0.5	1.69	0.3	0.69	0.2	2.4
11/8/10	0.5	2.70	0.1	1.71	0.4	1.6
11/8/10	0.5	2.83	0.2	1.24	0.2	2.3
11/15/10	0.5	2.80	0.8	1.28	0.1	2.2
11/15/10	0.5	2.47	0.4	0.96	0.2	2.6
11/22/10	0.5	1.62	0.1	0.58	0.2	2.8
11/22/10	0.5	1.33	0.3	0.83	0.1	1.6
11/29/10	2.0	1.23	0.2	0.71	0.2	1.7
11/29/10	2.0	1.17	0.2	0.87	0.1	1.3
12/6/10	2.0	1.93	0.3	0.67	0.6	2.9
12/6/10	2.0	1.95	0.3	1.11	0.1	1.8
12/13/10	2.0	2.54	0.6	1.49	0.4	1.7
12/13/10	2.0	2.09	0.1	1.37	0.3	1.5
12/20/10	2.0	2.09	0.2	0.89	0.2	2.4
12/20/10	2.0	1.56	0.1	0.75	0.2	2.1
12/27/10	2.0	1.49	0.1	0.95	0.0	1.6
12/27/10	2.0	1.37	0.2	1.19	0.2	1.1
1/3/11	2.0	1.75	0.1	1.10	0.2	1.6
1/3/11	2.0	1.68	0.2	0.76	0.1	2.2

Appendix E (Continued)

As stated in Chapter 7, the roughness data from the AFM did not reveal a significant difference in roughness between the feed and concentrate pilot membrane swatches. The root mean squared (RMS) and average (Ra) roughness values for the feed and concentrate pilot swatches and the feed/concentrate ratio of these values are presented in Table 7-5 for the no carbon loading portion and Table E-2 for the carbon loading portion of the study. All the RMS roughness and respective ratio data and the Ra roughness and ratio data are displayed in Figures E-1 and E-2 respectively.

Appendix E (Continued)

Table E-2 RMS and Ra roughness data and feed/concentrate ratio data

Date	Feed				Concentrate				RMS Ratio	Ra Ratio
	Avg RMS (nm)	Stdev	AVG Ra (nm)	Stdev	AVG RMS (nm)	Stdev	AVG Ra (nm)	Stdev		
8/30/10	149.672	56.001	108.777	40.396	112.647	23.144	85.797	14.699	1.33	1.27
8/30/10	119.322	30.470	92.247	21.894	75.288	7.477	57.827	4.206	1.58	1.60
9/6/10	91.613	14.152	71.872	10.645	110.317	36.247	86.173	29.699	0.83	0.83
9/6/10	107.763	6.599	83.357	7.431	98.865	42.324	71.930	25.672	1.09	1.16
9/13/10	59.429	13.306	46.189	10.303	65.644	17.815	47.932	12.718	0.91	0.96
9/13/10	68.134	6.169	52.508	8.162	60.913	16.248	46.027	13.092	1.12	1.14
9/20/10	67.208	18.598	48.135	12.686	67.165	9.629	48.711	6.494	1.00	0.99
9/20/10	58.539	14.458	44.243	10.199	54.460	14.066	40.841	9.553	1.07	1.08
9/27/10	44.292	10.253	31.934	6.233	55.901	18.412	41.408	15.224	0.79	0.77
9/27/10	61.543	10.519	44.087	9.099	74.962	20.835	56.174	13.384	0.82	0.78
10/4/10	62.204	9.719	39.459	3.392	52.640	11.384	38.791	6.864	1.18	1.02
10/4/10	47.186	11.650	34.282	8.984	47.790	6.686	36.022	4.950	0.99	0.95
10/11/10	75.799	12.353	54.513	10.848	74.950	10.788	54.130	12.929	1.01	1.01
10/11/10	86.936	15.689	58.148	9.672	97.968	30.990	73.229	24.398	0.89	0.79
10/18/10	50.418	6.480	38.757	4.662	77.918	40.198	50.946	20.577	0.65	0.76
10/18/10	76.405	21.797	58.762	17.170	70.019	12.948	53.183	12.103	1.09	1.10
10/25/10	49.974	16.824	36.560	11.171	43.585	7.908	29.958	3.280	1.15	1.22
10/25/10	78.044	49.577	60.008	38.855	43.052	7.347	30.322	3.560	1.81	1.98
11/22/10	52.897	1.440	40.358	0.993	50.214	8.553	38.570	6.238	1.05	1.05
11/22/10	61.817	9.951	49.348	7.754	64.584	31.838	47.081	21.855	0.96	1.05
11/29/10	71.632	42.997	54.365	36.148	67.340	8.389	51.021	6.876	1.06	1.07
11/29/10	51.278	10.009	38.694	5.828	81.313	33.886	62.210	24.397	0.63	0.62
12/6/10	119.397	121.090	86.621	85.281	48.220	16.737	34.854	10.662	2.48	2.49
12/6/10	68.110	31.538	53.487	24.007	45.115	4.976	34.725	3.485	1.51	1.54
12/13/10	46.106	3.704	35.066	2.974	46.063	9.775	35.056	8.016	1.00	1.00
12/13/10	50.864	1.982	37.540	2.696	58.311	16.140	46.433	12.782	0.87	0.81
12/20/10	55.005	15.820	41.263	10.685	45.035	6.364	33.900	3.463	1.22	1.22
12/20/10	53.092	26.196	38.443	14.720	58.188	12.052	40.650	6.597	0.91	0.95
12/27/10	36.735	4.389	28.043	2.846	52.508	19.013	40.806	15.017	0.70	0.69
12/27/10	45.131	6.732	35.042	5.496	54.167	3.968	41.570	3.409	0.83	0.84
1/3/11	38.132	3.357	29.292	2.764	46.897	5.394	35.610	3.706	0.81	0.82
1/3/11	50.715	5.144	38.058	1.059	42.527	2.872	32.483	1.557	1.19	1.17

Appendix E (Continued)

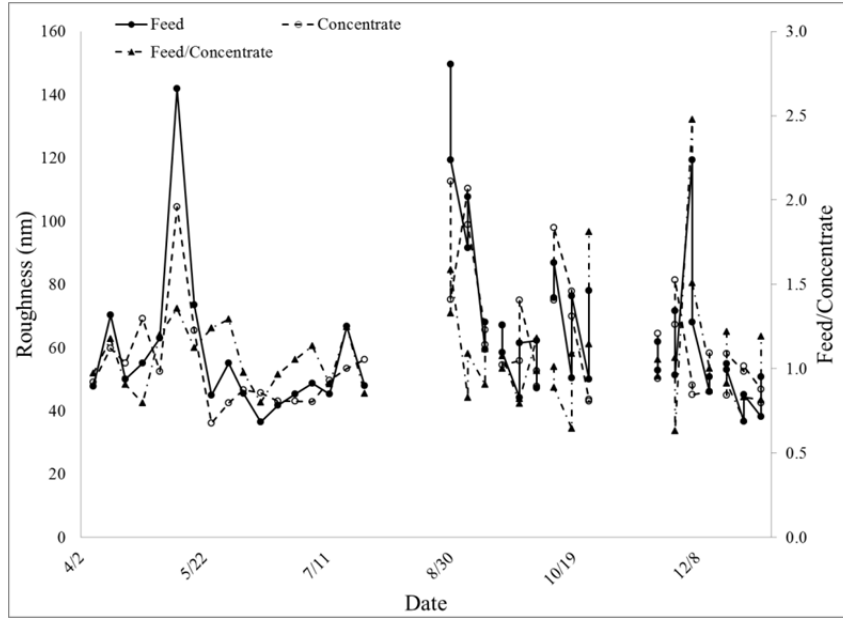


Figure E-1 RMS roughness for feed and concentrate and feed/concentrate ration throughout pilot study

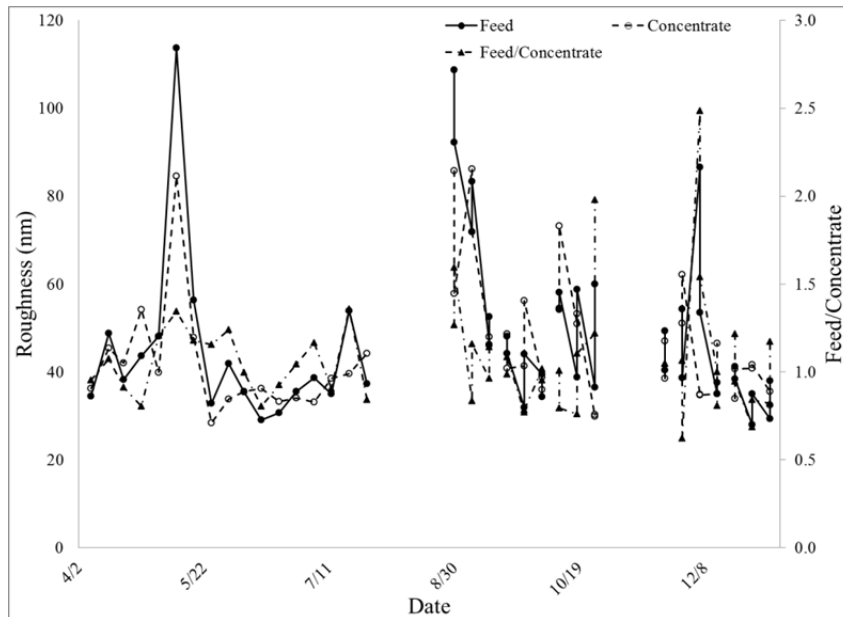


Figure E-2 Average roughness for feed and concentrate and feed/concentrate ration throughout pilot study

Appendix E (Continued)

The overall feed-concentrate fouling trends are presented in Chapter 7. Additionally, it was demonstrated that there was no statistical difference between the 50 GPM and 25 GPM flow rates for relative fouling rates. The overall ratio data and the data for the 50 GPM and 25 GPM flow rates are in Tables E-3, 7-16, and 7-17 respectively. The data from the 50 GPM and 25 GPM flow rates are represented graphically, Figures E-3 and E-4 respectively. These graphs display the same general trend as seen in the overall ratio analysis did, Chapter 7. Thus, there is a general increasing trend in the relative amount of foulant on the feed swatch with respect to the concentrate swatch as the level of carbon loading increases.

Table E-3 Overall feed/concentrate ratio data for protein, carbohydrate, and HPC at each carbon loading condition

Carbon Loading (g/m ² day)	Protein	Stdev	Carbohydrate	Stdev	HPC	Stdev
0	1.06	0.3	1.03	0.5	1.17	1.2
0.1	0.97	0.1	1.04	0.2	1.32	0.8
0.5	1.41	0.5	1.30	0.5	2.61	2.0
2	1.28	0.1	1.75	0.8	2.5	1.5

Appendix E (Continued)

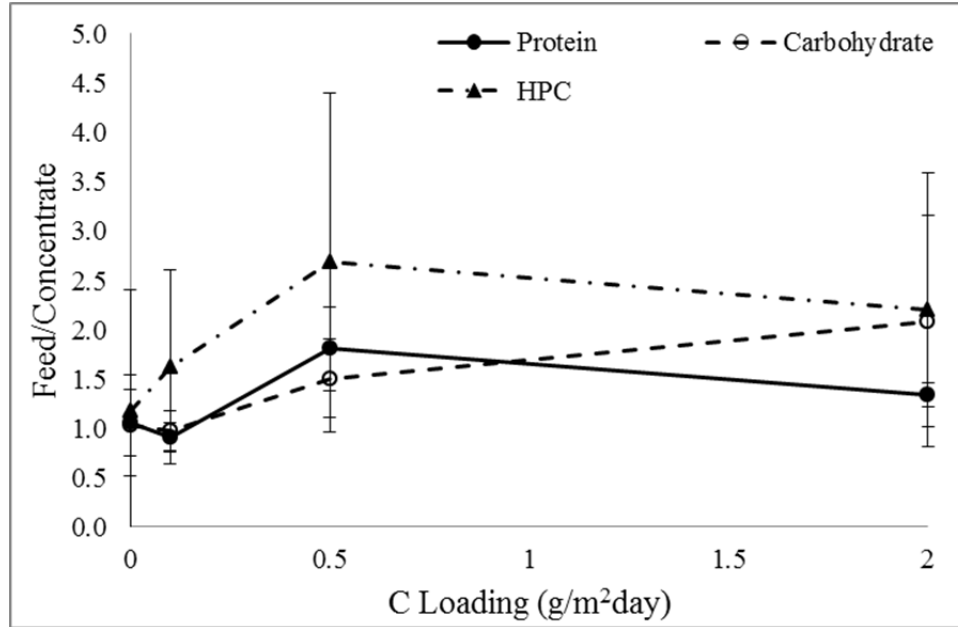


Figure E-3 The feed/concentrate ratio for the protein, carbohydrate and HPC concentrations plotted against carbon loading rate for the 50 GPM flow rate

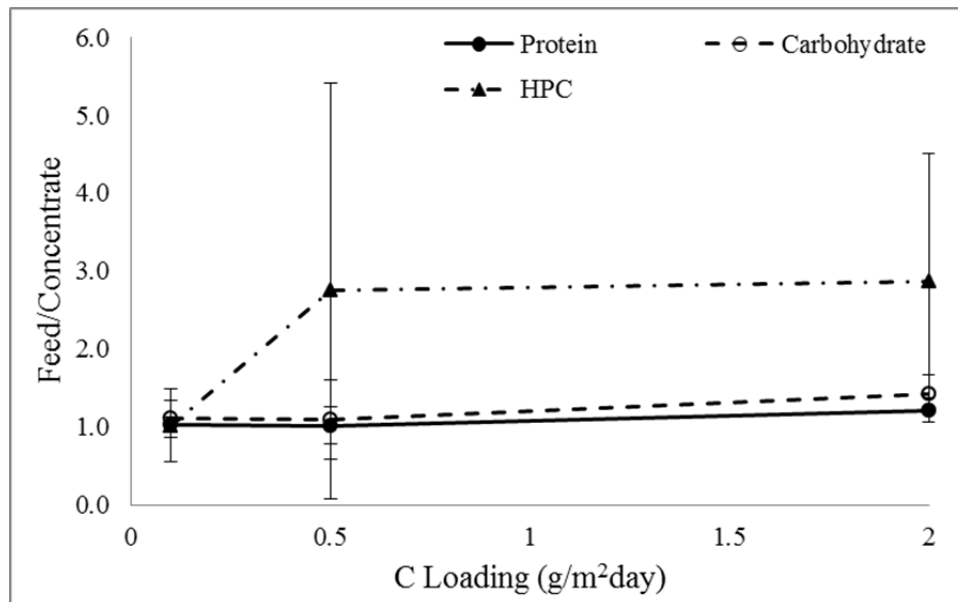


Figure E-4 The feed/concentrate ratio for the protein, carbohydrate and HPC concentrations plotted against carbon loading rate for the 25 GPM flow rate

Appendix E (Continued)

Additional Performance Analysis

The flux data presented in Chapter 7 indicated a greater loss of flux for the feed portion of the pilot system over the concentrate portion. Further, a greater difference between the two was observed as the level of carbon loading was increased, Figure 7-24. To generate these data points, the initial flux decline for each membrane swatch was calculated for each week and for each carbon loading condition. This was done by performing a linear approximation on the time lapse flux decline and taking the slope of the fit curve as described in Chapter 7.

Due to the variations in the operation system, such as power fluctuations, pump shut off, pilot shutdown, etc., many of the flux data points for the flat sheet modules are not useful for flux decline calculations. In order to obtain useful information, these points must first be removed from the data series. Additionally, after the initial flux decline, the subsequent flux decline is less dramatic. For the sake of obtaining comparable data, only the initial portion was used in these analyses.

Graphs of the initial flux decline for all flat sheet modules for the no carbon loading, 0.1 g C/m²day, 0.5 g C/m²day, and 2.0 g C/m²day portions of the study are in Figures E-5, E-6, E-7, and E-8 respectively. The slope of the curves represents the value of m (Equation 7.1), which is the initial loss of flux for the membrane material.

Appendix E (Continued)

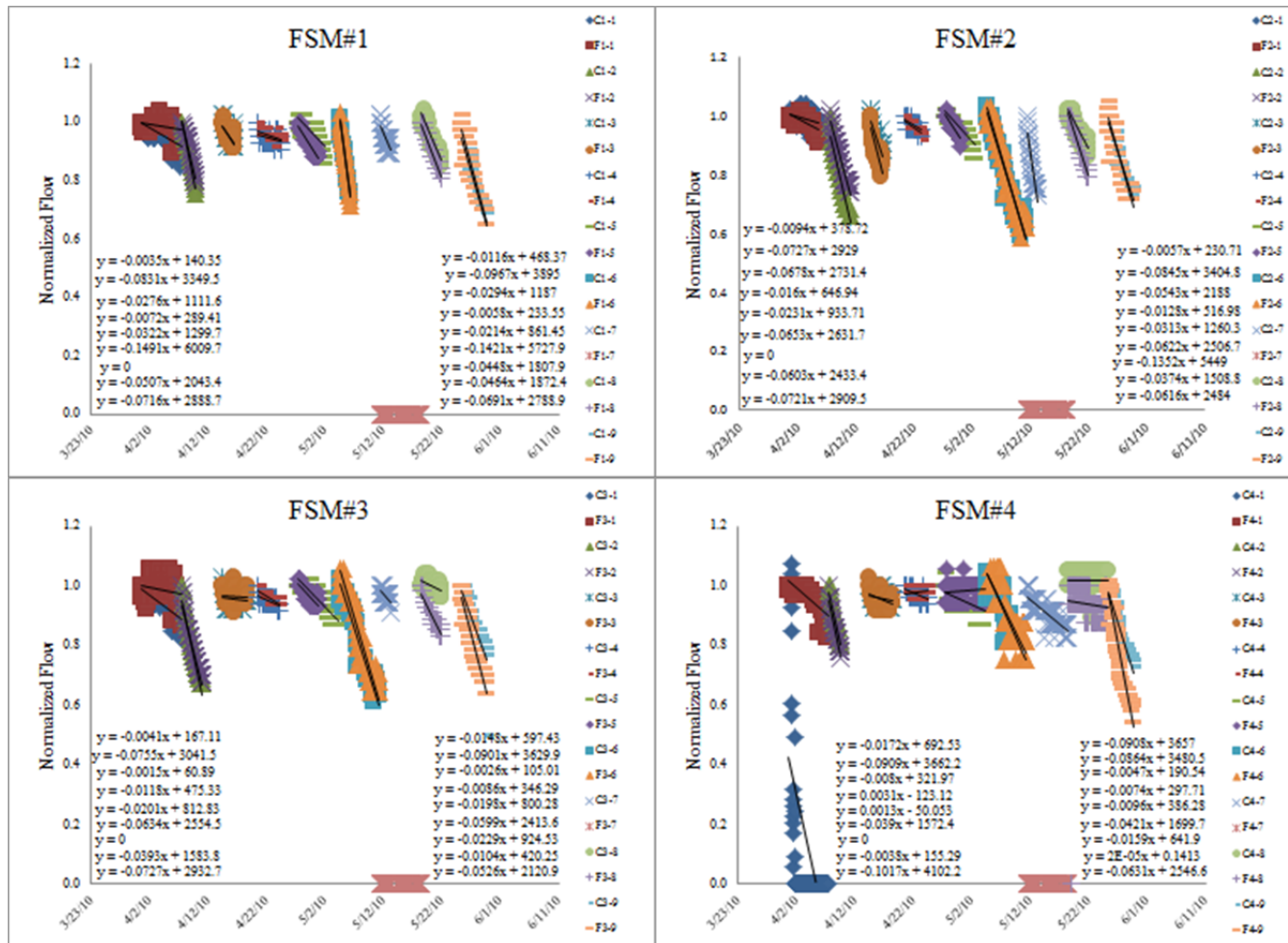


Figure E-5 Initial rate of fouling, m, for the no carbon loading portion of the study for all four FSMs

Appendix E (Continued)

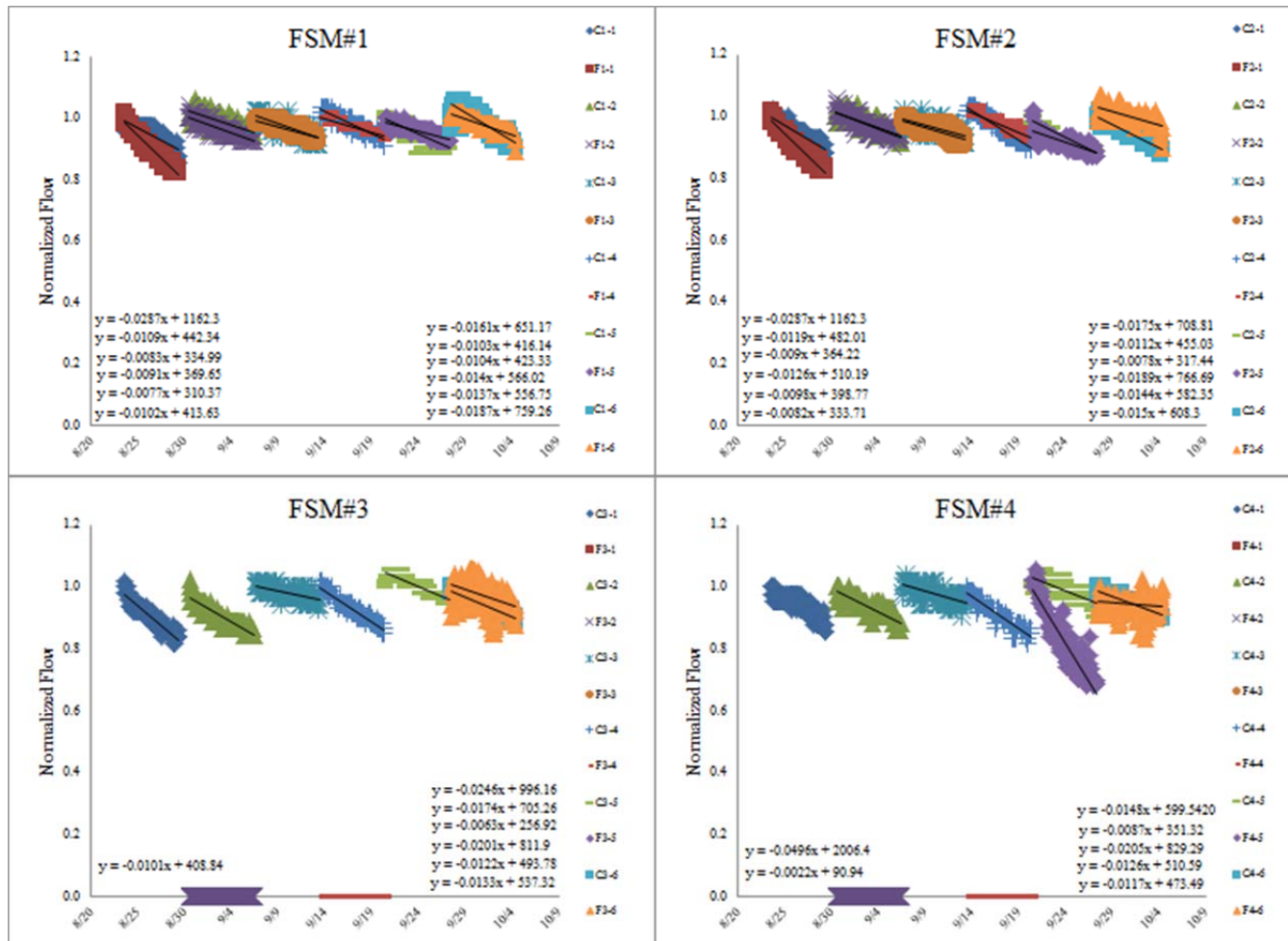


Figure E-6 Initial rate of fouling, m, for the 0.1 g C/m²day portion of the study for all four FSMs

Appendix E (Continued)

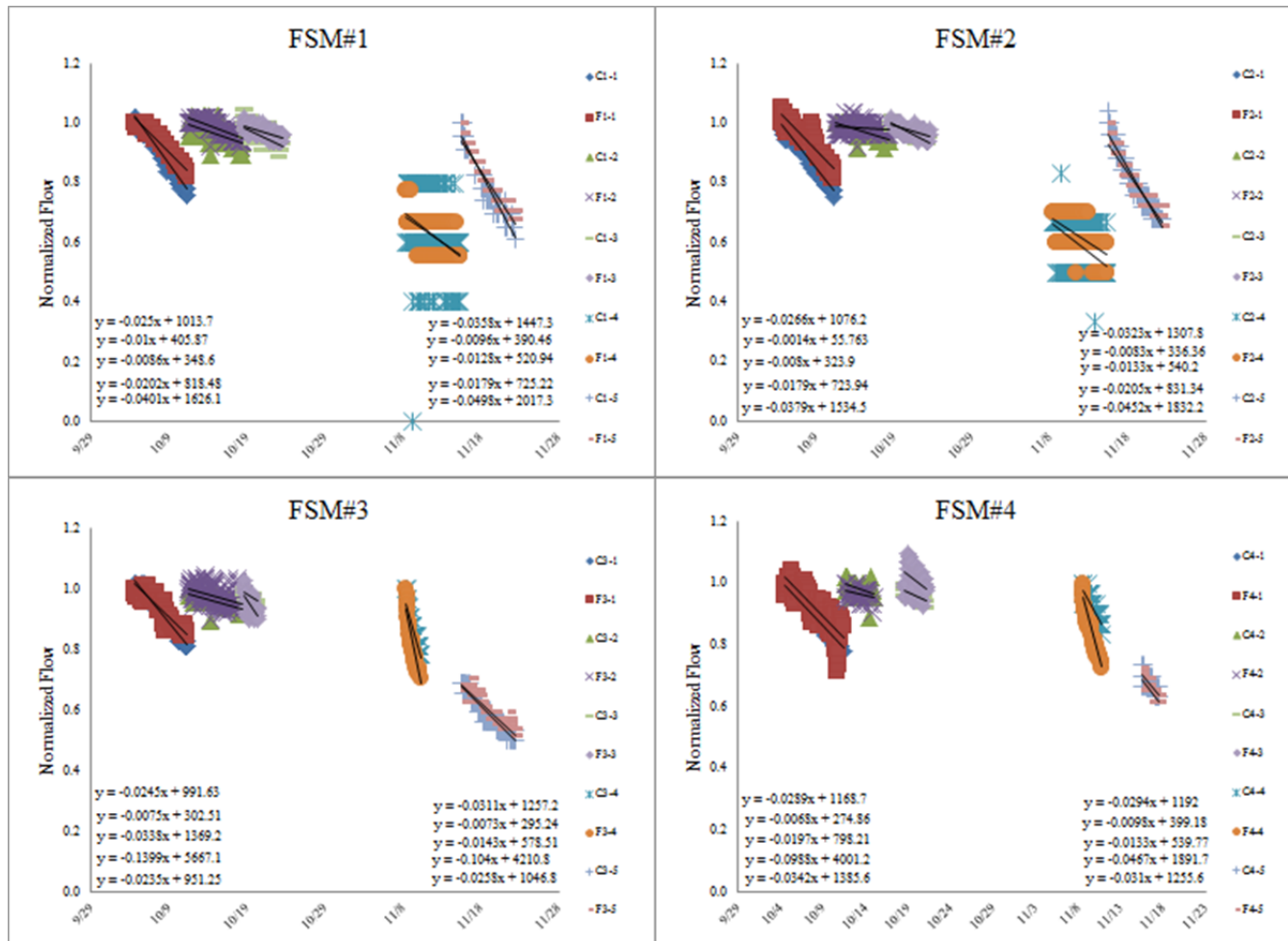


Figure E-7 Initial rate of fouling, m, for the 0.5 g C/m²day portion of the study for all four FSMs

Appendix E (Continued)

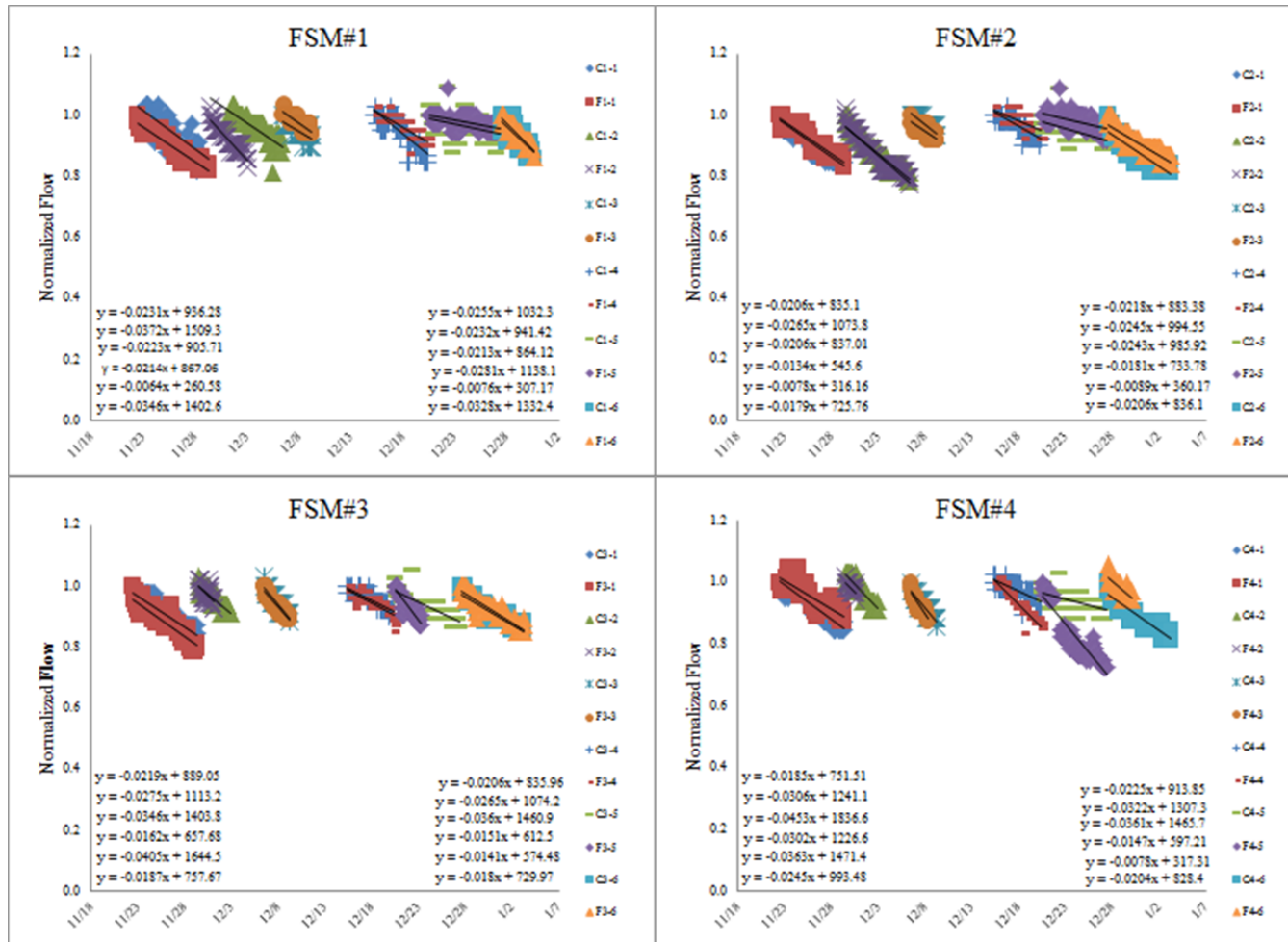


Figure E-8 Initial rate of fouling, m, for the 2.0 g C/m²day portion of the study for all four FSMs

Appendix E (Continued)

The values for m obtained from the graphs above for the feed and concentrate pilot membrane swatches were compared to determine relative fouling information. The average ratio, M (Equation 7.2), for each data point was averaged over the entire period for each carbon loading condition, although the first two data points were ignored for system equilibration purposes. The averaged M value for all for feed and all four concentrate membrane modules are in Tables E-4, E-5, E-6, and E-7 for the no carbon loading, 0.1 g C/m²day, 0.5 g C/m²day, and 2.0 g C/m²day portions of the study respectively.

Table E-4 Feed/concentrate ratio for initial flux decline for the zero external carbon loading portion of the study

<u>C Loading</u>	<u>Week#</u>	<u>Avg M</u>
0	1	0.74
0	2	0.90
0	3	1.12
0	4	0.86
0	5	0.93
0	6	1.02
0	7	-
0	8	2.16
0	9	1.30

Appendix E (Continued)

Table E-5 Feed/concentrate ratio for initial flux decline for the 0.1 g C/m²day portion of the study

C Loading	Week#	Avg M
0.1	1	1.22
0.1	2	1.06
0.1	3	0.98
0.1	4	0.66
0.1	5	1.73
0.1	6	0.51

Table E-6 Feed/concentrate ratio for initial flux decline for the 0.5 g C/m²day portion of the study

C Loading	Week#	Avg M
0.5	1	0.82
0.5	2	0.73
0.5	3	1.28
0.5	4	-
0.5	5	1.37
0.5	6	0.91

Table E-7 Feed/concentrate ratio for initial flux decline for the 2.0 g C/m²day portion of the study

C Loading	Week#	Avg M
2	1	0.93
2	2	1.17
2	3	1.03
2	4	1.16
2	5	2.31
2	6	1.04

Appendix E (Continued)

Statistics of Foulant Materials

Statistical analyses were performed on the data obtained from the foulant deposition tests to determine if there is a significant difference between the feed and concentrate membrane swatches. As stated in Chapter 7, ratio values greater than 1 indicates more fouling on the feed membrane sample than the concentrate. The significance of the ratio values (whether they are greater than 1) were tested and the results are presented here. The test results for proteins, carbohydrates, total direct count, HPC, RMS roughness, and Ra roughness are in Tables E-8, E-9, E-10, E-11, E-12, and E-13 respectively.

Table E-8 The t-test results from feed/concentrate ratio of protein concentration on pilot membrane samples

<u>C Loading</u>	<u>Mean</u>	<u>Stdev</u>	<u>n</u>	<u>t-value</u>	<u>Significant</u>
0.0	1.1	0.3	17	0.70	No
0.1	1.0	0.1	12	0.80	No
0.5	1.4	0.5	12	2.73	Yes
2.0	1.3	0.1	12	6.76	Yes

Table E-9 The t-test results from feed/concentrate ratio of carbohydrate concentration on pilot membrane samples

<u>C Loading</u>	<u>Mean</u>	<u>Stdev</u>	<u>n</u>	<u>t-value</u>	<u>Significant</u>
0.0	1.0	0.5	17	0.24	No
0.1	1.1	0.3	12	1.45	No
0.5	1.3	0.4	12	2.48	Yes
2.0	1.8	0.8	12	3.19	Yes

Appendix E (Continued)

Table E-10 The t-test results from feed/concentrate ratio of total direct count numbers on pilot membrane samples

C Loading	Mean	Stdev	n	t-value	Significant
0.0	1.6	0.9	11	2.32	Yes
0.1	1.4	0.4	4	2.13	No
0.5	1.8	0.6	12	4.65	Yes
2.0	1.8	0.5	12	5.97	Yes

Table E-11 The t-test results from feed/concentrate ratio of HPC concentration on pilot membrane samples

C Loading	Mean	Stdev	n	t-value	Significant
0.0	1.2	1.2	15	0.5	No
0.1	1.3	0.8	12	1.4	No
0.5	2.6	2.0	12	2.7	Yes
2.0	2.5	1.5	12	3.6	Yes

Table E-12 The t-test results from feed/concentrate ratio of root mean squared (RMS) roughness values for pilot membrane samples

C Loading	Mean	Stdev	n	t-value	Significant
0.0	1.1	0.2	17	1.39	No
0.1	1.1	0.2	12	0.90	No
0.5	1.1	0.3	8	0.64	No
2.0	1.1	0.5	12	0.71	No

Table E-13 The t-test results from feed/concentrate ratio of average roughness (Ra) values for pilot membrane samples

C Loading	Mean	Stdev	n	t-value	Significant
0.0	1.1	0.2	17	1.23	No
0.1	1.0	0.2	12	0.70	No
0.5	1.1	0.4	8	0.90	No
2.0	1.1	0.5	12	0.69	No

Appendix E (Continued)

The statistical analyses for the different carbon loading conditions for each of the tests performed were stated in Chapter 7. The results of these analyses for proteins, carbohydrates, feed carbohydrate/protein ratio, concentrate carbohydrate/protein ratio, total direct count, HPC, RMS roughness, and average roughness are in Tables E-14, E-15, E-16, E-17, E-18, E-19, E-20, and E-21 respectively.

Table E-14 Two-tailed t-test results between each carbon loading condition for protein concentration showing degrees of freedom (df), t-value, and indication of significance at 0.05

C Loading 1	C Loading 2	df	t-value	Significant
0.0	0.1	27	0.8623	No
0.0	0.5	27	2.2341	Yes
0.0	2.0	27	2.1619	Yes
0.1	0.5	22	2.843	Yes
0.1	2.0	22	5.4528	Yes
0.5	2.0	22	0.8454	No

Appendix E (Continued)

Table E-15 Two-tailed t-test results between each carbon loading condition for carbohydrate concentration showing degrees of freedom (df), t-value, and indication of significance at 0.05

C Loading 1	C Loading 2	df	t-value	Significant
0.0	0.1	27	0.5207	No
0.0	0.5	27	1.5256	No
0.0	2.0	27	2.9232	Yes
0.1	0.5	22	1.3097	No
0.1	2.0	22	2.5634	Yes
0.5	2.0	22	1.6696	No

Table E-16 Two-tailed t-test results between each carbon loading condition for feed carbohydrate/protein ratio showing degrees of freedom (df), t-value, and indication of significance at 0.05

C Loading 1	C Loading 2	df	t-value	Significant
0.0	0.1	27	2.5136	Yes
0.0	0.5	27	5.7208	Yes
0.0	2.0	27	7.8316	Yes
0.1	0.5	22	2.9149	Yes
0.1	2.0	22	3.7851	Yes
0.5	2.0	22	0.1352	No

Appendix E (Continued)

Table E-17 Two-tailed t-test results between each carbon loading condition for concentrate carbohydrate/protein ratio showing degrees of freedom (df), t-value, and indication of significance at 0.05

C Loading 1	C Loading 2	df	t-value	Significant
0.0	0.1	27	2.1674	Yes
0.0	0.5	27	6.2749	Yes
0.0	2.0	27	5.5708	Yes
0.1	0.5	22	3.5684	Yes
0.1	2.0	22	2.3772	Yes
0.5	2.0	22	1.6671	No

Table E-18 Two-tailed t-test results between each carbon loading condition for total direct count showing degrees of freedom (df), t-value, and indication of significance at 0.05

C Loading 1	C Loading 2	df	t-value	Significant
0.0	0.1	13	0.5563	No
0.0	0.5	21	0.5973	No
0.0	2.0	21	0.5811	No
0.1	0.5	14	1.3868	No
0.1	2.0	14	1.6983	No
0.5	2.0	22	0.0847	No

Appendix E (Continued)

Table E-19 Two-tailed t-test results between each carbon loading condition for HPC concentration showing degrees of freedom (df), t-value, and indication of significance at 0.05

C Loading 1	C Loading 2	df	t-value	Significant
0.0	0.1	25	0.3559	No
0.0	0.5	25	2.261	Yes
0.0	2.0	25	2.6189	Yes
0.1	0.5	22	2.0362	No
0.1	2.0	22	2.5116	Yes
0.5	2.0	22	0.0898	No

Table E-20 Two-tailed t-test results between each carbon loading condition for RMS roughness showing degrees of freedom (df), t-value, and indication of significance at 0.05

C Loading 1	C Loading 2	df	t-value	Significant
0.0	0.1	27	0.004	No
0.0	0.5	23	0.1566	No
0.0	2.0	27	0.3241	No
0.1	0.5	18	0.1288	No
0.1	2.0	22	0.2689	No
0.5	2.0	18	0.1306	No

Appendix E (Continued)

Table E-21 Two-tailed t-test results between each carbon loading condition for average roughness (Ra) showing degrees of freedom (df), t-value, and indication of significance at 0.05

C Loading 1	C Loading 2	df	t-value	Significant
0.0	0.1	27	0.096	No
0.0	0.5	23	0.6009	No
0.0	2.0	27	0.3561	No
0.1	0.5	18	0.5426	No
0.1	2.0	22	0.3395	No
0.5	2.0	18	0.092	No

The statistical results from a two-tailed t-test performed on the data from the 25GPM and 50GPM flow rate portions of the study discussed in Chapter 7 are presented here. The statistical results from the 0.1 g C/m²day, 0.5 g C/m²day, and 2.0 g C/m²day portions of the study are in Tables E-22, E-23, and E-24 respectively.

Table E-22 Two-tailed t-test results for the foulant analyses for 0.1 g C/m²day showing degrees of freedom (df), t-value, and indication of significance at 0.05

Test	C Loading	n	t-value	Significant
Protein	0.1	10	1.70	No
Carbohydrate	0.1	10	1.05	No
Feed				
Carbohydrate/Protein	0.1	10	0.18	No
Concentrate				
Carbohydrate/Protein			0.31	
HPC	0.1	10	1.35	No

Appendix E (Continued)

Table E-23 Two-tailed t-test results for the foulant analyses for 0.5 g C/m²day showing degrees of freedom (df), t-value, and indication of significance at 0.05

Test	C Loading	n	t-value	Significant
Protein	0.5	10	3.59	Yes
Carbohydrate	0.5	10	1.54	No
Feed				
Carbohydrate/Protein	0.5	10	0.31	No
Concentrate				
Carbohydrate/Protein			1.65	
HPC	0.5	10	0.23	No

Table E-24 Two-tailed t-test results for the foulant analyses for 2.0 g C/m²day showing degrees of freedom (df), t-value, and indication of significance at 0.05

Test	C Loading	n	t-value	Significant
Protein	2.0	10	1.56	No
Carbohydrate	2.0	10	1.47	No
Feed				
Carbohydrate/Protein	2.0	10	1.76	No
Concentrate				
Carbohydrate/Protein			0.80	
HPC	2.0	10	0.77	No